UNIVERSIDADE DE LISBOA
FACULDADE DE CIÊNCIAS

Tackling fungal resistance with new ketoconazole derivatives targeting plasma membrane sphingolipids

"Documento Definitivo"

Doutoramento em Bioquímica
Especialidade: Biofísica Molecular

Andreia Bento de Oliveira

Tese orientada por:
Doutor Rodrigo Freire Martins de Almeida

Documento especialmente elaborado para a obtenção do grau de doutor

2024

UNIVERSIDADE DE LISBOA

FACULDADE DE CIÊNCIAS

Tackling fungal resistance with new ketoconazole derivatives targeting plasma membrane sphingolipids

Doutoramento em Bioquímica

Especialidade: Biofísica Molecular

Andreia Bento de Oliveira

Tese orientada por:

Doutor Rodrigo Freire Martins de Almeida

Júri:

Presidente:

● João Manuel Pires da Silva, Professor Catedrático e Presidente do Departamento de Química e Bioquímica da Faculdade de Ciências da Universidade de Lisboa

Vogais:

● Doutora Maria de Fátima Guerreiro da Silva Campos Raposo, Professora Catedrática da Faculdade de Ciências e Tecnologia da Universidade NOVA de Lisboa;

● Doutor Jorge Manuel Martins, Professor Auxiliar da Faculdade de Ciências e Tecnologia da Universidade do Algarve;

● Doutor Nuno Fernando Duarte Cordeiro Correia dos Santos, Professor Associado com Agregação da Faculdade de Medicina da Universidade de Lisboa;

● Doutor Fábio Monteiro Fernandes, Professor Auxiliar do Instituto Superior Técnico da Universidade de Lisboa;

● Doutor Rodrigo Freire Martins de Almeida, Professor Associado da Faculdade de Ciências da Universidade de Lisboa (orientador).

Trabalho financiado pela Fundação para a Ciência e a Tecnologia através da bolsa de doutoramento SFRH/BD/145600/2019

Documento especialmente elaborado para a obtenção do grau de doutor

2024

Para o meu esposo

We live in a society exquisitely dependent on science and technology, in which hardly anyone knows anything about science and technology.

Carl Sagan

Acknowledgements

First and foremost, I must grant my special thanks to Professor Rodrigo de Almeida, my supervisor. Thank you *not only* for reading all my writings with the upmost patience, *but also* for carefully pointing any inaccuracies which allowed for my work to be as scientifically accurate as possible. *Besides* that, I am very grateful for the opportunity to work autonomously in this project. I appreciate all the meetings where my questions and doubts were answered, which were *typically* intercalated with talks about movies or food. *In fact*, my list of restaurants to try out is now *way* bigger than it should be. Finally, thank you for acknowledging my repeated use of an *array* of words and expressions with a gentle smile instead of judgment. *I think* this acknowledgement clearly highlights how much I paid attention to that… Thank you for all the kind words, mentoring and help throughout the years.

I would like to acknowledge the institutions that supported the execution of this project: to Fundação para a Ciência e a Tecnologia (FCT) for giving financial support with a PhD fellowship (SFRH/BD/145600/2019), research grants PTDC/BBB-BQB/6071/2014 (RESYEAST) and EXPL/BIA-BFS/1034/2021 (SphingOHmyces), and research units UID/Multi/00612/2013-2019 (Centro de Química e Bioquímica) and Centro de Química Estrutural, CQE, (UIDB/00100/2020; UIDP/00100/2020; LA/P/0056/2020); to Faculdade de Ciências da Universiadde de Lisboa (FCUL) for accepting me as a student; and to CQE facilities and equipment provided.

A special acknowledgement goes to Professor Radosław Starosta, who provided ketoconazole and its derivatives used in this work. More importantly were the caring yet critical words about the work we developed together that gave me the motivation for wanting to explore more and more the properties of these antifungal drugs. Never forgetting our conversations about gaming.

Thank you to Professor Liana Silva for all the help with the trickster molecule that is nystatin. I had the opportunity to go to some nice conferences because of you, for which I am very grateful.

I am also grateful to Professor Helena Soares, Professor Luísa Cyrne and Professor Susana Marinho for the support with yeast, particularly for using the Redox Biology laboratory and equipment to grow cells.

I also want to thank Doctor Pedro Paulo for the help with FLIM and other fluorescence measurements and the access to the facilities.

The yearly discussions with Professor Ana Coutinho and Professor Nuno Santos were highly inspiring and contributed to the progress of the project and development of new ideas. Thank you for all the feedback.

I realized that lab work is only amusing whenever you can share it with someone. And for that thank you to all the people that worked in the lab while I was there, and that became more than colleagues: Filipa, Joaquim, Beatriz, Mafalda, Helena, António and Elif. You have always kept the energy in the lab nice and *chill* (and at times full of fun), helping me navigate stressful periods, specially when things weren't going as expected. I must highlight the help and friendly words that Filipa and Joaquim always gave me. I am sure that without both, my first year would have been different.

I am very grateful to all the people I had the opportunity to "supervise" somehow: Margarida, Francesca, Chloe, Mathieu, Esperance, Arthur, Iryna, Tomás and Bruna. Working with you made me realize I truly enjoy mentoring.

Thank you to my friends, for keeping me sane during this project!

I am quite the *bully* to you Alexandra, and yet you keep asking me often how I am.

Thank you Tânia for sharing our issues with academia. I think having *war flashbacks* together really brought us closer, and I am very happy that I can call you friend now.

Although I rather prefer Mariana than you, I must thank you Inês. With some conversations about our many shared (or not) interests you helped me surpass some troublesome times. Even when you will be far away, I will bother you and make sure we remain friends.

I also appreciate how Joana (Pinto aka nº1) and Ana always want to share new adventures with me, that being going to a new restaurant, an escape room, or Egypt. Thank you, specially for the unsolicited hugs (that's for you Ana).

A special thanks to Joana and Iara who after all these years (11 now?!) still listen to my grievances and (pretend to?) laugh at my cringe jokes and never complained about unasked cat photos. When I was lacking motivation to continue working, one "small" call to you Iara, always put me back on track. Joana, whenever I was going through downer periods, sharing a beer with you always helped me out, laughing the pain away. You both always kept me happy and motivated and even when I was a little beach you never stopped being my closest friends.

Obrigada à minha família, por apesar de nem sempre compreenderem muito bem o que significa um doutoramento e que isso implica trabalhar em horários menos convencionais, falam com carinho e orgulho sobre o meu percurso. A minha sobrinha tem apenas meses

enquanto escrevo estas palavras, no entanto o seu nascimento renovou a minha vontade de alcançar uma carreira da qual me orgulho.

Agradeço também à família do meu marido (mãe Elisa, Miguel e Ana) por me terem aceite de braços abertos e pela sua demonstrada curiosidade em relação ao que eu faço.

Por fim e mais importante resta-me falar de quem terá tido o maior feito nestes quatro anos de doutoramento: aqueles que me aturam todos os dias, os meus gatos e esposo.

À Arriety, Gizmo e Méli, obrigada por me darem aquele momento diário de fofura que humaniza o meu coração em dias mais stressantes.

Nos quatro anos de doutoramento, muito aconteceu. Muitos períodos bons, menos bons e realmente maus. Em nenhuma altura senti que não me apoiavas no que quer que eu decidisse fazer. Mesmo quando as minhas inseguranças tomaram conta de mim, o teu carinho, respeito e abraço foram uma constante. É certo que sem ti não teria chegado ao fim desta tese. Fernando, obrigada por para além de seres um bom esposo seres o meu melhor amigo.

This work was developed under the supervision of:

Doctor Rodrigo Freire Martins de Almeida, Principal Investigator, Centro de Química Estrutural, and Assistant Professor, Departamento de Química e Bioquímica, Faculdade de Ciências, Universidade de Lisboa, Portugal.

This work was developed at:

Centro de Química e Bioquímica (grupo de Biofísica Molecular) and Centro de Química Estrutural (laboratório de Biofísica Molecular – grupo 8), Institute of Molecular Sciences, Departamento de Química e Bioquímica, Faculdade de Ciências, Universidade de Lisboa, Campo Grande, 1749-016 Lisboa, Portugal.

Andreia Bento de Oliveira was financially supported by Fundação para a Ciência e a Tecnologia (FCT) with a PhD fellowship SFRH/BD/145600/2019. The work developed during the PhD project was supported by FCT research grants PTDC/BBB-BQB/6071/2014 (RESYEAST) and EXPL/BIA-BFS/1034/2021 (SphingOHmyces), UID/Multi/00612/2013-2019 (Centro de Química e Bioquímica) and since January 1st, 2020, Centro de Química Estrutural (UIDB/00100/2020; UIDP/00100/2020) and Institute of Molecular Sciences (LA/P/0056/2020).

Preface

(written with a little help from ChatGPT)

It's quite fascinating to reflect on my journey when, at the onset of my PhD, outside of the academic realm, I'd often share that I was studying fungi.

"*Oh, you mean mushrooms?*" was the typical, proudly delivered response I always heard. However, fungi encompass so much more than mere culinary delights.

While I am genuinely captivated by their physiological, biochemical, and behavioral intricacies, I find myself compelled to shed light on the global challenge posed by fungal infections. Communicating the gravity of this issue and the arduous battle it entails has become a mission, portraying me as an unsung hero dedicated to fight a frequently overlooked problem for the greater well-being of society.

This might prompt the question of whether my delivery comes across as conceited. Yet, the typical answer is, "*So, you're researching treatments for nail fungal infections?*". Which I believe says that, yes, they do find me a conceited person, albeit one with some knowledge of these organisms.

This scenario offers a glimpse into my social circle but, more crucially, highlights the widespread disregard for fungi.

During these conversations, I introduce the topic of lipids, only to be met with further perplexity. Despite my efforts to convey the complexity and significance of these molecules in the tapestry of life, the response often boils down to an ironic, "*So, you work with fats - how cool.*"

Embracing my inner hipster, this only fueled my determination to focus on the aspects that many overlook. As I find myself nearing the culmination of my PhD, I continue to describe my work with the same terms and pride, aware that I've made a modest yet meaningful contribution to the scientific community. According to those who still inquire, thanks to a well-known tv show, I am still perceived as an unsung hero - now safeguarding the world from the threat of zombies.

List of publications

My contribution to the articles and chapters encompassed in this thesis:

1. A. Khmelinskaia J. T. Marquês, A. E.P. Bastos, C. A. C. Antunes, **A. Bento-Oliveira**, S. Scolari, G. M. da S. Lobo, R. Malhó, A. Herrmann, H. S. Marinho, R. F. M. de Almeida, "Liquid-ordered phase formation by mammalian and yeast sterols: a common evolutionary feature despite organizational differences." *Front. Cell Dev. Biol.* 2020, 8: 337. https://doi.org/10.3389/fcell.2020.00337
   Zymosterol and cholesterol GUV preparation, visualization (confocal microscopy) and image analysis.

2. **A. Bento-Oliveira**, F.C. Santos, J.T. Marquês, P. M. R. Paulo, T. Korte, A. Herrmann, H. S. Marinho, R. F. M. de Almeida, "Yeast Sphingolipid-Enriched domains and membrane compartments in the absence of mannosyldiinositolphosphorylceramide" *Biomolecules*, 2020, 10(6), 871. https://doi.org/10.3390/biom10060871
   Took an active part in the formal analysis, investigation, writing and preparation of the original draft, manuscript review and editing, and visualization. I conducted the fluorescence spectroscopy assays with *t*-PnA and DPH, and the protein heterogeneity determination, and respective data analysis.

3. F. C. Santos, J. T. Marquês, **A. Bento-Oliveira**, R. F. M. de Almeida, "Sphingolipid-enriched domains in fungi", *FEBS Letters*, 2020, 594 (22), 3698. https://doi.org/10.1002/1873-3468.13986
   Took an active part in writing-review and editing the manuscript. Wrote the original draft of the section on sphingolipid-enriched domains biological functions, which is featured in chapter I of this thesis.

4. C. Sousa, F. C. Santos, **A. Bento-Oliveira**, B. Mestre, L. C. Silva, R. F. M. de Almeida, "Chapter 14: Biophysical analysis of lipid domains in mammalian and yeast membranes by fluorescence spectroscopy." In *Lipid Rafts – Methods of isolation, visualization, and functional analysis* (e. Bieberich, ed.). Series *Methods in Molecular Biology,* 2021, Humana Press – Springer Nature, doi: 10.1007/978-1-0716-0814-2_14.
   Took an active part in the writing of the manuscript particularly the sections that mention studies with yeast.

5. **A. Bento-Oliveira**, M.-L.C.J. Moita, R.F.M. de Almeida, R. Starosta, "Unraveling environmental effects in the absorption and fluorescence spectra of p-methoxyphenylpiperazine derivatives", *Spectrochimica Acta Part A: Molecular and Biomolecular Spectroscopy*, 2024, https://doi.org/10.1016/j.saa.2023.123583.
   I conducted the fluorescence spectroscopy assays with 4MP, 4MOP 4M3P and 4M3OP in different solvents, including data analysis and figure design. Took an active part in the formal analysis, investigation, writing and preparation of the original draft, manuscript review and editing.

6. **A. Bento-Oliveira**, R. Starosta, R.F.M. de Almeida, "Interaction of the antifungal ketoconazole and its diphenylphosphine derivatives with lipid bilayers: insights into their antifungal action", *Archives of Biochemistry and Biophysics*, 2024. https://doi.org/10.1016/j.abb.2024.109919
   Took an active part in the planning of and performed all the experiments. Took an active part in the writing of the paper.

Publications to which I have contributed that are not included but are related to this thesis:

1. B. Demoro, **A. Bento-Oliveira**, F. Marques, J. C. Pessoa, L. Otero, D. Gambino, R. F.M. de Almeida, A. I. Tomaz, "Interaction with blood proteins of a Ruthenium(II) Nitrofuryl Semicarbazone Complex: Effect on the antitumoral activity", *Molecules*, 2019, 24(16): 2861. https://doi.org/10.3390/molecules24162861.
   I prepared the HSA-compound binding section of the article including conducting the fluorescence spectroscopy assays, analyzing the data, designing figures and writing.

2. A. M. de Matos, M. T. Blázquez-Sánchez, **A. Bento-Oliveira**, R. F. M. de Almeida, R. S. Nunes, P. Lopes, M. Machuqueiro, J. Cristovão, C. M. Gomes, C. S. Souza, I. G. El Idrissi, N. A. Colabufo, A. Diniz, F. Marcelo, M. C. Oliveira, O. López, J. G. Fernández-Bolaños, P. Dätwyler, B. Ernst, K. Ning, C. Garwood, B. Chen, A. P. Rauter, "Glucosylpolyphenols as inhibitors of Aβ-induced Fyn kinase activation and Tau phosphorylation: synthesis, membrane permeability, and exploratory target assessment within the scope of type 2 diabetes and Alzheimer's disease", *Journal of Medicinal Chemistry*, 2020, 63 (20), 11663, https://doi.org/10.1021/acs.jmedchem.0c00841
   I prepared the aggregation section of the article including conducting the assays, analyzing the data, designing figures and writing. The aggregation assays conducted in this work served as an optimization for other aggregation studies using absorption spectroscopy and static light scattering such as the ones present in chapters III and IV of the current thesis.

3. A. Alguacil, F. Scalambra, A. Romerosa, **A. Bento-Oliveira**, F. Marques, I. Maximiano, R.F.M. de Almeida, A.I. Tomaz, A. Valente, "Evaluation of the antiproliferative properties of CpRu complexes containing N-methylated triazaphosphaadamantane derivatives", *Bioinorganic Chemistry and Applications*, 2023: 6669394. https://doi.org/10.1155/2023/6669394.
   I prepared the HSA-compound binding section of the article including conducting the fluorescence spectroscopy assay, analyzing the data, designing figures and writing.

Abstract

The search for new antifungal drugs is a relevant and timely subject due to fungal resistance to antimicrobial agents which is an emerging public health threat. Recently developed diphenylphosphane derivatives of ketoconazole exhibited potential as antifungal therapeutic agents. The mode of action of these compounds is not yet fully uncovered, although evidence suggests that they might interact with sphingolipids in the fungal membrane, which are major component of sphingolipid-enriched gel domains (SLEDs). Moreover, it was shown that the antifungal polyene nystatin has pore-forming activity in highly ordered gel membranes that do not contain sterols, contradicting the classical ergosterol-dependent mode of action. Hence, SLEDs which are not found in animal membranes are promising targets for antifungal drugs and are possibly involved in certain antifungal drug action and resistance mechanisms.

The objectives of this thesis were 1) to explore the biophysical properties of the plasma membrane of the budding yeast *Saccharomyces cerevisiae* focusing on SLEDs, and 2) to uncover the preferential interaction of ketoconazole and diphenylphosphane derivatives, and nystatin with membranes containing specific fungal lipids and distinct biophysical properties as compared to mammalian ones, correlating this interaction with the drugs activity. Fluorescence spectroscopy was used together with an array of membrane systems, from intact cells in suspension to simpler systems such as isolated plasma membrane and liposomes prepared from *S. cerevisiae* lipid extracts or synthetic lipids.

For ketoconazole derivatives, this work also allowed to unravel how structural differences influence their interaction (partition and relative distribution) with membranes and how that could correlate with their biological activity through direct interference on the permeability of the plasma membrane.

Overall, the results presented herein point to SLEDs as promising targets for antifungal agents, with potential to uncover new approaches to fight antifungal drug resistance.

Keywords

Antifungal agents, Yeast plasma membrane, Fluorescence techniques, Sphingolipids, Membrane-drug interaction

Resumo

A resistência a fármacos por parte de fungos patogénicos e o aumento significativo de infeções fúngicas mundialmente são problemas graves para a saúde pública. A procura, desenvolvimento e/ou melhoria de antifúngicos para combater esta ameaça torna-se imperativa.

Como novos derivados difenilfosfano do cetoconazol apresentam potencial como antifúngicos, o seu modo de ação deve ser estudado aprofundadamente. Evidências sugerem que estes compostos interagem com esfingolípidos na membrana plasmática de fungos, *i.e.* com domínios ricos em esfingolipidos (SLEDs). Foi demonstrado que o antifúngico polieno nistatina forma poros em membranas altamente ordenadas, mas que não contêm esteróis, o que contradiz o modelo clássico de ação desta molécula dependente do ergosterol. Uma vez que os mesmos SLEDs não foram encontrados na membrana plasmática de mamíferos, estes domínios são alvos terapêuticos promissores, sendo relevante o estudo das suas propriedades.

O objectivo desta tese foi estudar as propriedades biofísicas da membrana plasmática da levedura *Saccharomyces cerevisiae* com foco nos SLEDs. Em parelo, foi averiguada a interação do antifúngico cetoconazol e seus derivados difenilfosfano, e da nistastina com membranas compostas por lípidos encontrados em membranas de fungo *vs* de mamífero com propriedades biofísicas próprias. A interação distinta destes compostos foi correlacionada com a sua actividade antifúngica. Para atingir estes objectivos, foi usada espectroscopia de fluorescência em conjunto com uma panóplia de sistemas membranares: de células intactas em suspensão a sistemas modelo com lípidos sintéticos ou extraídos da levedura.

Adicionalmente para os derivados do cetoconazol, os resultados apresentados demonstram como as diferenças estruturais entre compostos influenciam a sua interação (partição e distribuição transersal) com membranas, correlacionando esta interação com a sua atividade através da alteração da permeabilidade da membrana plasmática.

Assim, os resultados deste trabalho corroboram o potencial dos SLEDs como alvos terapêuticos. Este estudo apresenta, portanto, o potencial de contribuir para o combate às infeções fúngicas.

Palavras-chave

Antifúngicos, Membrana plasmática da levedura, Fluorescência, Esfingolípidos, Interação fármaco-membrana

Resumo alargado

A resistência a fármacos por parte de fungos patogénicos e o aumento significativo de infeções fúngicas mundialmente são atualmente um problema grave para a saúde pública. Como tal é essencial a procura, desenvolvimento e/ou melhoria de antifúngicos para combater esta ameaça.

O cetoconazol (Ke) é um azol antifúngico utilizado para tratamento de infeções fúngicas topicamente. Devido a efeitos secundários adversos, nomeadamente a nível hepático, o uso intravenoso deste fármaco é apenas permitido em casos extremos. O Ke impossibilita a produção de ergosterol (o principal esterol encontrado em fungos), inibindo um enzima da sua via de síntese. A redução dos níveis de ergosterol na membrana plasmática do fungo leva a uma perturbação da membrana com consequências fungistáticas. Os derivados difenilfosfano (KeP) e óxido de difenilfosfano (KeOP) do Ke apresentam atividade antifúngica maior e toxicidade contra células humanas menor que o composto pai. Apesar destes derivados inibirem o mesmo enzima que o Ke em células de fungo, estes continuam a ter atividade antifúngica contra uma estirpe de levedura que não produz ergosterol (*erg6*Δ), enquanto que o Ke tem uma atividade insignificante. A atividade destes dois derivados é menos dependente que o composto pai da expressão de proteínas responsáveis pelo efluxo de fármacos na membrana plasmática do fungo patogénico *Candida albicans*. Estas evidências apontam para possíveis modos de ação adicionais destes derivados através da interação direta com a membrana plasmática.

Tal como o Ke, a nitastina é um antifúngico que altera as propriedades da membrana, mas de forma direta. Este polieno agrega na membrana plasmática formando pequenos poros que perturbam a permeabilidade da membrana causando morte celular. Segundo o modo de ação clássico deste composto, a formação de poros na membrana é dependente da presença de esteróis, e a nistatina agrega em torno destes lípidos. No entanto, estirpes de levedura com diferentes esfingolipidomas na membrana plasmática, mas que mantêm a composição e nível de esteróis semelhante à estirpe selvagem (wt), apresentam sensibilidades diferentes à nistatina. Esta evidência aponta para um papel dos esfingolípidos na atividade deste antifúngico. Este polieno forma poros em membranas altamente ordenadas em fase gel e que não contêm esteróis, contestando o modelo clássico de ação da nistatina. Este resultado é particularmente interessante já que na membrana de levedura encontramos regiões na membrana plasmática denominadas domínios ricos em esfingolípidos (SLEDs) que são altamente ordenados em fase gel, com baixos níveis de esterol e que não são possíveis de encontrar em células de mamífero.

Já que certos antifúngicos atuam a nível da membrana plasmática, e que os SLEDs são potenciais alvos terapêuticos, o estudo das propriedades de membrana dos fungos, em particular dos SLEDs, é relevante e necessário para compreender a ação de certos antifúngicos e/ou desenvolver novos fármacos mais potentes e menos tóxicos.

Para além da presença de SLEDs na membrana plasmática de levedura, esta apresenta compartimentos espacio-temporalmente estáveis, com proteínas exclusivas e com funções específicas. Os dois compartimentos maiores e mais importantes na membrana plasmática da levedura são o que contem a H^+-ATPase Pma1p (MCP) e o que contem a permease de arginina Can1p (MCC). Certas evidências apontam para o MCP e o MCC serem ricos em esfingolípidos e esteróis respetivamente, ou pelo menos que estes lípidos sejam relevantes para a estabilidade das proteínas específicas destes compartimentos.

O primeiro objetivo desta tese foi estudar as propriedades biofísicas da membrana plasmática da levedura *Saccharomyces cerevisiae*, particularmente as propriedades dos SLEDs e qual a sua correlação com o MCP. Para tal, a estirpe wt e o mutante *ipt1*Δ da levedura *S. cerevisae* foram comparados. O mutante *ipt1*Δ é incapaz de produzir o esfingolípido complexo mais abundante na membrana plasmática da levedura, manosildiinositolfosforilceramida [$M(IP)_2C$], acumulando o seu percursor manosilinositolfosforilceramida (MIPC). A cabeça polar do MIPC não só é menor como também menos carregada. Células vivas, membrana plasmática isolada e vesículas unilamelares gigantes constituídas por lípidos extraídos da membrana plasmática foram marcados com diferentes sondas fluorescentes, cada uma com capacidade para reportar a presença e organização de domínios lipídicos, ordem global, e propriedades dielétricas da membrana. Adicionalmente, as proteínas Pma1p e Can1p foram marcadas com mRFP e GFP, respetivamente, em cada estirpe para avaliar a sua distribuição e organização usando microscopia confocal de fluorescência e imagiologia de tempos de vida de fluorescência (FLIM). A deleção do gene *IPT1* afeta significativamente a rigidez dos SLEDs, mas não a sua abundância relativa, e nenhuma alteração foi reportada para os domínios ricos em esteróis. Também foi observada uma alteração da distribuição da Pma1p na membrana na estirpe *ipt1*Δ em comparação com wt, sem alterações significativas na distribuição da Can1p. Estes resultados permitem concluir que a presença do $M(IP)_2C$ é importante para o empacotamento das cadeias dos esfingolípidos nos SLEDs das células wt; e que os SLEDs e o MCP estão correlacionados, e a distribuição da Pma1p depende das propriedades dos próprios SLEDs, *i.e.*, o MCP é provavelmente enriquecido em SLEDs.

Em paralelo, a interação de antifúngicos, nomeadamente do Ke e derivados difenilfosfano, e nistatina com membranas foi também estudada.

A partição do Ke, KeP e KeOP para membranas fluidas foi quantificada seguindo a fluorescência intrínseca destes compostos para diferentes concentrações de lípido em lipossomas. Apesar da afinidade a uma membrana fluída dos três azóis ser relativamente alta, o coeficiente de partição (K_p) determinado para os derivados (KeP: $(8.31\pm1.60)\text{x}10^5$; KeOP: $(4.66\pm0.72)\text{x}10^6$) foi maior que para o composto pai [$(3.31\pm0.36)\text{x}10^5$]. Estudos de permeabilidade com carboxifluoresceína revelaram que estes compostos aumentam a permeabilidade da membrana. Em particular o derivado KeOP para além de ser o composto com maior afinidade à membrana, é o mais rápido e mais eficiente a permeabilizá-la. Os mesmos estudos foram realizados para compostos mais pequenos (4MP e 4MOP) análogos estruturalmente simplificados do KeP e o KeOP respetivamente, nos quais a estrutura molecular do Ke é substituída por um metilo deixando apenas o grupo que terá sido adicionado ao Ke para formar os derivados respetivos. Não só a afinidade destes compostos à membrana fluída foi menor como também apresentam um menor efeito (praticamente inexistente) na permeabilidade da membrana. Por fim, estudos de extinção de fluorescência dos cinco compostos por parte da molécula hidrofílica acrilamida, permitiram estudar a sua localização relativa na membrana. Os compostos mais pequenos inserem-se numa zona mais superficial que os restantes. Assim, a presença estrutural do Ke concomitantemente com o grupo fosfina adicionado para formar os derivados, causa uma inserção mais profunda na membrana e uma maior afinidade a esta. A maior afinidade do KeOP e do 4MOP ($K_p = (5.21\pm0.82)\text{x}10^5$) quando comparados respetivamente com KeP e 4MP ($K_p = (4.29\pm0.17)\text{x}10^4$), confirma o papel do oxigénio presente nos derivados óxido que estará possivelmente a afetar a hidratação da membrana.

De forma a testar interações especificas do Ke com lípidos ou domínios lipídicos, foi quantificada a sua afinidade e capacidade de alterar a permeabilidade de membranas contendo o esterol ou base estrutural dos esfingolípidos maioritário de fungo (ergosterol e fitoceramida) ou de mamífero (colesterol e ceramida). A partição do Ke é mais eficiente para membranas fluidas, seguida de membranas que contêm ergosterol ($K_p = (1.51\pm0.19)\text{x}10^5$), fitoceramida ($K_p = (1.46\pm0.08)\text{x}10^5$) ou ceramida ($K_p = (1.34\pm0.17)\text{x}10^5$). O Ke possui menor afinidade para membranas contendo colesterol ($K_p = (4.44\pm2.51)\text{x}10^4$). Este azol causa perturbação semelhante em membranas com e sem ergosterol ou fitoceramida, e a alteração de permeabilidade foi a maior para sistemas com ceramida e a menor com sistemas com colesterol. A ação do Ke como agente permeabilizador foi menos rápida para membranas contendo os esteróis e mais rápida para membranas contendo esfingolípidos. Estes resultados apontam para a interação preferencial do Ke com membranas contendo ergosterol ao invés de colesterol,

enquanto a interação com fases gel ricas em esfingolípidos de fungo ou mamífero são semelhantes.

A interação da nistatina com lipossomas contendo ceramida ou fitoceramida também foi estudada. A fluorescência intrínseca da nistatina alterou-se com a presença de fitoceramida mas não de ceramida, o que sugere uma interação preferencial do antifúngico com fitoceramida ao invés da ceramida. Adicionalmente a nistatina teve uma influência mais forte nas propriedades de compressibilidade de monocamadas de fitoceramida do que de ceramida. A atividade da nistatina foi medida com um ensaio de permeabilidade de troca H^+/K^+ em lipossomas, que revelou que para períodos de incubação e/ou concentração da nistatina maior, a sua atividade é maior em lipossomas que contêm o esfingolípido fúngico, fitoceramida do que com ceramida. Estes resultados sugerem que a nistatina tem uma preferência por domínios ricos em fitoceramida, que mimetizam os SLEDs, *vs* domínios ricos em ceramida. Isto sugere que os SLEDs têm um papel na atividade antifúngica da nistatina.

De forma geral investigar a interação dos antifúngicos com membranas é relevante para compreender como uma alteração estrutural do próprio composto ou da composição membranar tem um efeito nessa interação, sendo importante para compreender a ação antifúngica destes compostos e é algo a considerar no *design* de novos fármacos.

Este trabalho realça a importância do estudo da membrana plasmática de fungo como alvo terapêutico, particularmente os seus domínios lipídicos característicos, SLEDs, permitindo o avanço do desenvolvimento ou melhoria de fármacos e o combate às infeções fúngicas.

Table of Contents

List of Abbreviations

3-carboxy-PROXYL	3 (carboxy)-2,2,5,5-tetramethyl-1-pyrrolidinyloxy
4MP	1-[(diphenylphosphino)methyl]-4-(4-methoxyphenyl)piperazine
4MOP	1-[(diphenylphosphoryl)methyl]-4-(4-methoxyphenyl)piperazine
5-DS	5-doxyl-stearic acid
16-DS	16-doxyl-stearic acid
AFM	Atomic force microscopy
ANEP	Aminonaphthylethenylpyridinium
Can1p	Arginine/H^+ symporter
CDC	Centers for Disease Control and Prevention
Cer	Ceramide
CF	5(6)-carboxyfluorescein
CHO	Chinese hamster ovarian
Chol	Cholesterol
CL	Cardiolipin
Cryo-EM	Cryogenic electron microscopy
DFT	Density-functional theory
DHE	Dehydroergosterol
Di-4-ANEPPS	6 [2 (*N,N* dibutylamino)naphthyl]ethenyl-4'-pyridinium propanesulfonate
Di-8-ANEPPS	4-[2-[6-(dioctylamino)-2-naphthalenyl]ethenyl]-1-(3-sulfopropyl)-pyridinium
DLS	Dynamic light scattering
DM-11	*N-N*-dimethylaminoethyl dodecanoate hydrochloride
DMSO	dimethylsulfoxide
DOPC	1,2-dioleoyl-*sn*-glycero-3-phosphocholine
DPH	1,6-diphenyl-1,3,5-hexatriene
DPPC	1,2-diparlmitoyl-*sn*-glycero-3-phosphocholine
EDTA	Ethylenediamine tetracetic acid
ER	Endoplasmic reticulum
Erg	Ergosterol
FCCP	Carbonyl cyanide-*p*-trifluoromethoxyphenylhydrazone
FDA	Food and Drug Administration
FLIM	Fluorescence lifetime imaging microscopy
FRAP	Fluorescence recovery after photobleaching
FTIR	Fourier transform infrared spectroscopy
GFP	Green fluorescent protein
GMPVs	Giant plasma membrane vesicles
GP	Generalized polarization
GPI	Glycosylphosphatidylinositol
GUVs	Giant unilamellar vesicles
HEPES	4-(2-hydroxyethyl)-1-piperazineethanesulfonic acid
HIV	Human immunodeficiency virus
HPLC	High performance liquid chromatography
IPC	Inositolphosphorylceramide
IPM	Isolated plasma membrane

ITC	Isothermal titration calorimetry
Ke	Ketoconazole
KeOP	Diphenylphosphane oxide derivative of ketoconazole
KeP	Diphenylphosphane derivative of ketoconazole
KeSeP	Diphenylphosphane selenide derivative of ketoconazole
KeSP	Diphenylphosphane sulphide derivative of ketoconazole
L_c	Lamellar crystalline phase
LCB	Long-chain base
l_d	Liquid-disordered
l_o	Liquid-ordered
LUVs	Large unilamellar vesicles
MCC	Membrane protein compartment containing Can1p
MCL	Membrane protein compartment containing the sterol transporter Ltc3/4
MCP	Membrane protein compartment containing Pma1p
MCT	Membrane protein compartment containing the target of rapamycin complex 2 TORC2
MCW	Membrane protein compartment containing the cell wall stress mechanosensory Wsc1
MD	Molecular dynamics
MEP	Molecular electrostatic potential
MIC	Minimal inhibitory concentration
MIPC	Mannosylinositolphosphorylceramide
$M(IP)_2C$	Mannosyldiinositolphosphorylceramide
MLVs	Multilamellar vesicles
mRFP	Monomeric red fluorescent protein
NBD-DPPE	*N*-(7-nitro-2-1,3-benzoxadiazol-4-yl)-1,2-dipalmitoyl-*sn*-glycero-3-phosphoethanolamine
NMR	Nuclear magnetic resonance
Nys	Nystatin
ODDC	Octenidine dihydrochloride
P45014DM	Cytochrome P450 sterol-14-α-demethylase
PA	Phosphatidic acid
PC	Phosphatidylcholine
PCM	Polarizable Continuum Model
PDI	Polydispersity index
PE	Phosphatidylethanolamine
PG	Phosphatidylglycerol
Phycer	Phytoceramide
PI	Phosphatidylinositol
Pma1p	H^+-ATPase
POPC	1-palmitoyl-2-oleoyl-*sn*-glycero-3-phosphocholine
PS	Phosphatidylserine
PSM	Palmitoyl-SM
Rhod-DOPE	*N*-(lyssamine Rhodamine B sulfonyl)-1,2-dioleoyl-*sn*-3-phosphatidylehanolamine
ROI	Region of interest
S.D.	Standard deviation
SLBs	Supported lipid bilayers
SLEDs	Sphingolipid-enriched domains

SM	Sphingomyelin
SRDs	Sterol-rich domains
SUVs	Small unillamellar vesicles
TCSPC	Time correlated single photon counting
TLC	Thin layer chromatography
TMA-DPH	Trimethylamine-diphenylhexatriene
t-PnA	*trans*-parinaric acid
VLC	Very long chain
wt	Wild-type
YPD	Yeast extract peptone dextrose medium
Zym	Zymosterol

List of Symbols

A	Average molecular area of a monolayer
A_{ex}	Average molecular excess area of a monolayer with more than one component
[C]	Compound concentration
C_S^{-1}	Compressional modulus
F_{100}	Maximum percentage of CF release
G	Grating factor
I	Fluorescence intensity
K_p	Molar partition coefficient
$K_{p,x}$	Mole-fraction partition coefficient
k_q	Bimolecular quenching rate constant
k_q^{app}	Apparent bimolecular quenching rate constant
k_r	Fluorescence radiative constant
k_{nr}	Fluorescence non-radiative constant
K_s	Static quenching constant
K_{sv}	Stern-Volmer constant
[L]	Total lipid concentration
L_{1h30}	Leakage of CF observed 1h30 after the addition of compound
L_{max}	Maximum leakage of CF
p_i	Pre-exponential factors of a fluorescence intensity decay
[Q]	Quencher concentration
R	Molar gas constant
$\langle r \rangle$	Fluorescence anisotropy
T	Temperature
T_m	Melting or transition temperature
[W]	Molar concentration of water
α_i	Normalized amplitudes of the fluorescence intensity decays
γ_L	Molar volume of lipid
γ_W	Molar volume of water
$\Delta G°$	Standard Gibbs energy
$\Delta\psi$	Transmembrane potential
λ_{em}	Emission wavelength
λ_{ex}	Excitation wavelength
λ_{max}	Maximum peak wavelength
π	Surface pressure
σ	Ratio of local compound/lipid concentration at the critical point
$\bar{\tau}$	Mean fluorescence lifetime (amplitude weighted)
$\langle \tau \rangle$	Mean fluorescence lifetime (intensity weighted)
$\langle \tau_L \rangle$	Average leakage time constant
τ_{long}	Long fluorescence lifetime component
Φ_F	Fluorescence quantum yield
χ_{Cer}	Mole-fraction of ceramide
χ_L	Mole-fraction of compound in the lipid phase
χ_{Phycer}	Mole-fraction of phytoceramide
ψ_d	Dipole potential
ψ_s	Surface potential

List of Figures

Chapter I

Chapter II

Chapter III

Chapter IV

Chapter V

Chapter VI

List of Tables

Chapter I

Chapter II

Chapter III

Chapter IV

Chapter V

Chapter VI

Outline

The increasing incidence of fungal infections is a health problem that should be duly addressed. To achieve this, it is important that new drugs and/or targets are discovered. The search for differences between mammalian and fungal cells becomes imperative. Biophysics is a powerful tool that together with the use of different membrane systems allows to unravel the properties of plasma membranes. In fact, published data from the Molecular Biophysics group, where this current thesis was developed, discovered a unique feature of the fungal plasma membrane – sphingolipid-enriched domains (SLEDs). In a collaborative work involving the Molecular Biophysics group, new ketoconazole derivatives were presented. Interestingly, their antifungal activity against *Saccharomyces cerevisiae* and *Candida albicans* suggested an additional mode of action for azoles through the direct interaction with the yeast plasma membrane, possibly overcoming certain drug resistance mechanisms. There are several antifungal drugs in the market that target the fungal plasma membrane, but until now, there has not been any published evidence which considers SLEDs as drug targets. This project was conducted considering this gap in research in hope to contribute for the discovery of new approaches to fight fungal infections.

A significant part of the data obtained during the execution of this work has already been published in international peer-reviewed scientific journals, hence the thesis is organized in a compilation of articles with an introductory chapter at the begginig and a concluding chapter at the end. The dissertation is divided into 7 chapters:

Chapter I – an introductory overview of the thematic that contextualizes the present thesis, with emphasis on 1) the yeast plasma membrane properties and 2) antifungal drugs which mode of action includes changes of the plasma membrane properties, such as the azole ketoconazole and the polyene nystatin. This chapter also includes a brief description of the basic principles of the biophysical characterization techniques used, mainly, fluorescence spectroscopy, and how it can be used to measure biophysical properties of different membrane systems and drug-membrane interactions. This general contextualization is followed by a small section where the aims proposed for this project are highlighted before any results are shown;

Chapter II – the entirety of the published article in *Biomolecules* (2020) which focuses on how the headgroup of complex sphingolipids in yeast cells changes the biophysical properties of the plasma membrane, and SLEDs, but also protein compartment organization;

Chapter III – the entirety of the published article in *Archives of Biochemistry and Biophysics* (2024) which focuses on quantification of ketoconazole and diphenylphosphane

derivatives interaction with a fluid bilayer and how this changes membrane permeability, correlating it with drug activity;

Chapter IV – a chapter prepared as a manuscript to be submitted in an international peer-reviewed scientific journal, which is a continuity study of the previous chapter focusing on the relative location of ketoconazole and diphenylphosphane derivatives in a fluid bilayer to a more detailed understanding of the interaction of these compounds with membranes and explore how different molecular groups in these compounds can change drastically the membrane-drug interaction and their antifungal activity;

Chapter V – a chapter prepared as a manuscript to be submitted in an international peer-reviewed scientific journal, which focuses on the interaction of ketoconazole with membranes containing the major fungal or mammalian sterol or sphingolipid backbone which allowed to unravel that the interaction of the azole depends on membrane fluidity and composition. To draw these conclusions, similarly to chapter III, the quantification of ketoconazole partition and its impact on membrane permeability were studied;

Chapter VI – a chapter prepared as a manuscript to be submitted in an international peer-reviewed scientific journal, which focuses on the preferential interaction of nystatin with the major fungal sphingolipid backbone *vs* the mammalian one;

Chapter VII – a general conclusion that ties all the data together, connecting antifungal activity with the unique properties of *S. cerevisiae* plasma membrane. This chapter also includes how the current thesis may influence upcoming research projects on the subjects described herein and how it contributes to future perspectives in antifungal therapy, namely against durg-resistant fungal strains.

CHAPTER I

INTRODUCTION

Section “3.3.1. SLEDs physiological role” of this chapter comprises the section with the same name of the review F. C. Santos, J. T. Marquês, **A. Bento-Oliveira**, R. F. M. de Almeida, “Sphingolipid-enriched domains in fungi”, *FEBS Letters*, 2020, 594 (22), 3698. https://doi.org/10.1002/1873-3468.13986

1. The overlooked problem of fungal infections

Fungi can cause fungal infections that can vary from mild skin diseases to bloodstream infections that can be deadly, and are responsible for approximately 1.7 million deaths annually (Bongomin et al. 2017). According to the Center for Disease Control and Prevention (CDC) the most common fungal diseases include fungal nail infections, ringworm, vaginal candidiasis, and *Candida* infections of the mouth, throat, and esophagus (Webpage: Fungal Diseases - CDC). These are not typically lethal, however fungal infections are particularly problematic for weakened immune systems such as those of patients with human immunodeficiency viruses (HIV) or cancer, or that underwent organ transplants. In these cases, even typically non-pathogenic fungus (such as *Saccharomyces cerevisiae*) can cause infections (Muñoz et al. 2005; Pérez-Torrado & Querol 2016). The number of immunosuppressed individuals is even higher in hospital and nursing homes. Weakened immune systems are easily susceptible to aspergillosis, candidiasis, mucormycosis, pneumocystis pneumonia and talaromycosis, which are all challenging to treat (Webpage: Fungal Diseases - CDC).

Besides all that was described until now, the overlooked problem of fungal infections arises not only from the small and not diverse number of antifungal drugs available (when compared to antiviral and antibacterial) but mainly from the resistance that certain species develop towards said drugs. This resistance in some cases is multi-drug related, and, hence, hard to eradicate. Particularly the yeast *Candida auris* has become a world-wide epidemic (Webpage: Fungal Diseases - CDC; Friedman & Schwartz 2019) due to its multi-drug resistance among other factors (Jeffery-Smith et al. 2017; Larkin et al. 2017; Sherry et al. 2017).

In addition to being a problem in healthcare, fungi are pathogenic towards plants, which has consequences in agriculture (Stukenbrock & Gurr 2023) and in the timber industry (Brischke & Alfredsen 2020).

Fungal infections are an overlooked problem that must be promptly addressed. The first line of defense should fall upon research to 1) study the fundamentals of these pathogenic organisms; 2) unravel mechanisms of resistance; and 3) search for new and/or improved antifungal drugs, including new targets for action.

2. General characteristics of fungi

The term fungus was first employed in the 16th century to refer to mushrooms, and it is thought to be a derivatization of the Greek *sphongos* which means sponge (Webpage: *Etymology of fungus by etymonline*). Fungi is a diverse group of organisms spanning from unicellular yeasts, such as *S. cerevisiae*, and multicellular filamentous molds, such as *Neurospora crassa*, to macroscopic filamentous fungi, that include mushrooms and toadstools.

The fungi kingdom accommodates such a plethora of organisms that has become challenging to restrict the group to a certain definition. The Merriam-Webster dictionary has the following entry on fungus: *fungus (noun) pl. fungi also funguses: any of a kingdom (Fungi) of saprophytic and parasitic spore-producing eukaryotic typically filamentous organisms formerly classified as plants that lack chlorophyll and include molds, rusts, mildews, smuts, mushrooms, and yeasts.* In *Introductory Mycology* (Alexopoulos & Mims 1979), Alexopoulos and Mims give a more biological characterization by defining the kingdom of fungi that which includes all *eukaryotic, spore-bearing, achlorophyllous organisms that generally reproduce sexually and asexually, and whose usually filamentous, branched somatic structures are typically surrounded by cell walls containing chitin or cellulose, or both of these substances, together with many other complex organic molecules.*

The present work is focused on the budding yeast *S. cerevisiae*.

2.1. Yeasts as model eukaryotic organisms

Yeasts are unicellular organisms with an average of 3-4 µm, that multiply by budding or fission a daughter cell off from the original parent cell (Figure 1.1). In society, yeasts, specifically *S. cerevisiae*, have an important role in brewing beer and baking bread.

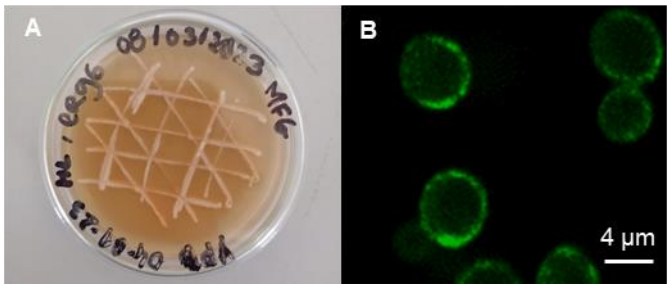

Figure 1.1: Yeast cells. A) *S. cerevisiae* culture in agar-YPD (yeast extract peptone dextrose) solid medium. Note the pastel color of each colony that is characteristic of *S. cerevisiae* cells. B) Confocal microscopy visualization of *S. cerevisiae*. In the bottom left corner, a cell is dividing. The membrane protein Can1p (arginine permease) is tagged with GFP (green fluorescent protein).

Additionally, *S. cerevisiae* is widely used as a model eukaryotic organism in research (please see review (Vanderwaeren et al. 2022)) due to a number of factors, including: 1) its

unicellular nature which facilitates handling and manipulation; 2) a well characterized genome, with a mutant library available to all (Webpage: *Saccharomyces Genome Database - SGD*); 3) a relatively simpler lipidome and proteome when compared with mammalian cells; 4) a short generation time; and 5) the presence of the eukaryotic metabolic "machinery" that is lacking in prokaryotic cells, particularly post-translational modifications (Yang et al. 2024). Furthermore, due to these characteristics, *S. cerevisiae* can easily be genetically engineered to produce molecules with pharmaceutical relevance (Kulagina et al. 2021). Particularly, yeast cells are used as factories for drug production, such as insulin (Kjeldsen et al. 2023) or subunits for vaccines (Kumar & Kumar 2019).

On another hand, some yeasts, such as most species from the genera *Candida* are pathogenic (Webpage: *Invasive Candidiasis - CDC*). Interestingly, even though *S. cerevisiae* is known as a non-pathogenic fungus, it can cause opportunistic infections in hospital environments where the number of immunosuppressed patients is increased (Muñoz et al. 2005; Pérez-Torrado & Querol 2016).

3. The yeast plasma membrane

Since some antifungal agents target the plasma membrane of fungi direct or indirectly, the study of this entity becomes an imperative matter not only in a fundamental fashion but also to help in the discovery of new improved antifungal agents. Moreover, developing antifungal drugs that act directly in the plasma membrane, increases the probability of escaping resistance mechanisms such as drug export overexpression (Sanglard et al. 2009).

As most biological membranes the fungal plasma membrane consists of a lipid bilayer where proteins and lipids distribute heterogeneously – an architectural organization that contributes to the proper function of the cell. The lipidome of fungi is slightly different when compared to that of mammals, which together with its membrane proteome account for a distinct plasma membrane organization, that to this day is still under study.

In the following sections the protein organization, lipid composition and lipid distribution of the yeast plasma membrane will be described, focusing on its unique properties that distinguishes it from the mammalian plasma membrane.

3.1. Membrane protein compartments

One major difference when compared to the mammalian plasma membrane is the presence of non-overlapping spatiotemporally stable compartments (Figure 1.2) that contain exclusively

certain proteins and are associated with specific cell functions (Athanasopoulos et al. 2019). Interestingly, while it is rather challenging to observe domains in the mammalian plasma membrane, due to its stability it is possible to visualize fungal protein compartments under a microscope (Athanasopoulos et al. 2019; Bento-Oliveira et al. 2020; Malinsky et al. 2013; Spira et al. 2012). Lipid and protein composition, morphology and inter-dynamics are what mainly characterizes these domains.

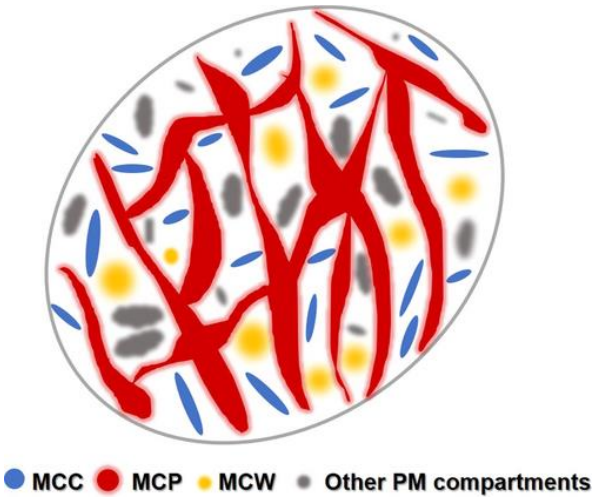

Figure 1.2: Schematic representation of the current distribution of protein compartments in the fungal plasma membrane (PM). The MCW is the membrane compartment that contains the cell wall stress mechanosensory Wsc1. (Santos et al. 2020)

The two major membrane protein compartments are the one containing the H^+-ATPase Pma1p (MCP) (Malínská et al. 2003) and the one containing the arginine permease Can1p (MCC) (Athanasopoulos et al. 2019). The MCC is also called MCC/eisosome due to presence of the eisosome, a large cytosolic protein scaffold that stabilizes the MCC's characteristic furrow-like invagination shape (Strádalová et al. 2009; Walther et al. 2006; Zahumensky & Malinsky 2019). This compartment acts as a sensor to membrane stress (Berchtold et al. 2012), having a role also in membrane adaptation to such stress (Athanasopoulos et al. 2019; Douglas & Konopka 2019; Douglas et al. 2011; Dupont et al. 2010; Pedroso et al. 2009) and lipid homeostasis regulation (Zahumensky & Malinsky 2019). Besides Can1p, other proteins are found in this compartment, such as the uracil permease Fur4p, and the high-affinity tryptophan permease Tat2p. The proper function of these nutrient transporters is dependent on ergosterol (Erg), the major sterol found in fungi (Spira et al. 2012; Zahumensky & Malinsky 2019). Certain evidence suggests that the MCC is enriched in Erg, particularly the labeling of cells with filipin - a 3'-β-sterol binding fluorescent polyene probe (Grossmann et al. 2007, 2008); and when specific proteins from the MCC are deleted, it is not only the compartment formation that becomes compromised but also the distribution of Erg in the plasma membrane

(Zahumensky & Malinsky 2019). Nevertheless, mass spectrometry of the lipidome surrounding proteins exclusively detected in either the MCC or MCP, show that there are similar amounts of Erg in these compartments (van 't Klooster et al. 2020).

The MCP is characterized by its relatively large size and network-like appearance distributed in the membrane along isolated foci (Gournas et al. 2018; Malinsky & Opekarová 2016). Moreover, Pma1p represents 25 to 50% of the total protein of the plasma membrane of *S. cerevisiae* (Serrano 1991). Regarding composition the MCP is thought to be enriched in sphingolipids through indirect data reported for its specific and exclusive protein, Pma1p. This ATPase is the most abundant protein in the plasma membrane of fungi (Serrano 1991) and its function is the creation and maintenance of membrane potential and in consequence intracellular pH regulation and ion concentration (Kane 2016). In *S. cerevisiae* (Bagnat et al. 2001; Gaigg et al. 2006) and *Cryptococcus neoformans* (Farnoud et al. 2014; Munshi et al. 2018) the oligomerization, traffic, activity and plasma membrane stability of Pma1p are affected by sphingolipid profile changes (Lauwers & André 2006; Lauwers et al. 2007; Lee et al. 2002; Wang & Chang 2002). Moreover, lipidomic of Pma1p purified and captured in nanodiscs with lipids that are in its microvicinity revealed that MCP is enriched in sphingolipids, with relatively low amount of Erg (van 't Klooster et al. 2020). Furthermore, as it will be described in chapter II, we used different fluorescent probes and Pma1p tagged with monomeric red fluorescent protein (mRFP) to show that yeast sphingolipid domains are important for protein distribution in the MCP (Bento-Oliveira et al. 2020). This evidence is further corroborated by the presence of a highly ordered lipid domain entrapped by Pma1p hexamers as seen using cryogenic electron microscopy (cryo-EM) (Zhao et al. 2021).

Although the MCC and the MCP are the major protein compartments, the fungal plasma membrane also includes other compartments such as the ones containing the target of rapamycin complex 2 TORC2 (MCT) (Berchtold & Walther 2009; Berchtold et al. 2012; Roelants et al. 2017), the sterol transporter Ltc3/4 (MCL) (Gatta et al. 2015; Murley et al. 2017) and the cell wall stress mechanosensory Wsc1 (MCW) (Kock et al. 2016). Each of these compartments has been associated with specific physiological roles, and due to the dynamics that characterize all biomembranes, there are inter-compartment relations between these, topics reviewed in detail elsewhere (Athanasopoulos et al. 2019).

3.2. Yeast membrane lipids

Lipids are relevant for signaling and regulatory functions, and as energy sources, among other functions in the cell (Czabany et al. 2007; Klug & Daum 2014; Rajakumari et al. 2008; Rego et al. 2014; Zweytick et al. 2000). Nevertheless, the major established role of lipids is as structural "blocks" of cellular membranes, which remains true for fungal cells.

The number of genes involved in lipid metabolism in yeast is smaller than in mammalian cells (Dujon 2015; Ejsing et al. 2009; Singh & Del Poeta 2016) which results in a relatively simpler lipidome. The main lipids that are possible to find in an eukaryotic membrane are glycerophospholipids, sphingolipids and sterols. In the budding yeast *S. cerevisiae* lipids comprise approximately 50% of the molecular components of the plasma membrane (Breslow 2013; Daum et al. 1998, 1999; Dickson & Lester 1999; Pedroso et al. 2009).

In Figure 1.3 the main lipid components in mammals and the yeast *S. cerevisiae* are depicted. Only sphingolipids and sterols are accounted for, since glycerophospholipids in both organisms have only small differences as it will be described in a future section.

The percentage of each class of lipids is relatively difficult to precise since it depends not only on the strain of the yeast, but also on the growth phase and environmental conditions. Additionally, there is a lack of uniformity regarding the experimental conditions, such as membrane isolation, lipid extraction and lipid quantification methodologies, that complicates the comparison of results from different studies. In Table 1.1 is a collection of some of the levels of sphingolipids, sterols and phospholipids obtained from different studies.

Table 1.1: Relative levels of each class of lipid in the plasma membrane of different *S. cerevisiae* strains. For the two last entries the sphingolipid weight at the plasma membrane is divided by the total protein in the plasma membrane. The *ipt1*Δ mutant lacks the major complex sphingolipid found in *S. cerevisiae,* $M(IP)_2C$ (mannosyldiinositolphosphorylceramide) and instead accumulates its precursor MIPC (mannosylinositolphosphorylceramide) in the plasma membrane. wt: wild-type strain.

Strain (background)	Sphingolipids	Sterols/Phospholipids	Reference
wt (W303-1B)	30.7 mol%	0.94 (mol/mol)	(Patton & Lester 1991)
wt (S288C)	-	0.365 (mol/mol)	(Bottema et al. 1983)
wt (X-2180)	-	3.31 (mol/mol)	(Zinser et al. 1991)
wt (X-2180)	0.28 mg/protein mg	0.91 (mg/mg)	(Leber et al. 1997)
*ipt1*Δ (X-2180)	0.52 mg/ protein mg	1.44 (mg/mg)	(Leber et al. 1997)

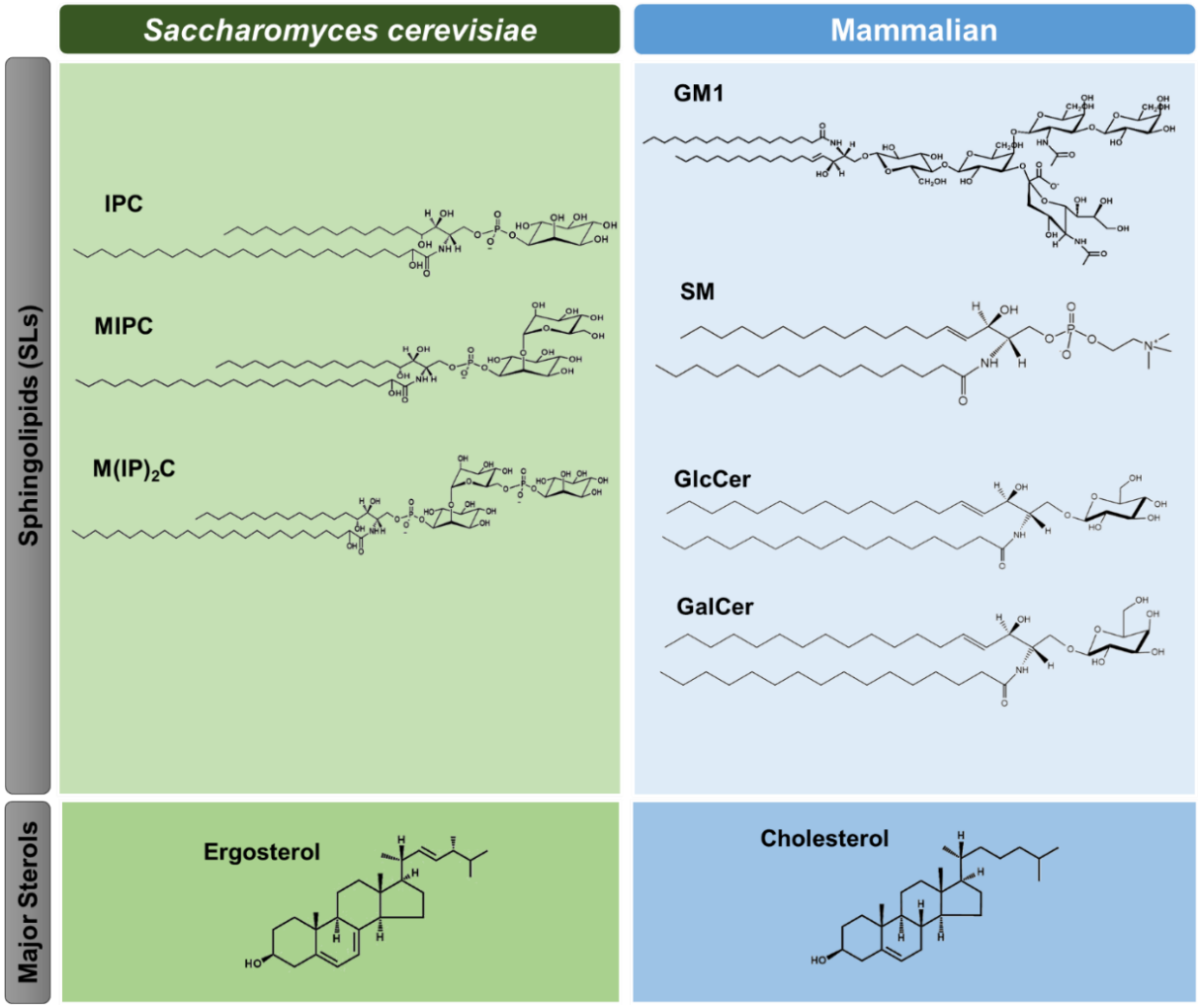

Figure 1.3: Molecular structure of the major complex sphingolipids and sterols found in the plasma membrane of the budding yeast *S. cerevisiae* (green) and mammals (blue). IPC – inositolphosphorylceramide; MIPC – mannosylinositolphosphorylceramide; $M(IP)_2C$ – mannosyldiinositolphosphorylceramide; GM1 - ganglioside GM1; SM – sphingomyelin; GlcCer – glucosylceramide; GalCer – galactosylceramide. The SM represented is particularly *N*-palmitoylsphingomyelin (PSM). Adapted from (Santos et al. 2020).

3.2.1. Lipids and their organization in biological membranes

Cellular membranes, including yeast membranes, can organize in different lipid domains with specific biophysical properties, such as fluidity, lipid packing and hydration that have been associated with a plethora of functions. These properties vary according to the environment and composition of the membrane itself and are reminiscent of the lipid phases found in membrane model systems (Marquês et al. 2015a): liquid-disordered (l_d), liquid-ordered (l_o) and solid-ordered (s_o) or gel, here listed from more fluid to more ordered and compact (Figure 1.4).

The general main lipid composition of membranes remained the same along different eukaryotic kingdoms (plantae, fungi and animalia): a mixture of glycerophospholipids, sphingophospholipids and sterols. Glycerophospholipids are the main "building blocks" of biomembranes. These phospholipids result from the conjugation of two fatty acyl chains and a

phosphate headgroup to a glycerol backbone. Sphingolipids also have a polar headgroup but are the result of an amide link between a sphingoid backbone and a fatty acyl chain. Alone, sphingolipids and glycerophospholipids form lipid bilayers in an aqueous solution that are organized either in a l_d or gel state, depending on the environment conditions, mainly temperature and pressure. All phospholipids below the melting temperature or transition temperature (T_m) are in a gel phase, while above it, a l_d phase is expected. Lipid phase diagrams are a collection of these transitions and vary from only one lipid to more complex mixtures (Figure 1.5). With more complex mixtures, more intricate situations can occur with unique phases and phase coexistence, depending always on the lipid and conditions, *e.g.* 1-palmitoyl-2-oleoyl-*sn*-glycero-3-phosphocholine (POPC)/Phytoceramide (Phycer), a system explained in more detail in section 3.2.3 of this chapter. Lipid phase diagrams can be determined using several techniques such as fluorescence spectroscopy and microscopy, and differential scanning calorimetry (de Almeida & Joly 2014).

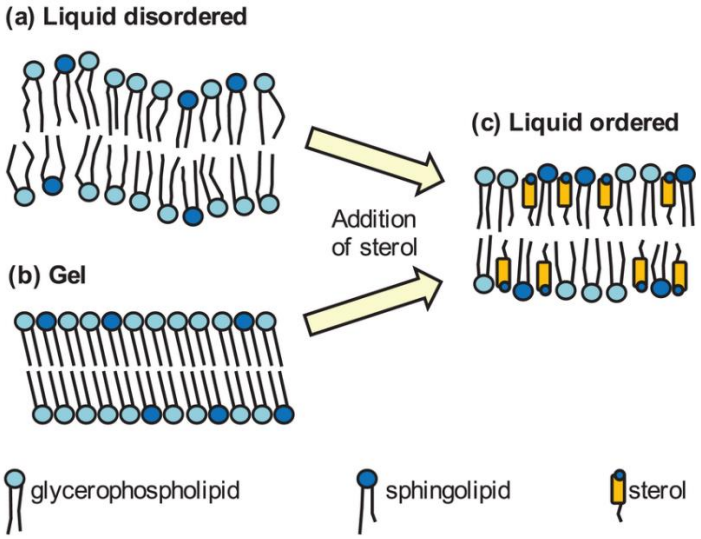

Figure 1.4: Schematic organization of the major lamellar lipid phases: (a) liquid-disordered (l_d), (b) solid-ordered or gel (s_o) and (c) liquid-ordered (l_o). The addition of certain sterols to a gel or a l_d phase causes the formation of l_o phase with opposite behaviors: the sterol addition fluidizes the gel but rigidifies the l_d. (Johnston et al. 2020)

The properties of a lipid phase vary mostly with the type of lipid that enriches it, particularly the headgroup size, polarity and charge, which also influences the hydration (Elson et al. 2010; Hartkamp et al. 2016). Moreover, lipids with long saturated acyl chains frequently concentrate in more ordered domains, while fluid domains are typically enriched in lipids with unsaturated chains. Also, unsaturated *trans* chains pack more orderly in membranes than *cis* ones, resulting in membranes with higher T_m. There are certain lipids that have been widely studied and characterized regarding their organization in membranes that allowed to draw these conclusions. For instance, POPC (Figure 1.5) is a glycerophospholipid commonly found in

membranes of eukaryotic organisms. At room temperature POPC exists in a l_d (Marsh 2012), because of the presence of a *cis*-unsaturated acyl chain in the *sn*-2 position, despite of the presence of a saturated acyl chain in the *sn*-1 position. In opposition, 1,2-dipalmitoyl-*sn*-glycero-3-phosphocholine (DPPC; Figure 1.5) at room temperature organizes in a gel phase due to the presence of two saturated acyl chains (Marsh 2012). Similarly, to DPPC, sphingomyelin (SM), one of the major sphingolipid found in mammalian membranes (Figure 1.3) at room temperature exists in a gel phase (de Almeida et al. 2003). In palmitoyl-SM (PSM) the sphingoid base has a *trans*-unsaturated bond that together with the presence of the saturated fatty acyl chain grants PSM the ability to form gel phases at room temperature. The amide nitrogen of SM can be both an acceptor and a donor for hydrogen bonding which results in a network of hydrogen bonds formed by the sphingolipid that maintains the membrane organized.

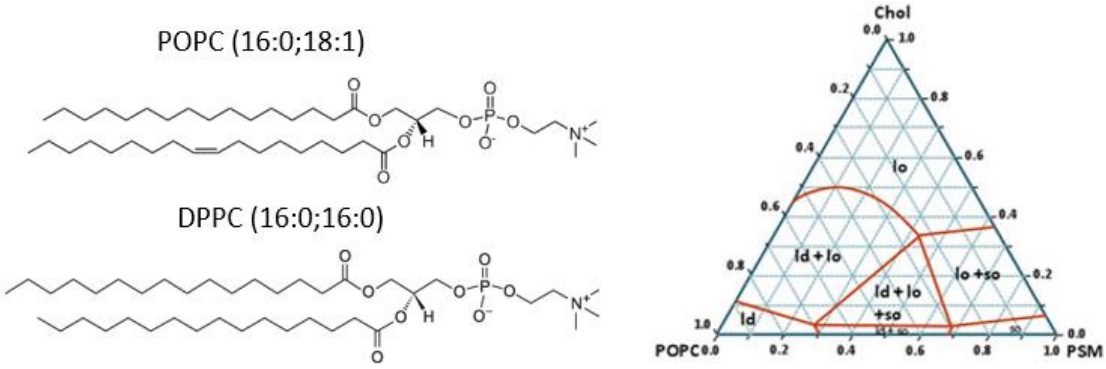

Figure 1.5: Ternary lipid phase diagram of *N*-palmitoylsphingomyelin (PSM), POPC and cholesterol (Chol) at 23°C. The molecular structures of two glycerophospholipids, POPC (1-palmitoyl-2-oleoyl-*sn*-glycero-3-phosphocholine) and DPPC (1,2-dipalmitoyl-*sn*-glycero-3-phosphocholine), are also represented. A ternary mixture of POPC/PSM/Chol at molar proportions 1:1:1 is considered a canonical mixture to study lipid rafts in mammalian plasma membrane models, *i.e.* this ternary mixture is a model of mammalian membranes. At this molar ratio there is a coexistence of l_d and l_o phases. Other phase coexistences are found such as l_o+gel (s_o), l_d+gel (for little to no amount of sterol and equimolar proportions of POPC and PSM) and the ternary coexistence l_d+l_o+gel. At relatively high percentages and 100 mol% of POPC the bilayer is in a fluid state (l_d), while with 100 mol% PSM the bilayer is in a gel phase. (de Almeida & Joly 2014; de Almeida et al. 2003)

In a gel phase, lipids organize in a tight packing configuration with the hydrocarbon chains in an all-*trans* conformation that leads to a slow rotation along the molecule long-axis, and to a cross-sectional area that is minimal and a maximal bilayer thickness (Elson et al. 2010; Goñi et al. 2014). This tight packing results is a slower lateral diffusion of gel phases when compared with l_d (Elson et al. 2010). Collected in Table 1.2 are the biophysical properties for a DPPC gel and l_d, that highlights certain biophysical differences between these two phases.

If certain sterols are mixed with phospholipids or sphingolipids at a certain molar proportion they will induce the formation of a third phase, the l_o phase (Figure 1.4) de Almeida & Joly 2014; Khmelinskaia et al. 2020), which in terms of fluidity is in between the l_d and the gel phase. In other words, the presence of sterols induces l_o formation preventing the abrupt

gel-fluid transition. This issue will be resumed in section 3.2.3 where the phase diagrams for mixture of DPPC with sterols are shown. Sterols are steroid alcohols that contain a four-ring nucleus that could be conjugated with different functional groups. Both the major sterol found in mammalian and fungal cells, cholesterol (Chol) and Erg (Figure 1.3), respectively, were shown to induce the formation of l_o phases with sphingolipids, or with saturated and mono-unsaturated phosphatidylcholines (PCs) (Khmelinskaia et al. 2020; Urbina et al. 1995). The interaction between the hydrophobic ring system and aliphatic chain of the sterols with the acyl chains of the phospholipids guarantees the extended chain conformation that characterizes the l_o phase. Please note that although sterols are the best known l_o forming agents, there are other. For instance, the hopanoid diplopterol found in bacteria is also able to form l_o phases with saturated lipids (Sáenz et al. 2012).

Table 1.2: Biophysical properties of a DPPC bilayer: hydration, thickness, head and chain rotation correlation time and lateral diffusion coefficient (D). Hydration levels were determined using calorimetry or spectroscopic methods. Bilayer thickness obtained from X-ray and freeze-fracture electron microscopy studies. The approximated head and chain correlation times were determined using spectroscopic techniques: vibrational Raman, Fourier transform infrared (FTIR) or fluorescence spectroscopy. The lateral diffusion coefficients (D) where obtained from fluorescence recovery after photobleaching (FRAP) assays. (de Almeida & Loura 2004; Marsh 2012)

Phase	Hydration (mol H_2O/mol lipid)	Bilayer thickness (nm)	Rotation		Lateral diffusion coefficient (D) (cm^2/s)
			Chain (s)	Head (s)	
Gel	0 - 10	~4.5	~10^{-7}	~$1.5x10^{-8}$	10^{-16} - 10^{-11}
l_d	5 - 35	~3.5	~10^{-9}	~$2.5x10^{-9}$	10^{-8} - 10^{-7}

An equimolar mixture of Chol, POPC and PSM is a model for mammalian membranes (Figure 1.5). This system has been widely used to study the properties of lipid rafts (de Almeida & Joly 2014; de Almeida et al. 2003). Although in the past the existence of these lipid domains was questioned, in 2006 lipid rafts were defined as "small (10–200 nm), heterogeneous, highly dynamic, sterol- and sphingolipid-enriched domains that compartmentalize cellular processes. Small rafts can sometimes be stabilized to form larger platforms through protein-protein and protein-lipid interactions." (Pike 2006). Since then the existence of these lipid domains was reported for different organisms associated with a plethora of functions in the cell. Its name arose from the domain being in an l_o phase which moves along the l_d bilayer similarly to a raft on water (Levental et al. 2020; Sezgin et al. 2017).

It is usually considered that biological membrane domains, are in a fluid state, and therefore are considered either l_d-like or l_o-like domains, although evidence in the past decade has emerged for the existence also of gel-like domains in living cells under physiological conditions, at least in yeast (Aresta-Branco et al. 2011; Bento-Oliveira et al. 2020; Santos et al. 2020; Vecer et al. 2014), and in sperm cells in latent state (Wolf 1995). Moreover, ceramide-

rich platforms that are characterized by being highly ordered gel phases (Silva et al. 2006c), are formed as a stress response in certain mammalian cells (Stancevic & Kolesnick 2010; Zhang et al. 2009).

Although the l_d, l_o and gel are the most commonly found lipid lamellar phases in nature, there are other, such as the L_c (crystalline phase) that is typically formed by lipids in an all-*trans* configuration, meaning they are fully extended and packed closely together, minimizing the space between them. This phase is often described as a "gel-like" state but it is less hydrated and lipids are more packed than in the gel phase (Marsh 2012). Lipids can also organize in non-lamellar phases such as the cubic or hexagonal phases. In the latter, lipid molecules - usually those with conical shapes such as phosphatidylethanolamines (PE) - organize into cylindrical tubes arranged in an hexagonal pattern (Jouhet 2013).

The type and abundance of domains can vary in each leaflet of the bilayer, but also, inside the cell, *e.g.* the plasma membrane is very different from the mitochondrial membrane and among different species. There are certain structural differences between each lipid class along evolution that resulted in different membranes with different functions (Dupont et al. 2021). For instance, the membrane domains found in plants and in fungi are overall more spatiotemporal stable and larger than the mammalian ones. Furthermore, as mentioned in the previous section, in yeast the plasma membrane is divided in different compartments with specific biophysical properties and lipid and protein composition (Athanasopoulos et al. 2019).

3.2.2. Yeast glycerophospholipids

The diversity of glycerophospholipids found in the plasma membrane lipidome of *S. cerevisiae* (and as in most organisms from different kingdoms) arises from 1) the different combinations of acyl moieties at the *sn*-1 and *sn*-2 positions, that can differ in length (in yeast, typically C_{16}-C_{18}), and if unsaturated, its location - in yeast, there are only monounsaturated or saturated acyl chains; additionally, 2) the polar headgroups at the *sn*-3 position can also vary: PC, PE, phosphatidylinositol (PI), phosphatidylserine (PS), phosphatidylglycerol (PG), and phosphatidic acid (PA) (Megyeri et al. 2016). Glycerophospholipids with PE, PI and PS headgroups are located preferentially in the inner leaflet of the plasma membrane of the yeast (Cheng & Michels 1991; Ikeda et al. 2006). As in other eukaryotic cells, a redistribution of these lipids in membrane leaflets is associated with specific cellular functions. For instance, in the bud neck of yeast cells in division, PE phospholipids accumulate in the outer leaflet of the plasma membrane, suggesting this glycerophospholipids are involved in cell polarity and actin filaments accumulation in this region (Iwamoto et al. 2004).

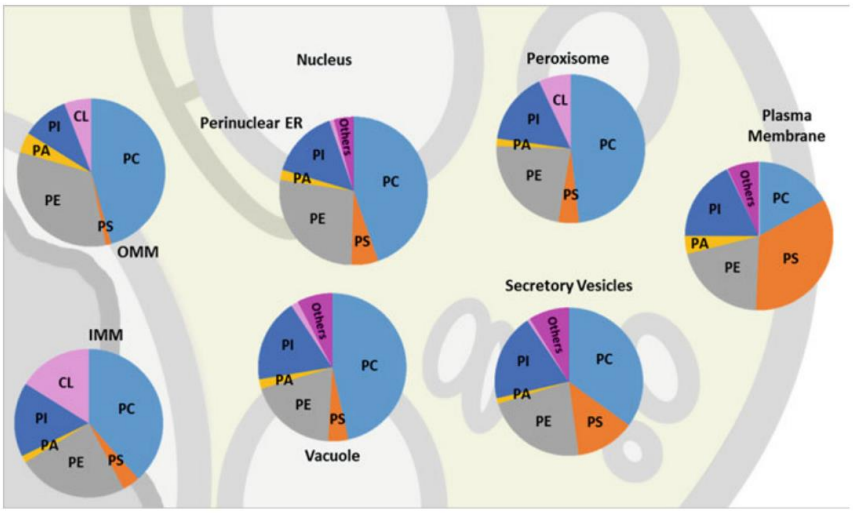

Figure 1.6: Distribution of the glycerophospholipids in yeast organelles membranes. The "others" slice includes lysophospholipids and the diacylglycerol. IMM – inner mitochondrial membrane; OMM – outer mitochondrial membrane. (Zaremberg et al. 2019)

The synthesis of glycerophospholipids is spatially restricted resulting in a differential distribution of these phospholipids along the organelle membranes of the yeast (Zinser et al. 1991) (Figure 1.6). It all starts in the endoplasmic reticulum (ER) with the acylation (acyl-CoA) of glycerol 3-phosphate or dihydroxyacetone phosphate to produce PA. PA can then function as a precursor for triacylglycerols, membrane phospholipids, PG and cardiolipin (CL) (Zaremberg et al. 2019).

3.2.3. The major fungal and mammalian sterols: ergosterol *vs* cholesterol

In Erg, the major sterol found in yeast, the four-ring nucleus, that characterizes sterols, is conjugated with a hydroxyl head group and an alkenyl side chain (Figure 1.3). Besides its relevance as a structural component of membranes, Erg can stimulate growth and proliferation (Aguilar et al. 2010) and inflammatory programmed cell death (Rodrigues 2018), contribute to mitochondrial DNA maintenance (Cirigliano et al. 2019) and stress adaptation (Montañés et al. 2011; Shakoury-Elizeh et al. 2010).

The highly conserved and regulated Erg biosynthetic pathway in the yeast *S. cerevisiae* is well characterized. This pathway is divided into three segments: 1) the mevalonate pathway, conserved across all eukaryotes; 2) the farnesyl pyrophosphate biosynthesis; and 3) the late pathway that has Erg as a final product (Figure 1.7). The first one occurs in the vacuole and mitochondria, the second in the vacuole, and the last one mainly in the ER (Jordá & Puig 2020).

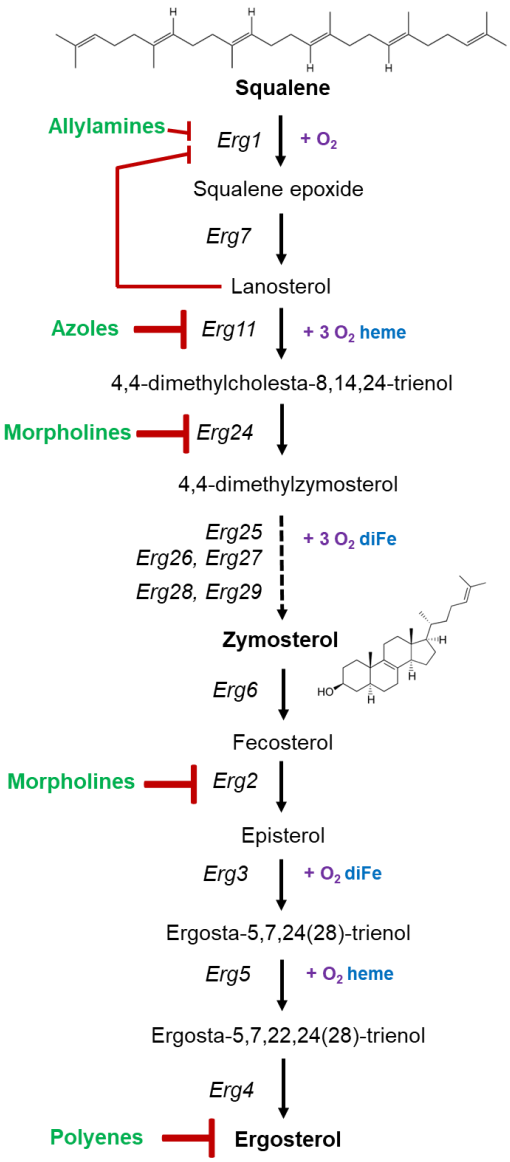

Figure 1.7: Late pathway of the Erg biosynthesis in *S. cerevisiae*. The target of certain antifungal drugs is represented. Zym molecular structure is also depicted. Enzymes: Erg1 – squalene epoxidase EC: 1.14.14.17; Erg7 – lanosterol synthase EC: 5.4.99.7; Erg11 – lanosterol C-14 demethylase EC: 1.14.14.154; Erg24 – sterol C-14 reductase EC: 1.3.1.70; Erg25 – sterol C-4 methyloxydase EC: 1.14.18; Erg26 – sterol C-3 dehydrogenase EC: 1.1.1.170; Erg27 – sterol C-3 ketoreductase EC: 1.1.1.270; Erg6 – sterol C-24 methyltransferase EC: 2.1.1.41; Erg2 – sterol C-8 isomerase EC: 5.-.-.-; Erg3 – sterol C-5 desaturase EC: 1.14.19.20; Erg5 – sterol C-22 desaturase EC: 1.14.19.41; Erg4 – sterol C-24 reductase EC: 1.3.1.71.

Due to the subcellular location of the sterol pathway, there is a differential distribution of the metabolites along the membranes of the organelles of the yeast cell. For instance, Erg comprises the majority of the sterols of the plasma membrane with approximately 80-90 mol% (Pedroso et al. 2009; Zinser et al. 1993), but other sterols are also present such as fecosterol, lanosterol and zymosterol (Zym) (Pedroso et al. 2009). In the Block pathway, Zym is also the precursor of Chol, the major sterol found in mammalian cells (Webpage: *PathBank - Bloch pathway (Cholesterol Biosynthesis) Homo sapiens*). Moreover, Zym is the first sterol of the Erg biosynthetic pathway that is incorporated in membranes (Zinser et al. 1993).

Only small differences can be found when comparing the structure of Chol, Erg and Zym (Figure 1.3 and Figure 1.7). One difference is the presence of a methyl group at carbon 24 of Erg that is not present in neither Chol nor Zym. Such difference has been considered important for the interaction of Erg with fungal sphingolipids (Eisenkolb et al. 2002), but not with the ability of Erg and Chol to induce l_o formation. Also, a saturated aliphatic chain is only found in Chol, when comparing with Erg and Zym, indicating its importance for the stronger ability of Chol to increase membrane dipole potential (Khmelinskaia et al. 2020).

Interestingly, Erg predominates in the inner leaflet of the fungal plasma membrane (55% inner *vs* 15% outer of the total Erg in yeast), and sphingolipids on the outer one (Solanko et al. 2018). This seems to go against the notion that evolution resulted in the optimal interaction between sterols and sphingolipids (Guan et al. 2009). So, the conditions to form lipid rafts in the yeast plasma membrane are not as suited as in the mammalian one. Hence, in the mammalian plasma membrane, interactions between sphingolipids and Chol seem to significantly influence the overall membrane properties. However, in the yeast plasma membrane, interactions between Erg and sphingolipids appear to be less frequent, which suggests that their impact on the general properties of the membrane is relatively minor.

An increasing number of studies address the question of how sterols influence membrane properties (Arora et al. 2004; Bastos et al. 2012; Endress et al. 2002a,b; Galván-Hernández et al. 2020; Khmelinskaia et al. 2020; Shrivastava & Chattopadhyay 2007; Urbina et al. 1995; Yoda 2022), in order to, *e.g.*, 1) establish a relationship from an evolutionary perspective between sterol structure and biological roles; 2) understand the basis of sterol ability to drive phase separation; 3) find out if any other sterol have the same ability as Chol to form lipid raft domains. The majority of the studies point in the same direction: Erg is able to decrease the area per molecule and increase the order of the acyl chains and bilayer thickness even more efficiently than Chol (Beattie et al. 2005; Czub & Baginski 2006; Frallicciardi et al. 2022; Henriksen et al. 2006; Hildenbrand & Bayerl 2005; Hsueh et al. 2005; Hung et al. 2016). The phase diagram of DPPC mixed with Erg or Chol, are comparable, showing very similar coexistence of phases with broader gel + l_o and l_d + l_o phase coexistence regions for Erg (Figure 1.8) (de Almeida & Joly 2014). Both Chol and Erg have the ability to induce l_o formation but with slightly different biophysical properties (Haldar et al. 2012; Khmelinskaia et al. 2020). For instance, the dipole potential of POPC or DPPC vesicles increases much more with the addition of Chol (>60% for 40 mol% of sterol), but less than 10% with 40 mol% of Erg (Haldar et al. 2012; Khmelinskaia et al. 2020). Moreover, Chol influences more the global properties of the membrane than Erg (Aresta-Branco et al. 2011; Khmelinskaia et al. 2020). This could be related

with the higher impact of Chol on phospholipids properties, such as ordering capacity, condensing effect and lateral diffusion, than Erg observed both *in vitro* (Bastos et al. 2012; Frallicciardi et al. 2022; Hung et al. 2016; Urbina et al. 1995) and *in silico* (Alavizargar et al. 2021).

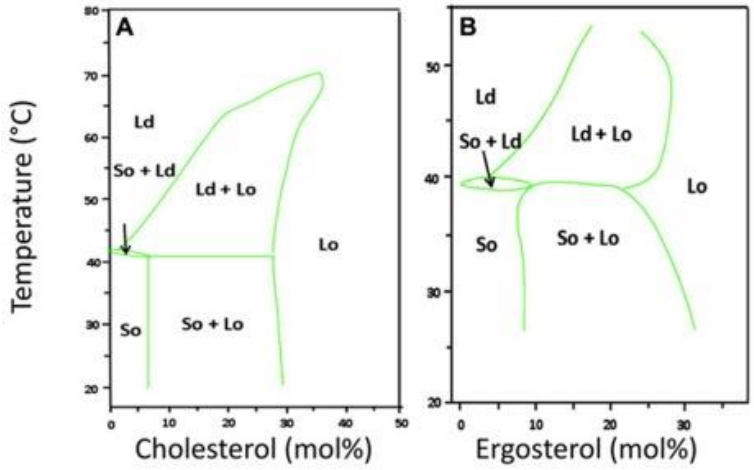

Figure 1.8: Phase diagrams for binary mixtures of DPPC with Chol (A) or Erg (B). Please note that although Erg and Chol are structurally similar, there are subtle differences in their phase diagram while mixing with the same phospholipid, a matter discussed in more detail in the text. (de Almeida & Joly 2014)

It is also relevant to mention that the mol% of Chol and Erg in the plasma membrane of mammals and yeast respectively, is very similar, which is approximately 30-40 mol% (Bezrukov et al. 2009; Das et al. 2013; Daum et al. 1999; Lange et al. 1989; Mitra et al. 2004; Pedroso et al. 2009). Nevertheless, the solubility of these two sterols in lipid bilayers is different. While for Chol the limit is at 65-70 mol% when mixing with saturated or monounsaturated PC lipids such as 1,2-dioleoyl-*sn*-glycero-3-phosphocholine (DOPC) and DPPC (Huang et al. 1999; Stevens et al. 2010); when mixed with the same lipids, the limit solubility for Erg is lower, 25-37 mol% (Hsueh et al. 2005; Mannock et al. 2010; Stevens et al. 2010; Urbina et al. 1995).

3.2.4. The simpler sphingolipidome of the budding yeast

In *S. cerevisiae* the sphingoid base, typically referred to as long-chain base (LCB), is C_{16}-C_{18}, while the fatty acyl chain (or very long chain, VLC) is longer with 24 or 26 carbons and completely saturated (Megyeri et al. 2016). In mammals the length of both the LCB and the VLC varies, particularly, but not only, with the type of cell and/or organelle.

In mammals regarding the headgroup, complex sphingolipids can be SMs or, if the headgroup is a sugar, glycosphingolipids (Figure 1.3). In the budding yeast *S. cerevisiae*, the major complex sphingolipids found in the plasma membrane are the inositolphosphorylceramides (Figure 1.3): inositolphosphorylceramide (IPC),

mannosylinositolphosphorylceramide (MIPC) and mannosyldiinositolphosphorylceramide ($M(IP)_2C$), in crescent order of size, but also amount in the plasma membrane (Dickson 2008; Zink et al. 2005). The biosynthetic pathway of these complex sphingolipids in *S. cerevisiae* is well characterized, and it is depicted in Figure 1.9.

The hydroxylation profile of both the LCB and the VLC is different in yeast and in mammals, however in fungi the hydroxylation levels is more diverse (Dickson & Lester 2002). The most abundant LCB in fungi is phytosphingosine, while in animals is sphingosine. Nevertheless, dihydrosphingosine is found in both kingdoms (Dickson 2008; Sarmento et al. 2020). The most abundant VLC in *S. cerevisiae* cells is 2-OH-26:0 (Dickson 2008).

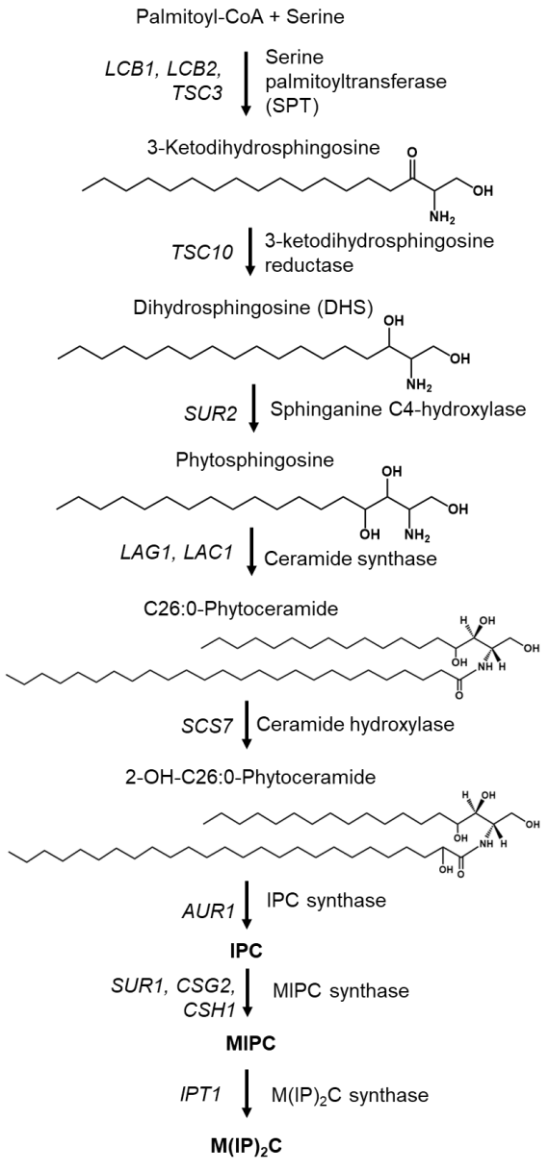

Figure 1.9: Schematic of the sphingolipid biosynthetic pathway in *S. cerevisiae*. The synthesis of sphingolipids in *S. cerevisiae* starts in the ER until phytoceramide (Phycer) is obtained, from which the more complex sphingolipids are synthetized at the Golgi complex. SPT: EC:2.3.1.50; 3-ketodihydrosphingosine: EC:1.1.1.102; sphinganine C4-hydroxylase: EC:1.-.-.-; ceramide synthase: EC:2.3.1.297; ceramide hydroxylase: EC:1.14.18.-; IPC synthase: EC:2.7.1.227; MIPC synthase: EC:2.4.1.370; $M(IP)_2C$ synthase: EC:2.7.1.228. Info gathered from (Dickson 2010).

Although, SM and varied glycosphingolipids have been studied biophysically, the same can not be said about yeast sphingolipids, and the main studies involve cells or isolated plasma membrane, rather than membrane model systems such as liposomes. The purification process of the IPCs is rather complex with little yield at the end, and still not available at a reasonable price. Nevertheless, the major sphingolipid backbone of fungi and mammals, Phycer and ceramide (Cer) respectively (Figure 1.10), have been characterized biophysically. At the molecular level both molecules result from an amide bond to a fatty acid. However, the sphingoid base of Phycer, phytosphingosine, has an additional hydroxyl group instead of a *trans* double bond at C-4, when compared to the sphingosine of Cer. Both molecules can induce the formation of highly ordered gel domains with different biophysical properties even when mixed with a fluid lipid, such as POPC (Figure 1.10) (Marquês et al. 2015b; Pinto et al. 2011). Phycer induces the formation of highly stable and rigid stoichiometric complexes in lipid bilayers with 3:1 and 1:2 POPC:Phycer which are stable at least from ~15 °C to ~55 °C. The existence of such complexes with Phycer, but not Cer, accounts for the existing stable membrane domains, particularly sphingolipid-enriched domains (SLEDs) – the topic of the following section.

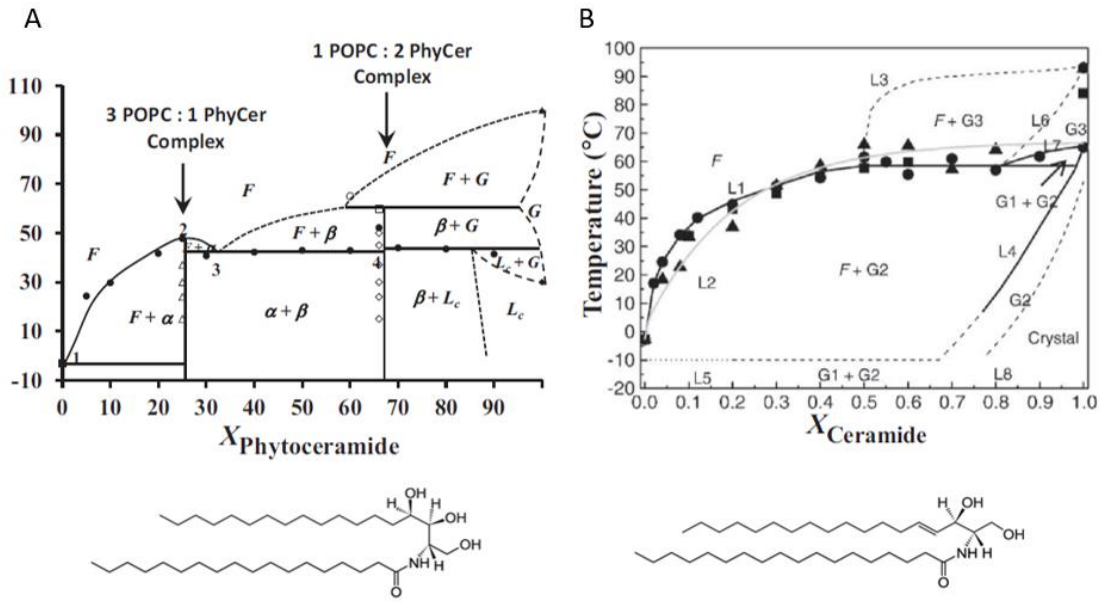

Figure 1.10: Lipid phase diagrams for POPC mixed with Phycer (A) or Cer (B). Below the phase diagram is the respective molecular structure of the sphingolipids, Phycer (*N*-stearoyl-4-hydroxysphinganine; t18:0;18:0) and Cer (*N*-stearoyl-D-*erythro*-sphingosine; d18:1;18:0). In A, α and β represent the 3:1 and 1:2 POPC:Phycer complexes, respectively. In B, G1 represents the POPC rich gel phase, G2 denotes the Cer rich gel phase and G3 concerns the highly ordered Cer rich gel phase. In both cases F stands for the fluid phase, L_c – lamellar crystalline and G – gel phase. The phase diagrams of POPC mixed with C16-Cer (d18:1;16:0 ; circles), C18-Cer (triangles) and C24-Cer (d18:1;24:0; squares) are represented in panel B. In both cases solid lines were experimentally determined and dashed lines represent the most probable and thermodynamically consistent way of completing the phase diagram. (Marquês et al. 2018)

3.3. Yeast lipid domains

In addition to the protein compartments mentioned herein, the plasma membrane of yeast has specific lipid domains with unique biophysical properties, organization, composition and in consequence functions. The two most relevant lipid domains are the sterol-rich domains (SRDs) and the SLEDs. Both these domains are distinct from the ones found in mammalian membranes, particularly lipid rafts which can be compared in terms of composition to both SLEDs and SRDs since typically lipid rafts are enriched in sphingolipids and sterols and l_o-like. However, SLEDs and SRDs are unique features of the fungal plasma membrane.

SRDs, which have been related mainly with membrane growth (Bagnat & Simons 2002), are not the main focus of this work. For more detail on this topic, please check review (Athanasopoulos et al. 2019).

Although under physiological conditions there has never been evidence for the presence of gel domains in the plasma membrane of mammals growing cells, that is not the case for fungi. In fact, the plasma membrane of three different fungal species – *S. cerevisiae* (Aresta-Branco et al. 2011; Vecer et al. 2014), *N. crassa* (Santos et al. 2017, 2018) and *C. neoformans* (Singh et al. 2012) - was shown to have SLEDs, that are sterol-depleted highly ordered gel domains. The high order and tight packing of sphingolipids in SLEDs is maintained by an H-bonding network that results from H-bonds between the hydroxyl and/or amide groups of sphingolipids with each other and/or the ester carbonyl group of glycerophospholipids, plus strong van der Waals interactions established with hydrocarbon chains (Hartkamp et al. 2016; Marquês et al. 2018; Meyer et al. 2014).

3.3.1. SLEDs physiological role

Following the discovery of SLEDs, their physiological relevance became a pressing question, motivating several studies aiming at finding an association between these domains and different cellular processes involving the fungal plasma membrane and the plethora of functions attributed to sphingolipids (Breslow & Weissman 2010; Dickson 2010; Mota Fernandes & Del Poeta 2020). The higher order and the ability to undergo a well-defined gel/fluid phase transition seem to be important features that differentiate SLEDs from other lipid domains (Aresta-Branco et al. 2011; Vecer et al. 2014), making them, for example, more responsive to thermal stress (Dickson 2008; Marquês et al. 2018).

The plasma membrane organization in yeast is deeply affected by depolarization, a subject reviewed in detail elsewhere (Malinsky et al. 2016). The strong connection between the

transmembrane potential of the fungal plasma membrane and the organization of membrane compartments and of the SLEDs was shown with multiple protocols, namely depolarization attained by external stimuli, such as electric fields and chemical agents, for example, lysosomotropic aminoester N-N-dimethylaminoethyl dodecanoate hydrochloride (DM-11) and octenidine dihydrochloride (ODDC) (Malinsky et al. 2016). DM-11 is an ionophore that makes the plasma membrane permeable to electrical stimuli and inhibits the plasma membrane H^+-ATPase activity, whereas ODDC is an ionophore with antimicrobial properties that binds to negatively charged cell surfaces and induces the permeabilization of the plasma membrane. Both these ionophores markedly decrease the abundance of gel domains in the plasma membrane (from 43% (wild-type (wt)) to ca. 12% (with DM-11) and 4% (with ODDC)). However, the rigidity of gel domains that decreases with the addition of DM-11 is essentially unchanged with the addition of ODDC (Herman et al. 2015). A reduction of the relative abundance of the gel domains, but not of their rigidity, was also observed in respiratory deficient strains (*cox7*Δ and *atp1*Δ), when compared to wt cells (Herman et al. 2015). In the same work, the authors used other methods to achieve membrane depolarization and, while in a few cases a small reduction in the rigidity of the gel domains could be noted, the constant observation was a drastic reduction of the relative abundance of gel domains (Herman et al. 2015).

The results above are of unquestionable physiological relevance, as they show that sphingolipid segregation into SLEDs in yeast depends on energy supply and transmembrane potential, that is, SLEDs are actively maintained in the membranes of living yeast cells and their modulation does not require changes in membrane composition (Malinsky & Opekarová 2016). Also, during the depolarization of the yeast plasma membrane, gel domains are dissipated, indicating that these lipid domains can quickly and reversibly respond to stress situations and environmental changes (Grossmann et al. 2007; Herman et al. 2015; Malinsky et al. 2016; Marquês et al. 2015b). Thus, one possible role of SLEDs is to sense, resist and/or respond to environmental stress. Furthermore, the increase of complex sphingolipids content in *S. cerevisiae* resulted in a membrane with more integrity and with increased osmotic tolerance (Zhu et al. 2020), which could be due to an higher amount of the highly rigid SLEDs in the membrane.

A decrease in the abundance of SLEDs was reported for cells that lack one of the enzymes necessary for Erg synthesis (*erg6*Δ mutant - Figure 1.7) or sphingolipids acyl chain 2-hydroxylation (*scs7*Δ mutants - Figure 1.9), and in both cases was accompanied by an increased global membrane order (as well as in spheroplasts, as will be discussed below), underpinning a possible general adaptation mechanism involving SLEDs (Aresta-Branco et al.

2011). This increase in the order of fluid domains in cells with impaired sphingolipid or sterol metabolism (or cell wall) was interpreted as resulting from a more homogeneous distribution of the sphingolipids in the membrane, which increases the order of the fluid regions, an effect that largely compensates for the decrease in the order resulting from a diminished relative abundance of the gel domains (Aresta-Branco et al. 2011). The significant reduction in the abundance of gel domains at the plasma membrane of intact wt *S. cerevisiae* cells invoked by cell depolarization using DM-11 or ODDC is accompanied by the homogenous dispersion of specific MCC H^+-symporters (Grossmann et al. 2007) and an increase in the order of fluid domains in the plasma membrane of *S. cerevisiae* (Herman et al. 2015). It was proposed that Erg is released from a specific pool in the MCC, ensuring the stabilization of sphingolipids in more disordered regions of the plasma membrane (Malinsky et al. 2016), contributing further to the observed global rigidification of the membrane.

SLEDs have been associated with *S. cerevisiae* cellular adaptation to hydrogen peroxide (H_2O_2) (Marquês et al. 2018). *S. cerevisiae* cells, when adapted to H_2O_2, have reduced levels of the hydroxylated VLC fatty acid 2-OH-C26:0, the major acyl chain in the complex sphingolipids of wt budding yeast, as compared to non-adapted cells (Pedroso et al. 2009). This sphingolipidome alteration is accompanied by a decrease in the permeability to H_2O_2 and alterations of the membrane order (Folmer et al. 2008; Pedroso et al. 2009).

Conidial cell death in *N. crassa* caused by heat shock and/or analogue-induced glucose deprivation was concomitant with an increase in Phycers production, correlating sphingolipids with cell death in this fungus, although gel domains were not directly addressed in this study (Plesofsky et al. 2008). More recently, it was shown that SLEDs abundance is increased in *N. crassa* conidia plasma membrane following 1 h challenge with staurosporine, a drug used in several organisms to induce programmed cell death, after 5 h germination. This change was accompanied by an increased fluidity in other membrane regions (Santos et al. 2018), again correlating a higher abundance of SLEDs with a lower global membrane order in fungi, and therefore suggesting an involvement of gel domains in the response of *N. crassa* to staurosporine.

Since the lateral diffusion in the gel phase is much slower than in less ordered phases, and discontinuous gel domains strongly hinder long range diffusion of membrane components in the fluid phase (Almeida et al. 1992; Ratto & Longo 2002; van 't Klooster et al. 2020), SLEDs might be important diffusion barriers for both lipids and proteins in fungal membranes (de Almeida & Joly 2014). In this way, they would contribute to the larger immobility or characteristic slower diffusion of proteins in the plasma membrane of fungi reported *e.g.* by

(Khan et al. 2015; Malinsky et al. 2013) when compared to the plasma membrane of animal cells (Bianchi et al. 2018; Valdez-Taubas & Pelham 2003). This guarantees a polarized distribution and stable spatiotemporal compartmentalization of proteins and lipids along the fungal plasma membrane (Marquês et al. 2015b).

Recently, it was reported that proteins of the MCP are surrounded (periprotein lipidome) by more sphingolipids and less Erg when compared to MCC proteins, indicating that proteins in the MCP would diffuse even more slowly due to their surrounding lipid environment (van 't Klooster et al. 2020). Moreover, sphingolipids play an important role in cell division, most likely at a late stage of cytokinesis and certainly in cell separation (Epstein et al. 2012). Additionally, there is evidence for the need of an integral sphingolipid biosynthesis pathway for the formation of diffusion barriers in the cortical ER at the bud neck, specifically necessary for the separation of mother and daughter cell components during budding (Clay et al. 2014).

SLEDs are also thought to be relevant for trafficking and signalling of certain proteins. Glycosylphosphatidylinositol (GPI) anchors in yeast have mostly a Phycer backbone, rather than being diacylglycerol-based as typically found in mammals, thus having the same hydrophobic backbone as the sphingolipids. When one of the enzymes involved in the remodelling of GPI-anchors is deleted as in *per1*Δ cells, the GPI anchor remains with an unsaturated acyl chain at the *sn*-2 position and the Cer-type anchor is not inserted. Moreover, this deletion leads to more rigid SLEDs (Aresta-Branco et al. 2011). These results indicate that SLEDs might contain a significant amount of GPI-anchored proteins, suggesting a role of these highly ordered domains in GPI-anchored proteins trafficking and signalling. It is also known that sphingolipids stabilize the association of GPI-anchored proteins with membranes and are required for trafficking from the ER to the Golgi (Gaigg et al. 2005; Heese-Peck et al. 2002; Watanabe et al. 2002). Moreover, the vesicles that transport GPI-anchored proteins from the ER to the Golgi are Phycer-enriched (Watanabe et al. 2002) and may already contain gel domains. Interestingly, the transport of GPI-anchored proteins is different between mammals and fungi (Lopez et al. 2019; Mañuel & Howard 2016), which may be justified by the fact that SLEDs are only found in fungi and not mammals.

SLEDs may play a crucial role in the maintenance of transmembrane proton gradient and ion homeostasis. In fact, evidence suggesting that Pma1p is associated with SLEDs has been accumulating. Sphingolipids with very long-chain fatty acids that typically form gel domains are required for Pma1p oligomerization (Bagnat et al. 2001; Lee et al. 2002; Wang & Chang 2002), traffic (Bagnat et al. 2001), stability at the plasma membrane (Wang & Chang 2002) and degradation (Gaigg et al. 2006). In *C. neoformans*, alteration of the sphingolipid biosynthesis

pathway affects Pma1p function and cell growth (Farnoud et al. 2014; Munshi et al. 2018). In *S. cerevisiae ipt1*Δ cells which lacks $M(IP)_2C$ and instead accumulate MIPC (Figure 1.3), the alteration of sphingolipid profile simultaneously affected the SLEDs rigidity and the distribution and environment of Pma1p (Bento-Oliveira et al. 2020), which in turn might interfere with Pma1p normal functioning (Kane 2016), and consequently with nutrient uptake by H^+-symporters at the MCC. Accordingly, SLEDs might be relevant for adapting the plasma membrane permeability when facing depolarization-induced stress (as described above), in a quicker and less energy-consuming manner than through active ion transport, and also for regulating membrane global order and protein distribution.

Finally, SLEDs may play a role in GPI-anchored proteins sorting to the cell wall (Gow et al. 2017), or in plasma membrane stabilization, when the cell wall is damaged or removed. These domains become less abundant in *S. cerevisiae* spheroplasts obtained from wt cells by cell wall enzymatic removal (Aresta-Branco et al. 2011), but the membrane becomes globally less fluid. Lipid and protein compartmentalization on the membrane is interconnected with the cell wall and is sensitive to cell wall stress (de Almeida 2018), further suggesting that SLEDs may be involved in the response to alterations in the cell wall. Sur7p, for instance, is a transmembrane protein involved in sphingolipid metabolism that is stabilized in the MCC, due to interactions between the cell wall and the plasma membrane (Young et al. 2002). Also, in *S. cerevisiae*, MIPC and/or Erg defective strains with hyperactivated cell wall integrity pathway, exhibit cell wall defects that are sensed by proteins located at the MCW, such as Wsc1 and 2 (Tanaka & Tani 2018). *N. crassa* slime strain lacks cell wall and has SLEDs with much tighter packing and higher melting temperature than the wt (Santos et al. 2017). Altogether, these studies point to different possible connections between the cell wall and the SLEDs in yeasts and filamentous fungi.

4. Study of the yeast plasma membrane properties and organization

4.1. Membrane systems for biophysical studies

In order to achieve the proposed goals of this project regarding the study of membrane biophysical properties, an array of different types of membrane systems was studied, each with different complexity and advantages (Figure 1.11). This allowed to have complementary information on a particular subject, and also to focus the study according to the proposed aim, *i.e.*, the membrane system was chosen according to the objective at hand.

For instance, studying directly cells allows to have answers regarding more complex information, without losing cell properties such as function, signaling, molecular synthesis, trafficking amongst many more that define metabolism and guarantees cell life. An example of the direct use of cells are the determination of minimal inhibitory concentration (MIC) (de Almeida et al. 2019) or in imaging techniques (Bento-Oliveira et al. 2020).

Please note that for the present project, yeast cells *S. cerevisiae* were used at a mid-exponential growth phase. This phase is characterized by 1) high metabolic activity and cell division, with a homogeneous population of cells; and 2) the cell wall is still developing, being relatively thin, which allows an easier plasma membrane labelling with fluorescent probes or dyes and/or isolation. Moreover, there are several previous studies in which the yeast cells were in this phase, *e.g.* (Aresta-Branco et al. 2011; Grossmann et al. 2008; Strádalová et al. 2009; Vandeputte et al. 2008), and thus being a well characterized system.

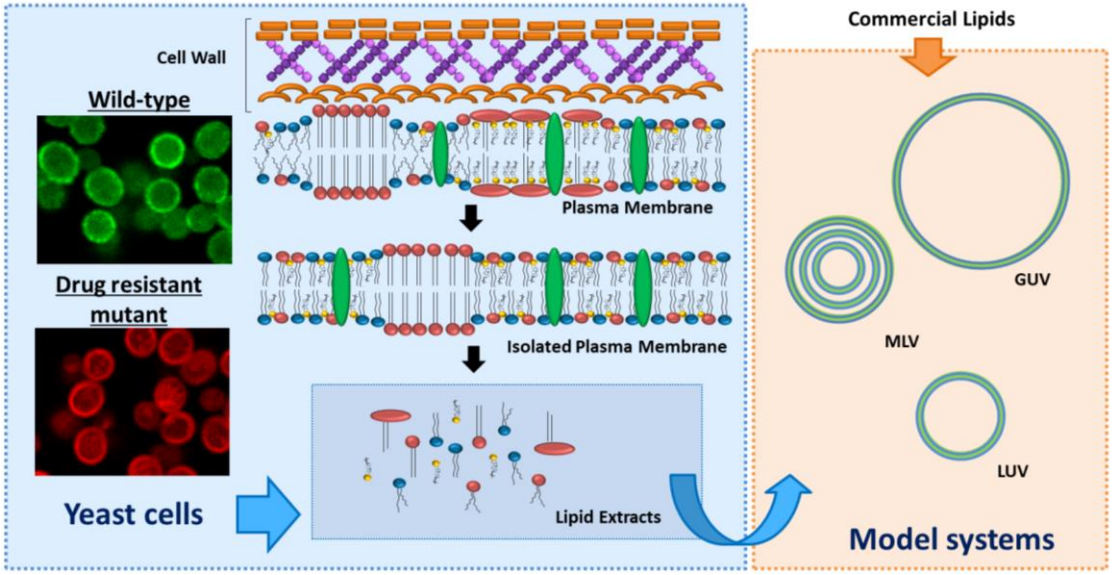

Figure 1.11: Schematic of the membrane systems used in this work. *S. cerevisiae* wt and mutant cells of the lipid biosynthetic pathway cells were studied. Additionally, the plasma membrane of these yeasts was isolated and studied also. Moreover, total lipid extracts or plasma membrane lipids were reconstituted into liposomes. Finally, liposomes containing commercial lipids were also prepared. These different membrane systems were chosen depending on the objective. GUV – giant unilamellar vesicle; MLV – multilamellar vesicle; LUV – large unilamellar vesicle. Adapted from (Marquês et al. 2015a).

For a more specific study of the membrane of organelles, without having the influence of other cell entities, it is possible to isolate different yeast components, such as lipid droplets (Castro et al. 2022), vacuole (Reinhard et al. 2023), ER (Reinhard et al. 2022) and the plasma membrane itself (Bento-Oliveira et al. 2020).

From the cell or even specific organelles as mentioned previously, lipids can be extracted, and used for lipidomic assays (Castro et al. 2022; Ejsing et al. 2009) or can be reconstituted into liposomes (Aresta-Branco et al. 2011; Bento-Oliveira et al. 2020). This type of approach

allows to draw conclusions from lipid composition and lipid-lipid interactions, without the interference of, *e.g.*, proteins.

On the other hand, to study more specific interactions such as a compound with a membrane (at least in a first approach), a more controlled system is required in order to characterize the possible partition and behavior of said compound to the membrane. Hence, typically liposomes that contain a particular amount of lipids, are used to achieve this goal, *e.g.* (dos Santos et al. 2017). Another example is the study of which biophysical properties of a bilayer depend on its composition (amount and type of lipids) *e.g.* (Khmelinskaia et al. 2020).

Liposomes can be multilamellar vesicles (MLVs) or unilamellar. According to the diameter of the liposomes there are small (15-30 nm; SUVs), large (100-400 nm; LUVs) or giant (1-100 μm; GUVs) unilamellar vesicles. Due to their bigger size that resemble cells, GUVs are typically used in imaging techniques, such as fluorescence microscopy, when labelled with fluorescent membrane probes *e.g.* (Bento-Oliveira et al. 2020; Khmelinskaia et al. 2020).

There are many more membrane systems that are used in biophysical studies such as proteoliposomes (Amati et al. 2020), giant plasma membrane vesicles (GMPVs) (Gerstle et al. 2018), supported lipid bilayers (SLBs)(Marquês et al. 2015b) and lipid monolayers at the air/water interface (Sarkis & Vié 2020).

All the systems mentioned herein can be coupled with a diverse range of techniques, such as atomic force microscopy (AFM), X-ray scattering (*e.g.* (Marquês et al. 2015b)), surface tension measurements and, the focus of this work, fluorescence spectroscopy and microscopy (*e.g.* (Khmelinskaia et al. 2020)).

4.2. Fluorescence fundamentals

Luminescence is the process by which a certain amount of energy in the form of radiation, excites a molecule, and when returning to the ground state, radiation is emitted (Figure 1.12). Both fluorescence and phosphorescence are luminescence processes, nevertheless, each of these phenomena occur in different timescales. In fluorescence the electron takes between 10^{-10} and 10^{-7} s to decay to the ground state, while in phosphorescence a longer period of time is expected, of approximately 10^{-6} to 10 s (Lakowicz 2006).

Regarding fluorescence, not all molecules can emit light under such circumstances, it is required the presence of a fluorophore that could entail the whole molecule or be part of it. This moiety typically contains delocalized electrons in rigid π systems, such as the ones found in aromatic rings or polyenes. Some examples of these molecules will be provided in future sections.

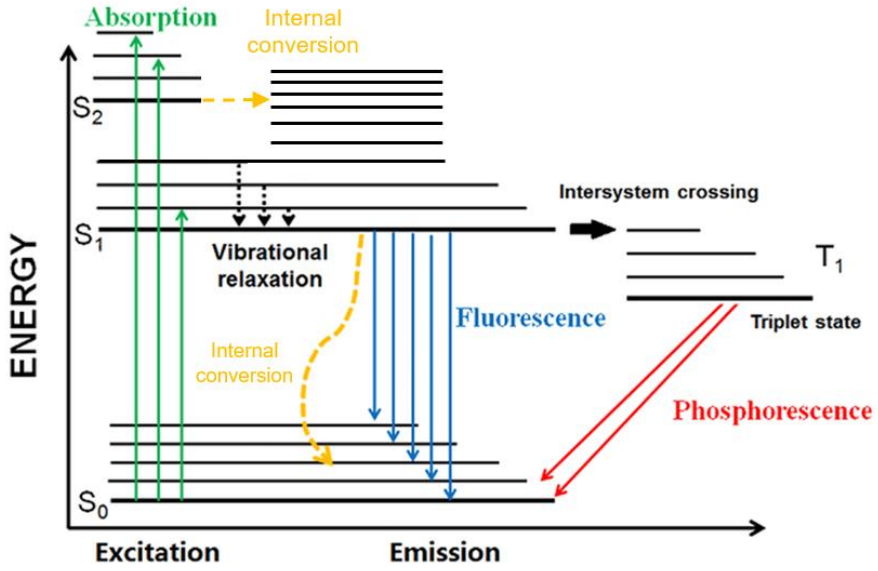

Figure 1.12: Perrin-Jablonski diagram representing the different electronic transitions upon radiative absorption. After a molecule absorbs radiative energy (green arrows), its electrons transition to higher electronic states. From this excited state it can then suffer non-radiative processes such as internal conversion (yellow arrows) or vibrational relaxation. Fluorescence (blue arrows) occurs when the electron returns to the ground state, emitting light. Moreover, intersystem crossing leads to a triplet excited state (T1) in which the excited molecule has an electron with the same spin as the ground state electron. From T1 the electron can return to the ground state via phosphorescence (red arrows), emitting light. Adapted from (Schweizer et al. 2021).

Two important characteristics of a fluorophore are its quantum yield (Φ_F) and its lifetime (τ). The first is the ratio of emitted photons to absorbed ones, meaning that a Φ_F closer to 1 belongs to a fluorophore that has brightest emission and it is easier to detect. As for the lifetime, it is the time that the molecule remains in the excited state before going back to the ground state.

Prior to fluorescence, when a molecule absorbs radiative energy, an electron transitions to more energetic orbitals and the molecule reaches higher electronic states. From this excited state it can then suffer non-radiative processes such as internal conversion. In consequence, the total decay constant for a fluorophore is the sum of the radiative constant (k_r) and the non-radiative constant (k_{nr}). A higher k_{nr} value signifies that there are more internal conversion processes occurring. Hence, a higher k_r and lower k_{nr} are associated with higher values of Φ_F. In fact, the Φ_F can also be described as the ratio of $k_r / (k_r + k_{nr})$.

Both the Φ_F and/or τ can change depending on the conditions surrounding the fluorophore, *e.g.*, refractive index, viscosity and polarity of the environment. For instance, after light absorption, solvent molecules can reorient around the fluorophore reducing the energy of the excited state. This stabilization process is known as solvent relaxation, and it depends mainly on the polarity and viscosity of the solvent/microenvironment that surrounds the fluorophore, among other factors. In fact, the viscosity of the medium can influence the flexibility/internal

motions that usually lead to internal conversion, thereby affecting the k_{nr}. Typically, a fluorophore in a more fluid environment, such as water, has lower Φ_F and shorter τ due to higher rates of internal conversion compared to a more rigid environment, such as a membrane. Moreover, a fluorophore distributed in a l_d membrane has lower Φ_F than in a gel phase. Nonetheless, viscosity is not the only parameter that influences fluorescence; other environmental factors such as temperature, pH, and specific molecular interactions also play significant roles (Lakowicz 2006; Valeur & Berberan-Santos 2001). Therefore, all conditions should be considered when analyzing fluorescence data.

We can take advantage of this sensitivity of the fluorophore to changes in the microenvironment to study properties of different solvents and environments. For instance, fluorescent probes can be used to study the biophysical properties of membranes (Bento-Oliveira et al. 2020; de Almeida et al. 2003; Marquês et al. 2015b), or the interaction of molecules with different solvents or microenvironments, such as the partition or bonding of compounds to membranes, *e.g.* (dos Santos et al. 2017). Both these approaches will be detailed in future sections.

The fluorescence intensity can be measured using a spectrofluorometer in a different array of measurements, explored next.

4.2.1. Fluorescence excitation and emission spectra

Fluorescence spectra represent the variation of the fluorescence intensity as a function of the wavelength. For the emission spectra, the wavelength used to excite the sample is fixed, and a range of emission wavelengths is scanned, and intensity is measured. While for the excitation spectra the emission wavelength is fixed, and it is the excitation wavelength that varies.

The excitation and emission spectra are typically a non-overlapping mirror image of each other, a consequence of two factors. First, according to the Franck-Codon principle, there are no changes in nuclear configuration of the molecule nor its microenvironment/solution sphere following fluorescence mechanisms, *i.e.* the assemble of distances and connection angles are not affected during the absorption and emission. This signifies that the transitions $S_0 \rightarrow S_1$ and $S_1 \rightarrow S_0$ are "vertical" resulting in the same peaks in excitation and emission. However, if the energy involved in absorption and emission were the same, the spectra would overlap. Moreover, the transitions are not truly just from one to another electronic state. A fluorophore is typically excited to higher vibrational levels (and even electronic), and before going back to the ground state, it relaxes to lowest vibrational levels of S_1, which occur in time rates that are faster than the decay to the ground state (Figure 1.12). The energy released during these

relaxation mechanisms, which are called internal conversion and vibrational relaxation, occurs through thermal loss that creates the "gap" between the excitation and the emission spectra. Furthermore, energy is translated in wavelength (or wavenumber), and this wavenumber interval between the peak of the spectra is called the Stokes-shift. A consequence of this (internal conversion, vibrational relaxation and the Franck-Codon principle) is that the same fluorescence emission spectrum is observed irrespective of the excitation wavelength used, varying only the integral fluorescence intensity (area under the spectrum). This is known as Kasha's rule.

Please note that there are certain exceptions to these rules and principles. Each case is a case study and should be analyzed accordingly.

4.2.2. Fluorescence anisotropy

Non polarized light contains an infinite possibility of radiative directional vectors. Using polarizers, it is possible to select only one of these vectors that either is reaching the sample (excitation) or that is detected (emission). By doing so, it is possible to determine the fluorescence anisotropy ‹r›, that can be calculated using the equation in Figure 1.13.

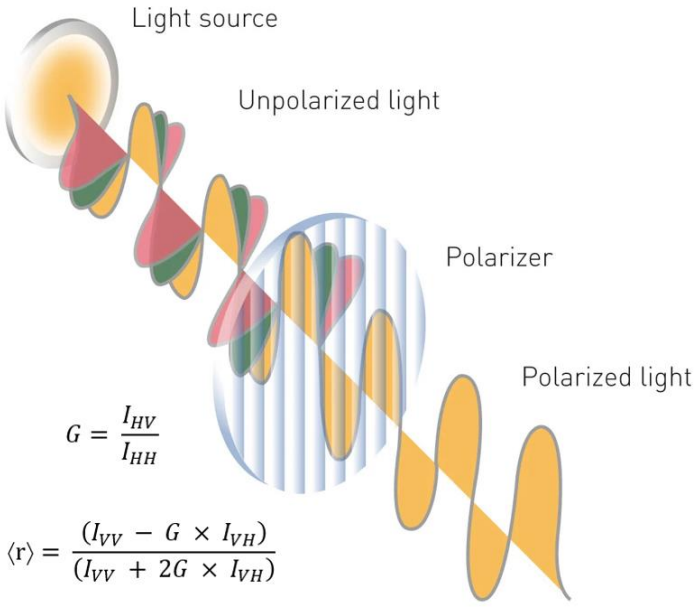

Figure 1.13: Fluorescence anisotropy, ‹r›, equation and schematic of how polarized light is obtained. In the equations $I_{X,Y}$ represents the polarized fluorescence intensity with the excitation (X) and emission (Y) at vertical (X and/or Y = V) or horizontal (X and/or Y = H) orientation. Also, the G is the grating factor that accounts for the different sensitivity of the detector to each light polarization plane. A polarizer can filter unpolarized light so that light waves oscillate in a single plane. Adapted from (Webpage: *Fluorescence Polarization - BMG Labtech*).

These type of measurements with polarized light takes advantage on the fact that fluorophores preferentially absorb photons whose electric vectors align parallel to the transition moment of the fluorophore. This means that upon excitation with polarized light, the fluorophores that have their transition moments aligned with the excitation vector become

preferentially excited, resulting in a photoselective population of excited fluorophores. During the excited state the fluorophore has enough time to rotate, changing the direction of the transition moment of the molecule and in consequence depolarizing the emission. Hence, anisotropy is inversely correlated with the rotational rate of the fluorophore, *i.e.*, higher anisotropies correspond to lower rotational rates (Lakowicz 2006).

Since the rotation of a molecule depends mainly on the size and the environment that surrounds the fluorophore, anisotropy measurements are used to study binding, membrane fluidity, molecular interactions, among others.

4.2.3. Fluorescence intensity decays

Using time-resolved fluorescence measurements it is possible to acquire fluorescence intensity or anisotropy decays. In these measurements, the sample is repeatedly exposed to a relatively short pulse of light at a specific wavelength, and the emitted photons of the sample are recorded individually with a high-speed detection system on the ns scale. During the measurement period, each detected photon is assigned to a time channel based on the time it takes to reach the detector, resulting in a histogram of photon counts as a function of time after the excitation pulse. Please note that the fluorophore emits randomly throughout the decay, and the probability of detecting a single photon after an exciting pulse, is proportional to the fluorescence intensity at time *t*. Hence these types of measurements are denominated Time Correlated Single Photon Counting – TCSPC. There are other setups that can be used to conduct time-resolved fluorescence measurements, such as Frequency-domain fluorescence measurements, nevertheless TCSPC was the technique used in the current work. In time-resolved measurements the fluorescence intensity decays acquired can be described by a mono-exponential decay function, in which the intensity decreases at a constant rate over time:

$$I(t) = I_0 \exp\left(-\frac{t}{\tau}\right) \quad (1)$$

where $I(t)$ is the fluorescence intensity at time t, I_0 is the initial fluorescence intensity and τ the fluorescence lifetime. Nevertheless, samples typically have more complex decays which can be described by a sum of n exponentials (decay components), according to the following equation:

$$I(t) = \sum_{i=1}^{n} p_i \exp\left(-\frac{t}{\tau_i}\right) \quad (2)$$

where *p* and τ are the pre-exponential factor and lifetime of component *i*, respectively. The pre-exponential is usually normalized, resulting in normalized amplitudes, α. Furthermore, since the equation is multi-exponential, it results in a number of *p* and τ, that is equal to the number of exponentials that describe the decay. Each of these components are usually assigned to a specific population of fluorophores according to the surrounding environment or conformation, when the radiative decay rate is the same. For instance, a two exponential decay has an α_1 and a τ_1 that characterize the fluorophores in one condition and, an α_2 and τ_2 that characterizes a different condition. In these situations, the α_i corresponds to the relative abundance of a fluorophore in that environment/conformation, while the τ_i is the according lifetime for that population.

From these parameters it is possible to determine the amplitude-weighted mean fluorescence lifetime, $\bar{\tau}$, and the intensity-weighted mean fluorescence lifetime, ‹τ›, using the following equations:

$$\langle \tau \rangle = \frac{\sum \alpha_i \tau_i^2}{\sum \alpha_i \tau_i} \tag{3}$$

$$\bar{\tau} = \sum_{i=1}^{n} \alpha_i \tau_i \tag{4}$$

Both are average lifetimes that consider the weighted average of the fluorophore populations. The $\bar{\tau}$ is proportional to the integral of the decay curve, being proportional to the steady-state intensity. The ‹τ› weighs each fluorescence decay component by its fractional intensity contribution, thus representing the average fluorescence decay behavior weighted by the intensity distribution.

A higher lifetime indicates that the fluorophore remains in the excited state for a longer period of time, which could be due to reasons highlighted previously, such as a more viscous surrounding environment and/or slower rotation rate. Nevertheless, there are exceptions to this.

4.2.4. Fluorescence quenching

Fluorescence quenching is any process by which the quantum yield of a fluorophore is decreased (Coutinho & Prieto 1993; Lakowicz 2006; Valeur & Berberan-Santos 2001). This could occur through a different range of processes and molecular interactions. For instance, in collisional or dynamic quenching there is no chemical alteration of the fluorophore, but its excited state is deactivated upon collision with the quencher. This quenching results from the diffusive encounters between the quencher and the fluorophore. The variation of the

fluorescence intensity of a fluorophore with the concentration of the quencher follows a linear behaviour according to the Stern-Volmer equation:

$$\frac{\mathrm{I}_0}{\mathrm{I}} = 1 + K_{\mathrm{SV}}[\mathrm{Q}] \quad (5)$$

where [Q] is the concentration of the quencher, K_{SV} is the Stern-Volmer constant and I and I_0 are the fluorescence intensity in the presence and absence of the quencher, respectively. It is possible to determine the bimolecular quenching constant, k_{q}, by using the following equation:

$$K_{\mathrm{SV}} \approx k_q \langle\tau\rangle_0 \quad (6)$$

where $\langle\tau\rangle_0$ is the intensity-weighted mean fluorescence lifetime of the compound in the absence of quencher. Typically, a higher k_{q} value is interpreted as the quencher being more effective at quenching the fluorophore, *i.e.* higher k_{q} values are associated with higher accessibility of the fluorophore towards the quencher.

Static quenching is another type of fluorescence quenching which occurs when the quencher creates a nonfluorescent complex with the fluorophore, through ground state quencher-fluorophore reactions. The dependence of fluorescence intensity on the concentration of quencher is linear according to the following equation:

$$\frac{\mathrm{I}_0}{\mathrm{I}} = 1 + K_{\mathrm{S}}[\mathrm{Q}] \quad (7)$$

where K_{S} is the association constant for complex formation (quencher-fluorophore).

For both pure collisional or pure static quenching, the variation of fluorescence intensity is linear in a Stern-Volmer plot (Figure 1.14 - A). Time-resolved measurements allow to distinguish between pure static and pure collisional quenching. For static quenching the lifetimes of the fluorophore remain unchanged because the formed complex is not fluorescent, and the observed fluorescence is from the non-complexed fluorophores. In this situation the ratio between the lifetime of the fluorophore in the absence and the presence of quencher is 1 ($\bar{\tau}_0/\bar{\tau} = 1$). However, for dynamic quenching, the excited state of the fluorophore is shortened, and the lifetime of the fluorophore is different in the presence of the quencher. Hence, the lifetime of the fluorophore can also be correlated with k_{q}, according to the following equation:

$$\frac{\bar{\tau}_0}{\bar{\tau}} = 1 + K_{\mathrm{SV}}[\mathrm{Q}] \quad (8)$$

If there is both collisional and static quenching occurring the variation of fluorescence intensity (I_0/I) follows a quadratic increase (Figure 1.14 - C), according to the following equation:

$$\frac{I_0}{I} = 1 + (K_{SV} + K_s)[Q] + (K_{SV}K_s)[Q]^2 \quad (9)$$

Collisional quenching depends on diffusion rates of both the quencher and the fluorophore. Faster diffusion rates increase the frequency of collisions, and thus the occurrence of quenching, *i.e.* higher K_{SV}. In fact, k_q is proportional do the diffusion coefficients of the quencher and the fluorophore. Since the diffusion rates are sensitive to temperature (higher temperature increases the diffusion rates) and viscosity (higher environment viscosity decreases the diffusion rates), collisional quenching is also sensitive to these conditions (Lakowicz 2006; Valeur & Berberan-Santos 2001).

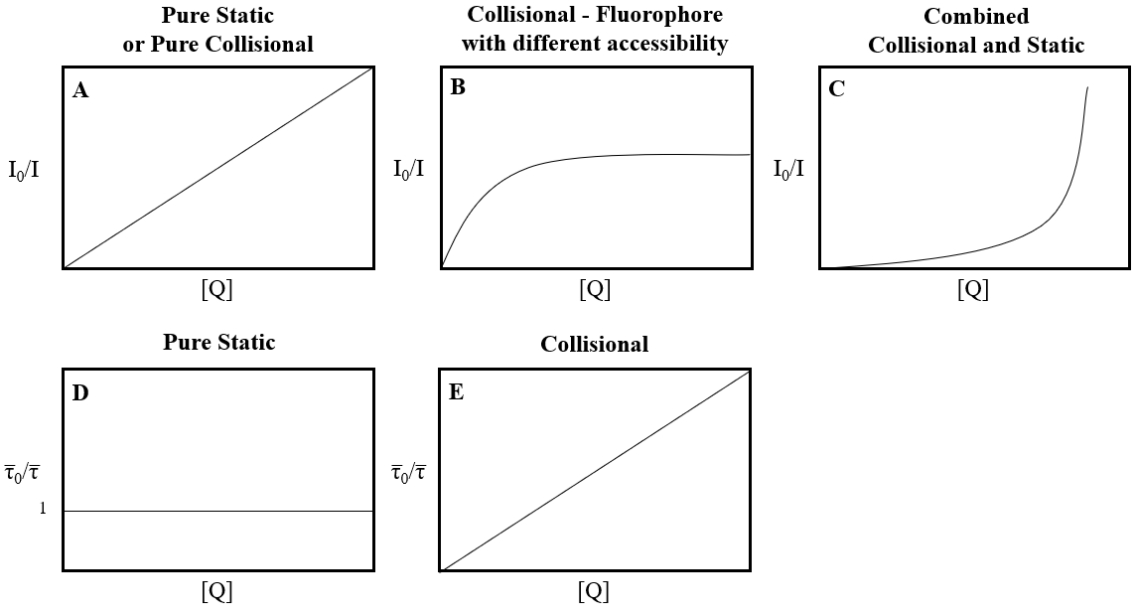

Figure 1.14: Summary of the most common variation of fluorescence intensity and lifetime with a quencher. Note that in A, B and C, the Y-axis is the ratio between fluorescence intensity in the absence (I_0) and presence of quencher (I), and in D and E the Y-axis is the ratio between the mean fluorescence lifetime in the absence ($\bar{\tau}_0$) and presence ($\bar{\tau}$) of quencher.

When there are fluorophores in solution with different accessibility towards the quencher, the Stern-Volmer plot is also non-linear (Figure 1.14 - B).

There are more exceptions to these quenching behaviors, *e.g.* the sphere of action model usually applies when the concentration of the quencher in solution is relatively high. Typically, this type of quenching results in a variation of steady-state fluorescence intensity similar to that of combined dynamic quenching with the formation of ground non fluorescent state complex (Figure 1.14 - C). Since it is a static process, the mean fluorescence lifetime is typically constant

(Figure 1.14– D). Note that combined dynamic and static quenching can occur with sphere of action quenching and in that case the mean fluorescence lifetime is affected due to the occurrence of dynamic quenching.

The study of the quenching processes gives information, particularly regarding the fluorophore spatial distribution, since for quenching to occur a proximity or contact between the quencher and the fluorophore is required. This allows, for example, to study the conformation of proteins (Eftink & Ghiron 1975; Mátyus et al. 2006), aggregation of molecules (Huang et al. 2019), and the depth of a fluorophore inserted in a membrane (Manuel Nuno & B., Miguel A. R. 2007) (more examples can be found in (Lakowicz 2006)).

4.3. Fluorescence probes as tools to study the yeast membrane

Fluorescent membrane probes have been widely used to study membrane properties, either in model systems or living cells. Typically, these probes partition towards different membrane regions reporting on the properties of such domains. Therefore, the use of a plethora of probes that grant access to different properties complement each other, unraveling biophysically membrane architecture and dynamics. Usually, the fluorescence quantum yield of membrane fluorescent probes is significantly lower in water than while the probe is distributed along the membrane. Moreover, the membrane/water partition coefficient is relatively high. Hence, the non-bound probe population is relatively small with lower fluorescence intensity not interfering with the fluorescence measurements for the membrane bound probe.

When working with these probes one must never forget that in certain conditions, they can also change the properties of the membrane, however as long as the concentration is kept at a relatively low value that does not lead to significant disturbance while keeping good fluorescence signal-to-noise ratio, fluorescent membrane probes can be a powerful tool for membrane biophysicists.

Once systems are labelled with fluorescent membrane probes, fluorescence spectroscopy (and, with some exceptions, microscopy) can be employed to characterize said system. Fluorescence properties of a fluorophore are sensitive to the microenvironment that surrounds it. The relevant measurements all depend on the probe used. For instance, fluorescence anisotropy and lifetimes are two parameters that report on relative lipid packing of the specific membrane region to which the probe is preferentially partitioning to. Usually, longer fluorescence lifetimes and higher fluorescence anisotropy indicate tighter packing order of the lipid region where the probe is inserted on, with few exceptions. This is due to the higher rigid environment that reduces the efficiency of nonradiative decay processes. Fluorescence

anisotropy and lifetimes are only two examples of the many fluorescence parameters that can provide information on membrane properties, all depending on the probe that is being used and the membrane system that is being labelled. Although typically one fluorescence parameter gives information about a certain membrane biophysical property, it is important to also analyze other fluorescence parameters, from intensity and spectra to anisotropy and lifetimes, to have a corroborative study all together.

Table 1.3: Summary of the fluorescent membrane probes used to study the fungal plasma membrane, including membrane model systems with fungal lipids such as Erg and IPCs. The properties reported by each probe are also represented. DPH - 1,6-diphenyl-1,3,5-hexatriene; ANEP – aminonaphthylethenylpyridinium; Rhod-DOPE - Rhodamine-1,2-dioleoyl-sn-glycero-3-phosphoethanolamine; *t*-PnA – *trans*-parinaric acid (*trans* -9,11,13,15-octadecatetraenoic acid).

Probe	Preferentially partitions towards	Most relevant parameter	Property reported	References in fungal systems
DPH	Equally to all membrane regions (except Cer-rich phases)	Fluorescence anisotropy (‹r›)	Membrane fluidity	(Abe & Hiraki 2009; Aresta-Branco et al. 2011; Bento-Oliveira et al. 2020; Dupont et al. 2021; Folmer et al. 2008; Kohli et al. 2002; Marquês et al. 2015b; Mishra et al. 2008; Mukhopadhyay et al. 2004; Park & Lee 2009; Santos et al. 2018; Silva et al. 2006a)
ANEP family	Sterol-rich regions	Excitation and emission spectra, Fluorescence lifetime (τ)	Dipole potential (R_{ex}), Sterol-rich regions packing and hydration, Erg levels	(Bastos et al. 2012; Bento-Oliveira et al. 2020; Khmelinskaia et al. 2020; Santos et al. 2018; Suchodolski et al. 2019)
Laurdan and derivatives	All membrane regions but in yeast it has higher Φ_F in sterol-rich regions	Excitation and emission spectra [generalized polarization (GP)]	Lipid order	(Klose et al. 2010; Learmonth & Gratton 2002; Suchodolski et al. 2019)
Rhod-DOPE	Liquid-disordered phases	Intensity, Fluorescence lifetime (τ)	Liquid-disordered phase packing order	(Bastos et al. 2012; Bento-Oliveira et al. 2020; Khmelinskaia et al. 2020)
***t*-PnA**	Gel domains	Fluorescence anisotropy (‹r›), Fluorescence lifetime (τ) (including other parameters such as τ_{long} and α_{long})	Presence of gel domains and their packing order	(Aresta-Branco et al. 2011; Bento-Oliveira et al. 2020; Herman et al. 2015; Marquês et al. 2015b; Santos et al. 2017, 2018; Singh et al. 2012; Vecer et al. 2014)

In the following sections we describe fluorescent membrane probes that have been used to study the membrane properties of the yeast plasma membrane. Table 1.3 summarizes such probes and what membrane properties they can report.

It is also possible to attach well characterized fluorophores to certain phospholipids. The dye conjugation should not interfere with the lipid distribution along the membrane nor with the properties of the membrane itself. These allows to report on the properties of the specific regions the phospholipid has preference for. Successful examples of this scenario are Rhod-DOPE (Rhodamine-1,2-dioleoyl-*sn*-glycero-3-phosphoethanolamine) (Webpage: *Avanti Polar Lipids - Rhod-DOPE*) and NBD-DPPE (N-(7-nitro-2-1,3-benzoxadiazol-4-yl)-1,2-dipalmitoyl-*sn*-glycero-3-phosphoethanolamine) (Webpage: *Avanti Polar Lipids - NBD-DPPE*), which partition preferentially towards fluid or ordered domains, respectively.

4.3.1. Gel domains characterization with *trans*-parinaric acid

Trans-parinaric acid (*t*-PnA) is a polyene that inserts in membranes with its tetraene motif buried in the hydrophobic core of the lipid bilayer (Figure 1.15). This fluorescent tetraene motif weakly fluoresces in water, however when incorporated in the membrane its Φ_F increases, particularly when partitioning towards gel phases rather than fluid ones (Aresta-Branco et al. 2011; Bento-Oliveira et al. 2020; de Almeida et al. 2009; Marquês et al. 2015b; Mateo et al. 1993, 1995; Sklar et al. 1977). This increased in Φ_F is due to a reduction in the efficiency of nonradiative decay processes in more rigid environment, leading also to an increase in the fluorescence lifetime of *t*-PnA. The fluorescence emission of this probe corresponds to a forbidden weak electronic transition which leads to long lifetimes (Sklar et al. 1977).

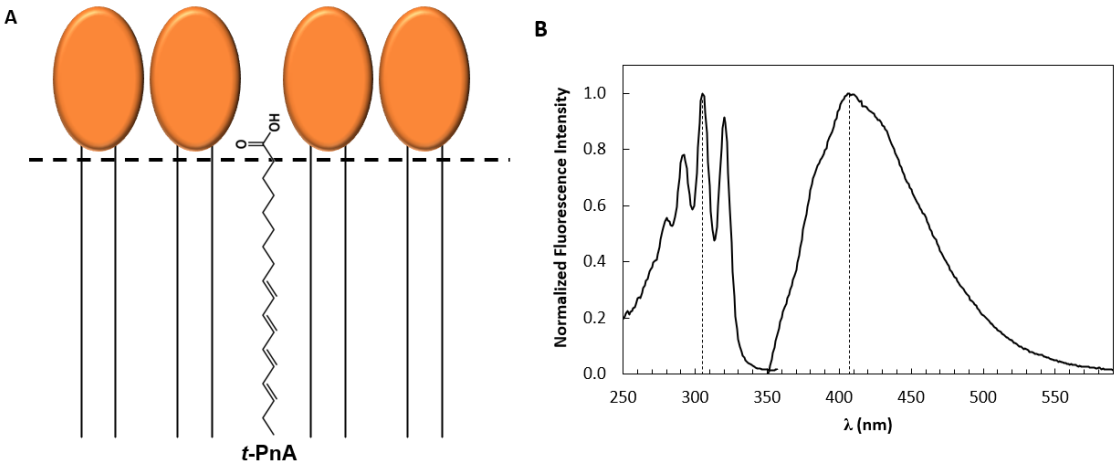

Figure 1.15: Molecular structure of *t*-PnA distributed along half a lipid bilayer (A). The excitation and emission spectra of *t*-PnA labelling isolated plasma membrane of *S. cerevisiae* is represented in B. The carboxyl group aligns with the polar headgroups of phospholipids, while the tetraene motif is buried in the hydrophobic core. A - (Santos et al. 2020)

The membrane/water partition coefficient of this probe towards membrane systems with l_d/l_o coexistence (1.8 ± 0.8) was significantly lower than the one obtained for membranes with l_d/gel coexistence (5 ± 2) (Mateo et al. 1995). Moreover, the partition coefficient between the two phases coexisting in membranes with POPC/Chol (l_d/l_o) is approximately 1 (0.8 ± 0.5)(Sklar 1980), showing that there is no preference for each of these two lipid phases, but rather for gel. Hence, the fluorescence of *t*-PnA is a reporter of the properties of gel domains.

Usually when *t*-PnA is incorporated in gel domains, its fluorescence intensity decay can be described by a multi-exponential equation (typically number of exponentials > 3) where the long lifetime component (τ_{long}) if longer than 30 ns is a fingerprint for the presence of gel domains, a criterion established using several model systems (de Almeida et al. 2009). Moreover, longer τ_{long} and mean fluorescence lifetime indicate higher rigidity of these domains. Furthermore, its corresponding normalized pre-exponential factor or amplitude (α_{long}) gives insight on the relative abundance of these gel domains (Mateo et al. 1993).

Unequivocally, *t*-PnA is the only fluorescent membrane probe reported on literature that allows the detection and characterization of gel domains in complex membrane systems.

T-PnA was used to label MLVs containing POPC with either Phycer or Erg. As mentioned previously, POPC is a lipid that at room temperature organizes preferentially in l_d (Marsh 2012). The time-resolved parameters obtained for *t*-PnA (particularly the τ_{long}) revealed that Phycer promotes the formation of gel phases, but Erg does not. Also, increasing amounts of Erg in a POPC/Phycer mixture abolishes the formation of gel phases (Aresta-Branco et al. 2011).

A more thorough study that included X-ray, confocal and AFM, and spectroscopic measurements of *t*-PnA labeling binary mixtures containing POPC and Phycer (Figure 1.10) in different percentages, showed that gel domains form with just approximately 5 mol% of Phycer at room temperature. However, with increasing amounts of the sphingolipid the formation of highly stable stoichiometric complexes with particular biophysical properties occurs (Marquês et al. 2015b). This approach allowed to determine the phase diagram for the POPC/Phycer mixture present in Figure 1.10, previously described in section 3.2.4 of this chapter.

Labeling different fungal species with *t*-PnA allowed to discover SLEDs in the plasma membrane of *S. cerevisiae* cells (Aresta-Branco et al. 2011; Bento-Oliveira et al. 2020; Herman et al. 2015; Vecer et al. 2014), in lipid extracts from *C. neoformans* (Singh et al. 2012), and in conidia of filamentous fungi *N. crassa* (Santos et al. 2017, 2018). The fluorescence intensity decay of *t*-PnA labeling yeast cells is characterized by a sum of 4 exponentials, with the fourth corresponding to the τ_{long} previously mentioned, that being longer than 30 ns (41.0 ± 1 ns) confirms the presence of gel domains, particularly SLEDs in *S. cerevisiae* (Aresta-Branco et al.

2011; Bento-Oliveira et al. 2020). This value is similar to that obtained at room temperature with *t*-PnA labelling MLVs containing POPC and 20 mol% of Phycer (Marquês et al. 2015b), a percentage similar to that of sphingolipids in the plasma membrane of the yeast (Daum et al. 1998, 1999; Dickson & Lester 1999; Pedroso et al. 2009). In isolated plasma membranes ($\tau_{long} \approx 46$ ns) or liposomes reconstituted with plasma membrane lipids ($\tau_{long} \approx 48$ ns) from *S. cerevisiae* where proteins are not present, the τ_{long} is significantly longer than the value obtained for cells in suspension (Aresta-Branco et al. 2011).

The T_m of SLEDs was also accessed by using *t*-PnA to label MLVs with lipids extracted from the plasma membrane of wt cells (Aresta-Branco et al. 2011) which was >42°C. The gel/fluid transition is similar to the one obtained for purified IPCs from yeast reconstituted in liposomes (Klose et al. 2010).

When the Erg biosynthetic pathway is altered, such as in *S. cerevisiae erg6*Δ mutants, the rigidity of SLEDs, *i.e.* the τ_{long} and the mean fluorescence lifetime of *t*-PnA are not altered (Aresta-Branco et al. 2011). These mutants lack C-24 methyltransferase accumulating cholesta-7,24-dienol, cholesta-5,7,24- trienol, cholesta-5,7,22,24-tetraenol and Zym (Heese-Peck et al. 2002) instead of Erg in the plasma membrane. Regarding sphingolipids, there are only minor differences such as lower amount of IPCs (Guan et al. 2009; Swain et al. 2002). Furthermore, *S. cerevisiae* plasma membrane suspensions with and without Erg (through removal with methyl-β-cyclodextrin) have similar τ_{long} of *t*-PnA (Aresta-Branco et al. 2011), confirming that sterol is not a major component of SLEDs and/or the sterol composition does not affect the properties of SLEDs.

The *t*-PnA was used to study the properties of SLEDs in *S. cerevisiae* mutants that have an impaired sphingolipid biosynthetic pathway. For instance, with both *scs7*Δ (Aresta-Branco et al. 2011) and *ipt1*Δ (Bento-Oliveira et al. 2020) mutant cells *t*-PnA reported an increase in the gel domains rigidity when compared with the wt strain. *Scs7*Δ cells accumulate complex sphingolipids that lack the hydroxylation in C2 of the sphingolipid acyl chain (Guan & Wenk 2006); while the major complex sphingolipid of the plasma membrane of *ipt1*Δ cells is MIPC instead of $M(IP)_2C$ (Dickson et al. 1997; Leber et al. 1997), and hence with a smaller and lower charged headgroup. These results obtained with *t*-PnA, evidence the structural relevance of both the headgroup and the hydroxylation of the acyl chain of sphingolipids for the proper lipid packing within SLEDs. Moreover, this evidences that the major molecular type of SLEDs is truly that of sphingolipids. This is further corroborated with studies of *t*-PnA were cells that lack sphingolipids, either through inhibition of the sphingolipids pathway with myriocin or

using a mutant with sphingolipid deficiency, *lcb1-100* cells (Vecer et al. 2014), have similar to the wt rigidity of the gel domains, but its relative abundance decreased.

4.3.2. Membrane global order – diphenylhexatriene probes

1,6-diphenyl-1,3,5-hexatriene (DPH) is a rod-shaped probe that incorporates in membranes with its long axis parallel to the lipid acyl chains of the bilayer (Figure 1.16). This probe partitions equally throughout different membrane regions independently of their fluidity and packing order (Davenport 1997; Florine-Casteel & Feigenson 1988), with a partition coefficient in different lipid systems close to 1 (de Almeida et al. 2009; Huang & Haugland 1991). Poorly hydrated Cer-rich phases that are in L_c phases such as the ones reported in specific conditions of systems with POPC/palmitoylceramide (Silva et al. 2006c), POPC/nervanonoylceramide (Pinto et al. 2008) or POPC/Phycer (Figure 1.10)(Marquês et al. 2015b), are an exception to this behavior, with an approximately null partition coefficient. However, for most cases the fluorescence anisotropy of DPH reports changes in the global membrane fluidity. The fluorescence anisotropy of DPH linearly correlates with membrane composition and temperature depending on the fraction of each phase in different binary and ternary lipid systems (de Almeida et al. 2003; Lentz 1988; Silva et al. 2007): the higher the fluorescence anisotropy of DPH the more rigid membranes are globally.

Typically, the steady-state anisotropy of DPH is enough to take conclusions regarding membrane global packing order. However, time-resolved measurements can also be performed to obtain relevant information, even though the lifetime of the probe does not have a marked dependence on the lipid phase. For instance, it was shown that at room temperature Chol and dehydroergosterol (DHE) have differential effects on fluid and gel lipid bilayers using DPH time-resolved measurements (Arora et al. 2004).

Regarding fungal systems, DPH was used to study the global order of POPC/Erg (Dupont et al. 2021; Silva et al. 2006a) and POPC/Phycer liposomes (Marquês et al. 2015b). The fluorescence intensity and anisotropy of DPH in the region of coexistence of l_d and a Phycer-rich gel phase behave similarly to typical systems with a coexistence of gel and l_d phases, and as reported by *t*-PnA, the hydrophobic packing is comparable to the one found for the global order of gel domains in yeast reported by DPH (Bento-Oliveira et al. 2020; Marquês et al. 2015b).

DPH was also used to label isolated plasma membrane and total lipids extracts reconstituted into MLVs (Bento-Oliveira et al. 2020) and *S. cerevisiae* cells (Aresta-Branco et al. 2011; Folmer et al. 2008). Interestingly, the results obtained with isolated plasma membrane

(‹r› = 0.23 ± 0.03) and total lipid extracts (‹r› = 0.21 ± 0.01) (Bento-Oliveira et al. 2020) are very similar but significantly higher than those obtained with yeast cells in suspension (‹r› = 0.14 ± 0.01) (Aresta-Branco et al. 2011; Bento-Oliveira et al. 2020). This is probably due to the fact that when using cells, DPH not only labels the plasma membrane but also the endomembrane system where global order is probably lower, due to the lack of complex sphingolipids which are mainly located at the plasma membrane (and in the Golgi complex where their synthesis occurs but with a short lifespan), and lower Erg levels. In fact, under a confocal microscope yeast cells plasma and internal membranes are labelled with DPH (Abe & Hiraki 2009).

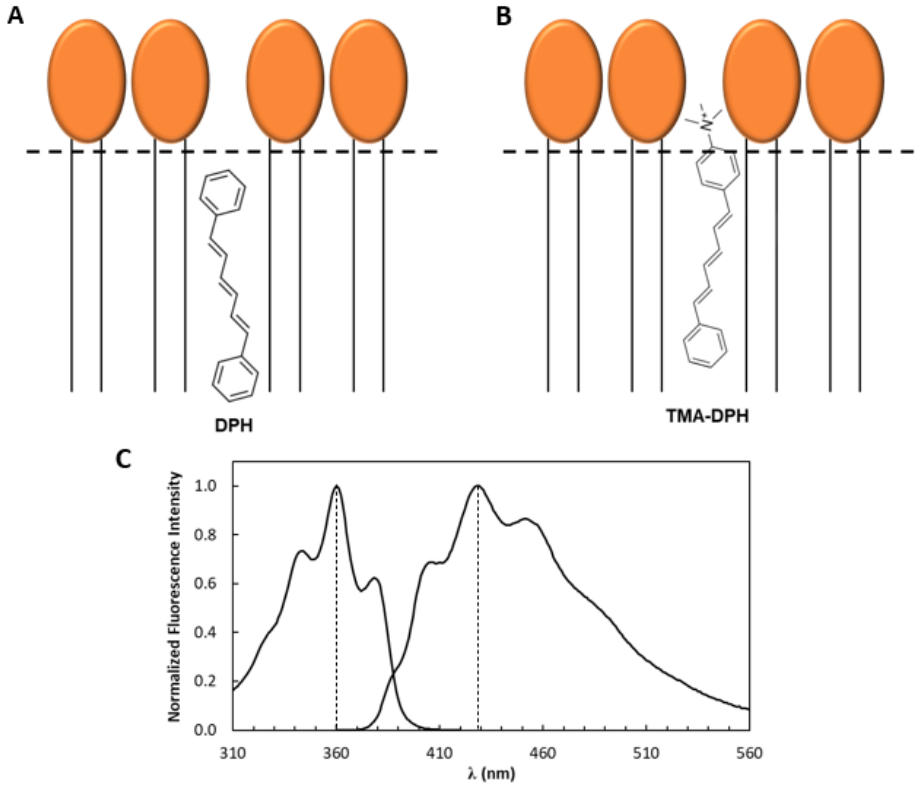

Figure 1.16: Molecular structure of (A) DPH and (B) TMA-DPH, and distribution along half of a lipid bilayer. The excitation and emission spectra of DPH labelling isolated plasma membrane of *S. cerevisiae* is represented in C. Both hexatrienes moieties of the probes locate along the hydrophobic core of the bilayer. Nevertheless, the charged trimethylamine anchors the probe to the polar headgroups. The differential distribution of each of these probes grants them the ability to report on different regions of the membrane.

Besides wt *S. cerevisiae*, DPH was also used to study the plasma membrane properties of several mutants. For instance, DPH was used to label living cells of *erg3*Δ and *erg6*Δ mutants which lack enzymes from the Erg biosynthetic pathway (Figure 1.7). *Erg3*Δ lacks C-5 desaturase accumulating ergosta-7,22-dienol (Smith et al. 1996). The global order of the plasma membrane of *erg3*Δ was lower than that of *wt* (Folmer et al. 2008) while the opposite was observed for *erg6*Δ (Aresta-Branco et al. 2011; Folmer et al. 2008).

Changes in sphingolipid profile of yeast, also lead to different membrane global order reported by the anisotropy of DPH. In *scs7*Δ cells the steady-state anisotropy of DPH was significantly higher than that of wt cells. On the other hand, the anisotropy of DPH in *ipt1*Δ isolated plasma membranes and liposomes reconstituted with extracted lipids, was lower (Bento-Oliveira et al. 2020). Note that, for each of these mutants, different systems were labeled: cells in suspension for *scs7*Δ, while isolated plasma membrane and lipid extracts reconstituted in MLVs were used for *ipt1*Δ. As mentioned previously results can be different according to what systems are labeled by DPH, so *scs7*Δ global order results can not be directly compared to those for *ipt1*Δ. Nonetheless, overall, it is possible to conclude that both changes in sphingolipid headgroup and hydroxylation pattern are changing the global order properties of yeast membranes.

No changes were reported for the global fluidity of membranes of *per1*Δ mutant cells (Aresta-Branco et al. 2011). These mutant cells lack the enzyme from the GPI anchor modeling pathway responsible for the reacylation of the GPI anchor at the *sn*-2 position, leading to an unsaturated acyl chain instead (Fujita et al. 2006). In principle this change would cause GPI anchor to be less efficiently accommodated in SLEDs.

DPH has also been used to report membrane fluidity in other yeast, such as pathogenic *Candida albicans* (Kohli et al. 2002; Mishra et al. 2008; Mukhopadhyay et al. 2004; Park & Lee 2009), and conidia of the filamentous fungus *N. crassa* (Santos et al. 2018). The fluorescence anisotropy of DPH whilst labelling *C. albicans* cells is similar to the values obtained for *S. cerevisiae* cells (Mishra et al. 2008). Moreover, spheroplasts obtained from *S. cerevisiae* (Aresta-Branco et al. 2011) or *C. albicans* (Mukhopadhyay et al. 2004) also have similar DPH fluorescence anisotropy (≈0.17 and ≈0.19, respectively). Furthermore, DPH labelling was also used to show that *C. albicans* strains that are resistant to azoles have lower membrane global order than azole sensitive strains (Mishra et al. 2008).

Derivatization of DPH lead to the development of new probes that similarly to DPH partition equally throughout the membrane reporting on global properties. Trimethylamine-diphenylhexatriene (TMA-DPH) anchors to the charged headgroups at the lipid-water interface (Figure 1.16) reporting on the acyl chain order closer to the interfacial region of the membrane (Kaiser & London 1998). In model membranes systems TMA-DPH fluorescence anisotropy decay and lifetime distribution is possible to use to detect and estimate approximate fractions of coexisting lipid phases (Sinha et al. 2003) an approach that has yet to be used in fungal systems. Moreover, no changes were detected for TMA-DPH fluorescence anisotropy in POPC/Erg mixtures containing different amounts of the sterol (Silva et al. 2006a). Nevertheless,

similarly, to DPH, TMA-DPH has also been used to study the fluidity of membranes of *S. cerevisiae* wt (Folmer et al. 2008) and *erg6*Δ, *scs7*Δ and other mutants with changes in sphingolipid and/or Erg composition (Abe & Hiraki 2009; Guan et al. 2009). Interestingly, the DPH fluorescence anisotropy values when labelling yeast cells are lower (0.14 ± 0.01) than when TMA-DPH is used (0.28 ± 0.01), which can be justified by the fact that DPH, has mentioned already, labels not only the plasma membrane but also internal membranes, while TMA-DPH due to its positive charge remains in the plasma membrane (Abe & Hiraki 2009).

Furthermore, the action of amphotericin B (an antifungal polyene) on pathogenic fungi *C. albicans* and *C. neoformans* was investigated using TMA-DPH, a study that showed the formation of pores by this drug in the yeast plasma membrane depends on its aggregation in an Erg-dependent fashion (Haynes et al. 1996).

4.3.3. Polarity sensitive probes - ANEP family

A lipid bilayer is characterized by three types of electrostatic potentials: the transmembrane potential ($\Delta\psi$), the surface potential (ψ_S) and the dipole potential (ψ_d) (Wang 2012). The dipole potential is a result of the alignment of dipoles of the membrane component such as lipids and water molecules.

The ANEP (aminonaphthylethenylpyridinium) membrane dyes belong to a family of styryl potentiometric fluorescent probes, that are able to quickly respond to changes in the dipole potential of the membrane. Particularly, shifts of the excitation spectra of these molecules when distributed in the membrane are commonly used to report on dipole potential changes collected at the red-edge of the emission spectrum (Haldar et al. 2012; Loew 1988). The emission spectra are not used due to the contribution of solvent relaxations processes that cause distortions and respond to fluidity as well as ψ_d changes, *i.e.* it is not possible to separate the contribution of changes in fluidity or ψ_d in the emission spectra. A ratio of two wavelengths of the excitation spectra is commonly used to normalize the measurements so it is possible to avoid contributions from probe or cell concentration, bleaching effects and uneven labelling of cells (Gross et al. 1994; Montana et al. 1989).

These probes are amphiphilic and their hydrocarbon chains anchor parallel to the acyl chains of phospholipids, while the charged hydrophilic groups align with lipids headgroups (Haldar et al. 2012; Loew 1996) (Figure 1.17). Following excitation of the probe, there is a large electronic charge shift that occurs parallel to the electric field within the membrane. Hence the charge redistribution occurring in the probe induced by excitation renders its excited spectrum sensitive to the voltage across the membrane. In consequence, when there is a change

of the dipole potential of the membrane there is a relatively small shift of the excitation spectra of the probe magnified in the ratio.

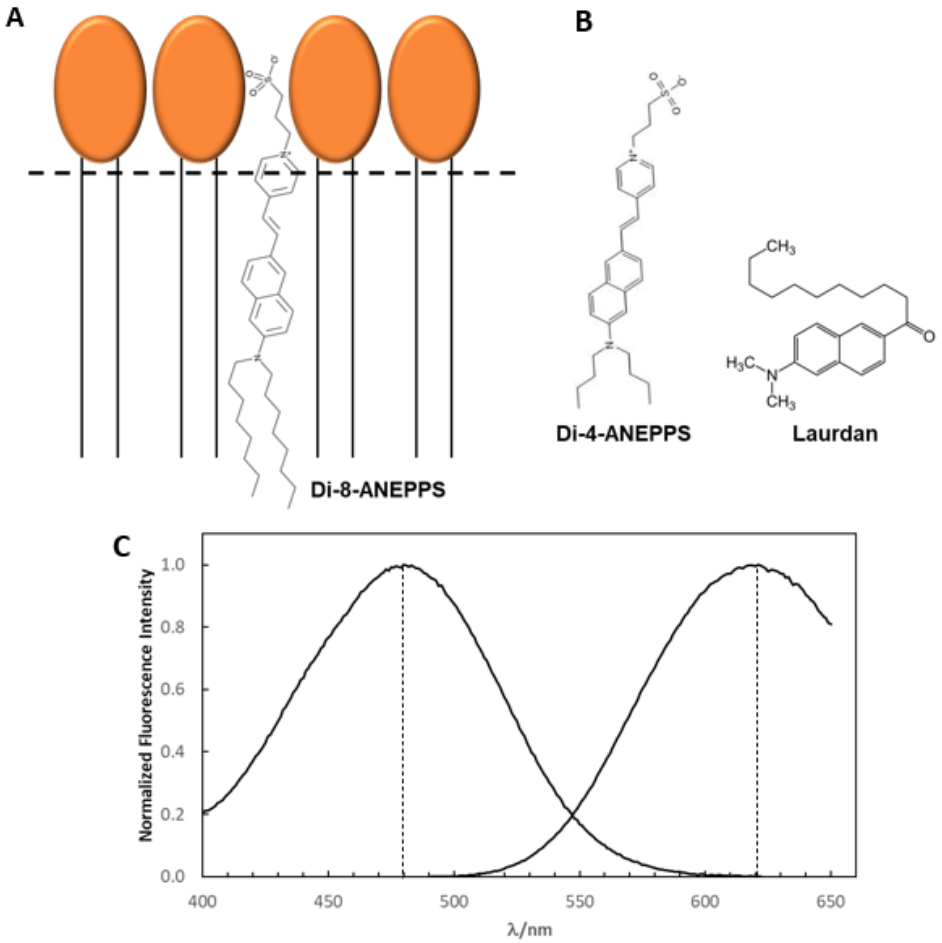

Figure 1.17: Molecular structure of di-8-ANEPPS and distribution along half of a lipid bilayer (A). (B) Molecular structures of di-4-ANEPPS and Laurdan. (C) Excitation and emission spectra of di-8-ANEPPS labelling isolated plasma membrane of *S. cerevisiae*. The charged moieties of di-8-ANEPPS anchor to the headgroup of phospholipids while the hydrocarbon chain aligns with the acyl chains of the lipids.

There is a vast variety of probes in this family (Loew 1988, 1996) and for the choice of the dye used one must consider what are the objectives. Depending on the dye, the sensitivity to the other two membrane potentials varies, which is something that can be relevant depending on the work. This sensitivity is associated mainly with the length of the chromophore and in consequence how the probe distributes along the membrane. For instance, ANNINE probes are longer than ANEP ones having higher sensitivity to transmembrane potential (Fromherz et al. 2008).

While labelling certain cells or MLVs, di-4-ANEPPS (6-[2-(*N*,*N*-dibutylamino)naphthyl]ethenyl-4'-pyridinium propanesulfonate) can rapidly be internalized due to spontaneous flip flop (Loew 1996). The longer hydrocarbon tail of di-8-

ANNEPS (4-[2-[6-(dioctylamino)-2-naphthalenyl]ethenyl]-1-(3-sulfopropyl)-pyridinium) decreases the probability to occur flip-flop, and in consequence internalization.

The dipole potential of the membrane is linearly dependent on the dipole moment of sterols present in the membrane (Haldar et al. 2012). Hence, ANNEPS probes have been used to report on sterol-related properties. In fact, styryl probes, such as di-4-ANNEPS or di-8-ANNEPS, have higher partition coefficients and quantum yield towards l_o phases than l_d and gel (Bastos et al. 2012; Bento-Oliveira et al. 2020; Khmelinskaia et al. 2014). Hence, these probes display an unique sensitivity to sterol-rich regions since the hydration and hydrogen bonding patterns at the membrane/water interface influences its fluorescence properties (Bastos et al. 2012; Haldar et al. 2012).

The mean fluorescence lifetime of these probes is sensitive to the conditions of the surrounding environment. The fluorescence lifetime of di-4-ANEPPS increases with Erg or Chol mole fraction for mixtures with POPC or DPPC (Bastos et al. 2012). Also, the presence of Erg or Chol influences differently a fluid (POPC) or gel (DPPC) membrane (Khmelinskaia et al. 2020). Overall, the fluorescence properties of di-4-ANEPPS are less sensitive to Erg than Chol (Bastos et al. 2012; Khmelinskaia et al. 2020). However, the $\bar{\tau}$ of di-4-ANEPPS correlates with Erg/phospholipid ratio in germinating conidia of *N. crassa* (Santos et al. 2018).

Fluorescence microscopy (steady-state and time-resolved) can be applied with samples labeled with ANEPS. For instance, GUVs reconstituted with plasma membrane lipids extracts of wt and *ipt1*Δ strain were labelled with di-8-ANEPPS and Rhod-DOPE, allowing to visualize l_o and l_d domains, respectively. Rhod-DOPE is a glycerophospholipid (DOPE) that, due to its two unsaturated acyl chains, preferentially partitions towards l_d phases, and the attached Rhodamine, a well characterized dye, grants it fluorescence properties that are different than di-8-ANEPPS. This co-labelling allowed to compare visually the two marked lipid phases in GUVs reconstituted from lipids of the plasma membrane of the two yeast strains, and also non-labelled regions which were assigned to gel domains. Furthermore, both in GUVs and in cells, fluorescence lifetime imaging microscopy (FLIM) was used to determine the mean fluorescence lifetime of di-8-ANEPPS in the membrane, allowing to compare the surrounding environment of the probe in wt cells vs the mutated ones.

There are other polarity and sterol sensitive dyes, such as Laurdan (Figure 1.17) and derivatives, which contain 2-hydroxy-6-dodecanoyl naphthalene (Amaro et al. 2017; Bagatoll et al. 1999; Golfetto et al. 2013; Levitan 2021; Mazeres et al. 2014). The emission spectra of Laurdan membrane probes suffers shifts according to the fluidity of the membrane. In fact, the generalized polarization (GP), which quantifies lipid packing, can be calculated from the

spectral shifts between different states of membrane order (Bagatoll et al. 1999; Golfetto et al. 2013; Levitan 2021; Mazeres et al. 2014). Moreover, Laurdan and/or derivatives have been used to label *S. cerevisiae* (Learmonth & Gratton 2002) and *C. albicans* (Suchodolski et al. 2019) cells, and liposomes with total lipid extracts from *S. cerevisiae* or selected extracted lipids (Klose et al. 2010). Nevertheless, while the absorption maximum of the ANEPS family ($\lambda_{exc} \approx$ 480-90 nm) is close to the wavelength of common pulsed excitation lasers that are used in FLIM, for Laurdan ($\lambda_{exc} \approx 360$ nm) two-photon fluorescence microscopy is necessary (Klose et al. 2010).

5. Antifungal drugs

Besides potency, the search for a proper efficient drug focus primarily in finding differences between the host and the pathogen, so that the drug can target the pathogen and leave the host unscathed. Since both animals (or plants) and fungi are eukaryotic, the differences between the two are relatively small. In fact, several antifungal drugs available in the market have toxic side effects (Vanreppelen et al. 2023).

Antifungal drugs can be natural products from plants, fungi or bacteria, or synthetic. Moreover, the antifungal agents now available in the market can be divided according to their target in the fungal cell: polyenes, pyrimidine analogs, azoles, allylamines and echinocandins (Vanreppelen et al. 2023). Table 1.4 presents a summary of the most common antifungal drugs in each class.

To fight resistance, a combined therapy of at least two antifungal agents from different classes that results in a synergistic therapy is frequently used (Campitelli et al. 2017). Another approach are improved delivery systems particularly the use of liposomal formulations which has been used with success, *e.g.* with amphotericin B (Jarvis et al. 2022). Currently, there are several new compounds and approaches being studied and on different clinical phases (Hoenigl et al. 2021; Van Daele et al. 2019).

This work focuses on antifungal drugs that act directly or indirectly in the plasma membrane of fungi, particularly the azole ketoconazole (**Ke**), and the polyene nystatin (Nys).

Table 1.4: Classes of antifungal drugs, according to their target. The list is organized from the oldest class to the most recently discovered.

Class	Main Source	Examples	Target	Consequences	Action
Polyenes	Natural	Nystatin (Hazen & Brown 1951), Amphotericin B (Donovick et al. 1955)	Sterols	Membrane pore formation, ROS formation	Fungicidal
Pyrimidine analogs	Synthetic	5-Flurocytosine (Polak & Scholer 1975)	DNA (thymidylate synthase) and protein (RNA) synthesis inhibition	DNA synthesis disruption, Amino acid pool and amino-acetylation of tRNA disruption	Fungistatic and Fungicidal
Azoles	Synthetic	Ketoconazole (Heeres et al. 1979), Fluconazole (Richardson et al. 1988)	Sterol synthesis (P450-dependent lanosterol 14-α-demethylase)	Membrane disruption, Toxic methylated sterol intermediates accumulation	Fungistatic
Allylamines	Synthetic*	Terbinafine (Birnbaum 1990)	Sterol synthesis (squalene epoxidase)	Membrane disruption, Squalene accumulation	Fungicidal
Morpholines	Synthetic	Amorolfine (Polak 1983)	Sterol synthesis (sterol C-14 reductase, sterol C-8 isomerase	Membrane disruption	Fungistatic and Fungicidal
Echinocandins	Natural	Pneumocandin B_0 (Wichmann et al. 1989), Caspofungin (Balkovec et al. 2014)	Glucan biosynthesis (β-(1,3)-glucan synthase)	Cell wall disruption	Fungistatic and Fungicidal

* Allylamines were first synthesized in the 70s and only recently it was discovered that *Lysinibacillus* is able to produce them (El-Sayed et al. 2021).

5.1. Ketoconazole and diphenylphosphine derivatives

Ke (Figure 1.18) was approved by the American Food and Drug Administration (FDA) and introduced to the market as Nizoral in 1981 to treat fungal infections. Nevertheless, the use of this imidazole-based antifungal drug was restricted in 2013 only for topical infections and life-threatening systematic mycoses due to its high hepatotoxicity (García Rodrĭguez et al. 1999; Knight et al. 1991). Nowadays, Nizoral is mainly used as a shampoo to diminish dandruff and control scalp fungus (Webpage: *Nizoral® Anti-Dandruff Shampoo - Ketoconazole 1%*).

The interest on **Ke** was renewed when results showed that it can also act against cancer cells (Chen et al. 2019; Naftalovich et al. 1991; Rochlitz et al. 1988; Weng et al. 2022) particularly prostatic cancer (Patel et al. 2018; Pont 1987; Trachtenberg 1984; Williams 1984), and Cushing's syndrome (Committee for Medicinal Products for Human Use (CHMP) 2014; Contreras et al. 1985).

As an azole the target of **Ke** is the Erg biosynthetic pathway, causing a decrease of Erg levels in the fungal cell, disturbing membrane structure and in consequence cell function and homeostasis. This occurs through **Ke** competitive inhibition of P450 sterol-14-α-demethylase (P45014DM) (Borelli et al. 1979; Loose et al. 1983; Shimokawa et al. 2005; Strushkevich et al. 2010; Van Tyle 1984) by the formation of a strong bond between the imidazole nitrogen of **Ke** and the heme iron of the enzyme.

Depending on the fungus, the mechanisms of resistance associated with azoles include target alteration through mutations in the Erg biosynthesis pathway (Casalinuovo et al. 2004; Morio et al. 2010), up-regulation of efflux transporters (Coleman & Mylonakis 2009; Sanglard et al. 2009) and/or cellular stress responses that include mediators such as the molecular chaperone Hsp90 (Cowen et al. 2009; Robbins et al. 2011).

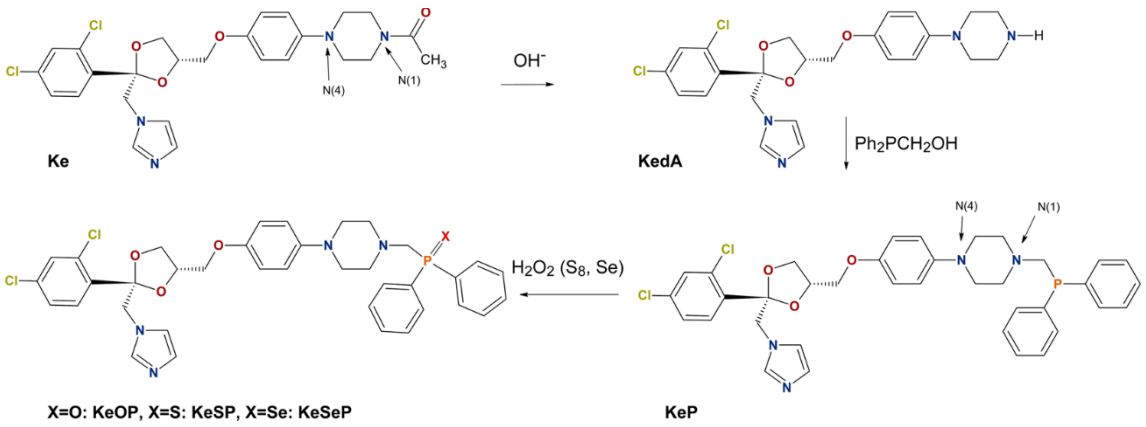

Figure 1.18: Schematic synthesis of Ke **derivatives. Ke** was deacylated to obtain **KedA** (deacylated **Ke**) from which, through a modified Mannich condensation reaction of hydroxymethylphosphanes with amines, **KeP** was obtained. PPh_2CH_2OH was obtained *in situ* from $PPh_2(CH_2OH)_2Cl$ by adding an excess of triethylamine. Chalcogenides were synthesized in a reaction of **KeP** with a stoichiometric amount of H_2O_2 (**KeOP**), resublimed sulphur (**KeSP**) or metallic selenium (**KeSeP**) in ultrasound bath. (de Almeida et al. 2019)

Ke can easily be deacylated generating a monosubstituted piperazine bearing a secondary amine group, a feature that is absent in other antifungal azoles such as fluconazole or miconazole. Its presence facilitates various modifications and addition of other functional groups that may alter biological properties of the parent molecule. For instance, de Almeida *et al.* presented aminomethylphosphine derived from **Ke** (**KeP**), synthesized from deacylated **Ke** through a modified Mannich condensation where the acetyl group of **Ke** was replaced by a diphenylphophinomethyl moiety. The respective chalcogenides were also synthetized: oxide (**KeOP**), sulphide (**KeSP**) and selenide (**KeSeP**) (Figure 1.18) (de Almeida et al. 2019). The addition of a phosphine group alters coordination properties of the molecule, particularly the possibility of creating complexes with soft metal ions such as Ruthenium (II) and Copper (I) (Płotek et al. 2015; Starosta et al. 2013, 2020). Moreover, aminomethylphosphines proved to

be air-stable in contrast to the trisaryl or trisalkylphosphines, which is a very desirable feature in the context of biological relevance.

As demonstrated by docking assays (Figure 1.19) these derivatives can also target P45014DM, and particularly **KeP** and **KeOP** have antifungal activity against strains of *S. cerevisiae* (MIC_{50} = 9.023 and 0.00416 μM, respectively) and *C. albicans* (MIC_{50} = 3.13 and 0.78 μM, respectively) with relative lower toxicity towards human cells (de Almeida et al. 2019). What is truly interesting about these compounds is that there are multiple evidence for a possible additional mode of action that could be through the direct perturbation of the membrane properties. As previously mentioned, *erg6*Δ *S. cerevisiae* cells lack sterol-24*C*-methyltransferase of the Erg biosynthetic pathway being unable to produce Erg, and instead accumulate Zym and other sterols in the plasma membrane (Heese-Peck et al. 2002). While **Ke** is not fungistatic against these cells, **KeP** and **KeOP** are (de Almeida et al. 2019). Moreover, a *C. albicans* mutant that lacks efflux transporters (Cdr1, Cdr2 and Mdr1) which overexpression has been associated with the development of resistance towards azoles, was 4-fold more susceptible to **KeP** and **KeOP** than the parental strain, while it was only 2.5 times more susceptible to **Ke**. Furthermore, *C. albicans* isolated from patients that have developed azole-resistance (from the overexpression of Mdr1) was 2 times more resistant to **KeOP** than the non-resistant strain, while **Ke** was 8 times higher (de Almeida et al. 2019). Hence, the activity of these two derivatives is less dependent on the expression of drug exporters at the plasma membrane of *C. albicans* than **Ke** itself. Furthermore, the presence of the $-CH_2PPh_2$ hydrophobic moiety increases the lipophilic nature of **KeP** and **KeOP** when compared with **Ke** and, in fact, these compounds are able to permeabilize the membrane (Bento-Oliveira et al. 2024) the subject of chapter III of the current thesis.

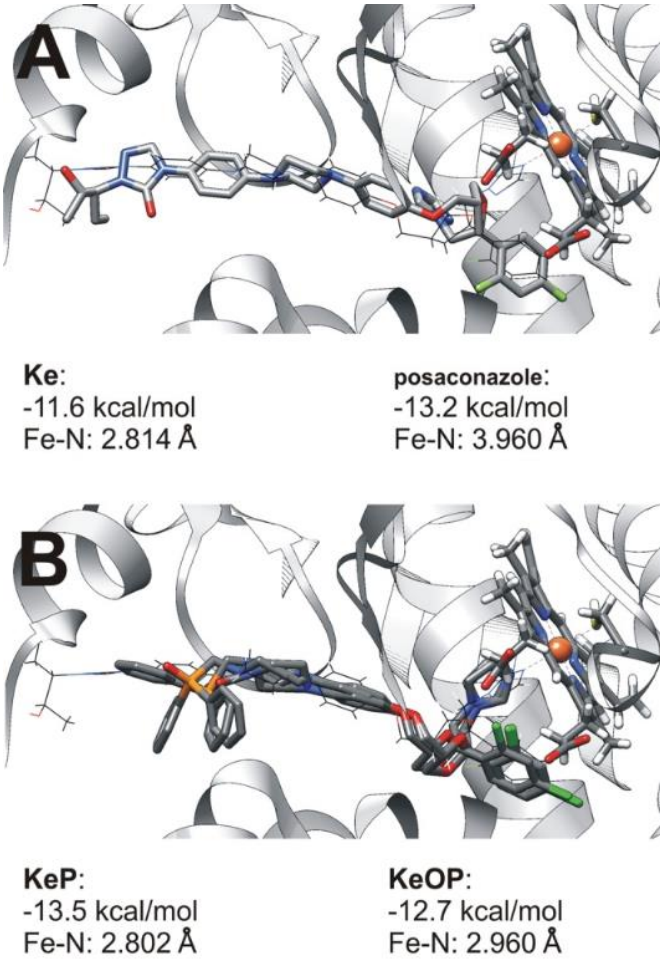

Figure 1.19: Docking results - heme of the C. albicans CYP51 and the best-fit docked compounds; posaconazole position from the original crystal structure (Webpage: *RCSB PDB - 5FSA: Crystal structure of sterol 14-alpha demethylase (CYP51) from a pathogenic yeast Candida albicans in complex with the antifungal drug posaconazole*) is also indicated (as a black wire). (A) docked posaconazole and **Ke**, (B) **KeP**, **KeOP**. (de Almeida et al. 2019)

5.2. Nystatin

Several studies have been conducted to better understand the mode of action of polyenes. Nys and amphotericin B are the two major polyenes used as antifungal drugs. This work focus mainly on Nys since 1) this drug has a broader spectrum of activity than amphotericin B (Stern et al. 1988); 2) several *C. albicans* strains are more sensitive to Nys than to amphotericin B (Sousa et al. 2023); and 3) unlike Nys, amphotericin B is not intrinsically fluorescent (unless under specific conditions) - there are several previous studies, *e.g.* (Coutinho & Prieto 1995, 2003; dos Santos et al. 2017; Silva et al. 2006a; Szomek et al. 2021), that focus on the fluorescence properties of Nys as a tool to unravel this polyene activity and membrane interaction, which is not possible to conduct for amphotericin B.

Nys is an FDA approved antifungal agent that, as a polyene, has a macrolactonic ring containing conjugated double bonds (2+4), conjugated with a D-mycosamine group (Figure

1.20). This macrolide is the oldest polyene antifungal and it was discovered in bacterium *Streptomyces noursei* in the early 1950s by Rachel Fuller Brown and Elizabeth Lee Hazen (Hazen & Brown 1951). Later, three different components of Nys were identified using HPLC (high performance liquid chromatography) and TLC (thin layer chromatography): A_1, A_2 and A_3 all with biological activity (Mitrofanova et al. 1991; Zielinski et al. 1988). Of these three, the component that is typically used in marketed drugs is A_1, being the one that is studied the most and used in the present work.

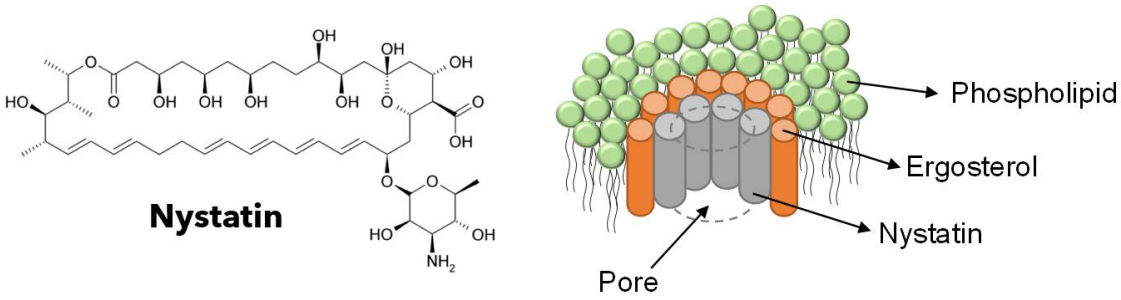

Figure 1.20: Nys molecular structure and the classical "barrel-state" model of the Nys pore in the membrane.

Nys has a broad-spectrum of activity, being fungicidal against a plethora of yeast and fungi, mainly from the *Candida* genus. Nevertheless, this drug has some side effects associated, such as nephrotoxicity, and easily aggregates in water, having a low absorption rate in the gastrointestinal tract. Currently it is used topically as a cream or ointment to treat *e.g.* vaginal yeast infections, and only rarely it is used orally (Webpage: *Nystatin Cream: Package Insert - Drugs.com*; Webpage: *Nystatin Uses, Side Effects & Warnings - Drugs.com*).

Mutations in the Erg biosynthesis pathway that leads to the accumulation of sterols other than Erg (target alteration), is the main resistance mechanisms of *Candida* associated with polyene drugs (Carolus et al. 2021; Rybak et al. 2022; Vandeputte et al. 2008; Vincent et al. 2013). Moreover, similarly to **Ke**, the chaperone Hsp90 activates the response to stress, due to antifungal drug activity (Vincent et al. 2013).

As most polyene antifungal agents, Nys is able to form small-diameter pores of approximately 0.8 nm of internal diameter (Andreoli et al. 1969; Holz & Finkelstein 1970), in the plasma membrane of fungi, through the formation of stoichiometric Nys-Erg complexes (Figure 1.20) that disrupts the membrane and in consequence the homeostasis of the cytoplasm, eventually leading to cell death. Nys aggregates in a cylindrical fashion with Erg around it. The exact Nys/Erg ratio is still debated. Moreover, the number of polyene molecules that are required to form the pore varies from 4 to 12 depending on the article (Andreoli 1974; Baginski et al. 1997; Coutinho & Prieto 2003; De Kruijff & Demel 1974; Moreno-Bello et al. 1988; Umegawa et al. 2022). The poly-hydroxylated region of the macrolide ring is facing the inside

of the channel, being protected from the hydrophobic core of the lipid bilayer. Moreover, the polyene chains are facing the outside of the channel which establish contacts with sterols. Furthermore, the polar moiety of the drug consists of ionizable groups that anchor the channel to the bilayer surface (Andreoli 1974; De Kruijff & Demel 1974; Holz 1974; Marty & Finkelstein 1975).

Although this is the classical mode of action of antifungal polyenes, there are many arguments regarding the role of Erg and if the mechanism for pore-formation is truly dependent on the sterol. The discussion became more relevant due to 1) the fact that there are yeast strains with similar sterol content but different sphingolipid profile that have different sensitivity to the drug (Komor et al. 1979; Leber et al. 1997); and 2) polyene macrolides are active in sterol-free lipid bilayers containing highly ordered gel domains (dos Santos et al. 2017). Due to this evidence some authors argue that Erg might not be directly involved in the pore-formation ability of Nys, but rather is relevant for membrane packing. The membrane packing seems in fact to be relevant for the activity of this drug, since Nys has a strong pore-forming activity in membranes with DPPC/POPC or PSM/POPC that have gel phases but no sterol. Also, the partition of Nys is stronger towards membranes containing gel phases (dos Santos et al. 2017) in opposition to more fluid membranes (Coutinho & Prieto 2003; dos Santos et al. 2017). Moreover, the tetraene motif of Nys is similar to that of *t*-PnA, which as mentioned previously is a fluorescent membrane probe that partitions preferentially towards gel domains (Aresta-Branco et al. 2011; Bento-Oliveira et al. 2020; de Almeida et al. 2009; Sklar et al. 1977). Due to this, it seems that Nys has a preference towards membranes containing gel-phases, even when no sterol is present. This evidence is particularly relevant when one considers the presence of SLEDs in the fungal plasma membrane but not in mammalian ones, and that in fact SLEDs are a possible target of Nys.

Another aspect to consider is that Nys has a preference for Erg, the major sterol found in fungi membranes, when compared to Chol. This preference grants selective toxicity of this compound against fungal cells (Coutinho et al. 2004; Silva et al. 2006a). Concerning the sterol structural requirements for antibiotic selectivity, the observations are controversial. Some authors state that the higher interaction between polyene antibiotics and Erg, as compared to Chol, is due to the presence of an extra double bond in the ring system (Charbonneau et al. 2001; Clejan & Bittman 1985), whereas others argue that a double bond in the sterol side chain is fundamental (Kawabata et al. 2001; Langlet et al. 1994), while there is also the possibility that both could be important (Silva et al. 2006b). In contrast, it is often proposed that the higher selectivity arises from the bulk membrane properties induced by the two sterols (González-

Damián & Ortega-Blake 2010; Récamier et al. 2010). This could explain Nys fluorescence intensity sensitivity to membrane fluidity and sterol content (Wilson-Ashworth et al. 2006). Moreover, Nys direct interaction with the plasma membrane was studied using UV-sensitive microscopy which showed that the polyene binds to mammalian cells, such as the chinese hamster ovarian (CHO) cells but does not affect the membrane dynamics of a fluorescent analog of Chol. In addition, studies with *S. cerevisiae* were performed and showed that the membrane staining of Nys was much more pronounced in yeast pre-loaded with Erg compared to yeast loaded with Chol. Also, the membrane fluorescence of Nys was more pronounced in yeast compared to mammalian cells (Szomek et al. 2021).

The answer could be that both the molecular structure of the sterols could affect the properties of the lipid domains and general biophysical properties of the membrane and in consequence the action of Nys.

6. Tools to study membrane-drug interaction

There is a diverse number of techniques that can be used to study membrane-drug interactions. It all depends on the objective of the work. Spectroscopic techniques together with model membrane systems, such as LUVs, have been widely used as a first approach to study drug-membrane interactions (see Review (Loura et al. 2003)). Fluorescence spectroscopy is useful particularly if the compound is intrinsically fluorescent. However, it is still possible to conduct such experiments by labelling the compound or if that is not possible or influences the drug interaction with the membrane, the use of fluorescent probes is also another option. Moreover, the use of fluorescent probes together with the compound (even if intrinsically fluorescent) might provide information regarding how the membrane-drug interaction is affecting membrane properties or if the compound is partitioning towards a specific region of the membrane that is selectively labelled with the probe used.

One can also use solid-state nuclear magnetic resonance (NMR) for membrane-bound molecules (Umegawa et al. 2022), or isothermal titration calorimetry (ITC) which is very resourceful to measure affinities, stoichiometry and enthalpies involved in the binding of the drug to the membrane (Moreno et al. 2010). Finally, molecular dynamics (MD) simulations can provide a good insight on a simpler system to a detail that is not possible in experimental approaches (Baginski et al. 2002).

6.1. Using drug intrinsic fluorescence to detect interaction with the membrane

Typically, when an intrinsically fluorescent compound interacts with a lipid in an aqueous solution, the fluorescence properties of that compound are affected. The transfer of the compound from an aqueous solution towards a less polar environment, *i.e.* the lipid bilayer, could change the compound quantum yield, the wavelength of the peak of the excitation and emission spectrum, anisotropy, and/or the mean fluorescence lifetime (Santos et al. 2003).

As mentioned previously, a change in the microenvironment that surrounds a fluorophore influences greatly the fluorescence properties of the molecule (Lakowicz 2006). Some typical results observed from the interaction between a fluorescent molecule and a lipid bilayer are (Loura et al. 2003):

1) An increase of the fluorophore fluorescence intensity with the presence of lipid that reflects an increase of the Φ_F, that is due to a decrease of the k_{nr}. Due to this reason, it is also possible to observe an increase of the fluorophore $\bar{\tau}$;

2) Spectral shifts, due to changes in solvent relaxation with solvent polarity. With the partition of a fluorescent compound towards the lipid bilayer, while the environment surrounding the molecule becomes less polar, this solvent effect on the excited state is reduced, which typically results in a blue-shift of emission spectra;

3) An increase of the fluorophore fluorescence anisotropy could occur when it interacts with a membrane. This increase indicates a reduction of rotational diffusion of the compound, which reinforces the hypothesis that the environment around the fluorophore is becoming more viscous with the presence of lipid, *i.e.* that the compound is being incorporated in the membrane.

It is important to add that these changes do not necessarily happen in parallel, and typically it only takes one to confirm drug-membrane interaction. Also, although these are some of the expected changes found in the fluorescence properties of compounds when partitioning from an aqueous medium to a membrane, there are some exceptions namely for complex membrane partition when the equilibrium of compound in water and in lipid is affected by processes such as aggregation of the compounds in aqueous solution or in the membrane, or self-quenching.

The membrane-compound interaction of several molecules was studied using this approach (Loura et al. 2003; Santos et al. 2003). For example, following the polyene Nys intrinsic fluorescent properties it was possible to compare the partition and interaction of the antifungal Nys towards different lipid bilayers such as the ones containing POPC or SM (dos Santos et al.

2017), DPPC (Coutinho & Prieto 1995, 2003) and POPC mixed with different sterols such as Chol and Erg (Coutinho et al. 2004; Silva et al. 2006b,a).

6.2. Relative membrane location of the drug

Aqueous fluorescence quenchers, such as acrylamide, iodide and 3-carboxy-PROXYL (3-(carboxy)-2,2,5,5-tetramethyl-1-pyrrolidinyloxy), have been used to characterize compounds and proteins in aqueous solution and to explore the accessibility to the aqueous medium of fluorophores interacting with the membrane (De Granada-Flor et al. 2019; Manuel Nuno & B., Miguel A. R. 2007; Sónia Troeira & Miguel A. R. B. 2005). Since these compounds are hydrophilic, and thus do not cross or partition towards the membrane, its quenching efficiency in this situation depends on how deeply buried the compound is in the membrane: the more superficial the fluorophore membrane location, the more efficient is the quenching (Figure 1.21 – A and B).

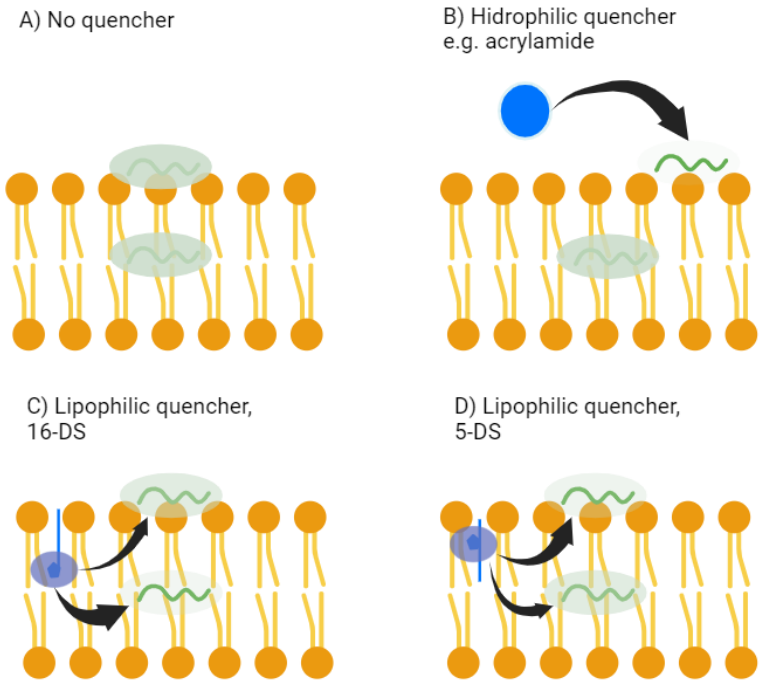

Figure 1.21: Exemplificative approaches with fluorescence quenching of molecule-membrane bound. The quencher (blue) used can be hydrophilic (B) and solely dissolve in the aqueous medium, or lipophilic (C and D) and distribute along the membrane affecting the fluorescence of the molecule (green wave line) depending on its location in the membrane. The intensity of the fluorescence of the molecule is correlated with the intensity of the surrounding green circle: the darker the green the more the molecule is able to fluoresce. In C and D since the moiety that is able to quench fluorescence is in different positions, it leads to differential quench of the molecule. For more details, please check the text. Created with BioRender.com.

Derivatized spin-labeled fatty acids can also be used as fluorescence quenchers to study the depth of a certain fluorophore in a membrane (Coutinho & Prieto 2003; Sónia Troeira & Miguel A. R. B. 2005). 5- and 16-doxyl-stearic acids (5- and 16-DS, respectively) are two commonly used lipophilic probes, that distribute vertically in a lipid bilayer, *i.e.* parallel to the

lipid acyl chain of the lipids (Ellena et al. 1988). These molecules have a doxyl group in a different position (5 and 16) that when inserted in a bilayer is in a different depth (Figure 1.21 - C and D). This results in different quenching efficiency by 5- or 16-DS, that can also include hydrophilic quenchers, for a fluorophore inserting in the bilayer and, using the parallax method (London & Chattopadhyay 1987) it is possible to determine the transversal position of a compound in a membrane.

In silico techniques are also tools that can unravel in more detail compound-membrane interaction. Although these are only theoretical approaches, they allow to gain insight about certain specific information that due to limitations of the procedures are not experimentally accessible. A complementary study with both is the ideal situation, which is not always available.

6.3. Measuring membranotropic effects

The compound interaction with the membrane, might change the properties of the membrane itself, including lipid packing order, membrane potential, hydration, thickness and vesicle fusion, amongst other.

The change in biophysical properties of the membrane due to its interaction with a molecule can be measured using the same approaches that are usually used to study membrane properties, such as AFM and X-ray diffraction, and with fluorescent membrane probes, with a similar approach as the one described in the previous sections. For the latter, one relevant aspect to consider is if the compound/molecule in study can interact with the membrane probes. For instance, the molecule can quench the probe fluorescence, and the membrane properties reported are affected.

Dynamic light scattering is another technique that is commonly used to study changes in vesicle size and stability. Moreover, it is possible under a confocal microscope to visualize vesicle morphological changes after the addition of membranotropic agents to labelled GUVs.

In this work, we focused on measuring the membranotropic ability of antifungal agents, especially regarding changes in permeability and compressibility properties.

6.3.1. Permeability assays

To confirm if a compound changes the overall permeability of a lipid bilayer it is possible to perform a permeability assay by using a fluorescent probe that at high concentration undergoes self-quenching (Figure 1.22), *e.g.* 5(6)-carboxyfluorescein (CF).

In this type of assay, liposomes are prepared with high concentrations of the probe encapsulated, in which its fluorescence is significantly quenched and in consequence the fluorescence intensity is low. The outside of the liposome must be kept without any probe, so that when a disturbing agent is added to the preparation, and the permeability of the liposome increases, there is leakage of the probe, and its local concentration outside is not as high as the inside or overall. Hence, the fluorescence intensity increases. After the addition of the compound of interest, a strong detergent is added disassembling the liposomes, freeing completely the remaining CF. This allows the determination of the maximum percentage of CF release (F_{100}). It is possible to track the changes in CF fluorescence intensity, *i.e.* the permeation of encapsulated CF through the lipid bilayer (Martinho et al. 2023; Starosta et al. 2023), along a certain period of time.

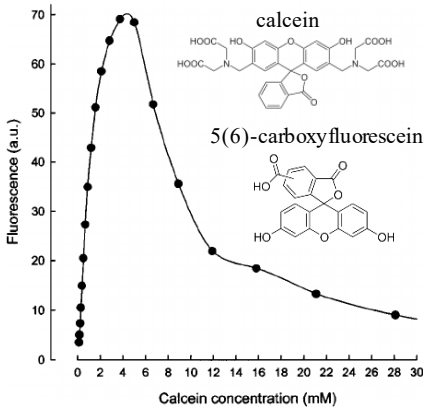

Figure 1.22: Self-quenching of calcein. Above ca. 4 mM of calcein the fluorescence intensity tends to relatively low values. The molecular structures of calcein and 5(6)-carboxyfluoresein (CF) are also represented. Adapted from (Hamann et al. 2002). The data are corrected for inner filter effects.

There are other permeability assays that are specific towards the membranotropic agent studied. For instance, the formation of Nys channels on lipid bilayers can be quantified by studying the potassium permeability of lipid vesicles through H^+/K^+ exchange assays across the membrane bilayer (dos Santos et al. 2017). This approach takes advantage of pyranine fluorescence emission which is sensitive to the pH in the medium (Figure 1.23 - A). It consists of forming vesicles with a buffer that has a high potassium concentration and pyranine. Then, all the pyranine that is outside the vesicles is removed by performing a molecular exclusion chromatography. Free equilibration of H^+ ions is then achieved by adding FCCP (carbonyl cyanide-*p*-trifluoromethoxyphenylhydrazone), a protonophore, followed by the formation of the potassium gradient by the addition of a buffer with no potassium. When Nys is added to these vesicles, if it is interacting with the lipid bilayer and forming pores, the medium inside the vesicle becomes more acid due to the proton flow that results from the efflux of potassium, and there is a shift in the fluorescence excitation wavelenght maximum of pyranine from 450

to 405 nm. This leads to a decrease in the ratio of emission of pyranine after excitation at 450 and 405 nm (Figure 1.23 - B). Due to this, the data is expressed as the ratio of pyranine fluorescence intensity at 510 nm obtained upon excitation at 450 nm and 405 nm which correspond to the maximum excitation wavelength when pyranine is at neutral or acidic pH, respectively.

It is possible to quantify the effectiveness of Nys pore formation by determining the dissipation of the potassium gradient. To do this the values obtained from the addition of Nys are compared with the total dissipation of the gradient (100% of gradient dissipation) which is achieved by the addition of the ionophore valinomycin (Figure 1.23 - B). Finally, a strong detergent, Triton X-100, is used to disassemble the liposomes which causes the fluorescence to go back to baseline values (Figure 1.23 - B).

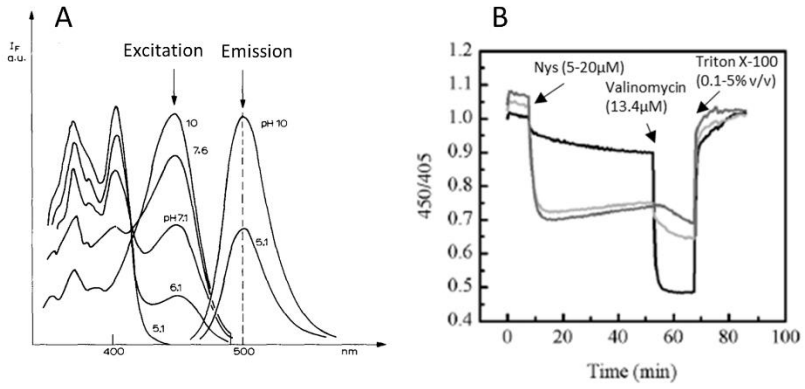

Figure 1.23: (A) Pyranine fluorescence excitation and emission spectra dependence on pH (Launay et al. 1980)**. (B) Pyranine permeability assay result (adapted from** (dos Santos et al. 2017)**).** In B, the fluorescence emission of pyranine was measured at 510 nm after excitation at 405 and 450 nm, first for 10 min to have a baseline, and then for 42 min after the addition of Nys, 10 min after adding the ionophore, valinomycin, and finally 20 min after adding the strong detergent Triton X-100. The ratio 450/405 represents the fluorescence intensity of pyranine after excitation at 450 nm divided by the intensity after excitation at 405 nm. The black, light grey and dark grey lines represent vesicles prepared with POPC containing 20, 50 and 70 mol% of SM, respectively.

6.3.2. Surface pressure perturbation

Lipid monolayers in the water/air interface have been widely used as membrane model systems. These are formed by placing carefully a relatively small amount of (amphipathic) lipids on top of water, in which the molecules will organize in a lipid film with the polar headgroups in contact with the water and the acyl chains facing the air. Usually, these monolayers are prepared on a Langmuir-Blodgett trough in between two barriers which can slide horizontally changing the lateral pressure of the monolayer. Placed in the middle is a probe that can measure the superficial tension, such as a Wilhelmy plate. With this apparatus it is possible to measure surface pressures (π) along average molecular areas (A) that are required to keep the monolayer stable without collapsing. From the curve $A(\pi)$ obtained at constant

temperature it is possible to detect phase transitions. These curves are called surface pressure-area isotherms (Figure 1.24). (de Almeida & Loura 2004; Dynarowicz-Latka et al. 2024; Oliveira et al. 2022; Stillwell 2016)

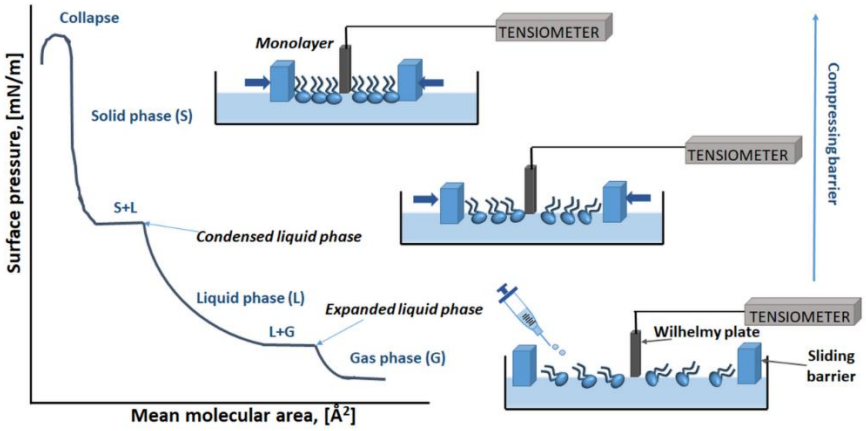

Figure 1.24: Example of a surface pressure-area isotherm $A(\pi)$ of a monolayer in the water/air interface and schematic illustration of the setup in a Langmuir-Blodgett trough. The compressing barriers decrease the mean molecular area which causes the increase of the surface pressure (π) until the monolayer collapses and the surface pressure decreases. In this representation the expanded and condensed liquid phase are analogous to the l_d and gel phases in lipid bilayers, respectively. (Rojewska et al. 2021)

In a typical setup the barriers are first completely extended, and a baseline without the lipid is measured, followed by the addition of the lipid to the water. After the surface stabilizes, the surface pressure is measured while the barriers are closing, decreasing the mean molecular area. With increasing surface pressure, it is possible to detect abrupt changes in slope, often displaying *plateaus* with constant mean molecular area which correspond to phase transitions and in the *plateau* there is coexistence of the two phases. At some point the monolayer reaches a limit packing order, and the barriers collapse the lipid film. (de Almeida & Loura 2004; Stillwell 2016)

The compressibility behaviour of a curve changes with lipid composition (type of lipid and quantity), temperature and the composition of the aqueous phase. These measurements allow to compare different lipid systems regarding their compressibility behaviour, *e.g.*, point of collapse, stability, phase transitions, and the compressional modulus (C_S^{-1}). This last parameter represents changes in terms of two-dimensional compressibility and is sensitive to lateral interactions, thus reporting on lateral packing elasticity of the monolayer. A high maximum C_S^{-1} of an isothermal curve means higher rigidity ability of the lipid system (Rojewska et al. 2021). This parameter can be calculated using the following equation:

$$C_S^{-1} = -A\left(\frac{d\pi}{dA}\right) \tag{10}$$

With more complex setups it is also possible to measure other parameters such as the surface potential. Interestingly, after measuring the compressibility properties, if a solid support is submerged in the lipidic film, the monolayer is transferred to that support in which other techniques are possible to conduct, such as AFM which allows to study the topography of the lipid system. (de Almeida & Loura 2004; Dynarowicz-Latka et al. 2024; Oliveira et al. 2022; Stillwell 2016)

After measuring the compressibility properties of a certain lipid system, it is possible to add another component, for instance a drug, and measure how that compound changes the compressibility behaviour of the monolayer. In other words, it is possible to measure/quantify membrane-drug interactions. This approach was previously used to study *e.g.* the interaction of the antifungal polyene Nys (Hąc-Wydro & Dynarowicz-Łatka 2006) and amphotericin B (Hąc-Wydro et al. 2005; Lance et al. 1996; Wang & Zhu 2021) with monolayers containing DPPC, Erg or Chol.

7. References

Abe F, Hiraki T. 2009. Mechanistic role of ergosterol in membrane rigidity and cycloheximide resistance in Saccharomyces cerevisiae. *Biochim. Biophys. Acta - Biomembr.* 1788(3):743–52

Aguilar PS, Heiman MG, Walther TC, Engel A, Schwudke D, Gushwa N, Kurzchalia T, Walter P. 2010. Structure of sterol aliphatic chains affects yeast cell shape and cell fusion during mating. *Proc. Natl. Acad. Sci. U. S. A.* 107(9):4170–75

Alavizargar A, Keller F, Wedlich-Söldner R, Heuer A. 2021. Effect of Cholesterol Versus Ergosterol on DPPC Bilayer Properties: Insights from Atomistic Simulations. *J. Phys. Chem. B*. 125(28):7679–90

Alexopoulos CJ, Mims CW. 1979. *Introductory Mycology*. John Wiley & Sons, Inc. 3rd editio ed.

Almeida PFF, Thompson TE, Vaz WLC. 1992. Lateral Diffusion and Percolation in Two-Phase, Two-Component Lipid Bilayers. Topology of the Solid-Phase Domains In-Plane and Across the Lipid Bilayer. *Biochemistry*. 31(31):7198–7210

Amaro M, Reina F, Hof M, Eggeling C, Sezgin E. 2017. Laurdan and Di-4-ANEPPDHQ probe different properties of the membrane. *J. Phys. D*. 50(13):

Amati AM, Graf S, Deutschmann S, Dolder N, von Ballmoos C. 2020. Current problems and future avenues in proteoliposome research. *Biochem. Soc. Trans.* 48(4):1473–92

Andreoli TE. 1974. The structure and function of amphotericin B-cholesterol pores in lipid bilayer membranes. *Ann. N. Y. Acad. Sci.* 235(0):448–68

Andreoli TE, Dennis VW, Weigl AM. 1969. The effect of amphotericin B on the water and nonelectrolyte permeability of thin lipid membranes. *J. Gen. Physiol.* 53(2):133–56

Aresta-Branco F, Cordeiro AM, Marinho HS, Cyrne L, Antunes F, de Almeida RFM. 2011. Gel domains in the plasma membrane of Saccharomyces cerevisiae: highly ordered, ergosterol-free, and sphingolipid-enriched lipid rafts. *J. Biol. Chem.* 286(7):5043–54

Arora A, Raghuraman H, Chattopadhyay A. 2004. Influence of cholesterol and ergosterol on membrane dynamics: A fluorescence approach. *Biochem. Biophys. Res. Commun.* 318(4):920–26

Athanasopoulos A, André B, Sophianopoulou V, Gournas C. 2019. Fungal plasma membrane domains. *FEMS Microbiol. Rev.*

Avanti Polar Lipids - NBD-DPPE. https://avantilipids.com/product/810144. Accessed: 02/22/2024

Avanti Polar Lipids - Rhod-DOPE. https://avantilipids.com/product/810150. Accessed: 02/22/2024

Bagatoll LA, Parasassi T, Fidelio GD, Gratton E. 1999. A Model for the Interaction of 6-Lauroyl-2-(N,N-dimethylamino)naphthalene with Lipid Environments: Implications for Spectral Properties. *Photochem. Photobiol.* 70(4):557–64

Baginski M, Resat H, Borowski E. 2002. Comparative molecular dynamics simulations of amphotericin B-cholesterol/ergosterol membrane channels. *Biochim. Biophys. Acta - Biomembr.* 1567(SUPPL.):63–78

Baginski M, Resat H, McCammon JA. 1997. Molecular properties of amphotericin B membrane channel: a molecular dynamics simulation. *Mol. Pharmacol.* 52(4):560–70

Bagnat M, Chang A, Simons K. 2001. Plasma membrane proton ATPase Pma1p requires raft association for surface delivery in yeast. *Mol. Biol. Cell.* 12(12):4129–38

Bagnat M, Simons K. 2002. Cell surface polarization during yeast mating. *Proc. Natl. Acad. Sci. U. S. A.* 99(22):14183–88

Balkovec JM, Hughes DL, Masurekar PS, Sable CA, Schwartz RE, Singh SB. 2014. Discovery and development of first in class antifungal caspofungin (CANCIDAS®)--a case study. *Nat. Prod. Rep.* 31(1):15–34

Bastos AEP, Marinho HS, Cordeiro AM, de Soure AM, de Almeida RFM. 2012. Biophysical properties of ergosterol-enriched lipid rafts in yeast and tools for their study: characterization of ergosterol/phosphatidylcholine membranes with three fluorescent membrane probes. *Chem. Phys. Lipids*. 165(5):577–88

Beattie ME, Veatch SL, Stottrup BL, Keller SL. 2005. Sterol structure determines miscibility versus melting transitions in lipid vesicles. *Biophys. J.* 89(3):1760–68

Bento-Oliveira A, Santos FC, Marquês JT, Paulo PMR, Korte T, Herrmann A, Marinho HS, de Almeida RFM. 2020. Yeast sphingolipid-enriched domains and membrane compartments in the absence of mannosyldiinositolphosphorylceramide. *Biomolecules*. 10(6):1–24

Bento-Oliveira A, Starosta R, de Almeida RFM. 2024. Interaction of the antifungal ketoconazole and its diphenylphosphine derivatives with lipid bilayers: insights into their antifungal action. *Arch. Biochem. Biophys.*

Berchtold D, Piccolis M, Chiaruttini N, Riezman I, Riezman H, Roux A, Walther TC, Loewith R. 2012. Plasma membrane stress induces relocalization of Slm proteins and activation of TORC2 to promote sphingolipid synthesis. *Nat. Cell Biol. 2012 145*. 14(5):542–47

Berchtold D, Walther TC. 2009. TORC2 plasma membrane localization is essential for cell viability and restricted to a distinct domain. *Mol. Biol. Cell*. 20(5):1565–75

Bezrukov L, Blank PS, Polozov I V., Zimmerberg J. 2009. An adhesion-based method for plasma membrane isolation: evaluating cholesterol extraction from cells and their membranes. *Anal. Biochem.* 394(2):171–76

Bianchi F, Syga L, Moiset G, Spakman D, Schavemaker PE, Punter CM, Seinen AB, Van Oijen AM, Robinson A, Poolman B. 2018. Steric exclusion and protein conformation determine the localization of plasma membrane transporters. *Nat. Commun. 2018 91*. 9(1):1–13

Birnbaum JE. 1990. Pharmacology of the allylamines. *J. Am. Acad. Dermatol.* 23(4 Pt 2):782–85

Bongomin F, Gago S, Oladele RO, Denning DW. 2017. Global and Multi-National Prevalence of Fungal Diseases—Estimate Precision. *J. Fungi 2017, Vol. 3, Page 57*. 3(4):57

Borelli D, Bran JL, Fuentes J, Legendre R, Leiderman E, Levine HB, Restrepo A, Stevens DA. 1979. Ketoconazole, an oral antifungal: laboratory and clinical assessment of imidazole drugs. *Postgrad. Med. J.* 55(647):657–61

Bottema CDK, McLean-Bowen CA, Parks LW. 1983. Role of sterol structure in the thermotropic behavior of plasma membranes of Saccharomyces cerevisiae. *Biochim. Biophys. Acta - Biomembr.* 734(2):235–48

Breslow DK. 2013. Sphingolipid Homeostasis in the Endoplasmic Reticulum and Beyond. *Cold Spring Harb. Perspect. Biol.*

5(4):1–16
Breslow DK, Weissman JS. 2010. Membranes in Balance: Mechanisms of Sphingolipid Homeostasis. *Mol. Cell.* 40(2):267
Brischke C, Alfredsen G. 2020. Wood-water relationships and their role for wood susceptibility to fungal decay. *Appl. Microbiol. Biotechnol. 2020 1049*. 104(9):3781–95
Campitelli M, Zeineddine N, Samaha G, Maslak S. 2017. Combination Antifungal Therapy: A Review of Current Data. *J. Clin. Med. Res.* 9(6):451
Carolus H, Pierson S, Muñoz JF, Subotić A, Cruz RB, Cuomo CA, Van Dijck P. 2021. Genome-Wide Analysis of Experimentally Evolved Candida auris Reveals Multiple Novel Mechanisms of Multidrug Resistance. *MBio*. 12(2):
Casalinuovo IA, Di Francesco P, Garaci E. 2004. Fluconazole resistance in Candida albicans: a review of mechanisms. *Eur. Rev. Med. Pharmacol. Sci.* 8(2):69–77
Castro IG, Shortill SP, Dziurdzik SK, Cadou A, Ganesan S, Valenti R, David Y, Davey M, Mattes C, Thomas FB, Avraham RE, Meyer H, Fadel A, Fenech EJ, Ernst R, Zaremberg V, Levine TP, Stefan C, Conibear E, Schuldiner M. 2022. Systematic analysis of membrane contact sites in Saccharomyces cerevisiae uncovers modulators of cellular lipid distribution. *Elife*. 11:
Charbonneau C, Fournier I, Dufresne S, Barwicz J, Tancrède P. 2001. The interactions of amphotericin B with various sterols in relation to its possible use in anticancer therapy. *Biophys. Chem.* 91(2):125–33
Chen Y, Chen HN, Wang K, Zhang L, Huang Z, Liu J, Zhang Z, Luo M, Lei Y, Peng Y, Zhou ZG, Wei Y, Huang C. 2019. Ketoconazole exacerbates mitophagy to induce apoptosis by downregulating cyclooxygenase-2 in hepatocellular carcinoma. *J. Hepatol.* 70(1):66–77
Cheng Q, Michels CA. 1991. MAL11 and MAL61 encode the inducible high-affinity maltose transporter of Saccharomyces cerevisiae. *J. Bacteriol.* 173(5):1817
Cirigliano A, Macone A, Bianchi MM, Oliaro-Bosso S, Balliano G, Negri R, Rinaldi T. 2019. Ergosterol reduction impairs mitochondrial DNA maintenance in S. cerevisiae. *Biochim. Biophys. acta. Mol. cell Biol. lipids*. 1864(3):290–303
Clay L, Caudron F, Denoth-Lippuner A, Boettcher B, Frei SB, Snapp EL, Barral Y. 2014. A sphingolipid-dependent diffusion barrier confines ER stress to the yeast mother cell. *Elife*. 2014(3):
Clejan S, Bittman R. 1985. Rates of amphotericin B and filipin association with sterols. A study of changes in sterol structure and phospholipid composition of vesicles. *J. Biol. Chem.* 260(5):2884–89
Coleman JJ, Mylonakis E. 2009. Efflux in Fungi: La Pièce de Résistance. *PLoS Pathog.* 5(6):
Committee for Medicinal Products for Human Use (CHMP). 2014. Assessment report Ketoconazole HRA, Procedure No. EMEA/H/C/003906/0000
Contreras P, Altieri E, Liberman C, Gac A, Rojas A, Ibarra A, Ravanal M, Serón-Ferré M. 1985. Adrenal rest tumor of the liver causing Cushing's syndrome: treatment with ketoconazole preceding an apparent surgical cure. *J. Clin. Endocrinol. Metab.* 60(1):21–28
Coutinho A, Prieto M. 1993. Ribonuclease T1 and alcohol dehydrogenase fluorescence quenching by acrylamide: A laboratory experiment for undergraduate students. *J. Chem. Educ.* 70(5):425
Coutinho A, Prieto M. 1995. Self-association of the polyene antibiotic nystatin in dipalmitoylphosphatidylcholine vesicles: a time-resolved fluorescence study. *Biophys. J.* 69(6):2541–57
Coutinho A, Prieto M. 2003. Cooperative partition model of nystatin interaction with phospholipid vesicles. *Biophys. J.* 84(5):3061–78
Coutinho A, Silva L, Fedorov A, Prieto M. 2004. Cholesterol and ergosterol influence nystatin surface aggregation: relation to pore formation. *Biophys. J.* 87(5):3264–76
Cowen LE, Singh SD, Köhler JR, Collins C, Zaas AK, Schell WA, Aziz H, Mylonakis E, Perfect JR, Whitesell L, Lindquist S. 2009. Harnessing Hsp90 function as a powerful, broadly effective therapeutic strategy for fungal infectious disease. *Proc. Natl. Acad. Sci. U. S. A.* 106(8):2818–23
Czabany T, Athenstaedt K, Daum G. 2007. Synthesis, storage and degradation of neutral lipids in yeast. *Biochim. Biophys. Acta - Mol. Cell Biol. Lipids*. 1771(3):299–309
Czub J, Baginski M. 2006. Modulation of Amphotericin B Membrane Interaction by Cholesterol and ErgosterolA Molecular Dynamics Study. *J. Phys. Chem. B*. 110(33):16743–53
Das A, Goldstein JL, Anderson DD, Brown MS, Radhakrishnan A. 2013. Use of mutant 125I-Perfringolysin O to probe transport and organization of cholesterol in membranes of animal cells. *Proc. Natl. Acad. Sci. U. S. A.* 110(26):10580–85
Daum G, Lees ND, Bard M, Dickson R. 1998. Biochemistry, Cell Biology and Molecular Biology of Lipids of Saccharomyces cerevisiae. *Yeast*. 14:1471–1510
Daum G, Tuller G, Nemec T, Hrastnik C, Balliano G, Cattel L, Milla P, Rocco F, Conzelmann A, Vionnet C, Kelly DE, Kelly S, Schweizer E, Schüller HJ, Hojad U, Greiner E, Finger K. 1999. Systematic analysis of yeast strains with possible defects in lipid metabolism. *Yeast*. 15(7):601–14
Davenport L. 1997. Fluorescence probes for studying membrane heterogeneity. *Methods Enzymol.* 278:487–512
de Almeida RFM. 2018. A route to understanding yeast cellular envelope – plasma membrane lipids interplaying in cell wall integrity. *FEBS J.* 285(13):2402–4
de Almeida RFM, Fedorov A, Prieto M. 2003. Sphingomyelin/phosphatidylcholine/cholesterol phase diagram: boundaries and composition of lipid rafts. *Biophys. J.* 85(4):2406–16
de Almeida RFM, Joly E. 2014. Crystallization around solid-like nanosized docks can explain the specificity, diversity, and stability of membrane microdomains. *Front. Plant Sci.* 5:72
de Almeida RFM, Loura LMS. 2004. *Tópicos de Biofísica de Membranas*. LIDEL ed.
de Almeida RFM, Loura LMS, Prieto M. 2009. Membrane lipid domains and rafts: current applications of fluorescence lifetime spectroscopy and imaging
de Almeida RFM, Santos FC, Marycz K, Alicka M, Krasowska A, Suchodolski J, Panek JJ, Jezierska A, Starosta R. 2019. New diphenylphosphane derivatives of ketoconazole are promising antifungal agents. *Sci. Rep.* 9(1):
De Granada-Flor A, Sousa C, Filipe HAL, Santos MSCS, De Almeida RFM. 2019. Quercetin dual interaction at the membrane

level. *Chem. Commun.* 55(12):1750–53
De Kruijff B, Demel RA. 1974. Polyene antibiotic-sterol interactions in membranes of Acholeplasma laidlawii cells and lecithin liposomes. III. Molecular structure of the polyene antibiotic-cholesterol complexes. *Biochim. Biophys. Acta - Biomembr.* 339(1):57–70
Dickson RC. 2008. New insights into sphingolipid metabolism and function in budding yeast. *J. Lipid Res.* 49(5):909–21
Dickson RC. 2010. Roles for Sphingolipids in Saccharomyces cerevisiae. *Adv. Exp. Med. Biol.* 688:217
Dickson RC, Lester RL. 1999. Yeast sphingolipids. *Biochim. Biophys. Acta - Gen. Subj.* 1426(2):347–57
Dickson RC, Lester RL. 2002. Sphingolipid functions in Saccharomyces cerevisiae. *Biochim. Biophys. Acta - Mol. Cell Biol. Lipids*. 1583(1):13–25
Dickson RC, Nagiec EE, Wells GB, Nagiec MM, Lester RL. 1997. Synthesis of mannose-(inositol-P)2-ceramide, the major sphingolipid in Saccharomyces cerevisiae, requires the IPT1 (YDR072c) gene. *J. Biol. Chem.* 272(47):29620–25
Donovick R, Gold W, Pagano JF, Stout HA. 1955. Amphotericins A and B, antifungal antibiotics produced by a streptomycete. I. In vitro studies. *Antibiot. Annu.* 3:579–86
dos Santos AG, Marquês JT, Carreira AC, Castro IR, Viana AS, Mingeot-Leclercq M-P, de Almeida RFM, Silva LC. 2017. The molecular mechanism of Nystatin action is dependent on the membrane biophysical properties and lipid composition. *Phys. Chem. Chem. Phys.* 19(44):30078–88
Douglas LM, Konopka JB. 2019. Plasma membrane architecture protects Candida albicans from killing by copper. *PLoS Genet.* 15(1):
Douglas LM, Wang HX, Keppler-Ross S, Dean N, Konopka JB. 2011. Sur7 promotes plasma membrane organization and is needed for resistance to stressful conditions and to the invasive growth and virulence of Candida albicans. *MBio*. 3(1):1–12
Dujon B. 2015. Basic principles of yeast genomics, a personal recollection. *FEMS Yeast Res.* 15(5):
Dupont S, Beney L, Ritt JF, Lherminier J, Gervais P. 2010. Lateral reorganization of plasma membrane is involved in the yeast resistance to severe dehydration. *Biochim. Biophys. Acta - Biomembr.* 1798(5):975–85
Dupont S, Fleurat-Lessard P, Cruz RG, Lafarge C, Grangeteau C, Yahou F, Gerbeau-Pissot P, Abrahão Júnior O, Gervais P, Simon-Plas F, Cayot P, Beney L. 2021. Antioxidant Properties of Ergosterol and Its Role in Yeast Resistance to Oxidation. *Antioxidants (Basel, Switzerland)*. 10(7):
Dynarowicz-Latka P, Wnętrzak A, Chachaj-Brekiesz A. 2024. Advantages of the classical thermodynamic analysis of single- and multi-component Langmuir monolayers from molecules of biomedical importance-theory and applications. *J. R. Soc. Interface.* 21(210):
Eftink MR, Ghiron CA. 1975. Dynamics of a protein matrix revealed by fluorescence quenching. *Proc. Natl. Acad. Sci.* 72(9):3290–94
Eisenkolb M, Zenzmaier C, Leitner E, Schneiter R. 2002. A specific structural requirement for ergosterol in long-chain fatty acid synthesis mutants important for maintaining raft domains in yeast. *Mol. Biol. Cell.* 13(12):4414–28
Ejsing CS, Sampaio JL, Surendranath V, Duchoslav E, Ekroos K, Klemm RW, Simons K, Shevchenko A. 2009. Global analysis of the yeast lipidome by quantitative shotgun mass spectrometry. *Proc. Natl. Acad. Sci. U. S. A.* 106(7):2136–41
Ellena JF, Archer SJ, Dominey RN, Hill BD, Cafiso DS. 1988. Localizing the nitroxide group of fatty acid and voltage-sensitive spin-labels in phospholipid bilayers. *Biochim. Biophys. Acta*. 940(1):63–70
El-Sayed SE, Abdelaziz NA, Osman H-EH, El-Housseiny GS, Aleissawy AE, Aboshanab KM. 2021. *Lysinibacillus* Isolate MK212927: A Natural Producer of Allylamine Antifungal 'Terbinafine'. *Molecules*. 27(1): 201-20
Elson EL, Fried E, Dolbow JE, Genin GM. 2010. Phase separation in biological membranes: integration of theory and experiment. *Annu. Rev. Biophys.* 39(1):207–26
Endress E, Bayerl S, Prechtel K, Maier C, Merkel R, Bayerl TM. 2002a. The Effect of Cholesterol, Lanosterol, and Ergosterol on Lecithin Bilayer Mechanical Properties at Molecular and Microscopic Dimensions: A Solid-State NMR and Micropipet Study. *Langmuir*. 18(8):3293–99
Endress E, Heller H, Casalta H, Brown MF, Bayerl TM. 2002b. Anisotropic motion and molecular dynamics of cholesterol, lanosterol, and ergosterol in lecithin bilayers studied by quasi-elastic neutron scattering. *Biochemistry*. 41(43):13078–86
Epstein S, Castillon GA, Qin Y, Riezman H. 2012. An essential function of sphingolipids in yeast cell division. *Mol. Microbiol.* 84(6):1018–32
Etymology of fungus by etymonline. https://www.etymonline.com/word/fungus. Accessed: 01/17/2024
Farnoud AM, Mor V, Singh A, Del Poeta M. 2014. Inositol phosphosphingolipid phospholipase C1 regulates plasma membrane ATPase (Pma1) stability in Cryptococcus neoformans. *FEBS Lett.* 588(21):3932–38
Florine-Casteel K, Feigenson GW. 1988. On the use of partition coefficients to characterize the distribution of fluorescent membrane probes between coexisting gel and fluid lipid phases: an analysis of the partition behavior of 1,6-diphenyl-1,3,5-hexatriene. *BBA - Biomembr.* 941(1):102–6
Fluorescence Polarization - BMG Labtech. https://www.bmglabtech.com/en/fluorescence-polarization/. Accessed: 05/22/2024
Folmer V, Pedroso N, Matias AC, Lopes SCDN, Antunes F, Cyrne L, Marinho HS. 2008. H2O2 induces rapid biophysical and permeability changes in the plasma membrane of Saccharomyces cerevisiae. *Biochim. Biophys. Acta*. 1778(4):1141–47
Frallicciardi J, Melcr J, Siginou P, Marrink SJ, Poolman B. 2022. Membrane thickness, lipid phase and sterol type are determining factors in the permeability of membranes to small solutes. *Nat. Commun. 2022 131*. 13(1):1–12
Friedman DZP, Schwartz IS. 2019. Emerging Fungal Infections: New Patients, New Patterns, and New Pathogens. *J. fungi (Basel, Switzerland)*. 5(3):
Fromherz P, Hübener G, Kuhn B, Hinner MJ. 2008. ANNINE-6plus, a voltage-sensitive dye with good solubility, strong membrane binding and high sensitivity. *Eur. Biophys. J.* . 37(4):509
Fujita M, Umemura M, Yoko-O T, Jigami Y. 2006. PER1 Is Required for GPI-Phospholipase A2 Activity and Involved in Lipid Remodeling of GPI-anchored Proteins. *Mol. Biol. Cell.* 17(12):5253
Fungal Diseases - CDC. https://www.cdc.gov/fungal/index.html. Accessed: 01/22/2024
Gaigg B, Timischl B, Corbino L, Schneiter R. 2005. Synthesis of sphingolipids with very long chain fatty acids but not

ergosterol is required for routing of newly synthesized plasma membrane ATPase to the cell surface of yeast. *J. Biol. Chem.* 280(23):22515–22

Gaigg B, Toulmay A, Schneiter R. 2006. Very long-chain fatty acid-containing lipids rather than sphingolipids per se are required for raft association and stable surface transport of newly synthesized plasma membrane ATPase in yeast. *J. Biol. Chem.* 281(45):34135–45

Galván-Hernández A, Kobayashi N, Hernández-Cobos J, Antillón A, Nakabayashi S, Ortega-Blake I. 2020. Morphology and dynamics of domains in ergosterol or cholesterol containing membranes. *Biochim. Biophys. Acta - Biomembr.* 1862(2):183101

García Rodrĭguez LA, Duque A, Castellsague J, Pérez-Gutthann S, Stricker BHC. 1999. A cohort study on the risk of acute liver injury among users of ketoconazole and other antifungal drugs. *Br. J. Clin. Pharmacol.* 48(6):847–52

Gatta AT, Wong LH, Sere YY, Calderón-Noreña DM, Cockcroft S, Menon AK, Levine TP. 2015. A new family of StART domain proteins at membrane contact sites has a role in ER-PM sterol transport. *Elife.* 4(MAY):1–46

Gerstle Z, Desai R, Veatch SL. 2018. Giant Plasma Membrane Vesicles: an Experimental Tool for Probing the Effects of Drugs and other Conditions on Membrane Domain Stability. *Methods Enzymol.* 603:129

Golfetto O, Hinde E, Gratton E. 2013. Laurdan fluorescence lifetime discriminates cholesterol content from changes in fluidity in living cell membranes. *Biophys. J.* 104(6):1238–47

Goñi FM, Sot J, Alonso A. 2014. Biophysical properties of sphingosine, ceramides and other simple sphingolipids. *Biochem. Soc. Trans.* 42(5):1401–8

González-Damián J, Ortega-Blake I. 2010. Effect of membrane structure on the action of polyenes II: nystatin activity along the phase diagram of ergosterol- and cholesterol-containing POPC membranes. *J. Membr. Biol.* 237(1):41–49

Gournas C, Gkionis S, Carquin M, Twyffels L, Tyteca D, André B. 2018. Conformation-dependent partitioning of yeast nutrient transporters into starvation-protective membrane domains. *Proc. Natl. Acad. Sci. U. S. A.* 115(14):E3145–54

Gow NAR, Latge J-P, Munro CA. 2017. The Fungal Cell Wall: Structure, Biosynthesis, and Function. *Microbiol. Spectr.* 5(3):

Gross E, Bedlack RS, Loew LM. 1994. Dual-wavelength ratiometric fluorescence measurement of the membrane dipole potential. *Biophys. J.* 67(1):208

Grossmann G, Malinsky J, Stahlschmidt W, Loibl M, Weig-Meckl I, Frommer WB, Opekarová M, Tanner W. 2008. Plasma membrane microdomains regulate turnover of transport proteins in yeast. *J. Cell Biol.* 183(6):1075

Grossmann G, Opekarová M, Malinsky J, Weig-Meckl I, Tanner W. 2007. Membrane potential governs lateral segregation of plasma membrane proteins and lipids in yeast. *EMBO J.* 26(1):1–8

Guan XL, Souza CM, Pichler H, Dewhurst G, Schaad O, Kajiwara K, Wakabayashi H, Ivanova T, Castillon GA, Piccolis M, Abe F, Loewith R, Funato K, Wenk MR, Riezman H. 2009. Functional interactions between sphingolipids and sterols in biological membranes regulating cell physiology. *Mol. Biol. Cell.* 20(7):2083–95

Guan XL, Wenk MR. 2006. Mass spectrometry-based profiling of phospholipids and sphingolipids in extracts from Saccharomyces cerevisiae. *Yeast.* 23(6):465–77

Hąc-Wydro K, Dynarowicz-Łatka P. 2006. Interaction between nystatin and natural membrane lipids in Langmuir monolayers--the role of a phospholipid in the mechanism of polyenes mode of action. *Biophys. Chem.* 123(2–3):154–61

Hąc-Wydro K, Dynarowicz-Łątka P, Grzybowska J, Borowski E. 2005. How does the N-acylation and esterification of amphotericin B molecule affect its interactions with cellular membrane components-the Langmuir monolayer study. *Colloids Surf. B. Biointerfaces.* 46(1):7–19

Haldar S, Kanaparthi RK, Samanta A, Chattopadhyay A. 2012. Differential effect of cholesterol and its biosynthetic precursors on membrane dipole potential. *Biophys. J.* 102(7):1561–69

Hamann S, Kiilgaard JF, Litman T, Alvarez-Leefmans FJ, Winther BR, Zeuthen T. 2002. Measurement of Cell Volume Changes by Fluorescence Self-Quenching. *J. Fluoresc.* 12(2):139–45

Hartkamp R, Moore TC, Iacovella CR, Thompson MA, Bulsara PA, Moore DJ, McCabe C. 2016. Investigating the Structure of Multicomponent Gel-Phase Lipid Bilayers. *Biophys. J.* 111(4):813–23

Haynes MP, Chong PLG, Buckley HR, Pieringer RA. 1996. Fluorescence studies on the molecular action of amphotericin B on susceptible and resistant fungal cells. *Biochemistry.* 35(24):7983–92

Hazen EL, Brown R. 1951. Fungicidin, an antibiotic produced by a soil actinomycete. *Proc. Soc. Exp. Biol. Med.* 76(1):93–97

Heeres J, Backx LJJ, Mostmans JH, Van Cutsem J. 1979. Antimycotic imidazoles. part 4. Synthesis and antifungal activity of ketoconazole, a new potent orally active broad-spectrum antifungal agent. *J. Med. Chem.* 22(8):1003–5

Heese-Peck A, Pichler H, Zanolari B, Watanabe R, Daum G, Riezman H. 2002. Multiple functions of sterols in yeast endocytosis. *Mol. Biol. Cell.* 13(8):2664–80

Henriksen J, Rowat AC, Brief E, Hsueh YW, Thewalt JL, Zuckermann MJ, Ipsen JH. 2006. Universal Behavior of Membranes with Sterols. *Biophys. J.* 90(5):1639

Herman P, Vecer J, Opekarova M, Vesela P, Jancikova I, Zahumensky J, Malinsky J. 2015. Depolarization affects the lateral microdomain structure of yeast plasma membrane. *FEBS J.* 282(3):419–34

Hildenbrand MF, Bayerl TM. 2005. Differences in the modulation of collective membrane motions by ergosterol, lanosterol, and cholesterol: a dynamic light scattering study. *Biophys. J.* 88(5):3360–67

Hoenigl M, Sprute R, Egger M, Arastehfar A, Cornely OA, Krause R, Lass-Flörl C, Prattes J, Spec A, Thompson GR, Wiederhold N, Jenks JD. 2021. The Antifungal Pipeline: Fosmanogepix, Ibrexafungerp, Olorofim, Opelconazole, and Rezafungin. *Drugs.* 81(15):1703–29

Holz R, Finkelstein A. 1970. The Water and Nonelectrolyte Permeability Induced in Thin Lipid Membranes by the Polyene Antibiotics Nystatin and Amphotericin B. *J. Gen. Physiol.* 56(1):125–45

Holz RW. 1974. The effects of the polyene antibiotics nystatin and amphotericin B on thin lipid membranes. *Ann. N. Y. Acad. Sci.* 235(0):469–79

Hsueh YW, Zuckermann M, Thewalt J. 2005. Phase diagram determination for phospholipid/sterol membranes using deuterium NMR. *Concepts Magn. Reson. Part A.* 26A(1):35–46

Huang J, Buboltz JT, Feigenson GW. 1999. Maximum solubility of cholesterol in phosphatidylcholine and phosphatidylethanolamine bilayers. *Biochim. Biophys. Acta*. 1417(1):89–100

Huang Y, Xing J, Gong Q, Chen LC, Liu G, Yao C, Wang Z, Zhang HL, Chen Z, Zhang Q. 2019. Reducing aggregation caused quenching effect through co-assembly of PAH chromophores and molecular barriers. *Nat. Commun. 2019 101*. 10(1):1–9

Huang Z, Haugland RP. 1991. Partition coefficients of fluorescent probes with phospholipid membranes. *Biochem. Biophys. Res. Commun.* 181(1):166–71

Hung WC, Lee MT, Chung H, Sun YT, Chen H, Charron NE, Huang HW. 2016. Comparative Study of the Condensing Effects of Ergosterol and Cholesterol. *Biophys. J.* 110(9):2026

Ikeda M, Kihara A, Igarashi Y. 2006. Lipid asymmetry of the eukaryotic plasma membrane: functions and related enzymes. *Biol. Pharm. Bull.* 29(8):1542–46

Invasive Candidiasis - CDC. https://www.cdc.gov/fungal/diseases/Candidiasis/invasive/. Accessed: 01/17/2024

Iwamoto K, Kobayashi S, Fukuda R, Umeda M, Kobayashi T, Ohta A. 2004. Local exposure of phosphatidylethanolamine on the yeast plasma membrane is implicated in cell polarity. *Genes Cells*. 9(10):891–903

Jarvis JN, Lawrence DS, Meya DB, Kagimu E, Kasibante J, Mpoza E, Rutakingirwa MK, Ssebambulidde K, Tugume L, Rhein J, Boulware DR, Mwandumba HC, Moyo M, Mzinganjira H, Kanyama C, Hosseinipour MC, Chawinga C, Meintjes G, Schutz C, Comins K, Singh A, Muzoora C, Jjunju S, Nuwagira E, Mosepele M, Leeme T, Siamisang K, Ndhlovu CE, Hlupeni A, Mutata C, van Widenfelt E, Chen T, Wang D, Hope W, Boyer-Chammard T, Loyse A, Molloy SF, Youssouf N, Lortholary O, Lalloo DG, Jaffar S, Harrison TS. 2022. Single-Dose Liposomal Amphotericin B Treatment for Cryptococcal Meningitis. *N. Engl. J. Med.* 386(12):1109–20

Jeffery-Smith A, Taori SK, Schelenz S, Jeffery K, Johnson EM, Borman A, Manuel R, Browna CS. 2017. Candida auris: a Review of the Literature. *Clin. Microbiol. Rev.* 31(1):

Johnston EJ, Moses T, Rosser SJ. 2020. The wide-ranging phenotypes of ergosterol biosynthesis mutants, and implications for microbial cell factories. *Yeast*. 37(1):27–44

Jordá T, Puig S. 2020. Regulation of Ergosterol Biosynthesis in Saccharomyces cerevisiae. *Genes (Basel)*. 11(7):1–18

Jouhet J. 2013. Importance of the hexagonal lipid phase in biological membrane organization. *Front. Plant Sci.* 4(DEC):70496

Kaiser RD, London E. 1998. Location of diphenylhexatriene (DPH) and its derivatives within membranes: comparison of different fluorescence quenching analyses of membrane depth. *Biochemistry*. 37(22):8180–90

Kane PM. 2016. Proton Transport and pH Control in Fungi. *Adv. Exp. Med. Biol.* 892:33–68

Kawabata M, Onda M, Mita T. 2001. Effect of aggregation of amphotericin B on lysophosphatidylcholine micelles as related to its complex formation with cholesterol or ergosterol. *J. Biochem.* 129(5):725–32

Khan A, McQuilken M, Gladfelter AS. 2015. Septins and Generation of Asymmetries in Fungal Cells. *Annu. Rev. Microbiol.* 69(1):487–503

Khmelinskaia A, Ibarguren M, De Almeida RFM, López DJ, Paixão VA, Ahyayauch H, Goñi FM, Escribá P V. 2014. Changes in membrane organization upon spontaneous insertion of 2-hydroxylated unsaturated fatty acids in the lipid bilayer. *Langmuir*. 30(8):2117–28

Khmelinskaia A, Marquês JMT, Bastos AEP, Antunes CAC, Bento-Oliveira A, Scolari S, Lobo GM da S, Malhó R, Herrmann A, Marinho HS, De Almeida RF. 2020. Liquid-ordered phase formation by mammalian and yeast sterols: a common feature with organizational differences. *Front. Cell Dev. Biol.* 8:337

Kjeldsen T, Andersen AS, Hubálek F, Johansson E, Kreiner FF, Schluckebier G, Kurtzhals P. 2023. Molecular engineering of insulin for recombinant expression in yeast. *Trends Biotechnol.*

Klose C, Ejsing CS, García-Sáez AJ, Kaiser HJ, Sampaio JL, Surma MA, Shevchenko A, Schwille P, Simons K. 2010. Yeast Lipids Can Phase-separate into Micrometer-scale Membrane Domains. *J. Biol. Chem.* 285(39):30224

Klug L, Daum G. 2014. Yeast lipid metabolism at a glance. *FEMS Yeast Res.* 14(3):369–88

Knight TE, Shikuma CY, Knight J. 1991. Ketoconazole-induced fulminant hepatitis necessitating liver transplantation. *J. Am. Acad. Dermatol.* 25(2 Pt 2):398–400

Kock C, Arlt H, Ungermann C, Heinisch JJ. 2016. Yeast cell wall integrity sensors form specific plasma membrane microdomains important for signalling. *Cell. Microbiol.* 18(9):1251–67

Kohli A, Smriti, Mukhopadhyay K, Rattan A, Prasad R. 2002. In Vitro Low-Level Resistance to Azoles in Candida albicans Is Associated with Changes in Membrane Lipid Fluidity and Asymmetry. *Antimicrob. Agents Chemother.* 46(4):1046

Komor E, Weber H, Tanner W. 1979. Greatly decreased susceptibility of nonmetabolizing cells towards detergents. *Proc. Natl. Acad. Sci. U. S. A.* 76(4):1814–18

Kulagina N, Besseau S, Godon C, Goldman GH, Papon N, Courdavault V. 2021. Yeasts as Biopharmaceutical Production Platforms. *Front. Fungal Biol.* 2:733492

Kumar R, Kumar P. 2019. Yeast-based vaccines: New perspective in vaccine development and application. *FEMS Yeast Res.* 19(2):7

Lakowicz JR. 2006. Principles of fluorescence spectroscopy. , pp. 530–73. New York: Springer. 3rd ed. ed.

Lance MR, Washington C, Davis SS. 1996. Evidence for the formation of amphotericin B-phospholipid complexes in Langmuir monolayers. *Pharm. Res.* 13(7):1008–14

Lange Y, Swaisgood MH, Ramos B V., Steck TL. 1989. Plasma membranes contain half the phospholipid and 90% of the cholesterol and sphingomyelin in cultured human fibroblasts. *J. Biol. Chem.* 264(7):3786–93

Langlet J, Bergès J, Caillet J, Demaret JP. 1994. Theoretical study of the complexation of amphotericin B with sterols. *Biochim. Biophys. Acta*. 1191(1):79–93

Larkin E, Hager C, Chandra J, Mukherjee PK, Retuerto M, Salem I, Long L, Isham N, Kovanda L, Borroto-Esoda K, Wring S, Angulo D, Ghannoum M. 2017. The Emerging Pathogen Candida auris: Growth Phenotype, Virulence Factors, Activity of Antifungals, and Effect of SCY-078, a Novel Glucan Synthesis Inhibitor, on Growth Morphology and Biofilm Formation. *Antimicrob. Agents Chemother.* 61(5):

Launay M, Tripier M, Guizerix J, Viriot ML, Andre JC. 1980. Pyranine used as a fluorescent tracer in hydrology: pH effects

in determination of its concentration. *J. Hydrol.* 46(3–4):377–83
Lauwers E, André B. 2006. Association of yeast transporters with detergent-resistant membranes correlates with their cell-surface location. *Traffic*. 7(8):1045–59
Lauwers E, Grossmann G, André B. 2007. Evidence for coupled biogenesis of yeast Gap1 permease and sphingolipids: Essential role in transport activity and normal control by ubiquitination. *Mol. Biol. Cell*. 18(8):3068–80
Learmonth RP, Gratton E. 2002. Assessment of Membrane Fluidity in Individual Yeast Cells by Laurdan Generalised Polarisation and Multi-photon Scanning Fluorescence Microscopy. . 241–52
Leber A, Fischer P, Schneiter R, Kohlwein SD, Daum G. 1997. The yeast mic2 mutant is defective in the formation of mannosyl-diinositolphosphorylceramide. *FEBS Lett.* 411(2–3):211–14
Lee MCS, Hamamoto S, Schekman R. 2002. Ceramide biosynthesis is required for the formation of the oligomeric H+-ATPase Pma1p in the yeast endoplasmic reticulum. *J. Biol. Chem.* 277(25):22395–401
Lentz BR. 1988. Membrane "Fluidity" From Fluorescence Anisotropy Measurements. In *Spectroscopic Membrane Probes*, ed. LM Loew, p. 41. Boca Raton, USA: CRC Press
Levental I, Levental KR, Heberle FA. 2020. Lipid Rafts: Controversies Resolved, Mysteries Remain. *Trends Cell Biol.* 30(5):341–53
Levitan I. 2021. Evaluating membrane structure by Laurdan imaging: Disruption of lipid packing by oxidized lipids. *Curr. Top. Membr.* 88:235
Loew LM. 1988. How to Choose a Potentiometric Membrane Probe. In *Spectroscopic Membrane Probes Volume 2*, pp. 139–51. Boca Raton: CRC Press
Loew LM. 1996. Potentiometric dyes: Imaging electrical activity of cell membranes. *Pure Appl. Chem.* 68(7):1405–9
London E, Chattopadhyay A. 1987. Parallax Method for Direct Measurement of Membrane Penetration Depth Utilizing Fluorescence Quenching by Spin-Labeled Phospholipids. *Biochemistry*. 26(1):39–45
Loose DS, Kan PB, Hirst MA, Marcus RA, Feldman D. 1983. Ketoconazole blocks adrenal steroidogenesis by inhibiting cytochrome P450-dependent enzymes. *J. Clin. Invest.* 71(5):1495
Lopez S, Rodriguez-Gallardo S, Sabido-Bozo S, Muñiz M. 2019. Endoplasmic Reticulum Export of GPI-Anchored Proteins. *Int. J. Mol. Sci.* 20(14):
Loura LMS, de Almeida RFM, Coutinho A, Prieto M. 2003. Interaction of peptides with binary phospholipid membranes: application of fluorescence methodologies. *Chem. Phys. Lipids*. 122(1–2):77–96
Malínská K, Malínský J, Opekarová M, Tanner W. 2003. Visualization of protein compartmentation within the plasma membrane of living yeast cells. *Mol. Biol. Cell*. 14(11):4427–36
Malinsky J, Opekarová M. 2016. New Insight Into the Roles of Membrane Microdomains in Physiological Activities of Fungal Cells. In *International Review of Cell and Molecular Biology*, Vol. 325, pp. 119–80
Malinsky J, Opekarová M, Grossmann G, Tanner W. 2013. Membrane Microdomains, Rafts, and Detergent-Resistant Membranes in Plants and Fungi. *https://doi.org/10.1146/annurev-arplant-050312-120103*. 64:501–29
Malinsky J, Tanner W, Opekarova M. 2016. Transmembrane voltage: Potential to induce lateral microdomains. *Biochim. Biophys. Acta*. 1861(8 Pt B):806–11
Mannock DA, Lewis RNAH, McElhaney RN. 2010. A calorimetric and spectroscopic comparison of the effects of ergosterol and cholesterol on the thermotropic phase behavior and organization of dipalmitoylphosphatidylcholine bilayer membranes. *Biochim. Biophys. Acta - Biomembr.* 1798(3):376–88
Mañuel M, Howard R. 2016. Trafficking of glycosylphosphatidylinositol anchored proteins from the endoplasmic reticulum to the cell surface. *J. Lipid Res.* 57(3):352–60
Manuel Nuno M, B., Miguel A. R. C. 2007. Omiganan interaction with bacterial membranes and cell wall models. Assigning a biological role to saturation. *Biochim. Biophys. Acta*. 1768(5):1277–90
Marquês JT, Antunes CAC, Santos FC, de Almeida RFM. 2015a. Biomembrane Organization and Function: The Decisive Role of Ordered Lipid Domains. In *Advances in Planar Lipid Bilayers and Liposomes*, Vol. 22, pp. 65–96. Elsevier B.V.
Marquês JT, Cordeiro AM, Viana AS, Herrmann A, Marinho HS, de Almeida RFM. 2015b. Formation and Properties of Membrane-Ordered Domains by Phytoceramide: Role of Sphingoid Base Hydroxylation. *Langmuir*. 31(34):9410–21
Marquês JT, Marinho HS, de Almeida RFM. 2018. Sphingolipid hydroxylation in mammals, yeast and plants – An integrated view. *Prog. Lipid Res.* 71:18–42
Marsh D. 2012. *Handbook of Lipid Bilayers*. Boca Raton FL.: CRC Press Taylor & Francis Group. 2nd ed. ed.
Martinho N, Marquês JMT, Todoriko I, Prieto M, de Almeida RFM, Silva LC. 2023. Effect of Cisplatin and Its Cationic Analogues in the Phase Behavior and Permeability of Model Lipid Bilayers. *Mol. Pharm.* 20(2):918–28
Marty A, Finkelstein A. 1975. Pores formed in lipid bilayer membranes by nystatin, Differences in its one-sided and two-sided action. *J. Gen. Physiol.* 65(4):515–26
Mateo CR, Acuña AU, Brochon JC. 1995. Liquid-crystalline phases of cholesterol/lipid bilayers as revealed by the fluorescence of trans-parinaric acid. *Biophys. J.* 68(3):978–87
Mateo CR, Brochon JC, Lillo MP, Acuña AU. 1993. Lipid clustering in bilayers detected by the fluorescence kinetics and anisotropy of trans-parinaric acid. *Biophys. J.* 65(5):2237–47
Mátyus L, Szöllosi J, Jenei A. 2006. Steady-state fluorescence quenching applications for studying protein structure and dynamics. *J. Photochem. Photobiol. B Biol.* 83(3):223–36
Mazeres S, Joly E, Lopez A, Tardin C. 2014. Characterization of M-laurdan, a versatile probe to explore order in lipid membranes. *F1000Research*. 3:
Megyeri M, Riezman H, Schuldiner M, Futerman AH. 2016. Making Sense of the Yeast Sphingolipid Pathway. *J. Mol. Biol.* 428(24 Pt A):4765–75
Meyer T, Baek DJ, Bittman R, Haralampiev I, Müller P, Herrmann A, Huster D, Scheidt HA. 2014. Membrane properties of cholesterol analogs with an unbranched aliphatic side chain. *Chem. Phys. Lipids*. 184:e1–6
Mishra NN, Prasad T, Sharma N, Gupta DK. 2008. Membrane fluidity and lipid composition of fluconazole resistant and

susceptible strains of Candida albicans isolated from diabetic patients. *Brazilian J. Microbiol.* 39(2):219
Mitra K, Ubarretxena-Belandia I, Taguchi T, Warren G, Engelman DM. 2004. Modulation of the bilayer thickness of exocytic pathway membranes by membrane proteins rather than cholesterol. *Proc. Natl. Acad. Sci. U. S. A.* 101(12):4083–88
Mitrofanova VG, Shenin ID, Mirgorodskaia O, Derzhavets AA, Matveeva E, Grinberg GE, Apter IM, Golubkova L. 1991. [Determination of nystatin component composition using HPLC and TLC with densitometry]. *Antibiot. i khimioterapiia = Antibiot. chemoterapy [sic]*
Montana V, Farkas DL, Loew LM. 1989. Dual-wavelength ratiometric fluorescence measurements of membrane potential. *Biochemistry*. 28(11):4536–39
Montañés FM, Pascual-Ahuir A, Proft M. 2011. Repression of ergosterol biosynthesis is essential for stress resistance and is mediated by the Hog1 MAP kinase and the Mot3 and Rox1 transcription factors. *Mol. Microbiol.* 79(4):1008–23
Moreno-Bello M, Bonilla-Marín M, González-Beltrán C. 1988. Distribution of pore sizes in black lipid membranes treated with nystatin. *Biochim. Biophys. Acta*. 944(1):97–100
Moreno MJ, Bastos M, Velazquez-Campoy A. 2010. Partition of amphiphilic molecules to lipid bilayers by isothermal titration calorimetry. *Anal. Biochem.* 399(1):44–47
Morio F, Loge C, Besse B, Hennequin C, Le Pape P. 2010. Screening for amino acid substitutions in the Candida albicans Erg11 protein of azole-susceptible and azole-resistant clinical isolates: new substitutions and a review of the literature. *Diagn. Microbiol. Infect. Dis.* 66(4):373–84
Mota Fernandes C, Del Poeta M. 2020. Fungal sphingolipids: role in the regulation of virulence and potential as targets for future antifungal therapies. *Expert Rev. Anti. Infect. Ther.* 18(11):1083–92
Mukhopadhyay K, Prasad T, Saini P, Pucadyil TJ, Chattopadhyay A, Prasad R. 2004. Membrane sphingolipid-ergosterol interactions are important determinants of multidrug resistance in Candida albicans. *Antimicrob. Agents Chemother.* 48(5):1778–87
Muñoz P, Bouza E, Cuenca-Estrella M, Eiros JM, Pérez MJ, Sánchez-Somolinos M, Rincón C, Hortal J, Peláez T. 2005. Saccharomyces cerevisiae fungemia: An emerging infectious disease. *Clin. Infect. Dis.* 40(11):1625–34
Munshi MA, Gardin JM, Singh A, Luberto C, Rieger R, Bouklas T, Fries BC, Del Poeta M. 2018. The Role of Ceramide Synthases in the Pathogenicity of Cryptococcus neoformans. *Cell Rep.* 22(6):1392–1400
Murley A, Yamada J, Niles BJ, Toulmay A, Prinz WA, Powers T, Nunnari J. 2017. Sterol transporters at membrane contact sites regulate TORC1 and TORC2 signaling. *J. Cell Biol.* 216(9):2679
Naftalovich S, Yefenof E, Eilam Y. 1991. Antitumor effects of ketoconazole and trifluoperazine in murine T-cell lymphomas. *Cancer Chemother. Pharmacol.* 28(5):384–90
Nizoral® Anti-Dandruff Shampoo - Ketoconazole 1%. https://nizoral.com/. Accessed: 02/20/2024
Nystatin Cream: Package Insert - Drugs.com. https://www.drugs.com/pro/nystatin-cream.html. Accessed: 07/17/2023
Nystatin Uses, Side Effects & Warnings - Drugs.com. https://www.drugs.com/mtm/nystatin.html. Accessed: 07/17/2023
Oliveira ON, Caseli L, Ariga K. 2022. The Past and the Future of Langmuir and Langmuir-Blodgett Films. *Chem. Rev.* 122(6):6459–6513
Park C, Lee DG. 2009. Fungicidal effect of antimicrobial peptide arenicin-1. *Biochim. Biophys. Acta - Biomembr.* 1788(9):1790–96
Patel V, Liaw B, Oh W. 2018. The role of ketoconazole in current prostate cancer care. *Nat. Rev. Urol.* 15(10):643–51
PathBank - Bloch pathway (Cholesterol Biosynthesis) Homo sapiens. http://pathbank.org/view/SMP0121057. Accessed: 02/05/2024
Patton JL, Lester RL. 1991. The phosphoinositol sphingolipids of Saccharomyces cerevisiae are highly localized in the plasma membrane. *J. Bacteriol.* 173(10):3101
Pedroso N, Matias AC, Cyrne L, Antunes F, Borges C, Malhó R, de Almeida RFM, Herrero E, Marinho HS. 2009. Modulation of plasma membrane lipid profile and microdomains by H2O2 in Saccharomyces cerevisiae. *Free Radic. Biol. Med.* 46(2):289–98
Pérez-Torrado R, Querol A. 2016. Opportunistic Strains of Saccharomyces cerevisiae: A Potential Risk Sold in Food Products. *Front. Microbiol.* 6:1522
Pike LJ, 2006. Rafts defined: a report on the Keystone symposium on lipid rafts and cell function. *J. Lipid Res.* 47(7):1597-98
Pinto SN, Silva LC, De Almeida RFM, Prieto M. 2008. Membrane domain formation, interdigitation, and morphological alterations induced by the very long chain asymmetric C24:1 ceramide. *Biophys. J.* 95(6):2867–79
Pinto SN, Silva LC, Futerman AH, Prieto M. 2011. Effect of ceramide structure on membrane biophysical properties: The role of acyl chain length and unsaturation. *Biochim. Biophys. Acta - Biomembr.* 1808(11):2753–60
Plesofsky NS, Levery SB, Castle SA, Brambl R. 2008. Stress-induced cell death is mediated by ceramide synthesis in Neurospora crassa. *Eukaryot. Cell*. 7(12):2147–59
Płotek M, Starosta R, Komarnicka UK, Skórska-Stania A, Jezowska-Bojczuk M, Stochel G, Kyzioł A. 2015. New ruthenium(II) coordination compounds possessing bidentate aminomethylphosphane ligands: synthesis, characterization and preliminary biological study in vitro. *Dalt. Trans.* 44(31):13969–78
Polak A. 1983. Antifungal activity in vitro of Ro 14-4767/002, a phenylpropyl-morpholine. *Sabouraudia*. 21(3):205–13
Polak A, Scholer HJ. 1975. Mode of action of 5-fluorocytosine and mechanisms of resistance. *Chemotherapy*. 21(3–4):113–30
Pont A. 1987. Long-term experience with high dose ketoconazole therapy in patients with stage D2 prostatic carcinoma. *J. Urol.* 137(5):902–4
Rajakumari S, Grillitsch K, Daum G. 2008. Synthesis and turnover of non-polar lipids in yeast. *Prog. Lipid Res.* 47(3):157–71
Ratto T V., Longo ML. 2002. Obstructed diffusion in phase-separated supported lipid bilayers: A combined atomic force microscopy and fluorescence recovery after photobleaching approach. *Biophys. J.* 83(6):3380–92
RCSB PDB - 5FSA: Crystal structure of sterol 14-alpha demethylase (CYP51) from a pathogenic yeast Candida albicans in complex with the antifungal drug posaconazole. https://www.rcsb.org/structure/5fsa. Accessed: 10/15/2021
Récamier KS, Hernández-Gómez A, González-Damián J, Ortega-Blake I. 2010. Effect of membrane structure on the action of

polyenes: I. Nystatin action in cholesterol- and ergosterol-containing membranes. *J. Membr. Biol.* 237(1):31–40
Rego A, Trindade D, Chaves SR, Manon S, Costa V, Sousa MJ, Côrte-Real M. 2014. The yeast model system as a tool towards the understanding of apoptosis regulation by sphingolipids. *FEMS Yeast Res.* 14(1):160–78
Reinhard J, Leveille CL, Cornell CE, Merz AJ, Klose C, Ernst R, Keller SL. 2023. Remodeling of yeast vacuole membrane lipidomes from the log (one phase) to stationary stage (two phases). *Biophys. J.* 122(6):1043–57
Reinhard J, Starke L, Klose C, Haberkant P, Hammarén H, Stein F, Klein O, Berhorst C, Stumpf H, Sáenz JP, Hub J, Schuldiner M, Ernst R. 2022. A new technology for isolating organellar membranes provides fingerprints of lipid bilayer stress. *bioRxiv*. 2022.09.15.508072
Richardson K, Cooper K, Marriott MS, Tarbit MH, Troke PF, Whittle PJ. 1988. Design and evaluation of a systemically active agent, fluconazole. *Ann. N. Y. Acad. Sci.* 544(1):4–11
Robbins N, Uppuluri P, Nett J, Rajendran R, Ramage G, Lopez-Ribot JL, Andes D, Cowen LE. 2011. Hsp90 governs dispersion and drug resistance of fungal biofilms. *PLoS Pathog.* 7(9):
Rochlitz CF, Damon LE, Russi MB, Geddes A, Cadman EC. 1988. Cytotoxicity of ketoconazole in malignant cell lines. *Cancer Chemother. Pharmacol.* 21(4):319–22
Rodrigues ML. 2018. The Multifunctional Fungal Ergosterol. *MBio*. 9(5):
Roelants FM, Leskoske KL, Marshall MNM, Locke MN, Thorner J. 2017. The TORC2-Dependent Signaling Network in the Yeast Saccharomyces cerevisiae. *Biomolecules*. 7(3):
Rojewska M, Smułek W, Kaczorek E, Prochaska K. 2021. Langmuir Monolayer Techniques for the Investigation of Model Bacterial Membranes and Antibiotic Biodegradation Mechanisms. *Membranes (Basel).* 11(9):
Rybak JM, Barker KS, Muñoz JF, Parker JE, Ahmad S, Mokaddas E, Abdullah A, Elhagracy RS, Kelly SL, Cuomo CA, Rogers PD. 2022. In vivo emergence of high-level resistance during treatment reveals the first identified mechanism of amphotericin B resistance in Candida auris. *Clin. Microbiol. Infect.* 28(6):838–43
Saccharomyces Genome Database - SGD. https://www.yeastgenome.org/. Accessed: 01/17/2024
Sáenz JP, Sezgin E, Schwille P, Simons K. 2012. Functional convergence of hopanoids and sterols in membrane ordering. *Proc. Natl. Acad. Sci. U. S. A.* 109(35):14236–40
Sanglard D, Coste A, Ferrari S. 2009. Antifungal drug resistance mechanisms in fungal pathogens from the perspective of transcriptional gene regulation. *FEMS Yeast Res.* 9(7):1029–50
Santos FC, Fernandes AS, Antunes CAC, Moreira FP, Videira A, Marinho HS, de Almeida RFM. 2017. Reorganization of plasma membrane lipid domains during conidial germination. *Biochim. Biophys. Acta* . 1862(2):156–66
Santos FC, Lobo GM, Fernandes AS, Videira A, De Almeida RFM. 2018. Changes in the biophysical properties of the cell membrane are involved in the response of neurospora crassa to staurosporine. *Front. Physiol.* 9(OCT):
Santos FC, Marquês JT, Bento-Oliveira A, de Almeida RFM. 2020. Sphingolipid-enriched domains in fungi. *FEBS Lett.* 594(22):3698–3718
Santos NC, Prieto M, Castanho MARB. 2003. Quantifying molecular partition into model systems of biomembranes: An emphasis on optical spectroscopic methods
Sarkis J, Vié V. 2020. Biomimetic Models to Investigate Membrane Biophysics Affecting Lipid–Protein Interaction. *Front. Bioeng. Biotechnol.* 8:513398
Sarmento MJ, Ricardo JC, Amaro M, Sachl R, J Sarmento CM, Sachl R, Heyrovsk J. 2020. Organization of gangliosides into membrane nanodomains. *FEBS Lett.* 594(22):3668–97
Schweizer T, Kubach H, Koch · Thomas. 2021. Investigations to characterize the interactions of light radiation, engine operating media and fluorescence tracers for the use of qualitative light-induced fluorescence in engine systems. *Automot. Engine Technol. 2021 63*. 6(3):275–87
Serrano R. 1991. Transport across yeast vacuolar and plasma membrane. In *The Molecular and Cellular Biology of the Yeast Saccharomyces: Genome Dynamics, Protein Synthesis, and Energetics*, eds. JR Broach, EW Jones, P J.R., pp. 523–85. NY, USA: Cold Spring Harbor Laboratory Press
Sezgin E, Levental I, Mayor S, Eggeling C. 2017. The mystery of membrane organization: composition, regulation and roles of lipid rafts. *Nat. Rev. Mol. Cell Biol. 2017 186*. 18(6):361–74
Shakoury-Elizeh M, Protchenko O, Berger A, Cox J, Gable K, Dunn TM, Prinz WA, Bard M, Philpott CC. 2010. Metabolic Response to Iron Deficiency in Saccharomyces cerevisiae. *J. Biol. Chem.* 285(19):14823
Sherry L, Ramage G, Kean R, Borman A, Johnson EM, Richardson MD, Rautemaa-Richardson R. 2017. Biofilm-Forming Capability of Highly Virulent, Multidrug-Resistant Candida auris. *Emerg. Infect. Dis.* 23(2):328–31
Shimokawa O, Niimi M, Kikuchi K, Saito M, Kajiwara H, Yoshida SI. 2005. Relationship between MIC and Minimum Sterol 14α-Demethylation-Inhibitory Concentration as a Factor in Evaluating Activities of Azoles against Various Fungal Species. *J. Clin. Microbiol.* 43(11):5547
Shrivastava S, Chattopadhyay A. 2007. Influence of cholesterol and ergosterol on membrane dynamics using different fluorescent reporter probes. *Biochem. Biophys. Res. Commun.* 356(3):705–10
Silva L, Coutinho A, Fedorov A, Prieto M. 2006a. Competitive binding of cholesterol and ergosterol to the polyene antibiotic nystatin. A fluorescence study. *Biophys. J.* 90(10):3625–31
Silva L, Coutinho A, Fedorov A, Prieto M. 2006b. Nystatin-induced lipid vesicles permeabilization is strongly dependent on sterol structure. *Biochim. Biophys. Acta - Biomembr.* 1758(4):452–59
Silva L, De Almeida RFM, Fedorov A, Matos APA, Prieto M. 2006c. Ceramide-platform formation and -induced biophysical changes in a fluid phospholipid membrane. *Mol. Membr. Biol.* 23(2):137–48
Silva LC, De Almeida RFM, Castro BM, Fedorov A, Prieto M. 2007. Ceramide-domain formation and collapse in lipid rafts: Membrane reorganization by an apoptotic lipid. *Biophys. J.* 92(2):502–16
Singh A, Del Poeta M. 2016. Sphingolipidomics: An important mechanistic tool for studying fungal pathogens. *Front. Microbiol.* 7(APR):183665
Singh A, Wang H, Silva LC, Na C, Prieto M, Futerman AH, Luberto C, Del Poeta M. 2012. Methylation of glycosylated

sphingolipid modulates membrane lipid topography and pathogenicity of Cryptococcus neoformans. *Cell. Microbiol.* 14(4):500–516
Sinha M, Mishra S, Joshi PG. 2003. Liquid-ordered microdomains in lipid rafts and plasma membrane of U-87 MG cells: a time-resolved fluorescence study. *Eur. Biophys. J.* 32(4):381–91
Sklar LA. 1980. The partition of cis-parinaric acid and trans-parinaric acid among aqueous, fluid lipid, and solid lipid phases. *Mol. Cell. Biochem.* 32(3):169–77
Sklar LA, Hudson BS, Simoni RD. 1977. Conjugated polyene fatty acids as fluorescent probes: Synthetic phospholipid membrane studies. *Biochemistry.* 16(5):819–28
Smith SJ, Crowley JH, Parks LW. 1996. Transcriptional regulation by ergosterol in the yeast Saccharomyces cerevisiae. *Mol. Cell. Biol.* 16(10):5427–32
Solanko LM, Sullivan DP, Sere YY, Szomek M, Lunding A, Solanko KA, Pizovic A, Stanchev LD, Pomorski TG, Menon AK, Wüstner D. 2018. Ergosterol is mainly located in the cytoplasmic leaflet of the yeast plasma membrane. *Traffic.* 19(3):198–214
Sónia Troeira H, Miguel A. R. B. C. 2005. Environmental factors that enhance the action of the cell penetrating peptide pep-1 A spectroscopic study using lipidic vesicles. *Biochim. Biophys. Acta.* 1669(2):75–86
Sousa F, Nascimento C, Ferreira D, Reis S, Costa P. 2023. Reviving the interest in the versatile drug nystatin: A multitude of strategies to increase its potential as an effective and safe antifungal agent. *Adv. Drug Deliv. Rev.* 199:114969
Souza CM, Schwabe TME, Pichler H, Ploier B, Leitner E, Guan XL, Wenk MR, Riezman I, Riezman H. 2011. A stable yeast strain efficiently producing cholesterol instead of ergosterol is functional for tryptophan uptake, but not weak organic acid resistance. *Metab. Eng.* 13(5):555–69
Spira F, Mueller NS, Beck G, Von Olshausen P, Beig J, Wedlich-Söldner R. 2012. Patchwork organization of the yeast plasma membrane into numerous coexisting domains. *Nat. Cell Biol. 2012 146.* 14(6):640–48
Stancevic B, Kolesnick R. 2010. Ceramide-rich platforms in transmembrane signaling. *FEBS Lett.* 584(9):1728–40
Starosta R, De Almeida RFM, Puchalska M, Białońska A, Panek JJ, Jezierska A, Szmigiel I, Suchodolski J, Krasowska A. 2020. New anticandidal Cu(I) complexes with neocuproine and ketoconazole derived diphenyl(aminomethyl)phosphane: luminescence properties for detection in fungal cells. *Dalt. Trans.* 49(25):8528–39
Starosta R, Komarnicka UK, Puchalska M. 2013. Luminescent copper(ı) (pseudo)halide complexes with neocuproine and a novel bulky tris (aminomethyl) phosphine derived from 2-piperazinopyridine. *J. Lumin.* 143:137–44
Starosta R, Santos TC, Dinis de Sousa AF, Santos MS, Corvo ML, Tomaz AI, de Almeida RFM. 2023. Assessing the role of membrane lipids in the action of ruthenium(III) anticancer compounds. *Front. Mol. Biosci.* 9:
Stern JC, Shah MK, Lucente FE. 1988. In vitro effectiveness of 13 agents in otomycosis and review of the literature. *Laryngoscope.* 98(11):1173–77
Stevens MM, Honerkamp-Smith AR, Keller SL. 2010. Solubility Limits of Cholesterol, Lanosterol, Ergosterol, Stigmasterol, and β-Sitosterol in Electroformed Lipid Vesicles. *Soft Matter.* 6(23):5882
Stillwell W. 2016. *An Introduction to Biological Membranes: Composition, Structure and Function: Second Edition*. Elsevier Inc.
Strádalová V, Stahlschmidt W, Grossmann G, Blažíková M, Rachel R, Tanner W, Malinsky J. 2009. Furrow-like invaginations of the yeast plasma membrane correspond to membrane compartment of Can1. *J. Cell Sci.* 122(Pt 16):2887–94
Strushkevich N, Usanov SA, Park HW. 2010. Structural basis of human CYP51 inhibition by antifungal azoles. *J. Mol. Biol.* 397(4):1067–78
Stukenbrock E, Gurr S. 2023. Address the growing urgency of fungal disease in crops. *Nat. 2023 6177959.* 617(7959):31–34
Suchodolski J, Muraszko J, Bernat P, Krasowska A. 2019. A Crucial Role for Ergosterol in Plasma Membrane Composition, Localisation, and Activity of Cdr1p and H+-ATPase in Candida albicans. *Microorganisms.* 7(10):
Swain E, Baudry K, Stukey J, McDonough V, Germann M, Nickels JT. 2002. Sterol-dependent regulation of sphingolipid metabolism in Saccharomyces cerevisiae. *J. Biol. Chem.* 277(29):26177–84
Szomek M, Reinholdt P, Petersen D, Caci A, Kongsted J, Wüstner D. 2021. Direct observation of nystatin binding to the plasma membrane of living cells. *Biochim. Biophys. Acta - Biomembr.* 1863(2):183528
Tanaka S, Tani M. 2018. Mannosylinositol phosphorylceramides and ergosterol coodinately maintain cell wall integrity in the yeast Saccharomyces cerevisiae. *FEBS J.* 285(13):2405–27
Trachtenberg J. 1984. Ketoconazole therapy in advanced prostatic cancer. *J. Urol.* 132(1):61–63
Umegawa Y, Yamamoto T, Dixit M, Funahashi K, Seo S, Nakagawa Y, Suzuki T, Matsuoka S, Tsuchikawa H, Hanashima S, Oishi T, Matsumori N, Shinoda W, Murata M. 2022. Amphotericin B assembles into seven-molecule ion channels: An NMR and molecular dynamics study. *Sci. Adv.* 8(24):2658
Urbina JA, Pekerar S, Le H biao, Patterson J, Montez B, Oldfield E. 1995. Molecular order and dynamics of phosphatidylcholine bilayer membranes in the presence of cholesterol, ergosterol and lanosterol: a comparative study using 2H-, 13C- and 31P-NMR spectroscopy. *Biochim. Biophys. Acta - Biomembr.* 1238(2):163–76
Valdez-Taubas J, Pelham HRB. 2003. Slow diffusion of proteins in the yeast plasma membrane allows polarity to be maintained by endocytic cycling. *Curr. Biol.* 13(18):1636–40
Valeur B, Berberan-Santos MN. 2012. *Molecular Fluorescence : Principles and Applications*. Wiley-VCH Verlag GmbH
van 't Klooster JS, Cheng T-Y, Sikkema HR, Jeucken A, Moody B, Poolman B. 2020. Periprotein lipidomes of Saccharomyces cerevisiae provide a flexible environment for conformational changes of membrane proteins. *Elife.* 9:
Van Daele R, Spriet I, Wauters J, Maertens J, Mercier T, Van Hecke S, Brüggemann R. 2019. Antifungal drugs: What brings the future? *Med. Mycol.* 57(Supplement_3):S328–43
Van Tyle JH. 1984. Ketoconazole. Mechanism of action, spectrum of activity, pharmacokinetics, drug interactions, adverse reactions and therapeutic use. *Pharmacotherapy.* 4(6):343–73
Vandeputte P, Tronchin G, Larcher G, Ernoult E, Bergès T, Chabasse D, Bouchara JP. 2008. A nonsense mutation in the ERG6 gene leads to reduced susceptibility to polyenes in a clinical isolate of Candida glabrata. *Antimicrob. Agents Chemother.*

52(10):3701–9
Vanderwaeren L, Dok R, Voordeckers K, Nuyts S, Verstrepen KJ. 2022. Saccharomyces cerevisiae as a Model System for Eukaryotic Cell Biology, from Cell Cycle Control to DNA Damage Response. *Int. J. Mol. Sci.* 23(19):
Vanreppelen G, Wuyts J, Van Dijck P, Vandecruys P. 2023. Sources of Antifungal Drugs. *J. Fungi.* 9(2):
Vecer J, Vesela P, Malinsky J, Herman P. 2014. Sphingolipid levels crucially modulate lateral microdomain organization of plasma membrane in living yeast. *FEBS Lett.* 588(3):443–49
Vincent BM, Lancaster AK, Scherz-Shouval R, Whitesell L, Lindquist S. 2013. Fitness Trade-offs Restrict the Evolution of Resistance to Amphotericin B. *PLOS Biol.* 11(10):e1001692
Walther TC, Brickner JH, Aguilar PS, Bernales S, Pantoja C, Walter P. 2006. Eisosomes mark static sites of endocytosis. *Nat. 2005 4397079*. 439(7079):998–1003
Wang J, Zhu H. 2021. Interaction between polyene antifungal drug and saturated phospholipid monolayer regulated by calcium ions at the air-water interface. *Colloids Surfaces B Biointerfaces*. 207:111998
Wang L. 2012. Measurements and implications of the membrane dipole potential. *Annu. Rev. Biochem.* 81:615–35
Wang Q, Chang A. 2002. Sphingoid base synthesis is required for oligomerization and cell surface stability of the yeast plasma membrane ATPase, Pma1. *Proc. Natl. Acad. Sci.* 99(20):12853–58
Watanabe R, Funato K, Venkataraman K, Futerman AH, Riezman H. 2002. Sphingolipids Are Required for the Stable Membrane Association of Glycosylphosphatidylinositol-anchored Proteins in Yeast. *J. Biol. Chem.* 277(51):49538–44
Weng N, Zhang Z, Tan Y, Zhang X, Wei X, Zhu Q. 2022. Repurposing antifungal drugs for cancer therapy. *J. Adv. Res.*
Wichmann CF, Liesch JM, Schwartz RE. 1989. L-671,329, a new antifungal agent. II. Structure determination. *J. Antibiot. (Tokyo).* 42(2):168–73
Williams G. 1984. Ketoconazole for prostate cancer. *Lancet.* 324(8404):696
Wilson-Ashworth HA, Bahm Q, Erickson J, Shinkle A, Vu MP, Woodbury D, Bell JD. 2006. Differential Detection of Phospholipid Fluidity, Order, and Spacing by Fluorescence Spectroscopy of Bis-pyrene, Prodan, Nystatin, and Merocyanine 540. *Biophys. J.* 91(11):4091–4101
Wolf DE. 1995. Lipid domains in sperm plasma membranes. *Mol. Membr. Biol.* 12(1):101–4
Yang S, Song L, Wang J, Zhao J, Tang H, Bao X. 2024. Engineering Saccharomyces cerevisiae for efficient production of recombinant proteins. *Eng. Microbiol.* 4(1):100122
Yoda T. 2022. Charged Lipids Influence Phase Separation in Cell-Sized Liposomes Containing Cholesterol or Ergosterol. *Membranes (Basel).* 12(11):
Young ME, Karpova TS, Brügger B, Moschenross DM, Wang GK, Schneiter R, Wieland FT, Cooper JA. 2002. The Sur7p family defines novel cortical domains in Saccharomyces cerevisiae, affects sphingolipid metabolism, and is involved in sporulation. *Mol. Cell. Biol.* 22(3):927–34
Zahumensky J, Malinsky J. 2019. Role of MCC/Eisosome in Fungal Lipid Homeostasis. *Biomolecules*. 9(8):
Zaremberg V, Ganesan S, Shabits BN. 2019. Metabolism and Regulation of Glycerolipids in Yeast. *Biog. Fat. Acids, Lipids Membr.* 315–39
Zhang Y, Li X, Becker KA, Gulbins E. 2009. Ceramide-enriched membrane domains—Structure and function. *Biochim. Biophys. Acta - Biomembr.* 1788(1):178–83
Zhao P, Zhao C, Chen D, Yun C, Li H, Bai L. 2021. Structure and activation mechanism of the hexameric plasma membrane H+-ATPase. *Nat. Commun. 2021 121*. 12(1):1–11
Zhu G, Yin N, Luo Q, Liu J, Chen X, Liu L, Wu J. 2020. Enhancement of Sphingolipid Synthesis Improves Osmotic Tolerance of Saccharomyces cerevisiae. *Appl. Environ. Microbiol.* 86(8):
Zielinski J, Golik J, Pawlak J, Borowski E, Falkowski L. 1988. The structure of nystatin A3, a component of nystatin complex. *J. Antibiot. (Tokyo).* 41(9):1289–91
Zink S, Mehlgarten C, Kitamoto HK, Nagase J, Jablonowski D, Dickson RC, Stark MJR, Schaffrath R. 2005. Mannosyl-diinositolphospho-ceramide, the major yeast plasma membrane sphingolipid, governs toxicity of Kluyveromyces lactis zymocin. *Eukaryot. Cell.* 4(5):879–89
Zinser E, Paltauf F, Daum G. 1993. Sterol composition of yeast organelle membranes and subcellular distribution of enzymes involved in sterol metabolism. *J. Bacteriol.* 175(10):2853
Zinser E, Sperka-Gottlieb CDM, Fasch E V., Kohlwein SD, Paltauf F, Daum G. 1991. Phospholipid synthesis and lipid composition of subcellular membranes in the unicellular eukaryote Saccharomyces cerevisiae. *J. Bacteriol.* 173(6):2026
Zweytick D, Leitner E, Kohlwein SD, Yu C, Rothblatt J, Daum G. 2000. Contribution of Are1p and Are2p to steryl ester synthesis in the yeast Saccharomyces cerevisiae. *Eur. J. Biochem.* 267(4):1075–82

AIMS

As mentioned in chapter I, due to the increasing incidence of fungal infections each year, it becomes imperative to search for new and/or improved antifungal drugs and targets. Hence, the work presented in this dissertation focus on two main goals, carried out in parallel in an effort to complement each other:

1) A fundamental study of the properties of the plasma membrane of the budding yeast *Saccharomyces cerevisiae*, with a special emphasis on sphingolipid organization in the membrane, which is unique in these organisms, and that can be a target for antifungal agents;
2) Unravel the membrane-interaction of different antifungal agents, to, correlating with the previous point, uncover why some are more efficient and less toxic to the host by targeting an exclusive feature of the fungal plasma membrane – sphingolipid-enriched domains (SLEDs).

These goals were achieved recurring mainly to fluorescence-based techniques - both steady-state and time-resolved fluorescence spectroscopy.

Specifically, this work aimed at answering pressing questions concerning the biophysical properties of the plasma membrane of *S. cerevisiae*:

- What sphingolipids are enriching SLEDs?
- What is the connection between SLEDs and protein membrane compartments, mainly MCP and MCC?
- How do sphingolipid structural differences (mainly regarding the polar headgroup) affect SLEDs and the overall membrane properties?

It also focused on studying the interaction of antifungal drugs with membranes, aiming at answering the following questions:

- Does azole antifungal drug ketoconazole have different affinity towards a fluid membrane than its phosphine derivatives?
- Does this membrane interaction influence the permeability of the membrane itself? If so, does it correlate with the activity of the compounds?
- What is the relative location of ketoconazole and phosphine derivatives in a fluid membrane?

- What are the molecular structural differences that are driving the distinct membrane interaction for each of the compounds?
- Do ketoconazole derivatives have different modes of action than ketoconazole itself?
- Is the interaction of ketoconazole preferential towards a specific lipid or lipid phase?
- Does nystatin have a preferential interaction with fungal sphingolipids when compared with mammalian ones?
- Is this preferential interaction affecting the pore-forming activity of nystatin?

CHAPTER II

YEAST SPHINGOLIPID-ENRICHED DOMAINS AND MEMBRANE COMPARTMENTS IN THE ABSENCE OF MANNOSYLDIINOSITOLPHOSPHORYLCERAMIDE

This chapter comprises the work published in *Biomolecules*, 2020, 10(6), 871 by **A. Bento-Oliveira***, F.C. Santos*, J.T. Marquês*, P. M. R. Paulo, T. Korte, A. Herrmann, H. S. Marinho, R. F. M. de Almeida (*equally contributing authors).

Contribution: Took an active part in the formal analysis, investigation, writing and preparation of the original draft, manuscript review and editing, and visualization. I conducted the fluorescence spectroscopy assays with *t*-PnA and DPH, and the protein heterogeneity determination, and respective data analysis.

biomolecules

MDPI

Article

Yeast Sphingolipid-Enriched Domains and Membrane Compartments in the Absence of Mannosyldiinositolphosphorylceramide

Andreia Bento-Oliveira [1,†], Filipa C. Santos [1,†], Joaquim Trigo Marquês [1,†], Pedro M. R. Paulo [2], Thomas Korte [3], Andreas Herrmann [3], H. Susana Marinho [1] and Rodrigo F. M. de Almeida [1,*]

1 Centro de Química Estrutural, Faculdade de Ciências, Universidade de Lisboa, 1749-016 Lisbon, Portugal; abdoliveira@fc.ul.pt (A.B.-O.); fpsantos@fc.ul.pt (F.C.S.); jmtmarques@fc.ul.pt (J.T.M.); hsmarinho@fc.ul.pt (H.S.M.)

2 Centro de Química Estrutural, Instituto Superior Técnico, 1049-001 Lisbon, Portugal; pedro.m.paulo@tecnico.ulisboa.pt

3 Department of Biology, Molecular Biophysics, IRI Life Sciences, Humboldt-Universität zu Berlin, 10115 Berlin, Germany; thomas.korte@rz.hu-berlin.de (T.K.); andreas.herrmann@rz.hu-berlin.de (A.H.)

* Correspondence: rfalmeida@fc.ul.pt; Tel.: +351-217-500-925

† These authors contributed equally to this work.

Abstract

The relevance of mannosyldiinositolphosphorylceramide [$M(IP)_2C$] synthesis, the terminal complex sphingolipid class in the yeast *Saccharomyces cerevisiae*, for the lateral organization of the plasma membrane, and in particular for sphingolipid-enriched gel domains, was investigated by fluorescence spectroscopy and microscopy. We also addressed how changing the complex sphingolipid profile in the plasma membrane could influence the membrane compartments (MC) containing either the arginine/ H^+ symporter Can1p (MCC) or the proton ATPase Pma1p (MCP). To achieve these goals, wild-type (*wt*) and *ipt1*Δ cells, which are unable to synthesize $M(IP)_2C$ accumulating mannosylinositolphosphorylceramide (MIPC), were compared. Living cells, isolated plasma membrane and giant unilamellar vesicles reconstituted from plasma membrane lipids were labelled with various fluorescent membrane probes that report the presence and organization of distinct lipid domains, global order, and dielectric properties. Can1p and Pma1p were tagged with GFP and mRFP, respectively, in both yeast strains, to evaluate their lateral organization using confocal fluorescence intensity and fluorescence lifetime imaging. The results show that *IPT1* deletion strongly affects the rigidity of gel domains but not their relative abundance, whereas no significant alterations could be perceived in ergosterol-enriched domains. Moreover, in these cells lacking $M(IP)_2C$, a clear alteration in Pma1p membrane distribution, but no significant changes in Can1p distribution, were observed. Thus, this work reinforces the notion that sphingolipid-enriched domains

distinct from ergosterol-enriched regions are present in the *S. cerevisiae* plasma membrane and suggests that $M(IP)_2C$ is important for a proper hydrophobic chain packing of sphingolipids in the gel domains of *wt* cells. Furthermore, our results strongly support the involvement of sphingolipid domains in the formation and stability of the MCP, possibly being enriched in this compartment.

Keywords: *Saccharomyces cerevisiae*; membrane compartments; sphingolipids; Pma1p; Can1p; fluorescence lifetime imaging microscopy (FLIM); fungal plasma membrane; inositolphosphorylceramides; fluorescence spectroscopy; giant unilamellar vesicles (GUVs)

1. Introduction

The plasma membrane of fungi contains a multitude of actively maintained membrane compartments, which have distinct protein markers, are stable in space and time, and are responsible for specific physiological functions [1–3]. Despite the growing interest in these compartments, the mechanism of their formation, their lipid composition, and their interrelations are still largely unknown [4].

In yeast and other fungi, as well as in plants, many plasma membrane proteins display slow lateral diffusion or are immobile, when compared to vertebrate biological membranes or artificial fluid lipid bilayers [2]. In some cases, this low mobility is dependent on plasma membrane sterols and sphingolipids [1,3,5–8]. In this regard, sphingolipid-enriched microdomains seem to be of particular relevance [9–11]. These domains found in the plasma membrane of *Saccharomyces cerevisiae* differ from the prototypical mammalian lipid raft both in composition, given they are ergosterol-depleted, and biophysically, as they are highly rigid gel domains [11]. Hence, the study of these domains is particularly important, as they may explain fundamental differences between fungal and mammalian membranes [9], providing potential targets that can be explored concerning antifungal drug development [12].

In the plasma membrane of yeast *S. cerevisiae* two major non-overlapping compartments can be found: the membrane compartment containing Can1p (MCC), an arginine permease, and the membrane compartment containing Pma1p (MCP), the plasma membrane H^+-ATPase. MCC is currently designated MCC/eisosome, as its characteristic furrow-like invaginating shape is stabilized by a large cytosolic protein scaffold, the eisosome, at the bottom of the MCC furrow [2,13,14]. A typical *S. cerevisiae* cell in exponential phase contains around 1.5–2.5 such invaginations per μm^2 of cell surface [8,13] covering roughly 25% of the membrane area. Fluorescence labeling with the 3'-β-sterol-binding filipin suggested that the MCC/eisosome is

ergosterol-enriched [15]. The deletion of proteins that are part of the MCC/eisosome, or are associated with it, compromises the formation of intact MCC/eisosome domains and influences ergosterol distribution in the plasma membrane [2]. Some of the well-known functions of the MCC/eisosome include the sensing of local membrane disturbances and deformations, *e.g.*, due to mechanical or osmotic stress [16], involvement in membrane adaptation to other types of stress [17–20], regulation of lipid homeostasis, in particular sensing sphingolipid levels [2], and protection against endocytosis/starvation [3]. Notably, membrane potential has been suggested to modulate the organization of MCC domains. Readily after membrane depolarization, proteins including Can1p are no longer confined to the MCC, acquiring a more homogeneous distribution in the plasma membrane [15,21]. Concomitantly, sphingolipid-enriched microdomains dissipate [22]. Thus, despite the stability of MCC and the low mobility of Can1p inside the MCC, its distribution in the plasma membrane is dynamic and regulated.

The MCP was first identified in *S. cerevisiae* by confocal fluorescence microscopy as a network-like compartment containing Pma1p [23], the most abundant plasma membrane protein in fungi [24]. This protein is responsible for the creation and maintenance of membrane potential of fungal cells, as well as regulation of the intracellular pH and ion concentration [25]. More recently, it has been suggested to be of relevance for signaling [3]. The electrochemical gradient established by Pma1p drives nutrient uptake, namely by symporters localized at the MCC, such as Can1p, establishing an important functional relation between MCP and MCC.

On the other hand, in *S. cerevisiae* [26,27] as well as in *Cryptococcus neoformans* [28,29], alterations of sphingolipid metabolic balance affect the oligomerization, traffic, activity, and plasma membrane stability of Pma1p [30–33]. These results point to an intimate relation between the MCP and the sphingolipids. Pma1p has relatively long hydrophobic transmembrane segments and is one of the yeast plasma membrane constituents with the longest residence time [34]. Thus, this compartment seems to be a good candidate to host sphingolipids. With very long hydrocarbon chains, they exhibit tendency to form highly ordered gel domains, and relatively low levels of ergosterol [15] are putatively found in the MCP. However, whether sphingolipids are major lipid components of those domains is also unproved, as is the sphingolipid enrichment in the MCC. Moreover, the labelling of sphingolipids is not straightforward, and only indirect evidence is available to support that hypothesis.

Based on the structure of their headgroup, complex sphingolipids are classified in three types in yeast, IPC (inositolphosphorylceramide), MIPC (mannosylinositolphosphorylceramide), and $M(IP)_2C$ (mannosyldiinositolphosphorylceramide). $M(IP)_2C$ is the most abundant complex sphingolipid in *S. cerevisiae*, regardless of whether the whole cell or specifically the plasma

membrane is considered [35,36]. Still, MIPC is also present in the plasma membrane of wild-type (*wt*) *S. cerevisiae* cells. The formation of terminal complex sphingolipid $M(IP)_2C$ from MIPC is catalyzed by an inositol phosphotransferase encoded by the *IPT1* gene [35,36]. In *ipt1*Δ cells, despite the major changes in sphingolipid composition, that are characterized by the lack of $M(IP)_2C$ and its replacement by MIPC, the sterol composition is similar to that of *wt* cells [35]. Some studies suggest that this gene deletion may enhance resistance to both nystatin and miconazole [35], and confers markedly higher resistance to zymocin [37], syringomycin E [38], and the plant defensin DmAMP1 produced by *Dahlia merckii* seeds [39]. The authors of the latter study proposed that the antifungal peptide targets membrane patches containing $M(IP)_2C$, although the specific contribution of each complex sphingolipid for the organization of the plasma membrane is still unclear.

In this work, in an attempt to clarify some of the issues described above, we have carried out a thorough biophysical characterization of the plasma membrane in *S. cerevisiae ipt1*Δ versus *wt* cells, addressing both lipid domains and membrane compartments. We found that the plasma membrane of *ipt1*Δ cells has more compact sphingolipid-enriched domains, whereas dielectric properties that are more specifically modulated by ergosterol remained essentially unchanged. Moreover, we present evidence that in *ipt1*Δ cells, where $M(IP)_2C$ is absent, the plasma membrane distribution of Pma1p is much more affected than that of Can1p.

2. Materials and methods

2.1. Materials and strains

Table 2.1 lists the S. cerevisiae strains used in this work. The *wt* and *ipt1*Δ strains were transformed using the lithium acetate procedure [40], with the integrative plasmid Ylp211-CAN1-GFP (*URA3*) or Ylp128-PMA1-mRFP (*LEU2*) kindly provided by Dr. Guido Grossmann and Professor Widmar Tanner (University of Regensburg, Germany).

Yeast extract, bactopeptone, yeast nitrogen base, and bacto-agar were purchased from Difco (Hampton, NH, USA). Amino acids, nucleotides and glucose used in the synthetic complete (SC) medium, sucrose, and organic solvents (of analytical grade for lipid extraction and spectroscopic grade for lipids and probes stock solutions) were obtained from Merck (Darmstadt, Germany). *Trans*-parinaric acid (*t*-PnA) was purchased from Santa Cruz Biotech. (Santa Cruz, CA, USA), 1,6-diphenylhexatriene (DPH) from Invitrogen (Carlsbad, CA, USA), 4-[2-[6-(dioctylamino)-2-naphthalenyl]ethenyl]-1-(3-sulfopropyl)-pyridinium (di-8-ANEPPS) was obtained from Biotium (Fremont, CA, USA), 1,2-dioleoyl-*sn*-glycero-3-phosphoethanolamine-*N*-(lissamine rhodamine B sulfonyl) (Rhod-DOPE) from Avanti Polar

Lipids (Alabaster, AL, USA), and Ludox (TM-50 colloidal silica, 50 wt.% suspension in water) acquired from Sigma-Aldrich (St. Louis, MO, USA).

Table 2. 1: *S. cerevisiae* strains used in this work, genotype description and growth media.

Strain	Genotype	Source	Growth Media
wild-type (*wt*; BY4741)	*MATa; his3Δ1; leu2Δ0; met15Δ0; ura3Δ0*	EUROSCARF (Frankfurt, Germany)	Synthetic Complete medium (SC)
***ipt1*Δ**	BY4741; *YMR272c::kanMX4*	EUROSCARF (Frankfurt, Germany)	SC
***wt*-Can1p-GFP**	BY4741*; Ylp211CAN::GFP*	This study	SC *ura*$^-$
***wt*-Pma1p-mRFP**	BY4741*; Ylp128PMA1:mRFP*	This study	SC *leu*$^-$
***ipt1*Δ-Can1p-GFP**	BY4741*; YMR272c::kanMX4; Ylp211CAN::GFP*	This study	SC *ura*$^-$
***ipt1*Δ-Pma1p-mRFP**	BY4741*; YMR272c::kanMX4; Ylp128PMA1::mRFP*	This study	SC *leu*$^-$

The fluorescent probes were quantified spectrophotometrically using the respective molar absorption coefficients: *t*-PnA, $\varepsilon_{ethanol}^{299.4\ nm} = 89{,}000\ M^{-1}cm^{-1}$; DPH, $\varepsilon_{methanol}^{350\ nm} = 88{,}000\ M^{-1}cm^{-1}$; di-8-ANEPPS, $\varepsilon_{methanol}^{498\ nm} = 37{,}000\ M^{-1}cm^{-1}$; Rhod-DOPE, $\varepsilon_{chloroform}^{559\ nm} = 37{,}000\ M^{-1}cm^{-1}$ [41,42].

2.2. Media and growth conditions

S. cerevisiae cells were inoculated at an A_{600nm} of 0.15 and cultured in SC medium (2% (*w/v*) glucose, 0.68% (*w/v*) yeast nitrogen base and amino acid composition given in [42]), except when specifically stated and for microscopy experiments using di-8-ANEPPS and Rhod-DOPE as membrane probes. In these cases, a similar growth procedure was performed using a culture medium containing 1% (*w/v*) yeast extract, 2% (*w/v*) peptone and 2% (*w/v*) glucose (YPD). Yeast cells were grown at 30 °C and 160 rpm overnight and reinoculated into the culture medium at an A_{600nm} of ~0.15. Upon reaching an A_{600nm} of 0.6, after a 5–6 h incubation, *i.e.*, in the mid-exponential phase, cells were harvested.

2.3. Plasma membrane isolation

The plasma membrane isolation was performed as described in [43] with minor adjustments. Briefly, cells were collected by centrifugation (5 min, 5000x g) and washed twice with 0.4 M sucrose in buffer A (25 mM imidazole HCl, pH 7.0) at 3500x g for 10 min. Harvested cells were resuspended in buffer A containing sucrose at 0.4 M and a mixture of protease inhibitors (Halt. protease inhibitor cocktail (100x) from Thermo Scientific (Waltham,

MA, USA)), and lysed gently with glass beads. To obtain a crude membrane extract, lysed cells were centrifuged at low speed (530x g) for 20 min, the supernatant was recovered and centrifuged at 22,000x g for 30 min. For the total lipid extracts preparation, the pellet containing the crude membrane extract was stored, while for the plasma membrane isolation it was resuspended in 2 mL of buffer A containing the protease inhibitor mixture. Then, it was applied on the top of a 10 mL discontinuous sucrose gradient (consisting of three layers of 2.25, 1.65, and 1.1 M sucrose in buffer A). The gradient centrifugation was carried out in a CP80NX Hitachi ultracentrifuge (Berkshire, United Kingdom) for 18 h at 80,000x g. Pure plasma membrane fractions were obtained from the interface between the 2.25 and 1.65 M sucrose layers and then they were resuspended in either buffer A (for lipid extraction) or B (for fluorescence analysis; 100 mM $NaH_2PO_4.H_2O$, 100 mM NaCl, 1 mM EDTA, pH 7.4) and pelleted by centrifugation at 30,000x g for 40 min.

2.4. Lipid Extraction

The extraction of the total lipids of the cell and of the plasma membrane was performed using a slightly modified Bligh–Dyer method [44]. The isolated plasma membrane (IPM) and the crude membrane extracts were separately incubated with 1 mL of buffer A and 19 mL of chloroform:methanol (1:2, *v/v*) at 20 °C with shaking at 140 rpm for 1 h. Chloroform was further added in order to have a chloroform:methanol ratio of 1:1 (*v/v*). The same volume of a 0.04% (*w/v*) $CaCl_2$ solution was added to the mixture, which was then vigorously stirred for 1 min (while relieving the pressure). Once two distinct phases were visible, both the organic phase and the interface were collected separately. The whole process was then repeated for the interface, from which the organic phase was collected, added to the previous one, dried under a stream of nitrogen and then stored at -20 °C. In plasma membrane suspensions and in lipid extracts, total phospholipid concentration was determined by phosphorus analysis [45]. Ergosterol molar proportion was assumed to be ca. 2:1 (phospholipid:ergosterol) [19,46]. Before use, total lipid extracts were redissolved in chloroform/methanol (2:1, *v/v*) and the adequate volume was taken to obtain suspensions of multilamellar vesicles (MLVs) in buffer B, at a final lipid concentration of ca. 0.3 mM (see [11] for further details).

2.5. Giant unilamellar vesicles (GUVs) preparation

GUVs were prepared by the electroformation method of Angelova et al. [47]. For GUV preparation, a 1 mM solution of the lipids extracted from yeast plasma membrane in chloroform: methanol (2:1, *v/v*) was used. The adequate volume of probe (di-8-ANEPPS and/

or Rhod-DOPE) stock solution was mixed to obtain a final lipid/probe ratio of 1:500 (mol:mol) and a chloroform:methanol ratio of (2:1, *v/v*). Then, 25 µL of this mixture, previously homogenized, was spread with a gas-tight syringe on the titanium plates of the GUV chamber. To remove any traces of organic solvent, the plates were placed on a vacuum desiccator for 30 min. The titanium chambers were assembled and filled with 700 µL of a 200 mM sucrose solution with sodium azide 15 mM, previously heated to 60 µC in a heat block, sealed, connected to the signal generator and placed in the heat block maintaining the system at 60 µC. A 10 Hz sinusoidal wave with a peak-to-peak amplitude of 0.4 V was initially applied and the voltage was increased to 2.0 V and kept overnight. The sinusoidal signal was then changed to 4 Hz frequency and 2.6 V voltage for 20 min. The vesicle suspension was kept at room temperature (24 °C) in the dark until use. For GUV visualization, 100 µL of each GUV suspension and 150 µL of glucose solution 200 mM were added to a well of an eight-well plastic plate from Ibidi® with glass like coverslip bottom.

2.6. Fluorescence spectroscopy measurements and data analysis

Fluorescence measurements were performed with a Fluorolog Model 3.22 spectrofluorimeter from Horiba Jobin Yvon (Villeneuve D'ascq, France) at 24.0 ± 1.0 °C in a sample compartment with temperature-control and magnetic stirring.

Harvested cells (*wt* and *ipt1*Δ) were washed twice with sterile water and then suspended in buffer B. Before starting the measurements, the probes DPH or *t*-PnA were added to the cell suspension to a final concentration of 2 µM and incubated at 24 °C (room temperature) for 20 and 5 min, respectively [11].

For fluorescence measurements, the IPM suspensions were incubated with *t*-PnA, DPH or di-8-ANEPPS for more than 5 min, 20 min, and 1 h respectively, at room temperature, to a final ratio of probe/lipid of 1/100, for DPH and t-PnA, and 1/200 for di-8-ANEPPS. The MLV suspensions made from total lipid extracts were labelled with DPH at a probe:phospholipid ratio of 1/200. Following a procedure previously described [48].

For fluorescence in the steady-state, the excitation and emission wavelengths were set to, respectively, 320 and 404 nm for *t*-PnA and 358 and 430 nm for DPH. The value of steady-state fluorescence anisotropy, ⟨r⟩, was determined through Equation (1):

$$\langle r \rangle = \frac{(I_{VV} - G \times I_{VH})}{(I_{VV} + 2G \times I_{VH})} \quad (1)$$

in which the subscripts indicate the orientation of the excitation and emission polarizers, where V and H correspond to vertical and horizontal orientations and G is a correction for the instrument different sensitivity to each light polarization plane. An adequate blank was subtracted from each intensity reading.

Time-resolved fluorescence measurements were carried out by the single photon timing technique, using a nanoLED N-320 from Horiba Jobin Yvon (Villeneuve D'ascq, France) for the excitation of *t*-PnA, and 404 nm as the emission wavelength. The scattering agent used to obtain the instrument response function (IRF) was Ludox®. The experimental fluorescence intensity decays were analyzed with the software TRFA® version 1.4 (Minsk, Belarus). To completely separate the emission of the probe from the autofluorescence of the cells, a method of global analysis was used [49]. The fluorescence intensity decays of the probe were described by a multiexponential model according to Equation (2):

$$I(t) = \sum_{i=1}^{n} \alpha_i \exp\left(-\frac{t}{\tau_i}\right) \quad (2)$$

After subtracting the contribution of the cells autofluorescence to the pre-exponential factor in each component i with lifetime τ_i, and after the thus obtained pre-exponential factors were normalized to obtain their relative amplitude α_i. Equation (3) was used to calculate the mean fluorescence lifetime (intensity weighted):

$$\langle\tau\rangle = \frac{\sum \alpha_i \tau_i^2}{\sum \alpha_i \tau_i} \quad (3)$$

and Equation (4) was used to compute the amplitude-weighted mean fluorescence lifetime:

$$\bar{\tau} = \sum_{i=1}^{n} \alpha_i \tau_i \quad (4)$$

The criteria for good quality of the fitting were the reduced global χ^2 close to 1 and the random distributions of weighted residuals and of residuals autocorrelation (see supplemental Figure S2.1).

Changes in membrane dipole potential were evaluated in IPM suspensions using the ratio of the steady-state fluorescence intensity values obtained from excitation of di-8-ANEPPS at 420 nm and at 520 nm, both with emission at 635 nm [50,51].

2.7. Fluorescence intensity and lifetime imaging by confocal microscopy

2.7.1. GUV and Living cells labeled with di-8-ANEPPS or rhod-DOPE

For fluorescence lifetime imaging microscopy (FLIM) with di-8-ANEPPS, after cell harvesting, the cellular suspension was labeled at room temperature (24 °C) with the probe at 1 μM, which was added from a concentrated methanol stock solution. After a 5 min incubation with the probe, the cells were centrifuged and suspended in buffer B.

Intensity images as well as FLIM measurements were taken in the confocal mode using an Olympus Fluoview 1000 (Olympus, Tokyo, Japan) upgraded with a LSM time-resolved kit (PicoQuant GmbH, Berlin, Germany) and an oil immersion objective, x60 (1.35 N.A.). For intensity images, di-8-ANEPPS was excited by a 488 nm line of a multiline argon laser and its emission detected in the range of 565–665 nm. Rhod-DOPE intensity images were acquired with excitation at 559 nm using a line of a multiline argon laser and detection in the range of 590–690 nm. Images with a frame size of 512 x 512 pixels were acquired. For FLIM measurements, di-8-ANEPPS was excited at 483 nm and Rhod-DOPE at 560 nm using pulsed-laser diodes and detected by a single photon avalanche photodiode (SPAD) using a 620 ± 30 nm bandpass filter. FLIM images were acquired for 60 s (45 frames with an average photon count rate of 2-4 x 10^4 count/s). Analysis of FLIM data was performed using the software from PicoQuant, SymPhoTime 64, (version 2.5), considering the convolution of the fluorescence decays with the IRF. The time distribution of photon counts in each pixel retrieved from the regions of interest were combined into a single decay curve which was analyzed by using a 2 exponentials model (Equation (2) with $i = 2$), judging the fitting quality from the distribution of the residuals and reduced χ^2 value. The intensity-weighted mean fluorescence lifetime τ and the amplitude weighted mean fluorescence lifetime $\bar{\tau}$ were calculated using Equations (3) and (4). The results are averaged over more than 50 GUV from at least 3 independent experiments and more than 400 cells from 4 independent experiments. The fluorescence lifetime of the probe was independent of the incubation time.

2.7.2. Yeast living cells tagged with GFP and mRFP

FLIM measurements as well as confocal images of harvested *S. cerevisiae wt* and *ipt1*Δ cells with GFP-tagged Can1p and mRFP-tagged Pma1p were performed on a time-resolved confocal fluorescence microscope, model MicroTime 200, from PicoQuant GmbH (Berlin, Germany), with details of the equipment setup described in [52].

The point-spread function of the setup was measured using fluorescent beads of size 100 nm, which afforded a lateral resolution of about 400 nm. Intensity images were obtained concomitantly with FLIM measurements. GFP and mRFP were excited at 480 nm using a pulsed-laser diode and detected by a SPAD using a the longpass filter above 510 nm. The images were obtained with a scanning resolution of 0.156 μm/pixel. All images were acquired with an excitation power of ca. 0.54 kW/cm^2 and further processed by creating a mask in which the cell membrane regions were visually selected using the region-of-interest (ROI) tools of SymPhoTime program, version 5.3.2.2. The fluorescence decays corresponding to the regions identified as cell membranes were obtained from the histograms of photon arrival times concerning only the pixels contained in these regions. Here, the same criteria as in Section 2.7.1. for the analysis of the FLIM data of proteins were employed. The results are averaged over ca. 400 cells from 3 independent experiments.

Confocal images were used to assess the distribution of Can1p-GFP and Pma1p-mRFP in the plasma membrane of yeast living cells. For numerical data extraction a line profile of the fluorescence intensity of the plasma membrane was obtained using Image Pro-Plus v6.0 and the fluorescence heterogeneity, *i.e.*, the fraction of pixels which have intensity higher or lower than the average plus or minus 10%, respectively (or plus or minus the standard deviation — both calculations yield the same relative results when comparing proteins or strains). It reflects to which extent the fluorescence intensity is concentrated in specific pixels and is independent on the total fluorescence intensity (see supplemental Figure S2.2). The heterogeneity was determined for the plasma membrane of each cell. For each transformed yeast strain, 4 independent experiments were performed, and more than 190 cells were analyzed.

2.8. Statistical Analysis

The results are presented as mean ± standard deviation (S.D.), unless stated otherwise, and the sample dimension and number of biologically independent replicates are given with the results. The statistical significance was determined using Student's *t*-test. Mean values were considered significantly different for *p*-values below or equal to 0.05.

3. Results

3.1. Sphingolipid-enriched domains are more compact in *ipt1*Δ cells

To understand how sphingolipid-enriched gel domains may change with an alteration of the sphingolipid profile, the plasma membrane of *S. cerevisiae* living cells was labelled with *t*-PnA. The fluorescence properties of this probe, especially the time-resolved, are sensitive to

changes in the amount and composition of highly ordered gel domains, into which it partitions very favorably in membrane model systems, undergoing a concomitant increase of its fluorescence quantum yield [48,53,54]. Additionally, the long lifetime component in *t*-PnA fluorescence intensity decay can be used as a fingerprint for gel domains when longer than 30 ns [11].

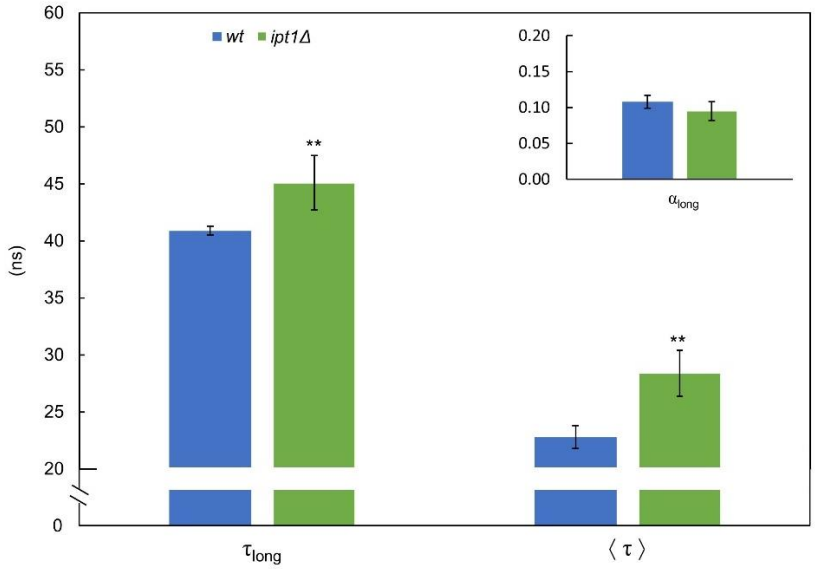

Figure 2. 1: The gel lipid domains of the plasma membrane of intact *S. cerevisiae* cells are more compact in *ipt1*Δ than in *wt* cells. The fluorescence intensity decay of the probe *t*-PnA in *S. cerevisiae* cellular suspensions was obtained at 24 °C, as described in the "experimental procedures". The long-component lifetime (τ_{long}) and normalized amplitude (α_{long}; see inset) and the mean fluorescence lifetime (‹τ›) are shown. The values are the mean ± S.D. of at least four biological replicates. ** $p \leq 0.01$.

The fluorescence intensity decay of *t*-PnA incorporated in the plasma membrane of *S. cerevisiae* cells is properly described by four exponentials, where the long component lifetime (τ_{long}) gives information about the relative degree of hydrophobic packing of gel domains and its amplitude (normalized pre-exponential) about their relative abundance [55]. For *wt* cells, the long lifetime component was 40.9 ± 0.4 ns, a value similar to that obtained in our previous work (~41 ns) [11], while for *ipt1*Δ cells it was 45.1 ± 2.4 ns (Figure 2.1 - τ_{long}). Since this parameter is higher than 30 ns for both strains, it reveals the presence of gel domains in the plasma membrane [11]. Moreover, both the long-lifetime component and the intensity weighted mean fluorescence lifetime (Figure 2.1 - ‹τ›) were even longer in *ipt1*Δ cells than *wt* cells. Similar results were obtained for cells grown in YPD medium (Supplementary Material Figure S2.3).

Regarding the relative abundance of the sphingolipid-enriched domains, the amplitude of the long lifetime component was somewhat lower in *ipt1*Δ cells, but the differences were not statistically significant. Taken together the results of packing and abundance of the sphingolipid-enriched domains contribute to the identical values obtained for the steady state

fluorescence anisotropy of *t*-PnA in living cells or IPM of *S. cerevisiae wt* and *ipt1*Δ cells (Supplementary Figure S2.4).

3.2. Membrane fluidity is altered in *ipt1*Δ cells

To further understand how the plasma membrane responds to alterations in the sphingolipid profile, the membrane of *S. cerevisiae* was labelled with DPH. Since DPH partitions equally throughout different lipid phases, it is sensitive to the membrane global properties, rather than to a particular type of domain [56,57], with the notable exception of poorly hydrated ceramide-rich phases [54]. DPH steady-state fluorescence anisotropy, ⟨r⟩, is a well-established parameter to report alterations in the global fluidity of the plasma membrane [11,58,59]. The fluorescence anisotropy of DPH changes linearly with composition (and temperature) along the gel/ liquid disordered (l_d) and l_d/ liquid ordered (l_o) phase coexistence region, *i.e.*, responds linearly to the fraction of each phase, in several binary and ternary lipid systems [12,54,58], including in the 1-palmitoyl-2-oleoyl-*sn*-glycero-3-phosphocholine (POPC)/ergosterol binary system [60]. Moreover, in the POPC/phytoceramide (the yeast sphingolipid backbone) system, the fluorescence anisotropy and intensity of DPH behave similarly to typical gel/ l_d systems in the region of coexistence of l_d and a phytoceramide-rich gel phase where the hydrophobic packing is comparable to the one found for the gel domains in yeast [48]. All these studies support the use of DPH anisotropy as a reporter of global membrane fluidity in yeast membranes.

As can be seen in Figure 2.2, for both the IPM suspensions and total lipid extracts reconstituted into multilamellar liposomes the steady-state anisotropy, ⟨r⟩, of DPH was significantly lower for *ipt1*Δ cells than for *wt* cells, but the values of ⟨r⟩ for IPM and total lipid extracts were similar for each strain.

In conclusion, the results suggest that the lack of $M(IP)_2C$ in *ipt1*Δ cells and/or the accumulation of MIPC [35,36] may lead to an alteration of the global fluidity of cellular membranes.

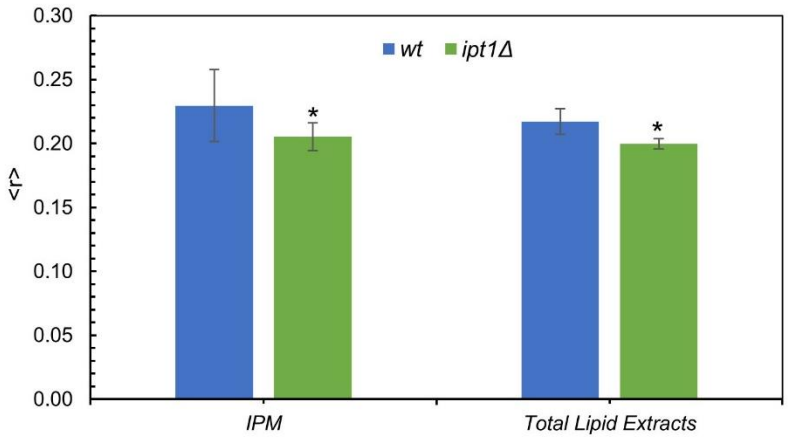

Figure 2. 2: The global order of the plasma membrane of *S. cerevisiae* is higher in *wt* than in *ipt1*Δ cells. The diphenylhexatriene (DPH) steady-state fluorescence anisotropy at 24 °C was obtained as described under "experimental procedures" for *wt* and *ipt1*Δ cells isolated plasma membrane (IPM) and multilamellar vesicles (MLVs) made from total lipid extracts obtained from cells in mid-exponential phase. The values are the mean ± S.D. of at least four biological replicates. * $p \leq 0.05$.

3.3. Plasma membrane fluid domains present similar properties in wt and *ipt1*Δ cells

Electrochromic dyes, such as di-8-ANEPPS, are suitable to report sterol-related properties [50,61]. In fact, the partition of another probe from ANEPPS family, di-4-ANEPPS, for the l_o phase formed in the presence of ergosterol is higher (~2.1x) than for the corresponding l_d phase in the same POPC/ergosterol phase coexistence tie-line. The probe also displays a higher fluorescence quantum yield in the l_o phase [62]. On the other hand, as already mentioned, *t*-PnA partitions preferentially towards gel domains [11,53,54]. Thus, complementary information can be retrieved by labelling the membranes with di-8-ANEPPS [59].

Unlike *t*-PnA, di-8-ANEPPS can be used in fluorescence microscopy studies due to its excitation and emission in the visible range and photostability. The imaging techniques enable to directly conclude from the labelling pattern if the probe is homogeneously distributed in the membrane or if brighter regions can be readily distinguished. We also used FLIM, which allows to selectively analyze the fluorescence lifetime for each region of interest (ROI) of the plasma membrane of living cells. In addition to intact cells, GUV reconstituted from plasma membrane lipid extracts pertaining to either *wt* or *ipt1*Δ cells were also used. These reconstituted systems were double-labelled both with di-8-ANEPPS and with Rhod-DOPE. Rhod-DOPE was only used to label GUVs since when added externally to an aqueous solution it will not incorporate efficiently into the lipid bilayer [49]. Rhod-DOPE, due to the unsaturated acyl chains of DOPE moiety, partitions preferentially towards l_d phase versus both gel [63] and ergosterol-induced l_o [62] domains. In a three-phase coexistence situation, it will be mostly excluded from the gel, but still with some partition into the lo regions of the membrane [63]. Thus, since di-8-ANEPPS

labels preferentially the l_o phase and Rhod-DOPE the l_d phase, their distribution in the membrane allows to evaluate the phase behavior of the GUV prepared from the plasma membrane lipid extracts. Both GUV and living cells were analyzed by confocal microscopy and FLIM (Figure 2.3).

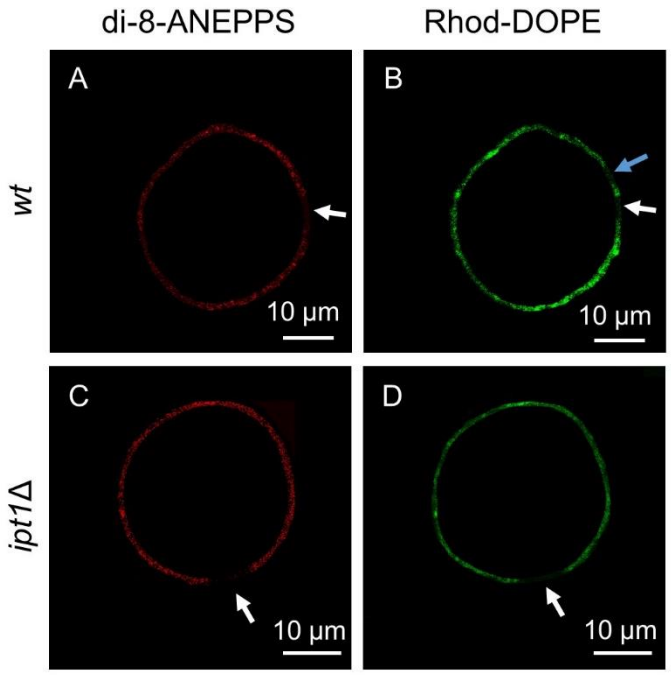

Figure 2. 3: *S. cerevisiae* plasma membrane lipids have complex phase behavior. Representative confocal microscopy images of giant unilamellar vesicles (GUVs) reconstituted from plasma membrane lipid extracts obtained from *wt* cells (A,B) or *ipt1*Δ cells (C,D) double-labelled with both di-8-ANEPPS and Rhod-DOPE. Images from di-8-ANEPPS channel (A,C) and Rhod-DOPE channel (B,D) are shown. White arrows indicate regions that were poorly labelled by both probes. The blue arrow points to a region that was poorly labelled by Rhod-DOPE but not at all by di-8-ANEPPS.

Confocal images of double-labelled GUVs prepared with plasma membrane lipid extracts from *wt* or *ipt1*Δ cells revealed that the fluorescence intensity of Rhod-DOPE and di-8-ANEPPS was not uniform throughout the GUV membrane. There were regions where the Rhod-DOPE signal was brighter, which indicated the presence of l_d domains. The same was observed for di-8-ANEPPS, which suggested the presence of regions where l_o predominates. Probe distribution throughout the membrane was clearly heterogeneous and despite the existence of regions where either the Rhod-DOPE or the di-8-ANEPPS signal was brighter it was not possible to accurately determine the relative proportion of l_d and l_o since these probes label most of the membrane, though with different intensity. Eventually, the size of the domains may be below the resolution of confocal fluorescence microscopy. Nonetheless, there were regions that were not labelled at all. These dark regions reveal lipid domains from which both probes were excluded. Both these probes are efficiently excluded from gel domains in

coexistence with l_d and l_o domains but have different distribution between l_d and l_o phases [49,64,65]. Therefore, those dark regions that are simultaneously unlabeled by both probes likely correspond to rigid gel domains, in agreement with the results obtained from the fluorescence spectroscopy of *t*-PnA (Figure 2.1).

FLIM experiments were carried out both on GUV and living yeast cells to study in more detail the biophysical properties of the plasma membrane regions probed by di-8-ANEPPS in *wt* versus *ipt1*Δ cells. In FLIM, the microscopy image generated is based on the fluorescence lifetime rather than fluorescence intensity. Electrochromic dyes such as ANEPPS display a complex relaxation kinetics, which translates into a multiexponential fluorescence decay. It is highly dependent on the density of dipoles and dielectric constant of the membrane interfacial region, polarity properties that can be strongly affected by the presence of sterols [61,66]. In the case of cells, ROI corresponding to the plasma membrane were selected (Figure 2.4 - A–D). The parameters describing the fluorescence intensity decays, namely the normalized pre-exponentials and the fluorescence lifetimes of the two exponential components, as well as the amplitude-weighted and intensity-weighted mean fluorescence lifetimes are presented in Table 2.2.

Table 2. 2: Fluorescence intensity decay parameters of di-8-ANEPPS incorporated in *S. cerevisiae wt* and *ipt1*Δ cells at 24 °C. The fluorescence intensity decays measured in cells were described by the sum of two exponentials, with amplitudes α_1 and α_2 and lifetimes τ_1 and τ_2. $\bar{\tau}$ is the amplitude-weighted mean fluorescence lifetime and $\langle\tau\rangle$ is the intensity-weighted mean fluorescence lifetime (Equations (3) and (4)). The values are the mean ± S.D. of more than 50 GUVs from three biological replicates and ca. 400 cells from four biological replicates.

Membrane System	Strain	τ_1 (ns)	α_1	τ_2 (ns)	α_2	$\bar{\tau}$ (ns)	$\langle\tau\rangle$ (ns)
GUV	*wt*	1.48±0.33	0.63±0.12	3.07±0.53	0.37±0.12	2.05±0.32	2.35±0.35
	ipt1Δ	1.37±0.29	0.66±0.09	3.11±0.54	0.34±0.09	1.95±0.33	2.30±0.37
Living cells	*wt*	1.43±0.40	0.38±0.07	3.00±0.31	0.62±0.07	2.43±0.12	2.70±0.06
	ipt1Δ	1.37±0.20	0.36±0.06	3.03±0.07	0.64±0.06	2.43±0.15	2.69±0.07

The lifetimes of the components describing the fluorescence decays obtained in GUV and in living cells are identical (Figure 2.4 - E, F) though their amplitudes are not (Figure 2.4 - G). Nonetheless, when comparing the two types of cells, *wt* and *ipt1*Δ, the decay parameters obtained were all very similar with no statistical differences found either in the plasma membrane of living cells or in reconstituted GUV, with a percent variation of less than 2%, if

at all. These results imply that the properties of the membrane reported by di-8-ANEPPS were not significantly affected by altering the composition of complex sphingolipids.

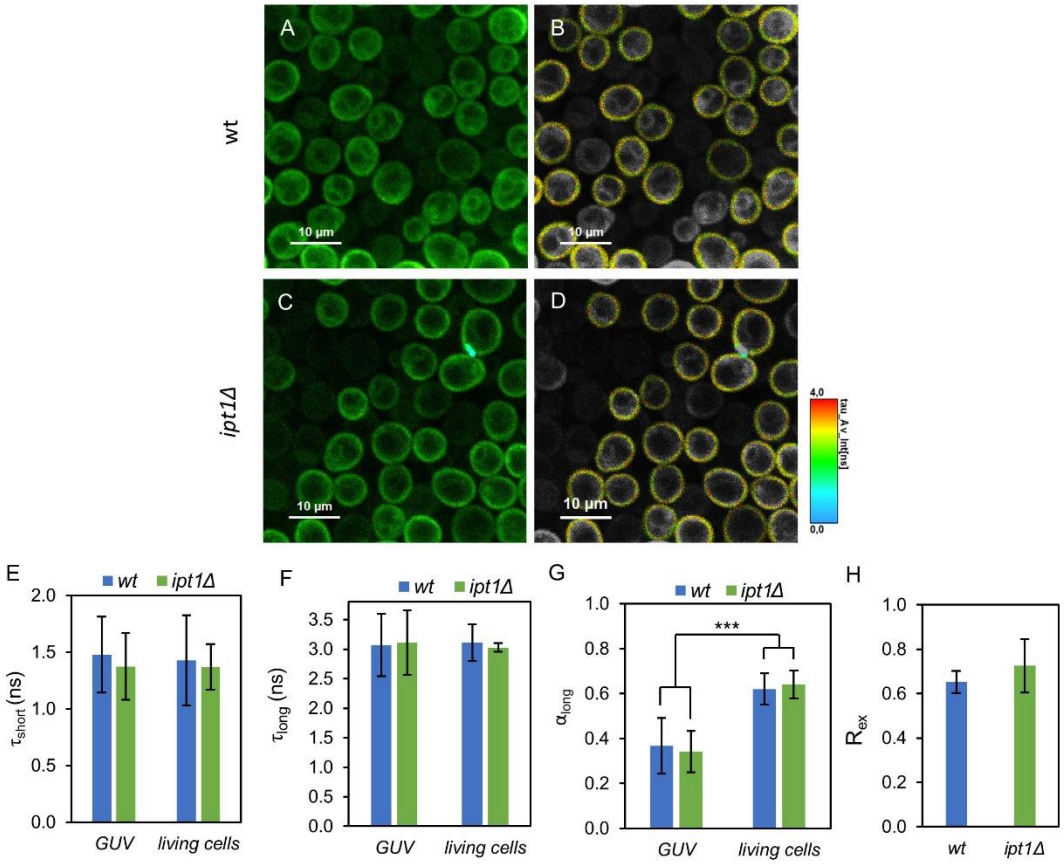

Figure 2. 4: Di-8-ANEPPS parameters are identical for *wt* and *ipt1*Δ cells in the different systems studied. Representative fluorescence lifetime imaging microscopy (FLIM) images of living *S. cerevisiae wt* (A,B) and *ipt1*Δ cells (C,D) labelled with di-8-ANEPPS. Panels (A,C) show representative intensity images, whereas in panels (B,D) the region-of-interest (ROI) selecting the plasma membrane is represented with the lifetime color scale obtained by FLIM. Lifetime components in GUVs obtained from plasma membrane lipids of *wt* and *ipt1*Δ cells and in living cells, (E) lifetime of the short component, (F) lifetime of the long component and (G) amplitude of the long component. The amplitude of the short component is 1-α_{long}. The values are the mean ± S.D. of at least three biological replicates with a total of at least 50 GUVs and 400 cells analyzed per strain. ***, $p \leq 0.001$. In panel (H) R_{ex} (420 nm/520 nm), which is linearly dependent on the membrane dipole potential, is shown for IPM suspensions labeled with di-8-ANEPPS ($n \geq 3$).

To further confirm that the properties of ergosterol-enriched domains are not affected by changes in the sphingolipid profile, the ratiometric value R_{ex} (420 nm/520 nm), which has a linear relationship with the membrane dipole potential [50], was determined from the excitation spectra of di-8-ANEPPS in the IPM of *S. cerevisiae* (Figure 2.4 - H). This parameter was not significantly different between *wt* and *ipt1*Δ cells, corroborating the previous conclusion.

The ⟨τ⟩ of Rhod-DOPE was also measured in GUVs reconstituted from lipids of *wt* cells yielding a value of 2.36 ± 0.02 ns, whereas in those prepared from lipids of *ipt1*Δ cells a value of 2.45 ± 0.04 ns was obtained. These values lay within those measured in phosphatidylcholine/ergosterol lipid bilayers, where a longer fluorescence lifetime points to a more fluid environment [62]. Thus, the fact that the fluorescence lifetime of Rhod-DOPE in

GUVs made from plasma membrane lipids is slightly longer for *ipt1*Δ cells than for *wt* cells, suggests a more fluid membrane in the deletion mutant, in agreement with the results obtained with the probe DPH.

3.4. The lateral organization of Pma1p but not Can1p is dependent on the sphingolipid profile

In order to evaluate the impact of changing sphingolipid composition of *S. cerevisiae* plasma membrane in the organization of MCC and MCP, the time-resolved fluorescence properties of Can1p tagged with GFP (Can1p-GFP) and Pma1p tagged with mRFP (Pma1p-mRFP) were studied by FLIM both in living *wt* and *ipt1*Δ cells. As already mentioned, Can1p is found in MCC domains that co-localize with ergosterol staining by filipin, whereas Pma1p is the hallmark of MCP which seems to be intimately related with sphingolipids, but with no direct evidence for sphingolipid enrichment [3].

The fluorescence decay parameters of the proteins mentioned above were collected for both *wt* and *ipt1*Δ cells (Figure 2.5 and Table S2.1). The decays are bi-exponential as expected when exciting GFP using a wavelength outside the absorption band of the protonated form and detecting emission above 500 nm [67–69]. Moreover, the lifetime and amplitude values obtained for each component of the fluorescence decay are in line with those reported in the literature [67–69]. The mean fluorescence lifetime obtained for GFP suggests that the protein is close to a medium with a high refractive index [70] as anticipated considering the membrane location of Can1p. For Can1p-GFP no differences were found between *wt* cells and *ipt1*Δ cells. On the contrary, for Pma1p-mRFP significant differences in the fluorescence decay parameters were found between the two strains studied (Supplementary Table S2.1). A statistically significant decrease was also observed in the intensity-weighted mean fluorescence lifetime, from 2.09 ± 0.04 ns in *wt* cells to 1.96 ± 0.07 ns in *ipt1*Δ cells (Figure 2.5 - B). This corresponds to, approximately, a 6% variation. This alteration reflects a different environment surrounding the protein in the two strains, which could be related to changes in the membrane refractive index, or to alterations in the pH or local ion concentration in the vicinity of the protein. Considering, *e.g.*, that the refractive index of a lipid membrane varies with the length and packing of the lipid hydrophobic chains [71] and also with polar headgroup chemistry [72], the change obtained in the mean fluorescence lifetime is particularly relevant since it would represent a variation equivalent to ~0.03 in terms of refractive index, or an increase of 20% (*v/v*) of glycerol in a water/glycerol mixture for a GFP in solution [70], which, in turn, is also

comparable *e.g.*, to a change of about 6 carbons in the length of a fatty acid chain monolayer [71].

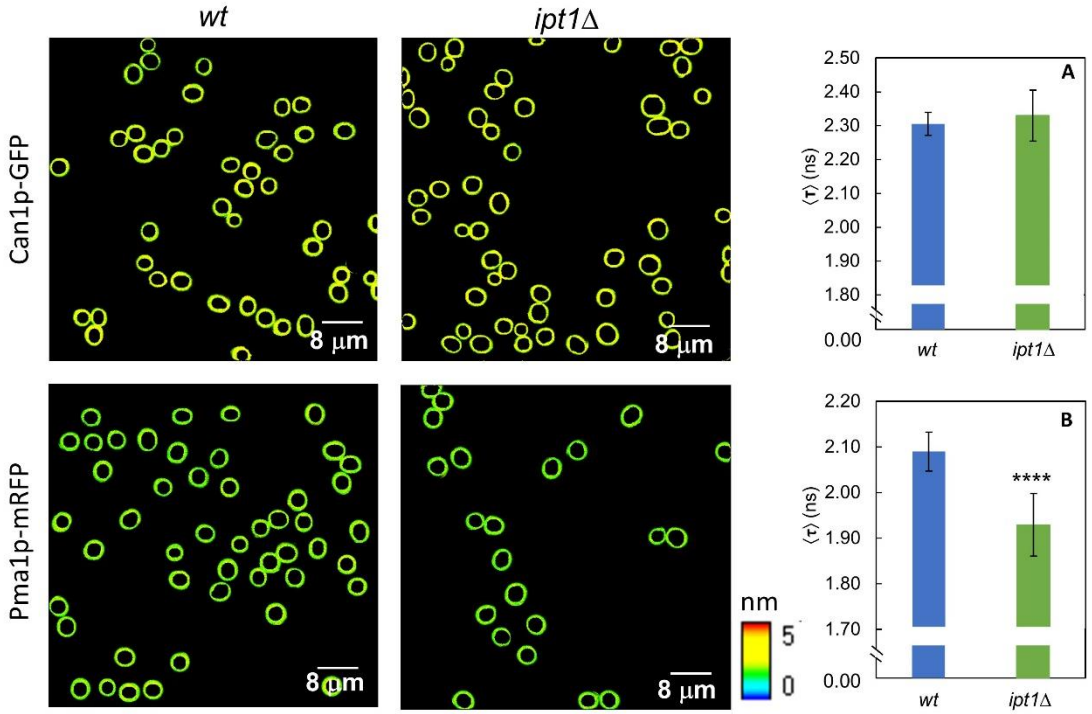

Figure 2. 5: The lack in M(IP)$_2$C leads to a change in the microenvironment surrounding Pma1p but not Can1p. Representative FLIM images of ROI comprising *S. cerevisiae wt* cells and *ipt1*Δ cells plasma membrane. Intensity-weighted mean fluorescence lifetime for *S. cerevisiae* cells. (**A**) *wt*-Can1p-GFP and *ipt1*Δ-Can1p-GFP cells and (**B**) *wt*-Pma1p-mRFP and *ipt1*Δ-Pma1p-mRFP cells. The values are the mean ± S.D. of three independent biological replicates with a total of ca. 400 cells analyzed for each strain. **** $p \leq 0.0001$.

The heterogeneity of Can1p and Pma1p distribution in the plasma membrane of *S. cerevisiae* was also assessed (see Section 2.7.2) to further evaluate the possible influence of the complex sphingolipids in the yeast membrane compartments MCC and MCP. The distribution heterogeneity was determined by confocal fluorescence microscopy [15,23], as described in the experimental section. These fusion proteins have been used previously to visualize and detect alterations in both membrane compartments in *S. cerevisiae* [15,23], or similar proteins, *e.g.*, Pma1p-GFP in other fungi such as *Neurospora Crassa* [73] or Pma1p tagged with hemagglutinin in *C. neoformans* [28].

In Figure 2.6, representative confocal images for the two strains labeled with either Pma1p-mRFP or Can1p-GFP are shown, as well as values obtained for the heterogeneity of their distribution in the plasma membrane for all the replicates. The fact that the heterogeneity values for Can1p and Pma1p distribution in the plasma membrane in *wt* cells are very similar, 0.68 ± 0.10 and 0.66 ± 0.12 respectively, can be due to the reported complementarity of the two membrane compartments. The heterogeneity of Can1p distribution is only slightly - if at all - affected by 3% in *ipt1*Δ cells relatively to *wt* cells (Figure 2.6 - A). In contrast, the heterogeneity

of Pma1p distribution in the plasma membrane is 15% higher in *ipt1*Δ cells than in *wt* cells (Figure 2.6 - B), a prominent change between strains especially when compared to the one found for Can1p. Interestingly, the quantification of fluorescence intensity at the plasma membrane (see supplementary Figure S2.5), reveals that Can1p-GFP has slightly higher average intensity in *ipt1*Δ plasma membrane than in the *wt*, whilst for Pma1p-mRFP, the intensity is significantly weaker in *ipt1*Δ cells. This difference in fluorescence intensity between strains indicates a change in the amount of protein at the plasma membrane, since the fluorescence quantum yield of Pma1p-RFP is only marginally lower in *ipt1*Δ cells, according to the measured amplitude-weighted mean fluorescence lifetimes (Supplementary Table S2.1) and pinpoints a potential defect in Pma1p accumulation at the plasma membrane in *ipt1*Δ cells. The mechanism underlying the lower Pma1p-mRFP levels at the plasma membrane of *ipt1*Δ cells can be related to alterations in the protein traffic or turnover or protein expression levels.

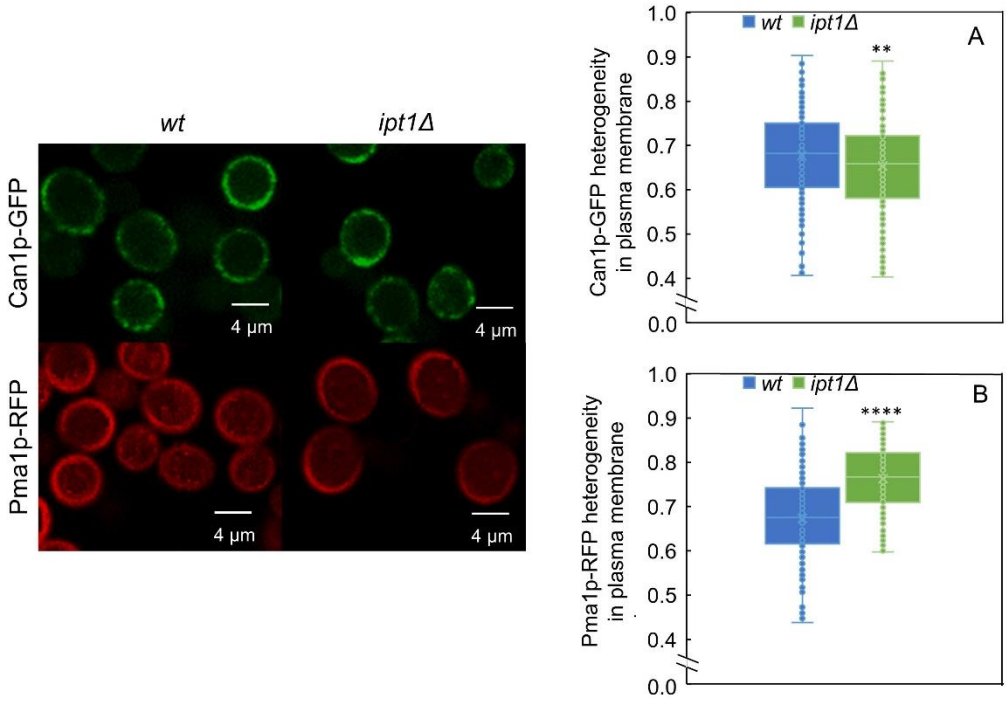

Figure 2. 6: MCP distribution in the plasma membrane is different in *wt* cells and *ipt1*Δ cells. The heterogeneity of Can1p-GFP and Pma1p-mRFP distribution along the plasma membrane was determined for *wt* cells (**A**) and *ipt1*Δ cells (**B**) as described in the experimental procedures. The values are the median ± S.D. of at least four biological replicates with a total of at least 190 cells analyzed per replicate. **, $p \leq 0.01$; ****, $p \leq 0.0001$. On the left, representative confocal fluorescence images of living *S. cerevisiae* cells with or without deletion of *IPT1* and expressing either Can1p-GFP or Pma1p-mRFP, as indicated, are shown.

4. Discussion

Sphingolipid-enriched gel domains in the plasma membrane of yeast [11] have been proposed to act as diffusion barriers [9] possibly contributing to the stability of the plasma membrane compartments [48] and to the separation of mother and daughter cell components during *S. cerevisiae* cell division that occurs at the budding neck [74]. Another possible function

might relate to cell viability in the absence of a cell wall since in the filamentous fungus *N. crassa*, a much tighter packing of sphingolipid-enriched domains occurs in the cell wall-less slime strain when compared to the *wt* strain under similar growth conditions [59] and membrane compartmentalization of lipids and proteins is interconnected to the cell wall and responds to cell wall stress [4]. Although it has been shown that sphingolipids are crucial for the formation and properties of such gel domains [10,11], it is still unclear if these domains contain a major sphingolipid class or if they are composed by a mixture of different sphingolipids. $M(IP)_2C$ is the most abundant complex sphingolipid in *S. cerevisiae*, particularly at the plasma membrane [35,75], but experimental support allowing the unequivocal identification of the components of gel domains is missing.

Considering the numerous relations between sphingolipids and/or C26 very long chain fatty acids with Pma1p [27,76], it is reasonable to predict that sphingolipid-enriched regions (gel domains) and MCP may co-localize at the yeast plasma membrane, but no direct evidence to confirm this hypothesis is available. Moreover, the impact of the sphingolipid headgroup on Pma1p distribution and microenvironment in the plasma membrane of *S. cerevisiae* has not been elucidated.

Recent observations support the hypothesis that MCC domains are ergosterol-enriched [7]. However, it is still unknown if complex sphingolipids, particularly $M(IP)_2C$, play a direct role in the organization of the MCC [3,15].

To address these questions, *wt* cells and *ipt1*Δ cells were compared regarding plasma membrane biophysical properties and distribution and organization of proteins referring to distinct membrane compartments. The deletion of the *IPT1* gene, which leads to the lack of $M(IP)_2C$ and its replacement by MIPC [35,36], allows to evaluate how changing the polar headgroup of complex sphingolipids influences the different plasma membrane lipid domains, namely, the sphingolipid-enriched gel domains, and also how it impacts on protein distribution and microenvironment. Thus, we aimed at establishing a more direct correlation between sphingolipid-enriched domains and MCP or MCC.

We showed in this work that the formation of gel domains was not hampered by the absence of $M(IP)_2C$ as the relative abundance of these domains in the plasma membrane was similar for both *S. cerevisiae wt* cells and *ipt1*Δ cells. In fact, in *ipt1*Δ cells, plasma membrane gel domains are even more rigid than those found in *wt* cells, as reported by *t*-PnA time-resolved fluorescence. This can be rationalized considering that $M(IP)_2C$ is a constituent of gel domains and in *ipt1*Δ cells is replaced by MIPC in those domains. The lack of a second inositol phosphate group makes the polar head of MIPC smaller and less charged than that of $M(IP)_2C$.

This may allow a tighter packing of these complex sphingolipids due to less electrostatic repulsion and/or steric hindrance at the headgroup level, which may result in a tighter packing and a more rigid environment at the hydrophobic membrane core. A similar proposal has been made to explain the tighter packing of gel domains found in the plasma membrane of *scs7*Δ cells, which lack the 2-OH group in the fatty acyl chain of all sphingolipids, when compared with *wt* cells [11]. On the other hand, the polar headgroups of $M(IP)_2C$ and MIPC may confer different average transversal positions to the sphingolipid amide group and sphingolipid backbone hydroxyl groups, which leads to distinct H-bonding network at the membrane surface [77] affecting the compactness of gel domains. The biophysical differences reported in this work between *wt* and *ipt1*Δ cells suggest that $M(IP)_2C$ is an important component of gel domains in *wt* cells. If sphingolipid-enriched domains were mainly composed by MIPC only, and independent of $M(IP)_2C$, then in *ipt1*Δ cells, which have a higher concentration of MIPC in the plasma membrane [46,78], we would observe an increase in the abundance of sphingolipid-enriched domains, but no changes in their packing. However, what we found is the opposite, *i.e.*, an increased packing and either no changes or a very small decrease in the abundance of sphingolipid-enriched domains. Thus, in *ipt1*Δ cells the sphingolipid-enriched domains are probably enriched in MIPC, as compared to *wt* cells. This can be due either to a direct effect, *i.e.*, the absence of $M(IP)_2C$ and its replacement by MIPC or an indirect effect that results from changing the balance of interactions between sphingolipids, including IPC, or between sphingolipids and other membrane lipids.

The loss of the *IPT1* gene leads to an increase in calcium tolerance [36,79], and differential drug resistance/sensitivity phenotypes [80], or an impaired uptake of miconazole [81,82]. Such results indicate that $M(IP)_2C$ differentially affects membranes permeability or the activity of membrane proteins [80], which suggests that different direct/indirect mechanisms may be at play. It has also been suggested that in *ipt1*Δ *S. cerevisiae* cells, lowered levels of $M(IP)_2C$ or altered levels of other sphingolipids may regulate the activity of some ABC transporters such as Pdr5p and Yor1p, which have been associated with controlling phospholipid content or distribution at the plasma membrane [83,84].

Thus, alterations of membrane components other than sphingolipids could be responsible, *e.g.*, for the decreased global fluidity of the plasma membrane in *ipt1*Δ cells. Sphingolipid-enriched gel domains have been proposed to serve as diffusion barriers [74], which may account, *e.g.*, for the slow diffusion of plasma membrane proteins in yeast. Thus, the alteration in their rigidity may influence the diffusion properties of several membrane components in the plasma membrane [85], conformational freedom of proteins residing in these domains [86] or

the partition of proteins in/out of these domains, namely glycosylphosphatidylinositol-anchored proteins [11].

While changing the sphingolipid headgroup has a measurable impact on the compactness of gel domains, it has no obvious effect on the lipid-dependent dipolar properties of sterol-enriched domains. With di-8-ANEPPS, our results for both fluorescence lifetime and membrane dipole potential measurements, were nearly identical for *wt* and *ipt1*Δ cells, regardless of the model system studied GUVs, living cells or IPM. This suggests that those biophysical properties, which are strongly dependent on sterol and sterol-lipid interactions [51,61], are less dependent on the major sphingolipid headgroup. In *erg6*Δ cells, which have an altered sterol profile, but no noticeable changes in sphingolipid profile when compared to *wt* cells [87,88], the rigidity of the gel domains is not changed [11], but the fluorescence lifetime of a sterol sensitive dye is significantly different from *wt* cells [51]. This behavior is opposite to that found for *ipt1*Δ cells where the rigidity of the gel domains is increased but the fluorescence properties of di-8-ANEPPS remain unchanged when compared to *wt* cells. Hence, sphingolipid-enriched and ergosterol-enriched regions seem to be to a certain extent independent in the plasma membrane of yeast. Those results thus support the recent observation that sphingolipids and ergosterol do not predominate in the same membrane leaflet [89]. Nonetheless, the occurrence of sphingolipid-enriched domains in the outer leaflet does not rule out the presence of ergosterol molecules in the inner leaflet of MCP.

Regarding the protein markers of membrane compartments, it was found that Pma1p plasma membrane distribution heterogeneity and fluorescence lifetime are changed in *ipt1*Δ cells when compared to *wt* cells, whereas the same parameters remain unaltered for Can1p. Since Pma1p and Can1p-specific membrane compartments have been described as spatially separated [1,3], and considering that changes were observed in the biophysical properties of sphingolipid-enriched domains but not in ergosterol-enriched domains, the results obtained in this work for Pma1p and Can1p support an independent compartmentalization of sphingolipid-enriched and sterol-enriched regions, and that these regions could be lipid domain counterparts of the MCP and the MCC, respectively. Currently, it is not certain which lipids compose either MCP or MCC apart from the lower ergosterol content of the former and the higher ergosterol content of the latter [15,23,86]. However, by using a lipidomic approach with styrene-maleic-acid polymers (SMAPLs) to determine which lipids surround Can1p and Pma1p, and other MCC or MCP specific proteins (periprotein lipidome), Klooster et al. [86] demonstrated that in fact the sphingolipid/ergosterol ratio is much higher in the MCP than in the MCC, while they do not differ much in periprotein phospholipid composition. The distribution pattern of Pma1p

as isolated foci in the plasma membrane has been associated to the honeycomb-like hexagonal lattices observed on the plasma membrane of *S. cerevisiae* [1]. Moreover, it has been suggested that the lipids contained in these structures should be very compact and display a gel arrangement [1]. The results here presented, and considering the body of knowledge on the relation between sphingolipids and sterols in MCP organization, *e.g.*, [1,26–33,86], are consistent with the presence of gel-forming sphingolipids in the composition of the MCP, providing the most simple explanation for the concomitant changes here observed in gel domains packing and Pma1p-mRFP, but not Can1p-GFP, distribution and fluorescence lifetime. The different fluorescence lifetime of Pma1p-mRFP in *wt* vs. *ipt1*Δ, cells reflects a different environment for the protein. This could be due to a different refractive index in the vicinity of the protein, which could be attributed to its relocation into different domains or changes in the thickness and packing of those domains, or it could also be due to misfunction of Pma1p leading to alterations of pH and ion concentration in the vicinity of the protein. This is a subject that certainly deserves further investigation. Our data strongly suggest that the MCC does not contain gel domains, since an alteration of their compactness did not affect the properties measured for Can1p. However, it should be noted that Can1p MCC partitioning is less affected than other MCC transporters by sphingolipid stress [3].

The labelling of GUV reconstituted from plasma membrane lipid extracts of *wt* cells or *ipt1*Δ cells with both di-8-ANEPPS and Rhod-DOPE revealed a complex phase behavior where three distinct types of domains can be distinguished and related to a three-phase coexistence (l_d/l_o/gel). DPH steady-state fluorescence anisotropy was lower in the IPM of *ipt1*Δ cells, pointing to a lower global order of the membrane, which seems to contradict the higher order of the gel domains. Therefore, it seems that the remainder of the membrane is more fluid. In particular, there could be a small increase in the relative abundance and/or fluidity of l_d-like domains. Upon *IPT1* deletion no alterations in l_o-like domains were apparent, since fluorescence decays of di-8-ANEPPS yielded similar components lifetimes and amplitudes in *ipt1*Δ and *wt* cells, and the gel domains became more rigid (and maybe slightly less abundant). Phytoceramide, the backbone of complex sphingolipids in yeast, can recruit up to 3 glycerophospholipid molecules per molecule of phytoceramide to form rigid gel phases [48]. It is possible that each $M(IP)_2C$ molecule can recruit a higher number of glycerophospholipid molecules, not only due to its double negative charge that could interact with the positive choline moiety of phosphatidylcholine, but especially because of the large size of its polar headgroup. MIPC, which is less charged and contains a smaller headgroup compared to $M(IP)_2C$, would recruit a lower number of glycerophospholipid molecules than $M(IP)_2C$. Thus,

in *ipt1*Δ cells, where $M(IP)_2C$ is missing and MIPC accumulates instead, gel domains would be more rigid due to the lower content in glycerophospholipids. On another hand, these low melting temperature lipids would become more available for the formation of disordered domains, contributing to the higher global fluidity of the membrane in *ipt1*Δ cells. Since gel domains are more rigid in *ipt1*Δ cells, this would suggest that liquid domains are more disordered in this strain. It was previously confirmed with DPPC and POPC membranes with and without cholesterol, labelled with Rhod-DOPE at different probe/lipid ratios [62,90], that the higher the ⟨τ⟩ values for Rhod-DOPE the more disordered are the membrane regions into which the probe is incorporating. Therefore, the fact that ⟨τ⟩ of Rhod-DOPE in GUVs reconstituted from lipids of *wt* cells is lower than those prepared from lipids of *ipt1*Δ cells supports the hypothesis that liquid regions in the plasma membrane of *ipt1*Δ cells are more disordered when compared to *wt* cells. Additionally, considering the recent results on the Pma1p periprotein lipidome [86], where this region of the membrane is sphingolipid-enriched, but there seems to be some ergosterol present, one might hypothesize that in *ipt1*Δ cells the sphingolipid-enriched domains /Pma1p periprotein lipidome become even more depleted in ergosterol, which could also lead to an increased rigidity of the domains, because ergosterol may actually fluidify these domains [11]. However, it is unlikely that the changes are due to ergosterol, because there were no changes in the fluorescence parameters of di-8-ANEPPS in *ipt1*Δ cell membrane and, in the *erg6*Δ cells strain lacking ergosterol mentioned above, the rigidity of the gel domains was not different from the *wt*.

This work points to a role of the polar headgroup of complex sphingolipids in the organization of Pma1p in the plasma membrane of *S. cerevisiae*. Also, in *C. neoformans* the complex sphingolipid headgroup has been related with Pma1p oligomerization and transport [28]. By regulating the rigidity/order of gel domains, sphingolipid polar headgroups may thus contribute to control Pma1p stability, distribution, and oligomerization in the plasma membrane. However, a specific interaction of $M(IP)_2C$, having an extra inositol phosphate group as compared to MIPC, with the protein cannot be ruled out. If the lipid annulus surrounding the protein is different, *e.g.*, in terms of number of lipid rings, the fraction of annular or non-annular complex sphingolipid may change, resulting in a different overall packing within the sphingolipid-enriched domains.

The present work shows how the headgroup structure of complex sphingolipids can be an important determinant in the organization of plasma membrane lipids and proteins in *S. cerevisiae*. Recently, we showed that the polyene antifungal nystatin forms active pores in membranes lacking any sterol, but containing gel domains [12], challenging the classical model

which describes the molecular mode of action of nystatin through an ergosterol-dependent mechanism. Moreover, the action of other antifungal drugs has been shown to involve an interplay with sphingolipids that is conditioned by their headgroup structure. *S. cerevisiae* cells defective in $M(IP)_2C$ are resistant to zymocin [37]. Moreover, zymocin requires an active Pma1p proton pump to exert its toxicity. These observations can be related to our results supporting a close relation between MCP and sphingolipid-enriched domains. The sphingolipid headgroup also influences the antifungal activity of the lipopeptide syringomycin E [38]. Fungi lacking $M(IP)_2C$, and accumulating MIPC, become resistant to syringomycin E. Syringomycin E acts on the membrane forming channels causing K^+ efflux and Ca^{2+} influx. The complete absence of $M(IP)_2C$ hampers syringomycin E toxicity. Since in *ipt1*Δ cells, gel domains become more tightly packed, this might hinder the insertion of syringomycin E acyl chain into the membrane. An independent study supporting the importance of sphingolipid-dependent biophysical properties shows that *scs7*Δ cells, where sphingolipid-enriched domains are also more rigid than in *wt* cells [11], are also more resistant to the action of syringomycin E. Since the lack of $M(IP)_2C$ leads to a tightening of gel domains, as well as to an altered distribution of Pma1p, it is possible that membrane proteins, alongside lipid composition, are also important for the susceptibility to syringomycin E. This is further supported by the observation that Pma1p proper functioning is crucial for the virulent activity of pathogenic fungi [28,91,92]. The apparent requirement of intact MCP/$M(IP)_2C$ domains for the action of syringomycin E is supported by the fact that cumulative conditions of MIPC accumulation and absence of $M(IP)_2C$ lead to resistance; yet higher levels of MIPC, when $M(IP)_2C$ is still produced, do not change the sensitivity phenotype [93]. A better understanding of sphingolipids role in yeast plasma membrane organization, particularly, in domain formation, may thus be an important contribute to clarify antifungal molecular targets and mode of action.

Gournas and collaborators showed that sphingolipids are required for the slower diffusion of Can1p in the MCC [8] and, presented different hypothesis for the still unknown mechanism [3]. Our results seem to rule out the hypothesis that $M(IP)_2C$ is directly required for the conformation-dependent anchoring of the protein transporters in the MCC, since its absence does not alter any measured property of Can1p. Also, in this work we observed diverse membrane reorganizations upon *IPT1* deletion, including changes in global plasma membrane fluidity, and yet no significant alterations were detected for Can1p, which seems to discard the hypothesis that the partitioning of Can1p into the MCC could be indirectly affected by a general alteration of plasma membrane organization. Our results did not confirm neither reject the possibility that sphingolipids depletion could lead to a concomitant decrease of ergosterol levels

in eisosomes, since ergosterol levels are similar in both *ipt1*Δ cells and *wt* cells and we show that some of the sterol-dependent properties are not significantly changed in the plasma membrane of *ipt1*Δ cells when compared to *wt* cells. However, another scenario is still possible, where sphingolipid-enriched domains act as diffusional barriers and are neighboring the MCC, thus preventing movement of Can1p. The change in sphingolipid levels may induce an alteration of the relative arrangement of yeast compartments, indirectly affecting those that are not sphingolipid-enriched.

5. Conclusions

There are still many unaddressed questions regarding lipid–protein interactions in the plasma membrane of fungi. Disclosing the mechanism of membrane compartments formation, their lipid composition and interrelations will hopefully lead to significant advances in membrane biology, but their investigation is also driven by the importance of some of these compartments in the pathogenicity of clinically relevant fungal species.

The identification of gel domains under physiological conditions was an important finding but the specific molecular constitution of those domains is unknown. Four different fluorescent probes, *t*-PnA, DPH, di-8-ANEPPS, and Rhod-DOPE, were used to label yeast plasma membrane, in living cells and IPM and in reconstituted systems, namely GUV made from plasma membrane lipid extracts. The set of probes employed yields complementary information that enables a comprehensive picture of the biophysical changes taking place at the plasma membrane upon the loss of $M(IP)_2C$ synthesis ability. With this work, it became clear that $M(IP)_2C$ is important for the regulation of gel domains in the plasma membrane of yeast, since in cells unable to synthesize this complex sphingolipid these domains are more rigid. In the future, co-localization studies with Pma1p-mRFP, and Can1p-GFP-containing *wt* cells [23], *ipt1*Δ cells and other strains with mutations in sphingolipid (and sterol) metabolism will provide invaluable insights to further understand the intricate relation between membrane lipid composition, biophysical properties, and membrane compartments organization and function in yeast.

Our results also help to clarify the interrelation between sphingolipids, $M(IP)_2C$ in this case, and Pma1p or Can1p. Diverse results in the literature point to a dependence of Pma1p proper sorting with intact sphingolipid synthesis. Here, we demonstrate a direct correlation between sphingolipid polar headgroup and protein distribution. Pma1p distribution is more heterogeneous in *ipt1*Δ cells, whereas Can1p distribution, if affected at all, becomes slightly more homogeneous. This suggests that $M(IP)_2C$ is directly involved in the organization of

MCP, but possibly not of MCC. The concomitant alteration in the rigidity of gel domains and Pma1p distribution supports a close communication between gel domains and MCP. On the other hand, MCC and ergosterol-enriched domains did not undergo any noticeable changes upon a major alteration of complex sphingolipid profile, which corroborates that MCC and ergosterol co-localize, further supporting that $M(IP)_2C$ is not an important constituent of ergosterol-enriched domains.

Acknowledgements

The authors thank Guido Grossmann and Widmar Tanner (University of Regensburg, Germany) that generously provided plasmid Ylp211-CAN1-GFP (*URA3*) and Ylp128-PMA1-mRFP (*LEU2*). We wish to thank Luísa Cyrne (Universidade de Lisboa, Portugal) for helping with the yeast cells transformation.

References

1. Malinsky, J.; Opekarova, M. New Insight into the Roles of Membrane Microdomains in Physiological Activities of Fungal Cells. *Int. Rev. Cell Mol. Biol.* **2016**, 325, 119–180.
2. Zahumensky, J.; Malinsky, J. Role of MCC/Eisosome in Fungal Lipid Homeostasis. *Biomolecules*. **2019**, 9, 305.
3. Athanasopoulos, A.; André, B.; Sophianopoulou, V.; Gournas, C. Fungal Plasma Membrane Domains. *FEMS Microbiol. Rev.* **2019**.
4. De Almeida, R.F.M. A route to understanding yeast cellular envelope—Plasma membrane lipids interplaying in cell wall integrity. *FEBS J.* **2018**.
5. Ganguly, S.; Singh, P.; Manoharlal, R.; Prasad, R.; Chattopadhyay, A. Differential dynamics of membrane proteins in yeast. *Biochem. Biophys. Res. Commun*. **2009**, 387, 661–665.
6. Valdez-Taubas, J.; Pelham, H.R. Slow di_usion of proteins in the yeast plasma membrane allows polarity to be maintained by endocytic cycling. *Curr. Biol. CB* **2003**, 13, 1636–1640.
7. Bianchi, F.; Syga, Ł.; Moiset, G.; Spakman, D.; Schavemaker, P.E.; Punter, C.M.; Seinen, A.-B.; van Oijen, A.M.; Robinson, A.; Poolman, B. Steric exclusion and protein conformation determine the localization of plasma membrane transporters. *Nat.Commun*. **2018**, 9, 501.
8. Gournas, C.; Gkionis, S.; Carquin, M.; Twyffels, L.; Tyteca, D.; André, B. Conformation-dependent partitioning of yeast nutrient transporters into starvation-protective membrane domains. *Proc. Natl. Acad. Sci. USA* **2018**, 115, E3145–E3154.
9. De Almeida, R.F.; Joly, E. Crystallization around solid-like nanosized docks can explain the specificity, diversity, and stability of membrane microdomains. *Front. Plant Sci.* **2014**, 5, 72.
10. Vecer, J.; Vesela, P.; Malinsky, J.; Herman, P. Sphingolipid levels crucially modulate lateral microdomain organization of plasma membrane in living yeast. *FEBS Lett.* **2014**, 588, 443–449.
11. Aresta-Branco, F.; Cordeiro, A.M.; Marinho, H.S.; Cyrne, L.; Antunes, F.; de Almeida, R.F. Gel domains in the plasma membrane of Saccharomyces cerevisiae: Highly ordered, ergosterol-free, and sphingolipid-enriched lipid rafts. *J. Biol. Chem*. **2011**, 286, 5043–5054.
12. Dos Santos, A.G.; Marquês, J.T.; Carreira, A.C.; Castro, I.R.; Viana, A.S.; Mingeot-Leclercq, M.P.; de Almeida, R.F.M.; Silva, L.C. The molecular mechanism of Nystatin action is dependent on the membrane biophysical properties and lipid composition. *Phys. Chem. Chem. Phys*. **2017**, 19, 30078–30088.
13. Stradalova,V.; Stahlschmidt,W.; Grossmann, G.; Blazikova, M.; Rachel, R.; Tanner,W.; Malinsky, J. Furrow-like invaginations of the yeast plasma membrane correspond to membrane compartment of Can1. *J. Cell Sci.* **2009**, 122, 2887–2894.
14. Walther, T.C.; Brickner, J.H.; Aguilar, P.S.; Bernales, S.; Pantoja, C.;Walter, P. Eisosomes mark static sites of endocytosis. *Nature* **2006**, 439, 998–1003.
15. Grossmann, G.; Opekarova, M.; Malinsky, J.; Weig-Meckl, I.; Tanner, W. Membrane potential governs lateral segregation of plasma membrane proteins and lipids in yeast. *EMBO J.* **2007**, 26, 1–8.
16. Berchtold, D.; Piccolis, M.; Chiaruttini, N.; Riezman, I.; Riezman, H.; Roux, A.; Walther, T.C.; Loewith, R. Plasma membrane stress induces relocalization of Slm proteins and activation of TORC2 to promote sphingolipid synthesis. *Nat. Cell Biol*. **2012**, 14, 542–547.
17. Douglas, L.M.; Konopka, J.B. Plasma membrane architecture protects Candida albicans from killing by copper. *PLoS Genet*. **2019**, 15, e1007911.

18. Douglas, L.M.; Wang, H.X.; Keppler-Ross, S.; Dean, N.; Konopka, J.B. Sur7 promotes plasma membrane organization and is needed for resistance to stressful conditions and to the invasive growth and virulence of Candida albicans. *mBio*. **2012**, 3.
19. Pedroso, N.; Matias, A.C.; Cyrne, L.; Antunes, F.; Borges, C.; Malho, R.; de Almeida, R.F.M.; Herrero, E.; Marinho, H.S. Modulation of plasma membrane lipid profile and microdomains by H2O2 in Saccharomyces cerevisiae. *Free Radic. Biol. Med*. **2009**, 46, 289–298.
20. Dupont, S.; Beney, L.; Ritt, J.F.; Lherminier, J.; Gervais, P. Lateral reorganization of plasma membrane is involved in the yeast resistance to severe dehydration. *Biochim. Biophys. Acta* **2010**, 1798, 975–985.
21. Grossmann, G.; Malinsky, J.; Stahlschmidt, W.; Loibl, M.; Weig-Meckl, I.; Frommer, W.B.; Opekarova, M.; Tanner, W. Plasma membrane microdomains regulate turnover of transport proteins in yeast. *J. Cell Biol*. **2008**, 183, 1075–1088.
22. Herman, P.; Vecer, J.; Opekarova, M.; Vesela, P.; Jancikova, I.; Zahumensky, J.; Malinsky, J. Depolarization affects the lateral microdomain structure of yeast plasma membrane. *FEBS J*. **2015**, 282, 419–434.
23. Malinska, K.; Malinsky, J.; Opekarova, M.; Tanner, W. Visualization of protein compartmentation within the plasma membrane of living yeast cells. *Mol. Biol. Cell* **2003**, 14, 4427–4436.
24. Serrano, R. Transport across yeast vacuolar and plasma membrane. In *The Molecular and Cellular Biology of the Yeast Saccharomyces: Genome Dynamics, Protein Synthesis, and Energetics*; Broach, J.R., Jones, E.W., Pringle, J.R., Eds.; Cold Spring Harbor Laboratory Press: Cold Spring Harbor, NY, USA, 1991; Volume 21, pp. 523–585.
25. Kane, P.M. Proton Transport and pH Control in Fungi. *Adv. Exp. Med. Biol*. **2016**, 892, 33–68.
26. Bagnat, M.; Chang, A.; Simons, K. Plasma membrane proton ATPase Pma1p requires raft association for surface delivery in yeast. *Mol. Biol. Cell* **2001**, 12, 4129–4138.
27. Gaigg, B.; Toulmay, A.; Schneiter, R. Very long-chain fatty acid-containing lipids rather than sphingolipids per se are required for raft association and stable surface transport of newly synthesized plasma membrane ATPase in yeast. *J. Biol. Chem*. **2006**, 281, 34135–34145.
28. Farnoud, A.M.; Mor, V.; Singh, A.; Del Poeta, M. Inositol phosphosphingolipid phospholipase C1 regulates plasma membrane ATPase (Pma1) stability in Cryptococcus neoformans. *FEBS Lett*. **2014**, 588, 3932–3938.
29. Munshi, M.A.; Gardin, J.M.; Singh, A.; Luberto, C.; Rieger, R.; Bouklas, T.; Fries, B.C.; Del Poeta, M. The Role of Ceramide Synthases in the Pathogenicity of Cryptococcus neoformans. *Cell Rep*. **2018**, 22, 1392–1400.
30. Wang, Q.; Chang, A. Sphingoid base synthesis is required for oligomerization and cell surface stability of the yeast plasma membrane ATPase, Pma1. *Proc. Natl. Acad. Sci. USA* **2002**, 99, 12853–12858.
31. Lauwers, E.; Andre, B. Association of yeast transporters with detergent-resistant membranes correlates with their cell-surface location. *Traffic.* **2006**, 7, 1045–1059.
32. Lauwers, E.; Grossmann, G.; Andre, B. Evidence for coupled biogenesis of yeast Gap1 permease and sphingolipids: Essential role in transport activity and normal control by ubiquitination. *Mol. Biol. Cell* **2007**, 18, 3068–3080.
33. Lee, M.C.; Hamamoto, S.; Schekman, R. Ceramide biosynthesis is required for the formation of the oligomeric H+-ATPase Pma1p in the yeast endoplasmic reticulum. *J. Biol. Chem*. **2002**, 277, 22395–22401.
34. Ferreira, T.; Mason, A.B.; Slayman, C.W. The yeast Pma1 proton pump: A model for understanding the biogenesis of plasma membrane proteins. *J. Biol. Chem*. **2001**, 276, 29613–29616.
35. Leber, A.; Fischer, P.; Schneiter, R.; Kohlwein, S.D.; Daum, G. The yeast mic2 mutant is defective in the formation of mannosyl-diinositolphosphorylceramide. *FEBS Lett.* **1997**, 411, 211–214.
36. Dickson, R.C.; Nagiec, E.E.; Wells, G.B.; Nagiec, M.M.; Lester, R.L. Synthesis of mannose-(inositol-P)(2)-ceramide, the major sphingolipid in Saccharomyces cerevisiae, requires the IPT1 (YDR072c) gene. *J. Biol. Chem.* **1997**, 272, 29620–29625.
37. Zink, S.; Mehlgarten, C.; Kitamoto, H.K.; Nagase, J.; Jablonowski, D.; Dickson, R.C.; Stark, M.J.R.; Schaffrath, R. Mannosyl-diinositolphospho-ceramide, the major yeast plasma membrane sphingolipid, governs toxicity of Kluyveromyces lactis zymocin. *Eukaryot. Cell* **2005**, 4, 879–889.
38. Stock, S.D.; Hama, H.; Radding, J.A.; Young, D.A.; Takemoto, J.Y. Syringomycin E inhibition of Saccharomyces cerevisiae: Requirement for biosynthesis of sphingolipids with very-long-chain fatty acids and mannoseand phosphoinositol-containing head groups. *Antimicrob. Agents Chemother*. **2000**, 44, 1174–1180.
39. Thevissen, K.; Cammue, B.P.; Lemaire, K.; Winderickx, J.; Dickson, R.C.; Lester, R.L.; Ferket, K.K.; Van Even, F.; Parret, A.H.; Broekaert, W.F. A gene encoding a sphingolipid biosynthesis enzyme determines the sensitivity of Saccharomyces cerevisiae to an antifungal plant defensin from dahlia (Dahlia merckii). *Proc. Natl. Acad. Sci. USA* **2000**, 97, 9531–9536.
40. Gietz, D.; St Jean, A.; Woods, R.A.; Schiestl, R.H. Improved method for high efficiency transformation of intact yeast cells. *Nucleic Acids Res*. **1992**, 20, 1425.
41. Johnson, I.; Spence, M.T.Z. (Eds.) *The Molecular Probes Handbook—A Guide to Fluorescent Probes and Labeling Technologies*; Life Technologies Corporation: Carlsbad, CA, USA, 2010.
42. Branco, M.R.; Marinho, H.S.; Cyrne, L.; Antunes, F. Decrease of H2O2 Plasma Membrane Permeability during Adaptation to H2O2 in Saccharomyces cerevisiae. *J. Biol. Chem*. **2004**, 279, 6501–6506.
43. Panaretou, B.; Piper, P. Isolation of yeast plasma membranes. *Methods Mol. Biol.* **2006**, 313, 27–32.
44. Bligh, E.G.; Dyer, W.J. A rapid method of total lipid extraction and purification. *Can. J. Biochem. Physiol.* **1959**, 37, 911–917.
45. McClare, C.W. An accurate and convenient organic phosphorus assay. *Anal. Biochem*. **1971**, 39, 527–530.
46. Daum, G.; Tuller, G.; Nemec, T.; Hrastnik, C.; Balliano, G.; Cattel, L.; Milla, P.; Rocco, F.; Conzelmann, A.; Vionnet, C.; et al. Systematic analysis of yeast strains with possible defects in lipid metabolism. *Yeast* **1999**, 15, 601–614.
47. Angelova, M.I.; Soléau, S.; Méléard, P.; Faucon, F.; Bothorel, P. Preparation of giant vesicles by external AC electric fields. Kinetics and applications. In *Trends in Colloid and Interface Science VI*; Steinkopff: Darmstadt, Germany, 1992; pp. 127–131.

48. Marques, J.T.; Cordeiro, A.M.; Viana, A.S.; Herrmann, A.; Marinho, H.S.; de Almeida, R.F. Formation and Properties of Membrane-Ordered Domains by Phytoceramide: Role of Sphingoid Base Hydroxylation. *Langmuir ACS J. Surf. Colloids* **2015**, 31, 9410–9421.
49. Bastos, A.E.; Scolari, S.; Stockl, M.; Almeida, R.F. Applications of fluorescence lifetime spectroscopy and imaging to lipid domains in vivo. In *Methods Enzymol*; Conn, P.M., Ed.; Academic Press: Burlington, MA, USA, 2012; Volume 504, pp. 57–81.
50. Haldar, S.; Kanaparthi, R.K.; Samanta, A.; Chattopadhyay, A. Differential Effect of Cholesterol and Its Biosynthetic Precursors on Membrane Dipole Potential. *Biophys. J.* **2012**, 102, 1561–1569.
51. Khmelinskaia, A.; Marques, J.M.; Bastos, A.E.; Antunes, C.A.; Bento-Oliveira, A.; Scolari, S.; Lobo, G.M.; Herrmann, A.; Marinho, H.S.; de Almeida, R.F. Liquid-ordered phase formation by mammalian and yeast sterols: A common feature with organizational differences. *Front. Cell Dev. Biol.* **2020**. Accepted.
52. Francisco, A.P.; Botequim, D.; Prazeres, D.M.F.; Serra, V.V.; Costa, S.M.B.; Laia, C.A.T.; Paulo, P.M.R. Extreme Enhancement of Single-Molecule Fluorescence from Porphyrins Induced by Gold Nanodimer Antennas. *J. Phys. Chem. Lett.* **2019**, 10, 1542–1549.
53. Sklar, L.A.; Hudson, B.S.; Simoni, R.D. Conjugated polyene fatty acids as fluorescent probes: Synthetic phospholipid membrane studies. *Biochemistry* **1977**, 16, 819–828.
54. De Almeida, R.F.; Loura, L.M.; Prieto, M. Membrane lipid domains and rafts: Current applications of fluorescence lifetime spectroscopy and imaging. Chem. Phys. Lipids **2009**, 157, 61–77.
55. Mateo, C.R.; Brochon, J.C.; Lillo, M.P.; Acuna, A.U. Lipid Clustering in Bilayers Detected by the Fluorescence Kinetics and Anisotropy of Trans-Parinaric Acid. *Biophys. J.* **1993**, 65, 2237–2247.
56. Davenport, L. [24] Fluorescence probes for studying membrane heterogeneity. In *Methods in Enzymology*; Academic Press: Cambridge, MA, USA, 1997; Volume 278, pp. 487–512.
57. Florine-Casteel, K.; Feigenson, G.W. On the use of partition coeffcients to characterize the distribution of fluorescent membrane probes between coexisting gel and fluid lipid phases: An analysis of the partition behavior of 1,6-diphenyl-1,3,5-hexatriene. *Biochim. Biophys. Acta (BBA) Biomembr.* **1988**, 941, 102–106.
58. Lentz, B.R. Membrane "Fluidity" from Fluorescent Anisotropy Measurements. In *Spectroscopic Membrane Probes*; Loew, M.L., Ed.; CRC Press: Boca Raton, FL, USA, 1988; pp. 13–41.
59. Santos, F.C.; Fernandes, A.S.; Antunes, C.A.; Moreira, F.P.; Videira, A.; Marinho, H.S.; de Almeida, R.F. Reorganization of plasma membrane lipid domains during conidial germination. *Biochim. Biophys. Acta* **2017**, 1862, 156–166.
60. Silva, L.; Coutinho, A.; Fedorov, A.; Prieto, M. Competitive binding of cholesterol and ergosterol to the polyene antibiotic nystatin. A fluorescence study. *Biophys. J.* **2006**, 90, 3625–3631.
61. Amaro, M.; Reina, F.; Hof, M.; Eggeling, C.; Sezgin, E. Laurdan and Di-4-ANEPPDHQ probe different properties of the membrane. J. Phys. D Appl. Phys. **2017**, 50.
62. Bastos, A.E.P.; Marinho, H.S.; Cordeiro, A.M.; de Soure, A.M.; de Almeida, R.F.M. Biophysical properties of ergosterol-enriched lipid rafts in yeast and tools for their study: Characterization of ergosterol/phosphatidylcholine membranes with three fluorescent membrane probes. *Chem. Phys. Lipids* **2012**, 165, 577–588.
63. De Almeida, R.F.; Borst, J.; Fedorov, A.; Prieto, M.; Visser, A.J. Complexity of lipid domains and rafts in giant unilamellar vesicles revealed by combining imaging and microscopic and macroscopic time-resolved fluorescence. *Biophys. J.* **2007**, 93, 539–553.
64. González-Ramírez, E.J.; Goñi, F.M.; Alonso, A. Mixing brain cerebrosides with brain ceramides, cholesterol and phospholipids. Sci. Rep. **2019**, 9, 13326.
65. Pinto, S.N.; Fernandes, F.; Fedorov, A.; Futerman, A.H.; Silva, L.C.; Prieto, M. A combined fluorescence spectroscopy, confocal and 2-photon microscopy approach to re-evaluate the properties of sphingolipid domains. *Biochim. Biophys. Acta* **2013**, 1828, 2099–2110.
66. Fluhler, E.; Burnham, V.G.; Loew, L.M. Spectra, membrane binding, and potentiometric responses of new charge shift probes. *Biochemistry* **1985**, 24, 5749–5755.
67. Cotlet, M.; Hofkens, J.; Maus, M.; Gensch, T.; Van der Auweraer, M.; Michiels, J.; Dirix, G.; Van Guyse, M.; Vanderleyden, J.; Visser, A.J.W.G.; et al. Excited-State Dynamics in the Enhanced Green Fluorescent Protein Mutant Probed by Picosecond Time-Resolved Single Photon Counting Spectroscopy. *J. Phys. Chem. B* **2001**, 105, 4999–5006.
68. Heikal, A.A.; Hess, S.T.;Webb,W.W. Multiphoton molecular spectroscopy and excited-state dynamics of enhanced green fluorescent protein (EGFP): Acid–base specificity. *Chem. Phys.* **2001**, 274, 37–55.
69. Suhling, K.; Siegel, J.; Phillips, D.; French, P.M.W.; Lévêque-Fort, S.; Webb, S.E.D.; Davis, D.M. Imaging the Environment of Green Fluorescent Protein. *Biophys. J.* **2002**, 83, 3589–3595.
70. Suhling, K.; Davis, D.; Petrasek, Z.; Siegel, J.; Phillips, D. Influence of the refractive index on EGFP fluorescence lifetimes in mixtures of water and glycerol. *Proc. SPIE* **2001**, 4259, 92–101.
71. Petrov, J.G.; Pfohl, T.; Möhwald, H. Ellipsometric Chain Length Dependence of Fatty Acid Langmuir Monolayers. A Heads-and-Tails Model. *J. Phys. Chem. B* **1999**, 103, 3417–3424.
72. Kienle, D.F.; de Souza, J.V.; Watkins, E.B.; Kuhl, T.L. Thickness and refractive index of DPPC and DPPE monolayers by multiple-beam interferometry. *Anal. Bioanal. Chem.* **2014**, 406, 4725–4733.
73. Fajardo Somera, R.A.; Bowman, B.; Riquelme, M. The plasma membrane proton pump PMA-1 is incorporated into distal parts of the hyphae independently of the Spitzenkorper in Neurospora crassa. *Eukaryot. Cell* **2013**, 12, 1097–1105.
74. Clay, L.; Caudron, F.; Denoth-Lippuner, A.; Boettcher, B.; Frei, S.B.; Snapp, E.L.; Barral, Y. A sphingolipid-dependent diffusion barrier confines ER stress to the yeast mother cell. *Elife* **2014**, 3.
75. Ejsing, C.S.; Sampaio, J.L.; Surendranath, V.; Duchoslav, E.; Ekroos, K.; Klemm, R.W.; Simons, K.; Shevchenko, A. Global analysis of the yeast lipidome by quantitative shotgun mass spectrometry. *Proc. Natl. Acad. Sci. USA* **2009**, 106, 2136–2141.

76. Gaigg, B.; Timischl, B.; Corbino, L.; Schneiter, R. Synthesis of sphingolipids with very long chain fatty acids but not ergosterol is required for routing of newly synthesized plasma membrane ATPase to the cell surface of yeast. *J. Biol. Chem*. **2005**, 280, 22515–22522.
77. Marques, J.T.; Marinho, H.S.; de Almeida, R.F.M. Sphingolipid hydroxylation in mammals, yeast and plants—An integrated view. *Prog. Lipid Res*. **2018**, 71, 18–42.
78. Tani, M.; Toume, M. Alteration of complex sphingolipid composition and its physiological significance in yeast Saccharomyces cerevisiae lacking vacuolar ATPase. *Microbiology* **2015**, 161, 2369–2383.
79. Dickson, R.C. Thematic Review Series: Sphingolipids. New insights into sphingolipid metabolism and function in budding yeast. *J. Lipid Res*. **2008**, 49, 909–921.
80. Hallstrom, T.C.; Lambert, L.; Schorling, S.; Balzi, E.; Goffeau, A.; Moye-Rowley,W.S. Coordinate control of sphingolipid biosynthesis and multidrug resistance in Saccharomyces cerevisiae. *J. Biol. Chem*. **2001**, 276, 23674–23680.
81. Tanaka, S.; Tani, M. Mannosylinositol phosphorylceramides and ergosterol coodinately maintain cell wall integrity in the yeast Saccharomyces cerevisiae. *FEBS J.* **2018**, 285, 2405–2427.
82. Morimoto, Y.; Tani, M. Synthesis of mannosylinositol phosphorylceramides is involved in maintenance of cell integrity of yeast Saccharomyces cerevisiae. *Mol. Microbiol*. **2015**, 95, 706–722.
83. Kean, L.S.; Grant, A.M.; Angeletti, C.; Mahé, Y.; Kuchler, K.; Fuller, R.S.; Nichols, J.W. Plasma membrane translocation of fluorescent-labeled phosphatidylethanolamine is controlled by transcription regulators, PDR1 and PDR3. *J. Cell Biol.* **1997**, 138, 255–270.
84. Decottignies, A.; Grant, A.M.; Nichols, J.W.; deWet, H.; McIntosh, D.B.; Go_eau, A. ATPase and Multidrug Transport Activities of the Overexpressed Yeast ABC Protein Yor1p. *J. Biol. Chem*. **1998**, 273, 12612–12622.
85. Ratto, T.V.; Longo, M.L. Obstructed di_usion in phase-separated supported lipid bilayers: A combined atomic force microscopy and fluorescence recovery after photobleaching approach. Biophys. J. **2002**, 83, 3380–3392.
86. Van't Klooster, J.S.; Cheng, T.Y.; Sikkema, H.R.; Jeucken, A.; Moody, B.; Poolman, B. Periprotein lipidomes of Saccharomyces cerevisiae provide a flexible environment for conformational changes of membrane proteins. Elife **2020**, 9.
87. Guan, X.L.; Souza, C.M.; Pichler, H.; Dewhurst, G.; Schaad, O.; Kajiwara, K.;Wakabayashi, H.; Ivanova, T.; Castillon, G.A.; Piccolis, M.; et al. Functional Interactions between Sphingolipids and Sterols in Biological Membranes Regulating Cell Physiology. *Mol. Biol. Cell* **2009**, 20, 2083–2095.
88. Swain, E.; Baudry, K.; Stukey, J.; McDonough, V.; Germann, M.; Nickels, J.T. Sterol-dependent regulation of sphingolipid metabolism in Saccharomyces cerevisiae. *J. Biol. Chem*. **2002**, 277, 26177–26184.
89. Solanko, L.M.; Sullivan, D.P.; Sere, Y.Y.; Szomek, M.; Lunding, A.; Solanko, K.A.; Pizovic, A.; Stanchev, L.D.; Pomorski, T.G.; Menon, A.K.; et al. Ergosterol is mainly located in the cytoplasmic leaflet of the yeast plasma membrane. *Traffic* **2018**, 19, 198–214.
90. Castro, B.M.; de Almeida, R.F.M.; Fedorov, A.; Prieto, M. The photophysics of a Rhodamine head labeled phospholipid in the identification and characterization of membrane lipid phases. *Chem. Phys. Lipids* **2012**, 165, 311–319.
91. Stewart, E.; Gow, N.A.; Bowen, D.V. Cytoplasmic alkalinization during germ tube formation in Candida albicans. *J. Gen. Microbiol*. **1988**, 134, 1079–1087.
92. Mahanty, S.K.; Gupta, P.; Banerjee, U.; Fotedar, R.; Prasad, R. Defective plasma membrane H(+)-ATPase or orthovanadate resistant mutants from Candida albicans, a pathogenic yeast. *Biochem. Int*. **1990**, 22, 11–20.
93. Stock, S.D.; Hama, H.; DeWald, D.B.; Takemoto, J.Y. SEC14-dependent secretion in Saccharomyces cerevisiae. Nondependence on sphingolipid synthesis-coupled diacylglycerol production. *J. Biol. Chem*. **1999**, 274, 12979–12983.

Supplementary material

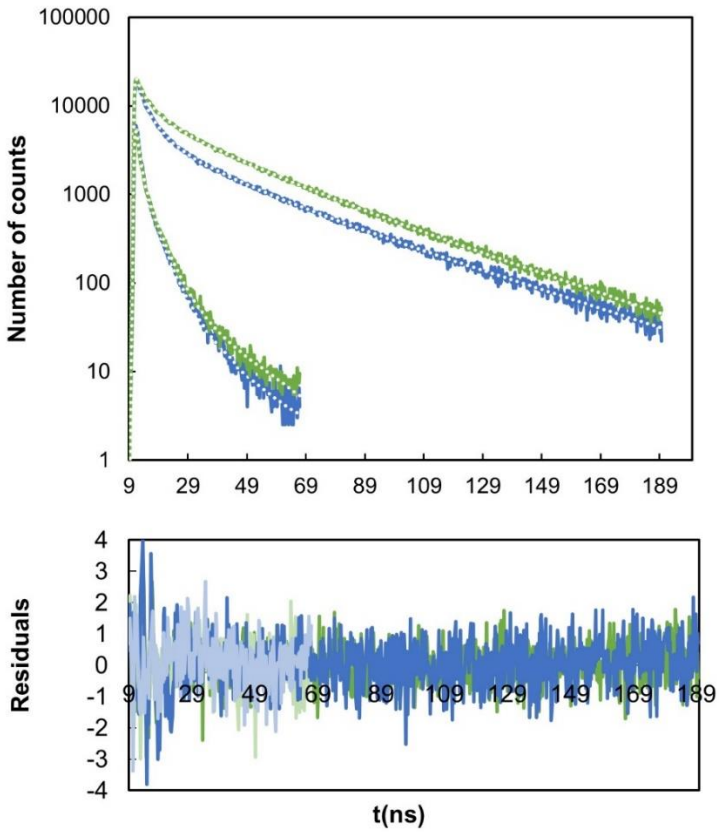

Figure S2. 1: Fluorescence intensity decay of *t*-PnA in *wt* (blue) and *ipt1*Δ (green) cell suspensions at 24 ºC. Top panel: experimental decays in *t*-PnA labelled and unlabeled cell suspensions (faded blue and green, respectively) and best fitting function with a sum of exponentials (white dashed line) obtained with a global analysis method. Bottom panel: Residues. *t-PnA* fluorescence decays were obtained as described in the experimental procedures.

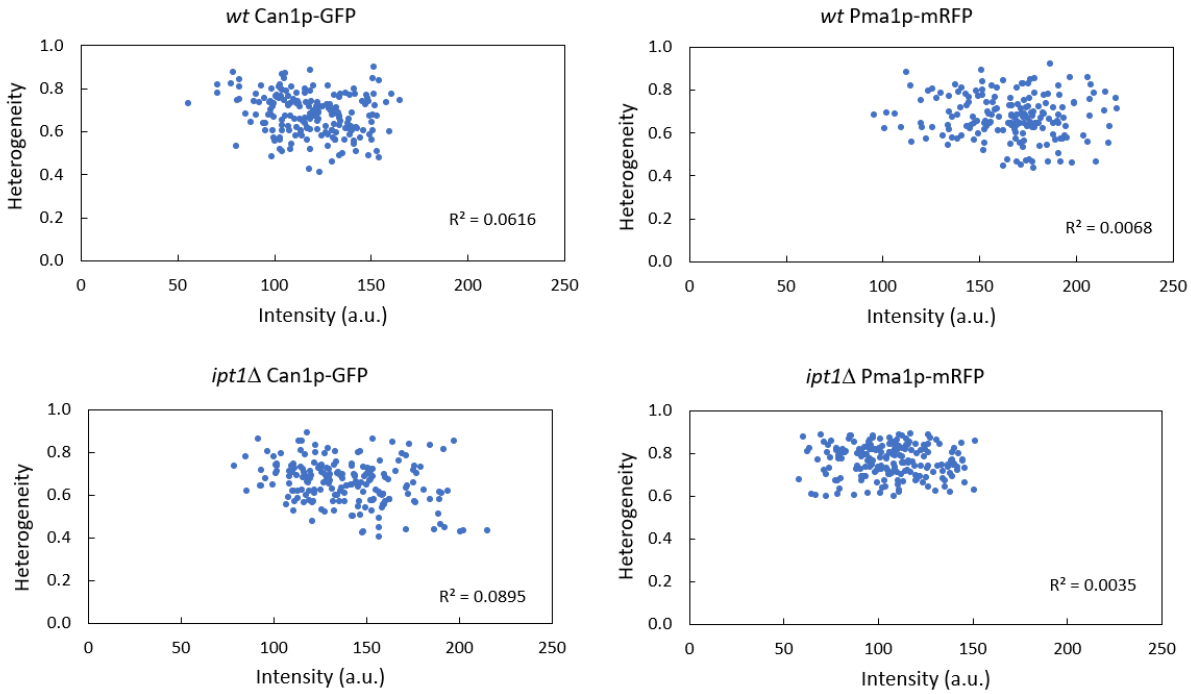

Figure S2. 2: Relation between the average fluorescence intensity of Can1p or Pma1p along the plasma membrane and their distribution heterogeneity. Heterogeneity has no correlation with the intensity of the signal (in arbitrary units), which is not only confirmed by the dispersion of the results throughout the graph but also by the very low value of the linear determination coefficients. Each data point corresponds to one cell.

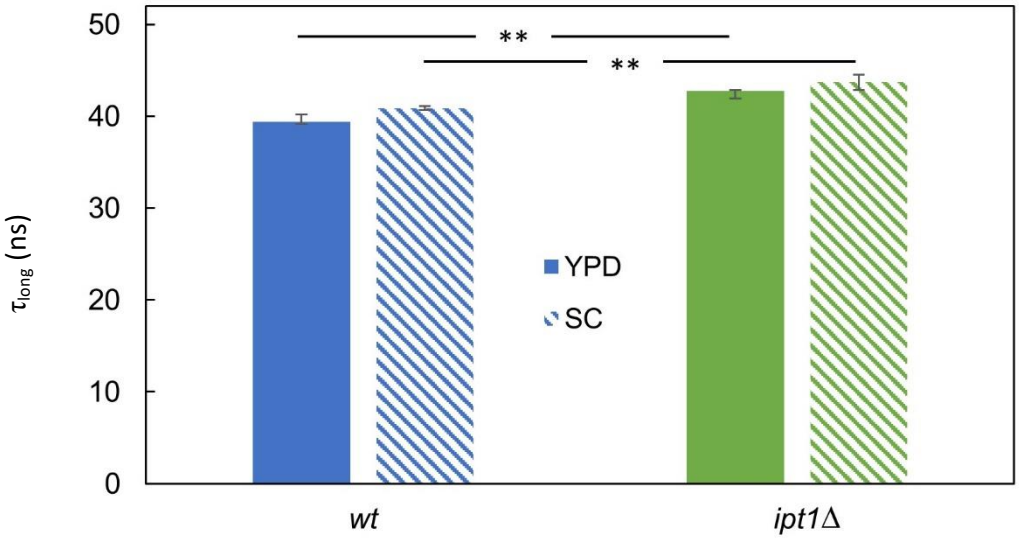

Figure S2. 3: The lifetime of the long component of *t*-PnA is essentially identical in growth media SC and YPD (yeast extract, peptone, dextrose). The fluorescence intensity decay of the probe in *S. cerevisiae* cellular suspensions at 24 ℃ was obtained as described in the "experimental procedures" for living *wt* and *ipt1*Δ cells in mid-exponential phase grown in SC or YPD (1 % (w/v) yeast extract, 2 % (w/v) peptone, 2 % (w/v) glucose) media. For both strains, the long component lifetime is tendentially shorter for cells grown in YPD. Nonetheless, the long component lifetime is always statistically longer in *ipt1*Δ than in *wt* cells. The values are the mean ± S.D. of at least four biological replicates. **, $p \leq 0.01$.

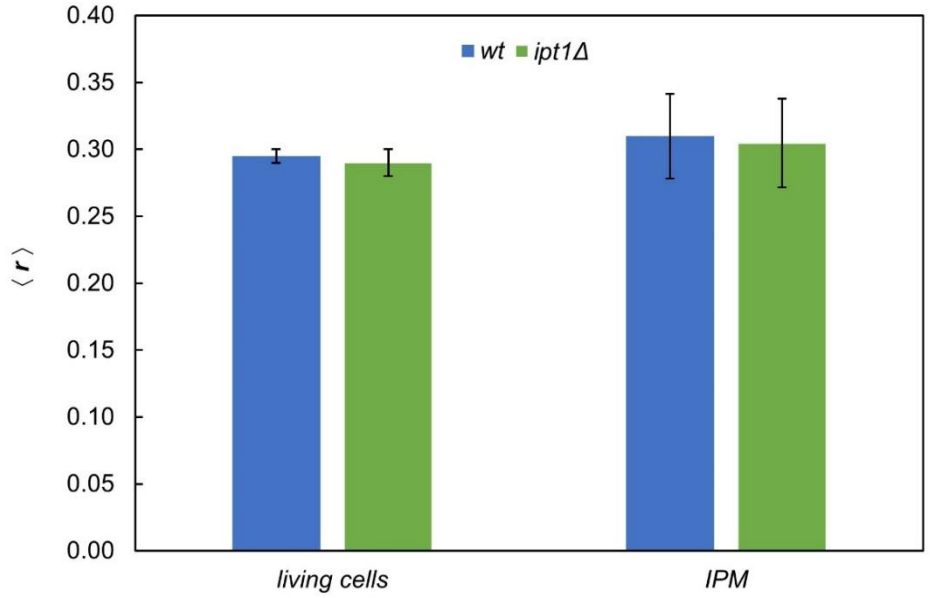

Figure S2. 4: The deletion of *IPT1* gene does not lead to significant differences between intact cells and isolated plasma membrane (IPM) in the sphingolipid-enriched domains. The *t*-PnA steady-state fluorescence anisotropy at 24 °C was obtained as described under "experimental procedures" in suspensions of living *wt* and *ipt1*Δ cells in mid-exponential phase and in IPM. The values are the mean ± S.D. of at least four biological replicates.

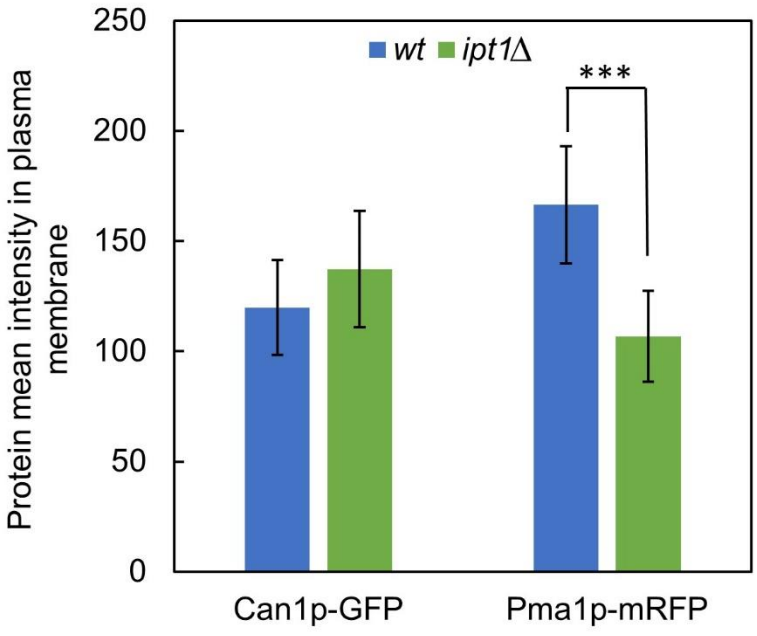

Figure S2. 5: Can1p-GFP and Pma1p-mRFP mean fluorescence intensity in the plasma membrane of *wt* (blue) and *ipt1*Δ (green) cells. The values are the mean ± S.D. of at least four independent biological replicates with a total of at least 200 cells analyzed per replicate. ***$p \leq 0.001$.

Table S2. 1: Parameters describing the fluorescence intensity decay obtained from FLIM experiments of the transformed fluorescent proteins in *S. cerevisiae wt* and *ipt1*Δ plasma membrane. The values are the mean ± S.D. of at least four independent biological replicates with a total of at least 200 cells analyzed per replicate.

Strains	α_1	α_2	τ_1 (ns)	τ_2 (ns)	$\bar{\tau}$ (ns)
***wt* Can1p-GFP**	0.81 ± 0.08	0.19 ± 0.08	1.82 ± 0.09	3.59 ± 0.45	2.10 ± 0.04
***ipt1*Δ Can1p-GFP**	0.83 ± 0.06	0.17 ± 0.06	1.86 ± 0.04	3.60 ± 0.15	2.14 ± 0.06
***wt* Pma1p-mRFP**	0.90 ± 0.01	0.10 ± 0.01	1.57 ± 0.01	4.03 ± 0.16	1.80 ± 0.02
***ipt1*Δ Pma1p-mRFP**	0.95 ± 0.02*	0.05 ± 0.02*	1.64 ± 0.02*	4.45 ± 0.32	1.77 ± 0.03*

* $p<0.001$ *vs wt* Pma1p-mRFP

CHAPTER III

INTERACTION OF THE ANTIFUNGAL KETOCONAZOLE AND ITS DIPHENYLPHOSPHINE DERIVATIVES WITH LIPID BILAYERS: INSIGHT INTO THEIR ANTIFUNGAL ACTION

This chapter comprises the work published in *Archives of Biochemistry and Biophysics*, 2024, 109919 by **A. Bento-Oliveira**, R. Starosta, R. F. M. de Almeida.
Contribution: Took an active part in the planning of and performed all the experiments. Took an active part in the writing of the paper.

Archives of Biochemistry and Biophysics 753 (2024) 109919

Contents lists available at ScienceDirect

Archives of Biochemistry and Biophysics

journal homepage: www.elsevier.com/locate/yabbi

Interaction of the antifungal ketoconazole and its diphenylphosphine derivatives with lipid bilayers: Insights into their antifungal action

Andreia Bento-Oliveira [a], Radosław Starosta [a,b], Rodrigo F.M. de Almeida [a,*]

[a] Centro de Química Estrutural, Institute of Molecular Sciences, Departamento de Química e Bioquímica, Faculdade de Ciências, Universidade de Lisboa, Campo Grande, 1749-016, Lisboa, Portugal
[b] Faculty of Chemistry, University of Wroclaw, F. Joliot-Curie 14, 50-383, Wroclaw, Poland

Abstract

Ketoconazole (**Ke**) is an important antifungal drug, and two of its diphenylphosphinemethyl derivatives (**KeP**: Ph_2PCH_2-Ke and **KeOP**: $Ph_2P(O)CH_2$-Ke) have shown improved antifungal activity, namely against a yeast strain lacking ergosterol, suggesting alternative modes of action for azole compounds. In this context, the interactions of these compounds with a model of the cell membrane were investigated, using POPC (1-palmitoyl-2-oleoyl-*sn*-glycero-3-phosphocholine) large unilamellar vesicles and taking advantage of the intrinsic fluorescence of **Ke**, **KeP** and **KeOP**. Steady-state fluorescence spectra and anisotropy, including partition and aggregation studies, as well as fluorescence lifetime measurements, were carried out. In addition, the ability of the compounds to increase membrane permeability was assessed through a carboxyfluorescein leakage assay. The membrane/water mole fraction partition coefficients ($K_{p,x}$): $(3.31 \pm 0.36) \times 10^5$, $(8.31 \pm 1.60) \times 10^5$ and $(4.66 \pm 0.72) \times 10^6$, for **Ke**, **KeP** and **KeOP**, respectively, show that all three compounds have high affinity for the lipid bilayer. Moreover, **KeP**, and particularly **KeOP** interact more efficiently with POPC bilayers than **Ke**, which correlates well with their *in vitro* antifungal activity. Furthermore, although the three compounds disturb the lipid bilayer, **KeOP** is the quickest and most efficient one. Hence, the higher affinity and ability to permeabilize the membrane of **KeOP** when compared to that of **KeP**, despite the higher lipophilicity of the latter, points to an important role of $Ph_2P(O)CH_2$-oxygen. Overall, this work suggests that membrane interactions are important for the antifungal activity of these azoles and should be considered in the design of new therapeutic agents.

Keywords: Ketoconazole, Drug-membrane interaction, Antifungal agents, Fluorescence Spectroscopy, Diphenylphosphanomethyl derivative, Phospholipid bilayer

Highlights

- Membrane partition of ketoconazole and diphenylphosphine derivatives was quantified;
- Both diphenylphosphine derivatives have higher membrane affinity than ketoconazole;
- All compounds distinctly and significantly increase the lipid bilayer permeability;
- The oxide derivative has the strongest membrane effects and antifungal activity;
- Drug-membrane interactions are relevant for azole antifungal activity.

Graphical abstract

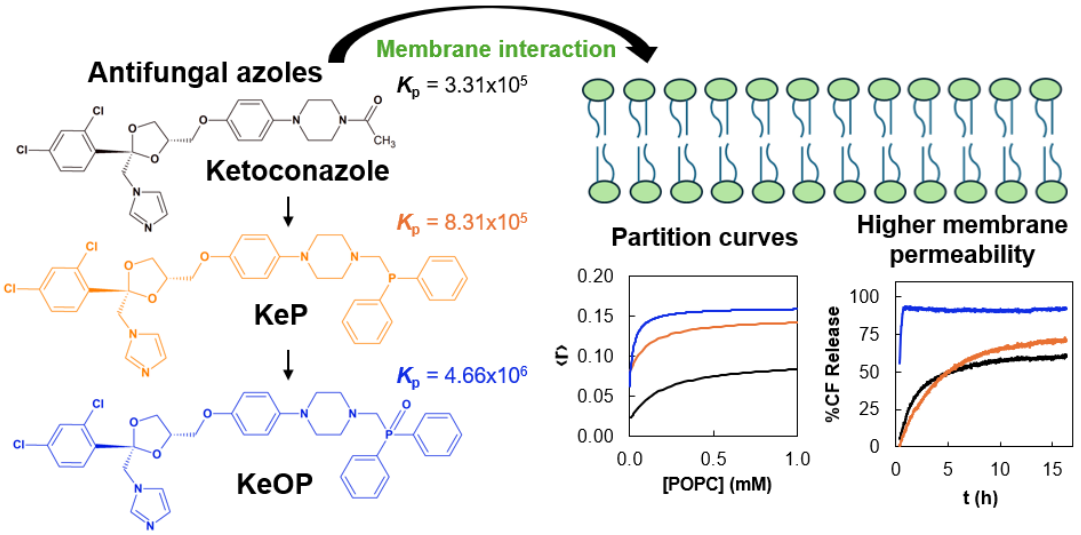

1. Introduction

Fungal infections are a serious health threat, especially for patients with weakened immune systems due to viral infections, cancer, organ transplants, or certain medications [1,2]. Although fungal infections outbreaks are rather rare, the emergence of pathogenic fungi resistant to commonly used antifungal drugs, is occurring at unprecedented rates [3, 4], which can easily change the global picture. Therefore, the search for new antifungal agents and alternative therapies has become increasingly important, as well as a better understanding of all the aspects of antifungal action. Ketoconazole (**Ke**: 1-[4-[4-[[2-(2,4-dichlorophenyl)-2-(imidazole-1-ylmethyl)-1,3-dioxolan-4-yl]methoxy]phenyl]piperazin-1-yl]ethanone) (Figure 3.1) is an imidazole-based antifungal drug. It was approved by the american Food and Drug Administration (FDA) and introduced to the market in 1981 as a first-line treatment for fungal infections. However, due to its hepatotoxicity [5,6], its use was restricted in 2013 to topical infections or certain life-threatening systematic mycoses. Nevertheless, the findings that **Ke** may be also a potential therapeutic agent in cancer combination therapy [7], treatment of

prostatic cancer [8–11] and Cushing's syndrome [12,13], and was able to inhibit the growth of several cancer cell lines [14], raised renewed interest in this molecule [15,16].

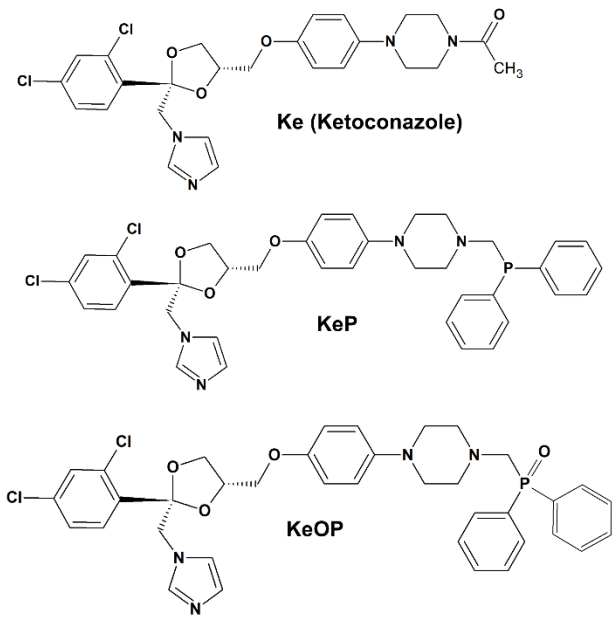

Figure 3. 1: Molecular structures of ketoconazole (Ke), Ph_2PCH_2-Ke (KeP), $Ph_2P(O)CH_2$-Ke (KeOP).

As in the case of other synthetic azoles, its primary molecular target is cytochrome P450 sterol-14-α-demethylase (P45014DM) [17–21]. By forming a strong bond between the imidazole nitrogen and the heme iron, **Ke** acts as a competitive inhibitor of the enzyme. Consequently, the inhibition of P45014DM results in a decrease in ergosterol levels of the fungal cell, disturbing membrane structure and function. For example, ergosterol deficiency in budding yeast leads to compromised vacuolar-type ATPase activity and, as a result, to the disruption of intracellular cation homeostasis [22].

Recently, we have presented an aminomethylphosphine derived from **Ke** (**KeP**), where the acetyl group of **Ke** was replaced by a diphenylphophinomethyl moiety, and its chalcogenides: oxide (**KeOP**), sulphide (**KeSP**) and selenide (**KeSeP**) [23]. Similarly to **Ke**, these derivatives can also target P45014DM as demonstrated by our docking assay [23]. Moreover, we have shown that these compounds are promising antifungal agents, especially **KeP** and **KeOP** (Figure 3.1), for selected strains of *Saccharomyces cerevisiae* and *Candida albicans*. Interestingly, the derivatives have antifungal activity against a *S. cerevisiae* strain that lacks sterol-24C-methyltransferase [23]. Cells of this strain are unable to produce ergosterol, and instead accumulate cholesta-5,7, 24-trienol and zymosterol [24]. Moreover, the Copper(I) complexes with **KeP** and 2,9-dimethyl-1,10-phenantroline proved to be very effective against *C. albicans* surpassing their typical drug resistance mechanisms [25]. These findings suggest

that there might be additional targets for these compounds. Therefore, we hypothesize that **KeP** and **KeOP** mode of action may include perturbation of the plasma membrane lipid bilayer. In support of this hypothesis, are: i) the activity against a yeast strain lacking ergosterol, which reduces the importance of the protein target P45014DM, ii) the activity against *C. albicans* of these compounds is less dependent on the expression of drug exporters at the plasma membrane than the activity of **Ke**, iii) the fact that the derivatives are likely more lipophilic due to the -CH_2PPh_2 hydrophobic moiety, and iv) our recent finding that triphenylphosphine (PPh_3) induces a relatively fast and extensive permeabilization of fluid lipid bilayers [26]. Several antifungal drugs can target directly the membrane or some of its components, such as proteins and/or lipids, or specific membrane domains, causing permeabilization of the membrane or even its disruption [27]. For instance, antifungal polyenes such as nystatin and amphotericin B, are believed to bind ergosterol in the fungal plasma membrane, forming pores that lead to cell death [28–31]. It has also been shown that nystatin can efficiently partition towards gel domains in coexistence with a fluid phase, suggesting that sphingolipid-enriched domains (SLEDs) in the fungal plasma membrane [32,33] could be a target for antifungal agents [34,35]. Moreover, the study of the interaction between azoles and lipid bilayers may promote the development and improvement of liposomal delivery systems, as already performed *e.g.* for voriconazole [36] and anidulafungin [37]. However, to the best of our knowledge, **Ke** direct interaction with lipid bilayers has not been investigated. Hence, in this work, the interaction of **Ke** and the two derivatives **KeP** and **KeOP** with 1-palmitoyl-2-oleoyl-*sn*-glycero-3-phosphocholine (POPC), forming fluid bilayers at room temperature, was studied. Since all these compounds display a clear dependence of their absorption and fluorescence properties on the environment [38,39], the intrinsic fluorescence of **Ke** and its derivatives was used as a tool to detect, quantify and characterize the partition of these azoles with the membrane. Moreover, a leakage assay was performed to determine if these compounds change the permeability of a fluid bilayer. We found that all three compounds interact with the lipid bilayer, with both derivatives having a stronger partition to the membrane than **Ke** itself. However, the compound with stronger membrane affinity, **KeOP**, is not the most lipophilic, but it is the one with the most interesting *in vitro* antifungal activities [23] and the quickest and most effective permeabilizer of the membrane. This study thus supports our hypothesis that **Ke** and particularly its phosphine derivatives may exert their action, at least partially, through their perturbation of the cell membrane lipid bilayer.

2. Materials and methods

2.1. Chemicals

POPC was obtained from Lipoid (Ludwigshafen, Germany). DMSO (spectroscopic grade) and HEPES were acquired from Fisher Chemical (Waltham, MA, USA). Other chemicals and solvents were purchased from Merck and used without further purification. POPC stock solutions in chloroform (spectroscopic grade) were kept at − 20 ◦C under nitrogen and their concentration was determined by phosphate quantification [40]. The syntheses of **KeP** and **KeOP** were described in one of our recent papers [23]. The compounds were pre-dissolved in DMSO and in all experiments the final DMSO concentration was 2 %.

2.2. Liposome preparation

LUVs with a mean diameter of 100 nm, containing POPC were prepared by the extrusion method in HEPES buffer (10 mM; pH 7.4), as previously described [26,34]. A buffer with low ionic strength was used to minimize aggregation of the compounds as revealed by the broadening of the excitation and emission spectra of the compounds when using a buffer with 150 mM NaCl (Figure S3.1).

2.3. Absorption and fluorescence spectroscopy and static light scattering

Absorption spectra were acquired with a Jasco V-560 spectrophotometer (Easton, MD, USA) at room temperature using quartz cuvettes with 1 cm optical path. A Fluorolog 3.22 spectrofluorimeter from Horiba Jobin Yvon (Villeneuve D'ascq, France) was used for fluorescence and static light scattering measurements both performed at 23.0 ± 1.0 °C in a sample compartment with magnetic stirring and temperature control, using quartz cuvettes QS from Hellma with optical path of 1 cm in excitation and 0.4 cm in emission. For the excitation spectra the emission was fixed at 370 nm, and the excitation wavelength was scanned from 260 to 350 nm. For the emission spectra excitation was fixed at 295 nm, and the emission wavelength was scanned from 310 to 575 nm, with wavelength increments of 1 nm. For spectra acquisition the bandwidths were typically 4 nm in both excitation and emission, and integration time 0.2 s. For steady-state fluorescence anisotropy measurements, the excitation and emission wavelengths were set to 295 nm and 370 nm, respectively for all compounds. To determine the value of steady-state fluorescence anisotropy, $\langle r \rangle$, the following Equation (1) was used:

$$\langle r \rangle = \frac{(I_{VV} - G \times I_{VH})}{(I_{VV} + 2G \times I_{VH})} \quad (1)$$

in which the subscripts indicate the orientation of the excitation and emission polarizers, where V and H correspond to vertical and horizontal orientations and G is a correction factor calculated from the ratio I_{HV}/I_{HH}. An adequate blank was subtracted from each intensity reading. For fluorescence anisotropy measurements the bandwidths were 8 nm. Time-resolved fluorescence measurements were carried out by the single photon timing technique, using a nanoLED N-280 (λ_{ex} = 279 nm) from Horiba Jobin Yvon (Villeneuve D'ascq, France), using 375 nm as the emission wavelength. The bandwidth was 14.7 nm. The resolution of the detector (TBX from Horiba) was 50 ps. Photon counts were accumulated until reaching 20 000 counts in the peak channel with a time scale of 0.02669 ps/channels, and the number of channels used for analysis was approximately 1000. To obtain the instrument response function, diluted Ludox® was used as the scattering agent. The experimental fluorescence intensity decays were analyzed using the software TRFA® version 1.4 (Minsk, Belarus). The fluorescence intensity decays were described by a two exponential model according to Equation (2):

$$I(t) = \sum_{i=1}^{n} p_i \exp\left(-\frac{t}{\tau_i}\right) \quad (2)$$

A third component was fixed to 10 ps to account for light scattering, and it was not used for the determination of the average fluorescence lifetimes. After normalizing the pre-exponential factors (p_i), to obtain the normalized pre-exponentials or amplitudes α_i, Equation (3) was used to determine the mean fluorescence lifetime (intensity weighted):

$$\langle\tau\rangle = \frac{\sum \alpha_i \tau_i^2}{\sum \alpha_i \tau_i} \quad (3)$$

A reduced $\chi 2$ close to 1 and random distributions of the weighted residuals and of the residuals autocorrelation were the conditions to consider a successful fitting.

2.3.1. Aggregation studies

Absorption, fluorescence, and light scattering measurements were performed for different concentrations of **Ke**, **KeP** and **KeOP** dissolved in 10 mM HEPES (pH 7.4, filtered through paper with 5 μm pores) with 2 % DMSO, incubated for 2 h protected from light at room temperature. Static light scattering (Rayleigh) was determined as previously described in reference [41] with both excitation and emission wavelengths set to 550 nm in right angle geometry.

2.3.2. Partition experiments

The fluorescence intensity measurements were optimized using different sets of parameters, to determine an exact K_p value for each compound. First, we obtained the emission spectra using the two possible cuvette configurations – an optical path of 1 cm in excitation and 0.4 cm in emission, and the opposite – and plotted the maximum intensity from the spectra, the area under the spectrum (both with and without polarizers at the magic angle) and the fluorescence intensity at the magic angle retrieved from the polarization components of emission (denominator in eq. (1)). We chose the method that for the three compounds **Ke**, **KeP** and **KeOP** yielded curves with less scattering of the data and with lower background contributions (data not shown). The best results were obtained using the intensity at a fixed wavelength: λ_{ex} = 295 nm and λ_{em} = 370 nm, with an optical path of 1 cm in excitation and 0.4 cm in emission without polarizers.

LUVs with 10 mM of POPC, were diluted in HEPES buffer to a final concentration that ranged from 0.025 mM to 2 mM. **Ke**, **KeOP**, **KeP** were added to the LUV suspensions to a final concentration of 5, 10 or 15 μM (the latter only for **KeP**) and 2 % DMSO and incubated for 1 h 30 min at 23.0 ± 1.0 °C. After 45 min of incubation the fluorescence properties (steady-state intensity, anisotropy and intensity decays) of the compounds were stable, but as a matter of precaution the incubation period of the compound was extended to 1 h 30 min to ensure that the system was fully equilibrated (data not shown).

2.3.3. Leakage assay

LUVs with 2 mM of POPC were prepared in 10 mM HEPES buffer containing 40 mM of 5(6)-carboxyfluorescein (CF). In order to remove the non-encapsulated CF, the pellet that resulted from LUV centrifugation at 150 000 rcf for 2h (Ultracentrifuge Hitachi CP80NX with P70AT rotor), was re-suspendend in HEPES buffer (50 mM, pH 7.4), and filtered through a Sephadex G-25 filtration column (Disposable PD Desalting Columns, Merck). The LUVs were then diluted in a 96-well plate to different lipid concentrations ranging from 0.1 to 0.25 mM. CF fluorescence intensity was measured every 1 min, during 14–16 h after the addition of 5–20 μM of **Ke**, **KeP** or **KeOP**. Finally, for total LUVs lysis 1 % (v/v) of Triton was added to each well, and fluorescence intensity was measured to determine the maximum percentage of CF release (F100). A microplate reader SpectraMAX GeminiEM spectrofluorimeter from Molecular Devices (San José, CA, USA) was used in the leakage assay to measure the

fluorescence intensity of CF, at 25 °C. The excitation and emission wavelengths were set to 492 nm and 530 nm, respectively, and a cut-off filter at 515 nm was used.

The CF leakage percentage was calculated using the following equation:

$$\%CF\ Leakage = \frac{F_t - F_0}{F_{100} - F_0} \tag{4}$$

where F_0 is the initial fluorescence intensity measured without the addition of compound, and F_t is the fluorescence intensity value at each time point [42].

Equation 5 [42] was fitted to the experimental data:

$$L = \sum_{i=1}^{n} L_i \left(1 - \exp\left(-\frac{t}{\tau_{Li}}\right)\right) \tag{5}$$

where L_i represents the maximum leakage associated with each kinetic constant, t is the time after the addition of the compounds, and τ_{Li} represents the time constants. The average leakage time constant, $\langle\tau_L\rangle$ can be calculated using the following equations:

$$\langle\tau_L\rangle = \sum \alpha_i \tau_{Li} \tag{6}$$

$$\alpha_i = \frac{L_i}{L_{max}} \tag{7}$$

$$L_{max} = \sum L_i \tag{8}$$

2.4. Statistical analysis

All the results, except the fluorescence spectra, and the CF leakage curves, are presented as mean ± standard deviation (S.D.) of at least three independent replicates. Representative fluorescence intensity spectra and CF leakage curves shown are the median result from at least three independent replicates. The statistical significance was determined using one-way ANOVA with post-hoc Tukey's test. Mean values were considered significantly different for *p*-values below or equal to 0.05.

3. Results

3.1. Interaction of Ke with POPC lipid bilayers

3.1.1. Fluorescence properties of Ke in the presence of POPC bilayers

Although **Ke** is an FDA approved drug with extensive literature regarding its mode of action and molecular properties [17,18,43], its interaction with lipid bilayers was never reported, to the best of our knowledge. Therefore, we began by addressing the question of whether **Ke** can interact with lipid bilayers to an extent that can be considered biologically relevant. **Ke** was studied in buffer solution and in the presence of a simple membrane model system made of POPC LUVs. POPC is a lipid commonly found in membranes of eukaryotic organisms [44,45]. At room temperature POPC exists in a fluid state (main phase transition temperature (T_m) = - 4 °C [45]), because of the presence of an unsaturated acyl chain at *sn*-2. Due to these characteristics, membrane model systems made of POPC only or containing POPC are widely used, *e.g.* Refs. [46–49]. LUVs were prepared with different concentrations of lipid (0.025 mM–1.5 mM of POPC) and the steady-state fluorescence of **Ke** was characterized, namely, fluorescence excitation and emission spectra and anisotropy (Figure 3.2). The concentration of **Ke** used was 10 μM, which ensures a good signal-to-noise ratio in the fluorescence measurements carried out. Moreover, at this concentration the absorbance is lower than 0.02, which avoids inner filter artifacts. Importantly, at 10 μM concentration **Ke** is active against several strains of *C. albicans* and *S. cerevisiae* [23].

In the absence of lipid, **Ke** presented an emission band with maximum at 379 nm and an excitation band at 285 nm (Figure 3.2 - A), which is in agreement with a previous photophysical characterization of **Ke** [38]. The presence of POPC caused a blue shift of the emission spectra and a red shift of the excitation spectra of **Ke**. The peak wavelength for excitation changed from 285 nm to ca. 293 nm (Figure 3.2 – B) while for emission it changed from 379 nm to ca. 371 nm (Figure 3.2 – C) as the concentration of lipid increased, also in agreement with our previous characterization of **Ke** luminescence in different solvents [38]. These shifts clearly show an alteration of the fluorophore microenvironment to a less polar one which allows to conclude that **Ke** is partitioning to the lipid bilayer.

Upon increasing the lipid concentration, the intensity of light emitted by **Ke** at 370 nm (Figure 3.2 – D) increased. The increased fluorescence intensity observed for **Ke** in the presence of lipid reflects the increase of **Ke** fluorescence quantum yield, which is most probably due to a decrease of its non-radiative rate constant, as expected upon the insertion of a molecule in a more viscous environment [50], in this case the lipid bilayer. This happens until a high partition

of the compound into the membrane is reached, which corresponds to an almost constant fluorescence intensity value. Some of the steady-state fluorescence properties of **Ke** in the absence and presence of lipid are summarized in Table 3.1.

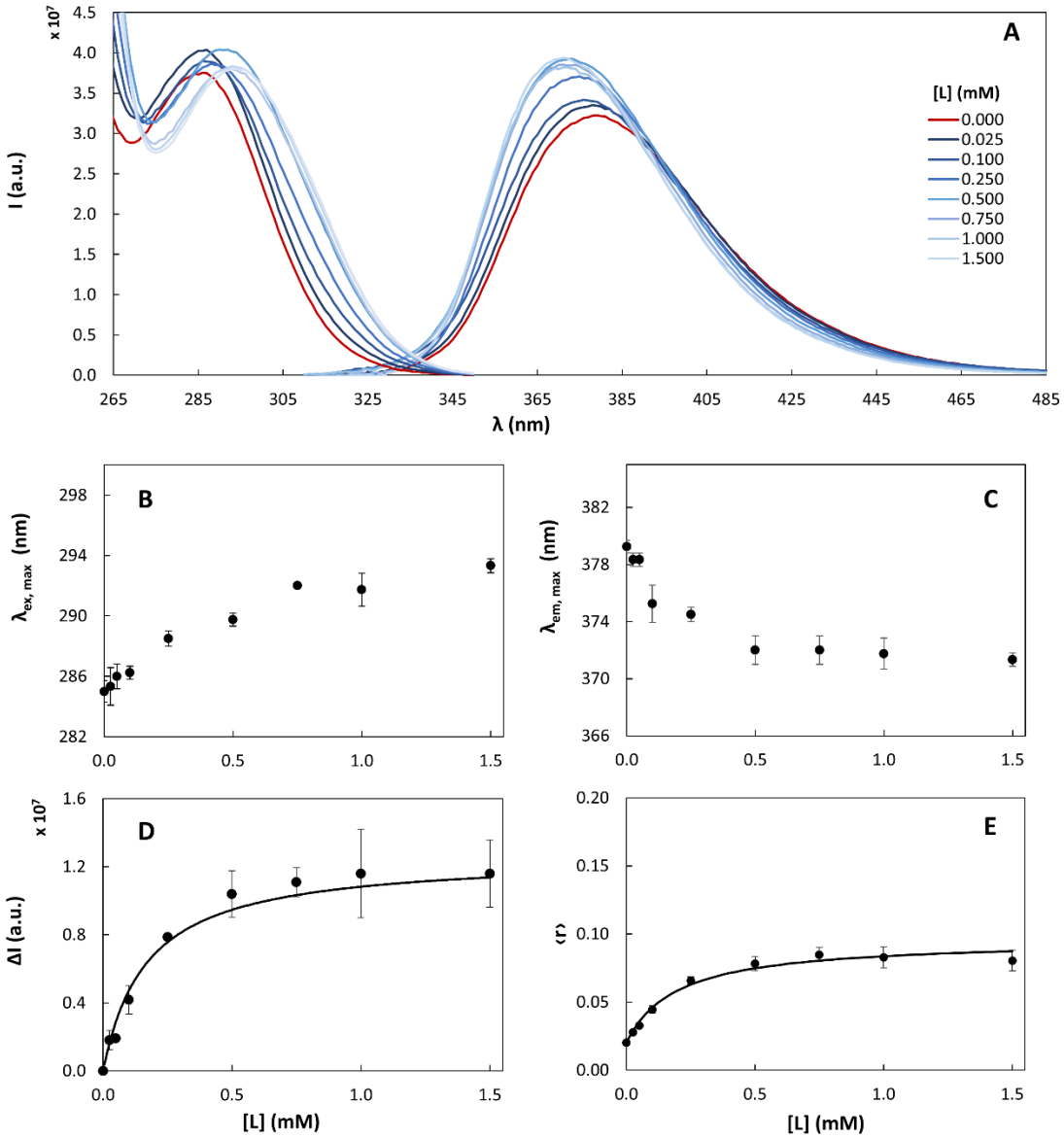

Figure 3. 2: Interaction of Ke **with POPC lipid bilayers monitored through its intrinsic fluorescence.** Fluorescence excitation and emission spectra (A), peak wavelength of excitation ($\lambda_{exc,max}$; B), and emission ($\lambda_{em,max}$; C) spectra, fluorescence intensity (variation from the value in water), ΔI (D) and steady-state fluorescence anisotropy, ⟨*r*⟩(E) of **Ke** for increasing lipid concentrations. The solid lines in D and E represent the fitting of equations (9) and (10), respectively, to the experimental data. Data in D and E was obtained with excitation at 295 nm and emission collected at 370 nm. The concentration of **Ke** was 10 μM. The results in B – E are the mean ± S.D. of at least three independent replicates.

The presence of lipid also induced an increase in the steady-state fluorescence anisotropy of **Ke** (Figure 3.2 – E). This indicates a hindering and/or slowing down of the rotational diffusion of the compound, which reinforces the hypothesis that the environment around the fluorophore is becoming more viscous with the presence of lipid, *i.e.* that the compound is being incorporated in the membrane. It is important to mention that these changes in fluorescence

anisotropy are not due to different fluorescence lifetimes of the compound in the presence of lipid, which just changed marginally (Table 3.1).

Table 3. 1: Equations used for the determination of the mole-fraction partition coefficient between POPC bilayer and water, of Ke, KeOP, KeP **at 23 °C; parameters obtained from the fit; maximum excitation and emission wavelengths and intensity-weighted mean fluorescence lifetimes.** ([C] = 10 µM, unless stated otherwise; $\lambda_{ex,max,i}$ and $\lambda_{em,max,i}$ are the peak wavelengths of the excitation and emission spectra, respectively, in water (i = aq) or with the highest lipid concentration (i = lip)). ΔG° was determined using equation S5.

Compound	Ke	KeOP	KeP
Equation	9	9	11 and 12
$K_{p,x}$	(3.31 ± 0.36) x10^5 [(2.40 ± 0.22) x10^5][a]	(4.66 ± 0.72) x10^6	[(8.31 ± 1.60) x10^5][b]
ΔI_{max} (a.u.)	(1.26 ± 0.26) x10^7 [(8.62 ± 0.17) x10^6][a]	(3.20 ± 0.26) x10^6	-
$\Delta G°$ (kJ/mol)	-31.30 ± 0.27	-37.81 ± 0.37	-33.56 ± 0.48
I_L/I_W	1.37 ± 0.02	1.51 ± 0.04	1.27[c]
σ	-	-	0.064
r_W	0.020 ± 0.001	0.051 ± 0.010	0.079 ± 0.013
r_L	0.094 ± 0.005	0.161 ± 0.006	0.149 ± 0.004
$\langle\tau\rangle_{aq}$ (ns)[d]	2.45 ± 0.02	1.40 ± 0.17	1.52 ± 0.12
$\langle\tau\rangle_{lip}$ (ns)[d]	2.36 ± 0.01	1.69 ± 0.48	1.53 ± 0.03
$\lambda_{ex,max,aq}$ (nm)	285	287	284
$\lambda_{ex,max,lip}$ (nm)	293	296	296
$\lambda_{em,max,aq}$ (nm)	379	382	368
$\lambda_{em,max,lip}$ (nm)	371	369	368

[a] values determined using 5 µM of compound.
[b] 5, 10 and 15 µM of **KeP** were used.
[c] from equation 10.
[d] determined using equation 3

3.1.2. Quantifying the partition of Ke between aqueous buffer and POPC bilayers

The change in **Ke** fluorescence intensity in the presence of increasing concentrations of lipid can be used to determine its membrane/water mole-fraction partition coefficient ($K_{p,x}$). $K_{p,x}$ reflects the equilibrium distribution of a compound between two phases, in this case the lipid phase, lipid bilayer, and the aqueous phase, the buffer solution. The determination of $K_{p,x}$ values allows to quantify thermodynamically the interaction of the compound with the membrane, *i.e.* in which phase the compound preferentially distributes [51–53].

The **Ke** lipid/water $K_{p,x}$ was determined using Equation (9) [34,52, 54,55]:

$$\Delta I = \frac{\Delta I_{max}\ K_{p,x}\ [L]}{[W] + K_{p,x}\ [L]} \quad (9)$$

where $\Delta I = I - I_W$ is the difference between the steady state fluorescence intensity at 370 nm of the compound measured in the presence (I) and in the absence (I_W) of LUVs; $\Delta I_{max} = I_L - I_w$ is the maximum value for that difference, with I_L the limiting value of I corresponding to complete membrane partition of the compound; [L] is the total lipid concentration in the suspension; $K_{p,x}$ is the mole-fraction partition coefficient of the antifungal between the lipid and aqueous phases; and [W] is the molar concentration of water at the assay temperature (55.5 M).

The results for **Ke** are shown in Figure 3.2 – D. The solid line represents the nonlinear fit of equation (9). The $K_{p,x}$ and ΔI_{max} values obtained for **Ke** at 23 °C were (3.31 ± 0.36) x 10^5 and (1.26 ± 0.26) x 10 a.u., respectively. These values were obtained by averaging the parameters obtained from the fit of equation (9) to each independent replicate. From these results, a ratio of intensities of **Ke** in the lipid and in aqueous phases I_L/I_W of 1.37 was determined. The parameters are summarized in Table 3.1.

The $K_{p,x}$ obtained for **Ke** at 5 μM – (2.40 ± 0.22) x 10^5 (Table 3.1; Figure S3.2), was not significantly different from the one obtained at 10 μM, according to Student's *t*-test. This indicates that the partition of **Ke** towards the POPC bilayers is not dependent on compound concentration in the range of 5–10 μM, validating the use of a partition model assuming an infinite dilution regime [52,56].

Changes in **Ke** fluorescence anisotropy at 10 μM can be used to estimate the steady-state fluorescence anisotropy of **Ke** in the lipid phase - r_L – by fitting equation (10) [57] to the fluorescence anisotropy data (Figure 3.2 – E).

$$\langle r \rangle = \frac{r_W \left(\frac{1}{\gamma_L [L]} - 1\right) + r_L K_p \frac{\Phi_L}{\Phi_W}}{\frac{1}{\gamma_L [L]} - 1 + K_p \frac{\Phi_L}{\Phi_W}} \quad (10)$$

The ratio Φ_L/Φ_W was taken as equal to I_L/I_W, γ_L is the molar volume of POPC in a fluid bilayer (0.763 M^{-1} [58]); and r_W is the steady-state fluorescence anisotropy value for the compound in aqueous solution (with no lipid). The value of $K_{p,x}$ previously obtained was also fixed and the only parameter optimized was r_L. Figure 3.2 – E shows that the best fitting curve describes very well the experimental values of ‹*r*›, which validates the K_p value obtained from the fluorescence intensity analysis. The fluorescence anisotropy of **Ke** in the lipid bilayer was 0.094 ± 0.005, more than 4-fold its value in water (Table 3.1).

3.2. Membrane interactions of Ke derivatives KeP and KeOP

Since **KeP** and **KeOP** are intrinsically fluorescent due to the presence of virtually the same fluorophore [38,39] as **Ke**, it is possible to 1) characterize the compounds in aqueous solution and 2) study the interaction of these compounds with the membrane by monitoring the fluorescence properties of the compounds.

3.2.1. Exploring the aggregation of KeOP and KeP

Before assessing the interaction of the two **Ke** derivatives with POPC membranes, it is important to characterize the aggregation of these compounds in aqueous environment, which is more likely to occur for these compounds than **Ke** due to the presence of an hydrophobic diphenylphosphine moiety, and in fact was observed for Cu(I) complexes with **KeP** [25]. The formation of aggregates in aqueous solution can influence the membrane/water partition of the compounds and require a different partition model [59,60] or a different experimental approach [61]. Therefore, the concentration dependence of the emission spectra and static light scattering intensity of **KeOP** and **KeP** in aqueous solution were studied (Figure 3.3). Aggregation leads to the presence of particles with larger size than the monomeric form, and consequently leads to an increase in light scattering intensity. These spectroscopic approaches have been previously used to address the aggregation of a variety of compounds [41,57]. **Ke** was used as a negative control, since it does not aggregate in aqueous solution [62].

The light scattering by **KeOP** was stronger than that by **Ke**, especially for the highest measured concentration (100 μM), while for **KeP** the light scattering intensity values were considerably higher than for **Ke** (and **KeOP**) above concentrations of 10 μM (Figure 3.3 – A). On the other hand, the emission spectra of **KeOP** displayed a second non-typical band at longer wavelengths for concentrations higher than 6 μM (Figure 3.3 – D), which was not observed for **KeOP** in organic solvents [38]. A similar behavior was found for **KeP** but for concentrations at least as low as 2 μM (Figure 3.3 – E). This is confirmed by the non-linear dependence of the fluorescence intensity at 375 nm on the concentration of **KeOP** and **KeP** (Figure 3.3 - C). A non-linear dependence of the absorbance of **KeOP** and **KeP** at the peak wavelength on concentration for both compounds was also observed (Figure S3.4 - B and C), further corroborating the aggregation of these two compounds. Furthermore, the fluorescence anisotropy of **KeOP** increased with concentration until it reaches a plateau at 8–10 μM, while for **KeP** the fluorescence anisotropy was constant in the range of concentrations used, 0.2–20 μM (Figure S3.3). Altogether, these results suggest that **KeP** has a stronger tendency to

aggregate than **KeOP**, and, since the values for light scattering intensity are markedly higher, **KeP** probably forms larger aggregates than the ones formed by **KeOP**. Moreover, **KeP** already aggregates at 2 µM, while **KeOP** aggregates for concentrations above 6 µM.

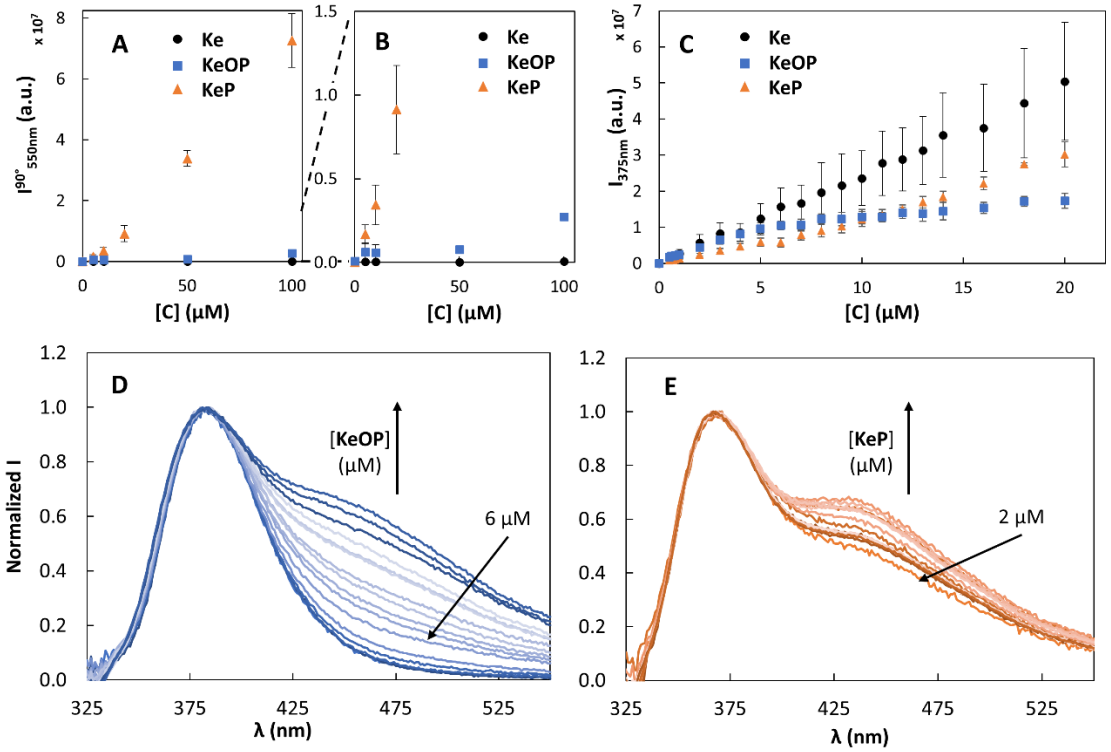

Figure 3. 3: Aggregation of KeOP **and** KeP **in aqueous solution.** (A and B) Static light scattering intensity at 550 nm and 90° for **Ke** (black circles), **KeOP** (blue squares) and **KeP** (orange triangles) with concentrations ranging from 5 to 100 µM. B is a Y-axis zoom in of A. (C) Fluorescence intensity at 375 nm as a function of the concentration of **Ke**, **KeOP** and **KeP** in HEPES buffer. (D and E) Normalized fluorescence emission spectra with different concentrations of **KeOP** (D) and **KeP** (E), in HEPES buffer ranging from 0.5 to 20 µM. The results in A – C are the mean ± S.D. of at least three independent replicates.

This stronger tendency of **KeP** to aggregate is consistent with its higher hydrophobicity compared to **KeOP**, and with the lower ground state dipole moment determined previously using density-functional theory (DFT), which was 3.03 D and 5.44 D for **KeP** and **KeOP** respectively [38].

3.2.2. Fluorescence properties of KeP and KeOP in the presence of POPC bilayers

To investigate possible interactions of **Ke** derivatives with lipid bilayers, the fluorescence excitation and emission spectra and anisotropy of **KeP** and **KeOP** were obtained in the presence of LUVs with different POPC concentrations (0.025 mM–2 mM; Figure 3.4). The concentration of **KeP** and **KeOP** used was 10 µM, the same as the one used for the assay with **Ke**. Ideally, the concentration of **KeOP** and **KeP** should be below the values for which aggregation is detected. However, for **KeP** that is not possible, since the compound aggregates at very low concentrations – 2 µM. **KeOP** on the other hand has a very low fluorescence quantum yield,

preventing its study in LUV suspensions at concentrations below 10 µM, due to the low signal-to-noise ratio.

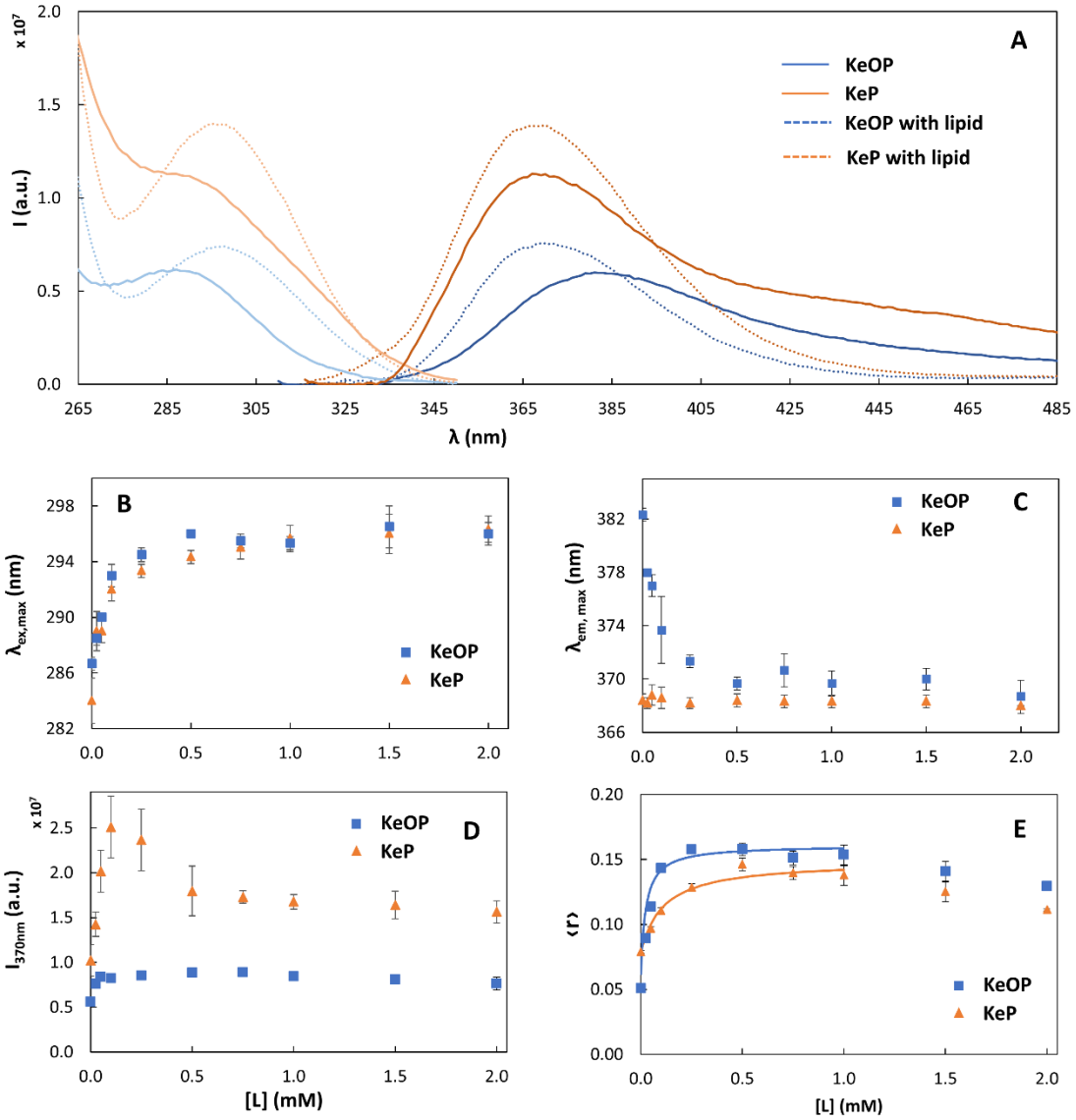

Figure 3. 4: Interaction of KeOP **and** KeP **with POPC lipid bilayers monitored through their intrinsic fluorescence.** (A) Fluorescence excitation (light blue and orange) and emission (dark blue and orange) spectra of **KeOP** (blue) and **KeP** (orange) in HEPES buffer (solid line) or in the presence of LUVs at 2 mM of POPC (dashed line). Peak wavelength of excitation ($\lambda_{exc,max}$; B) and emission ($\lambda_{em,max}$; C) spectra. Fluorescence intensity (variation from the value in water), ΔI (D) and steady-state fluorescence anisotropy, $\langle r \rangle$ (E) of **KeOP** (blue squares) and **KeP** (orange triangles) for increasing lipid concentrations. The solid line in E represents the fitting of equation (10) to the experimental data. Data in D and E was obtained with excitation at 295 nm and emission collected at 370 nm. The concentration of **KeP** and **KeOP** was 10 µM. The results in B - E are the mean ± S.D. of at least three independent replicates.

The peak wavelengths of **KeOP** and **KeP** in buffer were, respectively, 287 nm and 284 nm for excitation spectra and 382 nm and 368 nm for emission spectra (Figure 3.4 – A - C; Table 3.1). These values are in agreement with the ones obtained in our previous work [38]. The presence of POPC LUVs induced (1) an overall increase in the fluorescence intensity of both compounds (Figure 3.4 – D), (2) a redshift of the excitation spectra to a peak wavelength of ca. 296 nm (Figure 3.4 – B), and (3) for **KeOP** only, there was a blue shift of the emission spectra

until the peak wavelength reached a value of 369 nm (Figure 3.4 – C). Since the presence of the liposomes affected the fluorescence properties of both compounds, it is possible to conclude that **KeOP** and **KeP** also interact with POPC lipid bilayers.

The fluorescence properties of **KeOP** underwent similar changes in the presence of POPC as **Ke**. Both the fluorescence intensity and anisotropy at 370 nm increased with lipid concentration until they reached a constant value (Figure 3.4 – D and E), reflecting the progressive incorporation of compound in the membrane. However, for **KeOP** this increase amounts to 58 % and seems to be steeper than for **Ke**. The blue shift of the emission spectra of **KeOP** in the presence of lipid is also in agreement with its incorporation in the lipid bilayer. The maximum shift observed for **KeOP** was very similar to the one found for **Ke** (8–9 nm). However, the shift seems to be more abrupt for **KeOP** than for **Ke**, as noted for the increase in fluorescence intensity, which agrees with **KeOP** partitioning more efficiently into the lipid bilayer.

Although **KeP** did not show a shift in the peak wavelength of the emission spectra, for all three compounds, **Ke**, **KeOP** and **KeP**, the peak wavelength of the emission spectra in the presence of the highest concentration of lipid used, reached a similar value (between 368 and 371 nm – Table 3.1). Since the three compounds share the same fluorophore, this result points to a similar environment surrounding the three compounds in the lipid bilayer, *i.e.*, **Ke** and its two derivatives **KeOP** and **KeP** are probably inserted at similar depths in the membrane.

Even though the variation of fluorescence anisotropy of **KeP** was similar to the one found for **Ke** and **KeOP**, the fluorescence intensity of this compound did not follow the typical hyperbolic curve (Figure .4 – D). For 10 μM of **KeP**, the fluorescence intensity increases 150 % until 0.1 mM of POPC is reached, then it decreases to a value that is only 50 % higher than the intensity in the absence of lipid, and finally it remains fairly constant for lipid concentrations higher than 0.5 mM. Overall, there was an increase in the fluorescence intensity with the presence of lipid which, together with the variation of anisotropy and shift of the excitation spectra, points to the interaction of **KeP** with the lipid bilayer. However, no shift was observed in the emission spectra of **KeP**, indicating a more similar microenvironment for this compound in both the absence and the presence of liposomes, which corroborates the strong aggregation of **KeP** in aqueous solution shown in the previous section. In the aggregates most **KeP** molecules are surrounded by other lipophilic **KeP** molecules instead of water.

For concentrations of POPC above 1 mM the fluorescence anisotropy of **KeP** and **KeOP** started to decrease, which is most likely due to the increase of light scattering caused by the

high concentration of lipid. Therefore, the values of anisotropy for concentrations higher than 1 mM of lipid were not used in the determination of r_L (as described *e.g.* in Ref. [57]).

3.2.3. Quantifying the partition of KeOP and KeP between buffer and POPC bilayer

As stated in the previous section, the aggregation of **KeOP** was not as significant as for **KeP** in the lower compound concentration range, and there is no evidence for **KeOP** aggregation in the presence of lipid. In addition, the fluorescence intensity of this compound upon increasing lipid concentration followed a typical hyperbolic curve. Therefore, the partition of **KeOP** towards the POPC bilayer was quantified using equation (9) for determination of $K_{p,x}$ (Figure 3.5 - A). The $K_{p,x}$ and ΔI_{max} obtained from the fit (Figure 3.5 - A) were (4.66 ± 0.72) x 10^6 and (3.20 ± 0.26) x 10^6 a.u. respectively.

The variation of fluorescence intensity of **KeP** did not follow the typical hyperbolic curve for partition (Figure 3.4 – D). Moreover, the concentration of lipid where the trend of the curve changes (the fluorescence intensity starts to decrease) is different for each compound concentration (Figure 3.5 – B). This indicates that the processes influencing the interaction of the compound with the membrane are dependent on the concentration of the compound, or more precisely, on the compound/lipid ratio, particularly for low concentrations of lipid, where the compound/lipid ratios are high. In this region, the behavior of the system cannot be described by a partition of a solute at infinite dilution.

In order to quantify the partition behavior of **KeP** it was considered that there are two regimes as previously described for omiganan, an antimicrobial peptide [59] and the dengue virus fusion peptide [60]. In the first regime, there is an approximately linear increase in fluorescence intensity, and the system is described by the local compound/lipid ratio, σ, which is relatively high. The determination of this ratio allows quantifying the number of molecules of lipid that surround the compound. Afterwards, the system enters the second regime where the partition behavior of the compound between the two phases is characterized by the molar partition coefficient (K_p) as defined in Supporting Material (Equation S3). In this regime the local amount of lipid is now much larger than that of the compound, and the fluorescence intensity decreases. So, for the complex membrane/water partition behavior of **KeP**, the value of $K_{p,x}$ was determined using the following equation [59, 60]:

$$[C] = \frac{\sigma}{K_p \gamma_L} + \sigma [L]_c \qquad (11)$$

where [C] is the total compound concentration, $[L]_c$ is the total lipid concentration at the critical saturation point, σ is the ratio of local compound/lipid concentration at the critical point of the first regime, and γ_L is the molar volume of lipid. The critical points were considered those at which the maximum values of fluorescence intensity were reached (Figure 3.5 – B), *i.e.*, the points where K_p and σ both describe the system [59,60]. The value of γ_L for POPC bilayers in the fluid phase was considered 0.763 M^{-1} [58].

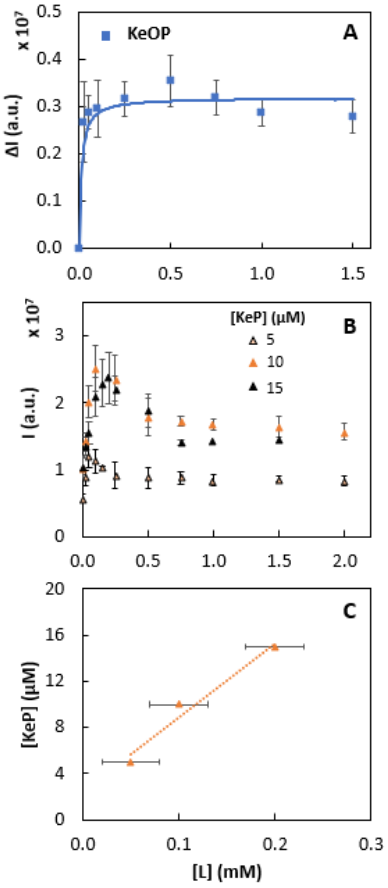

Figure 3. 5: Membrane/water partition of KeOP **and** KeP**.** (A) Fluorescence intensity of **KeOP** (blue squares) at 10 μM for increasing lipid concentrations. The solid line represents the fitting of equation (9) to the experimental data. (B) Fluorescence intensity of **KeP** (triangles), at 5 (light orange), 10 (orange) and 15 (dark orange) μM for increasing lipid concentrations. (C) **KeP** concentration as a function of lipid concentration at the critical point retrieved from (B). The results are the mean ± S.D. of at least three independent replicates. The bandwidth used to obtain the results in B were not the same, so the value of fluorescence intensity is not directly comparable between the different concentrations of **KeP**.

The total concentration of **KeP** was plotted as a function of the critical concentration of lipid in Figure 3.5 – C where the solid line is the linear fit of equation (11). The K_p estimated by this method was $(1.96 \pm 0.37) \times 10^4$. The σ obtained had a value of 0.064 which corresponds to approximately 15 molecules of lipid surrounding each molecule of **KeP** at the critical point. Interestingly, the minimum number of POPC molecules that need to surround a small molecule for it to avoid contact with another one in a lipid bilayer is ca. 12. So, 15 molecules of POPC

surrounding **KeP**, hinder the contact between **KeP** molecules in the bilayer, and prevent its aggregation.

K_p can be converted to $K_{p,x}$ through the following equation [63]:

$$K_{p,x} = K_p \frac{\gamma_L}{\gamma_W} \quad (12)$$

where γ_W is the molar volume of water, which was taken as 0.018 M^{-1} [64].

Using equation (12) the $K_{p,x}$ value obtained for **KeP** was (8.31 ± 1.60) x 10^5 . This value is higher than the one obtained for **Ke**, but lower than the one determined for **KeOP** (Table 3.1), which suggests that **KeOP** is the one among the three compounds that interacts more favorably with the lipid bilayer, followed by **KeP**. Interestingly, both derivatives have higher affinity for POPC bilayers than **Ke**.

The fact that **KeP** aggregation behavior in aqueous solution is much more marked than that of **KeOP** may help understand why the partition behavior of the former compound is not typical, unlike the one found for **KeOP**. One hypothesis is that the **KeOP** interaction with the membrane is inducing the disassembly of its aggregates, and it is manly the monomeric form of the compound that is partitioning into the lipid bilayer. This is confirmed by the vanishing of the non-typical band at longer wavelengths, which was assigned to the aggregate, even in the presence of the smallest concentration of lipid (Figure S3.5–D). For **KeP** the non-typical band only disappeared completely at the critical lipid concentrations (Figure S3.5 – A-C).

3.3. Effect of the compounds on lipid bilayer permeability

The relatively high membrane affinity of the compounds presented herein raises the question of whether these drugs are able to disturb the lipid bilayer, leading *e.g.* to increased permeability. Hence, if such membrane disruption occurs, it could be evidence for an additional mode of action of these azole drugs through direct interaction with the membrane.

To quantify how the partition of the compounds could be affecting the membrane permeability, LUVs encapsulating CF were prepared. CF is intrinsically fluorescent, but at high concentrations suffers self-quenching. Therefore, it is possible to measure the release of CF by following the increase of its fluorescence intensity, *i.e.* the permeation of encapsulated CF through the lipid bilayer [26,65].

After the addition of 10 μM **Ke**, **KeP** or **KeOP** to 0.1 mM POPC LUVs encapsulating CF, the fluorescence intensity of this molecule increased clearly above the values of the negative control (only 2 % DMSO added) (Figure 3.6 - A), indicating that **Ke**, **KeP** and **KeOP** all disturb

the POPC bilayer, increasing its permeability. Interestingly, **KeOP** is 1) the one inducing the fastest permeabilization, as revealed by the shortest average leakage time (9 ± 1 min; Figure 3.6 – C), and 2) the most effective permeabilizer, as it leads to the highest percentage of maximum leakage (Figure 3.6 – B). Although **KeP** has the longest average leakage time (265 ± 49 min; Figure 3.6 - C), the maximum percentage of CF release (73 ± 2 %) is higher than the one obtained for **Ke** (60 ± 1 %; Figure 3.6 - B). This longest average time for **KeP** is probably due to the presence of aggregates that dissociate gradually as the monomeric compound partitions to the membrane. This behavior is also apparent when comparing the leakage percentage after 1h30, *i.e.*, the same incubation time used for the partition experiments. After 1h30 incubation, **KeOP** already induced a very high leakage, whereas **KeP** has induced a lower leakage than **Ke**. Only at longer times (>5 h) **KeP** becomes the second most efficient permeabilizing agent.

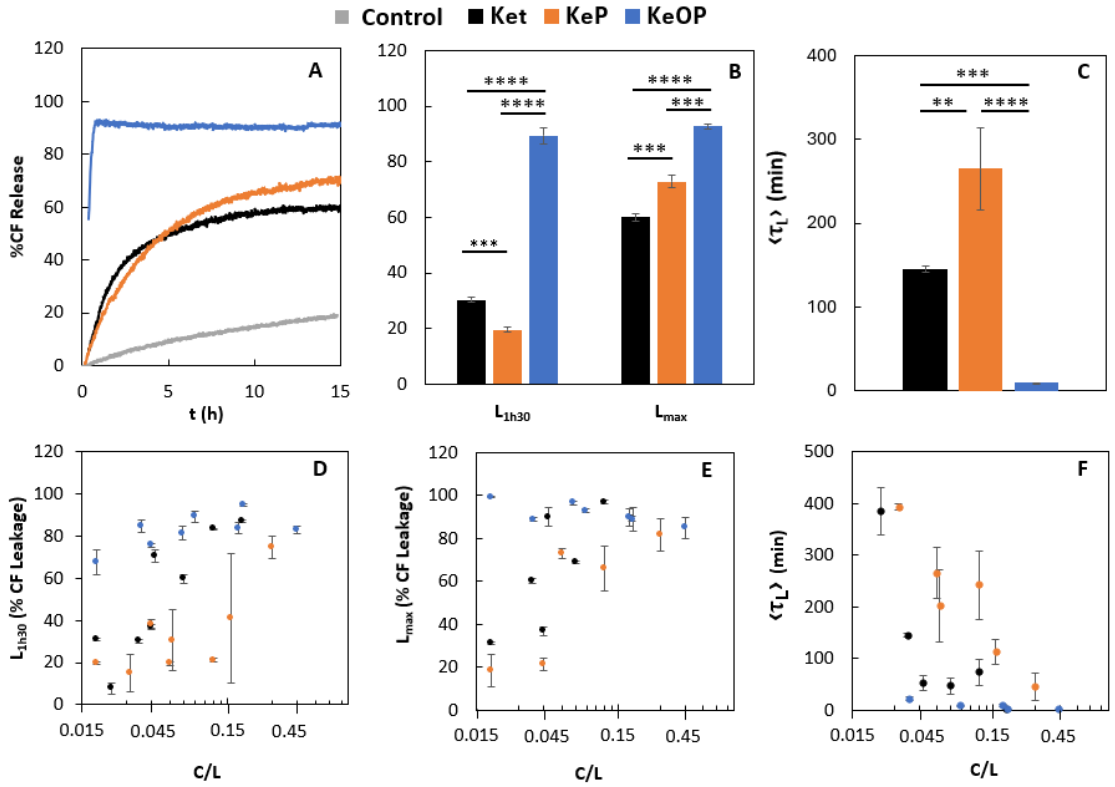

Figure 3.6: Effect of Ke, KeP **and** KeOP **on membrane permeability.** (A–C) The percentage of CF release from LUVs with 0.1 mM of POPC after the addition of 10 µM of each compound, was measured along 14-16 h. (B) Maximum percentage of CF release (L_{max}) and percentage of release 1h30 after the addition of the compound (L_{1h30}). (C) Average leakage time constant ($\langle\tau_L\rangle$) obtained for each compound. (D–F) L_{1h30} (D), L_{max} (E) and $\langle\tau_L\rangle$ (F) after the addition of **Ke**, **KeP** or **KeOP**, at different compound/lipid ratios (C/L). %CF Release was calculated using equation (4), while L_{max} and $\langle\tau_L\rangle$ were obtained from equations (5)–(8). The results in B–F are the mean ± S.D. of at least three independent replicates. ** *p*-value ≤0.01; *** *p*-value ≤0.001; **** *p*-value ≤0.0001.

The results discussed so far were carried out with the compounds at the same concentration used for most of the previous experiments. In this way, the permeabilizing activity of the compounds could be affected by the extent of membrane partition, *i.e.*, the effective local

concentration in the membrane is significantly different for each compound tested. Therefore, we tested different compound and lipid concentrations and calculated the effective compounds concentration in the membrane using the determined $K_{p,x}$ values (Table 3.1). In this way, we covered a broad range of compound/lipid ratios at the membrane (Figure 3.6 – D-F), showing that when considering the same local compound concentration in the membrane for the three compounds, **KeOP** continues to be the one inducing the fastest and most efficient membrane permeabilization. For the lowest compound/lipid ratios, which are probably those closest to the ratios reached under biological conditions, **KeOP** induces a fast and very extensive leakage, but the other two compounds have little permeabilizing activity.

4. Discussion

Although many antifungal drugs were shown to interact with membranes [34,66–68], the direct interaction of the FDA approved antifungal drug, **Ke**, with lipid membranes was not studied yet. In this work we were able to show that **Ke**, as well as its promising phosphine derivatives **KeP** and **KeOP**, can be transferred spontaneously from an aqueous solution to a POPC bilayer and increase its permeability. This was validated by the relatively high partition coefficients determined for all the compounds, which translate to an associated negative standard Gibbs energy (Table 3.1). According to the octanol/water (o/w) partition coefficient of **Ke** (experimental log $P_{o/w}$ of 4.35) [43], this molecule is lipophilic [41]. This value is similar to the log $P_{o/w}$ of other azoles that are fungicidal as well [66,69,70] and which interactions with lipid bilayers have been identified [66–68]. The changes in the fluorescence properties of **Ke** upon the addition of lipid show that this compound is partitioning towards the POPC bilayer. We determined a lipid/water $K_{p,x}$ at 23 °C of (3.31 ± 0.36) x 10^5 for **Ke**. This value corresponds to a log $K_{p,x}$ lipid/water of 5.52, which is one unit higher than the log $P_{o/w}$, suggesting that **Ke** has a higher affinity for a POPC bilayer than for a phase of octanol saturated with water. Both the lipophilicity of **Ke** and the shifts observed in the emission and excitation spectra in the presence of lipids indicate that the fluorophore of **Ke** is most likely interacting with the acyl chains of POPC.

Interestingly, the concentration of **Ke** used in the partition assay, ranged between 5 and 10 μM, which are in the same order of magnitude or higher than the minimal inhibitory concentration (MIC) against *S. cerevisiae* and *C. albicans*. Moreover, the administration of a single 200 mg dose of **Ke** in tablets leads to a mean peak plasma concentration of approximately 3.5 μg/mL which corresponds to ~6.6 μM, being in the same range of compound concentration used in this work [71]. The affinity of **KeP** and **KeOP** for a POPC bilayer was also characterized

in this work through the steady-state fluorescence measurements for different lipid concentrations. The value of the maximum emission wavelength in the presence of the highest lipid concentration used was similar for **Ke**, **KeP** and **KeOP**, and close to the ones obtained in 1-butanol [38], which points to a similar depth location in the membrane for the three compounds, since they share virtually the same fluorophore. The variation of fluorescence intensity of **KeOP** versus lipid concentration followed a typical hyperbolic curve. The same was not observed for **KeP**, which partition could be described by a model that depends on the concentration of compound. This different behavior was attributed to the strong tendency of **KeP** to aggregate in buffered aqueous solution for concentrations higher than 2 μM. Thus, instead of being described by a single equilibrium between monomer in water and in the membrane, the aggregation equilibria also had to be considered. **KeOP** was also shown to aggregate in buffer solution but with a markedly lower tendency than **KeP**, which could explain why **KeOP** followed the typical hyperbolic trend for membrane partition, analogously to **Ke**. Notably, this is consistent with the results obtained from static light scattering (Figure 3.3 - A) and other studies in aqueous solution (Figure S3.3–4) for compounds concentration ranging from 0.2 to 100 μM. Once liposomes were added to the system, the concentration of the compound in aqueous medium decreases, shifting the aggregation equilibrium towards the formation of monomer, causing the dissembly of the **KeOP** aggregates. This was confirmed by the analysis of the emission spectra of **KeOP** in aqueous solution, which has a second band, assigned to the aggregate, that disappears for samples containing the smallest concentration of POPC used (Figure S3.5–D). For **KeP**, even with higher concentrations of lipid the second non-typical emission band is still present, which confirms the persistence of aggregates in the sample. A single emission band is only identified for lipid concentrations higher than the critical saturation points for each concentration of **KeP**, *i.e.* the points where the behavior of the fluorescence dependence on lipid concentration switches, and the system is described by a membrane/water partition of the monomer in infinite dilution regime.

Although **KeP** is the most hydrophobic compound, as shown by the aggregation behavior and the calculated log $P_{o/w}$ (6.2 ± 1.1) higher than those of **KeOP** (5.5 ± 1.2) and **Ke** (3.6 ± 0.6) [72], the membrane/water Kp,x determined for **KeP** was not the highest. In fact, it was in the same order of magnitude of that for **Ke**, while for **KeOP** this coefficient was one order of magnitude higher. These results indicate that the diphenylphosphine moiety added to Ke allows for a stronger interaction with the membrane, which was somewhat expected given the hydrophobic character of this group. Furthermore, **KeOP** is, among the three compounds, the one that has the highest affinity for POPC bilayers, which seems to be granted by the presence

of the oxide in this drug that is missing in the other derivative. The highly polar P=O oxygen atom of **KeOP** can establish strong H-bonds with water molecules [39]. The membrane insertion of this compound would be stabilized in comparison with the other compounds, if in addition to hydrophobic interactions similar to those of **KeP**, the P=O oxygen could still be involved as an acceptor in H-bonding. This possibility, which requires further investigation would be compatible with an increased water penetration in the lipid bilayer due to **KeOP**, which would also justify its very high permeabilizing activity.

Sterol-14-α-demethylase P45014DM, the primary protein target of the three compounds, is a transmembrane protein of the endoplasmic reticulum (ER) [17,18,21,73]. To inhibit this enzyme, azole compounds must either cross the fungal plasma membrane or remain in the lipid bilayer and traffic through the endomembrane system to reach a target which is located in the lumen of the ER. A strong interaction with membrane lipids could mean that the compounds could more readily reach the ER where the target enzyme is located, due to the extensive cortical ER that is known to be present in yeast, with multiple contact points with the plasma membrane [74–76].

The permeability assay revealed that the three compounds have the ability to increase significantly the permeability of the POPC bilayer and thus to change membrane properties. **KeOP** was the one with the highest efficiency. These results together with the relative membrane affinity of **Ke**, **KeP** and **KeOP** found in this work could be relevant to understand some of our previous findings [23]. Namely, it was shown that **KeOP** had a lower MIC for wild-type *S. cerevisiae* (MIC = 0.00416 μM) than **Ke** (MIC = 0.865 μM) and **KeP** (MIC = 9.023 μM), *i.e.*, it was more efficient as an antifungal agent than both **Ke** and **KeP**. Moreover, both **KeP** and **KeOP** were active against a mutant strain of *S. cerevisiae* that lacks ergosterol in the plasma membrane, while **Ke** was not. Notably, that **KeOP** has 1) the highest membrane affinity and 2) the fastest and most efficient membrane permeabilization effect, correlates with the fact that this drug has the lowest MIC for *S. cerevisiae* wild-type when compared with **Ke** and **KeP** [23]. **KeOP** can induce an extensive membrane permeabilization under all conditions studied, including the lowest compound: lipid ratio used which compares with the MIC values ranging from 0.00416 to 3.13 μM against wild type *S. cerevisiae* with different genetic backgrounds. On another hand, against the same wild type strains, the parent compound **Ke** MIC values ranged between 0.865 and 6.25 μM, a value higher than obtained for **KeOP** [23]. This is in agreement with the fact that **Ke** induces a leakage higher than 50 % only at 10 μM or more, and higher compound:lipid ratios than **KeOP**. The MIC values and compound concentration range for membrane permeabilization indicate that this could be an

important additional mechanism of action for these compounds, especially **KeOP**, supporting further investigation of membrane interaction with these compounds. Considering that the $K_{p,x}$ values for **KeOP** and **KeP** are higher than for **Ke**, it is possible to conclude that $–CH_2PPh_2$ or $–CH_2P(O)Ph_2$ moiety strongly influences the affinity of **Ke** for lipid bilayers simultaneously enhancing its antifungal activity, with a cumulative effect of the oxygen atom in the phosphine group. Therefore, it is highly probable that **KeOP**, and even **KeP**, might have an additional mode of action related to their membrane perturbation ability, besides ergosterol biosynthesis inhibition. This would provide an explanation for the synergy observed between **KeOP** and another azole inhibiting 14α-demethylase, fluconazole [77], against *C. albicans*.

Several antifungal drugs are known for membranotropic properties and their effects on the membrane are an important part of their mode of action and contribute to their antifungal activity. For instance, nystatin and amphotericin B are both antifungal polyenes which, by inserting in the lipid bilayer increase membrane permeability and under certain conditions form pores that lead to fungal death [28–31]. Another example is fluconazole which affects the physico-chemical properties and architecture of dipalmitoylphosphatidylcholine (DPPC) liposomes [78], effects that have been correlated with the activity of the drug [77]. The addition of fluconazole to DPPC liposomes led to a decrease of the gel/fluid phase transition temperature and stabilized the lamellar rippled phase, $P_{\beta'}$ [78]. **Ke**, and especially its derivatives, are larger compounds than fluconazole, particularly the most hydrophobic moiety or moieties, suggesting that the insertion of the molecule, even in its monomeric form, can have a significant impact on membrane biophysical properties underlying the observed increase in membrane permeability. On the other hand, if **Ke** and derivatives affect membrane properties of fungal membranes, this could, in principle, be extended to mammalian membranes, and hence justify why **Ke** is hepatotoxic when administered orally [5,6], which is still not clarified, but could also be relevant for its anticancer activity [7–11].

Our studies could be also relevant to understand fungal drug resistance. Changes in membrane fluidity and asymmetry constitute putatively two of the resistance mechanisms found in *C. albicans* against azole antifungal drugs [79]. In a work with a mutant strain of *C. albicans* an increased membrane rigidity was correlated with the hindered entrance of fluconazole in the cell [80]. Nevertheless, those cases of resistance can also be interpreted considering that the compounds also act by disturbing (and permeabilizing) the membrane, and fungal strains with different membrane composition and properties can be more resilient to the membrane perturbation induced by the compounds. Finally, the drug-membrane interaction studies reported here could be relevant for the possible formulation of new delivery systems to better

improve the efficiency and reduce toxicity of **Ke**, since, as aforementioned, its oral administration is correlated with adverse side effects. This strategy as already been used with other antifungal agents, such as miconazole [81], amphotericin B [82,83], fluconazole and others [66].

We expect that the alterations of membrane permeability caused by **Ke** and derivatives and their relative affinity to the membrane will be dependent on membrane composition and biophysical properties. In the fungal plasma membrane, drug-membrane interactions are affected by the presence of proteins and different lipids, particularly ergosterol, the single most abundant component in the membrane of wild type yeast cells, and also sphingolipids which can comprise ~18 mol% of plasma membrane lipids, and other glycerophospholipids, such as phosphatidylethanolamine or phosphatidylinositol [84]. Also, not only the compounds might have preferential interaction with certain lipids, but also with specific lipid phases/domains, as reported for example for polyene antifungal drugs. The study here presented, carried out with a simple lipid system, which allowed successful quantification of membrane partition taking into account the different aggregation behavior of the compounds, paved the way for future studies of the interaction of **Ke** and its derivatives with more complex membranes.

5. Conclusion

In this work the affinity of the antifungal drug **Ke** and two of its derivatives, **KeP** and **KeOP**, for a fluid lipid bilayer was quantified, using fluorescence spectroscopic assays that relied on the intrinsic fluorescence of these compounds. We found that **Ke** and two diphenylphosphane derivatives, **KeP** and **KeOP**, interact with membranes under biologically relevant conditions. It was also possible to conclude that the phosphine moiety allows more effective membrane interaction. Moreover, the three compounds increase the permeability of the membrane. Chiefly, **KeOP** was the quickest and most effective in disturbing the bilayer, which, together with its highest partition coefficient, suggests an important role of the P=O bond. This oxygen atom establishes strong H-bonds with water molecules [39], which may favor an increased water penetration through the lipid bilayer, which thus becomes more permeable. Further investigation is required to fully understand these interactions at the molecular level. Studies involving membranes with different compositions would be relevant to explore possible preferences for certain lipids, such as ergosterol, or even lipid domains such as SLEDs (sphingolipid-enriched domains), and the impact of the compounds on lateral membrane organization. Nonetheless, our data strongly suggests that membrane

permeabilization is important for the antifungal activity of these compounds, particularly of **KeOP**.

Drug-membrane interaction studies, such as the one carried out in this work, are crucial for drug design and characterization since they allow further predicting the pharmaco-kinetic and -dynamic mechanisms of these compounds and could disclose new antifungal targets, such as fungal SLEDs. Furthermore, this line of work is also relevant for the design of new drug-delivery systems in which the compound is delivered in liposomes.

On the other hand, this work is relevant for membrane biophysics in a broader context, since a series of structurally related compounds were studied regarding membrane partition and microenvironment. Currently, we are investigating compounds in which the diphenylphosphinomethyl motif is structurally dominant to further test if the concomitant presence of **Ke** and diphenylphosphine moieties is indeed required for the increased membrane affinity of **KeP** and **KeOP**. We expect that this will help to identify how different parts of a molecule contribute to drug-lipid interactions and to establish new structure-activity relationships.

Acknowledgements

This work was funded by Fundação para a Ciência e Tecnologia (FCT), I.P./MCTES through national funds under projects EXPL/BIA-BFS/ 1034/2021, UIDB/00100/2020 (https://doi.org/10.54499/UIDB/00100/2020), UIDP/00100/2020 (https://doi.org/10.54499/UIDP/00100/2020) and LA/P/0056/2020 (https://doi.org/10.54499/LA/P/0056/2020), and doctoral scholarship to A.B.-O. (SFRH/BD/145600/ 2019).

References

[1] Center for Disease Control and Prevention, Centers for Disease Control and Prevention, Antifungal Resistance, 2023. https://www.cdc.gov/fungal/antifung al-resistance.html. (Accessed 7 March 2023).
[2] E. Rayens, K.A. Norris, Prevalence and healthcare burden of fungal infections in the United States, 2018, Open Forum Infect. Dis. 9 (2022) 1–12, https://doi.org/ 10.1093/OFID/OFAB593.
[3] M.C. Fisher, N.J. Hawkins, D. Sanglard, S.J. Gurr, Worldwide emergence of resistance to antifungal drugs challenges human health and food security, Science 360 (2018) 739–742, https://doi.org/10.1126/science.aap7999.
[4] J. Rhodes, Rapid worldwide emergence of pathogenic fungi, Cell Host Microbe 26 (2019) 12–14, https://doi.org/10.1016/J.CHOM.2019.06.009.
[5] L.A. García Rodrïguez, A. Duque, J. Castellsague, S. P´erez-Gutthann, B.H. C. Stricker, A cohort study on the risk of acute liver injury among users of ketoconazole and other antifungal drugs, Br. J. Clin. Pharmacol. 48 (1999) 847–852, https://doi.org/10.1046/J.1365-2125.1999.00095.X.
[6] T.E. Knight, C.Y. Shikuma, J. Knight, Ketoconazole-induced fulminant hepatitis necessitating liver transplantation, J. Am. Acad. Dermatol. 25 (1991) 398–400, https://doi.org/10.1016/0190-9622(91)70214-M.
[7] S. Naftalovich, E. Yefenof, Y. Eilam, Antitumor effects of ketoconazole and trifluoperazine in murine T-cell lymphomas, Cancer Chemother, Pharmacol 28 (1991) 384–390, https://doi.org/10.1007/BF00685694.
[8] V. Patel, B. Liaw, W. Oh, The role of ketoconazole in current prostate cancer care, Nat. Rev. Urol. 15 (2018) 643–651, https://doi.org/10.1038/S41585-018-0077-Y.
[9] A. Pont, Long-term experience with high dose ketoconazole therapy in patients with stage D2 prostatic carcinoma, J. Urol. 137 (1987) 902–904, https://doi.org/ 10.1016/S0022-5347(17)44290-X.
[10] J. Trachtenberg, Ketoconazole therapy in advanced prostatic cancer, J. Urol. 132 (1984) 61–63, https://doi.org/10.1016/S0022-5347(17)49464-X.
[11] G. Williams, Ketoconazole for prostate cancer, Lancet 324 (1984) 696, https://doi. org/10.1016/S0140-6736(84)91253-4.
[12] P. Contreras, E. Altieri, C. Liberman, A. Gac, A. Rojas, A. Ibarra, M. Ravanal, M. Seron-Ferr ´ ´e, Adrenal rest tumor of the liver causing Cushing's syndrome: treatment with ketoconazole preceding an apparent surgical cure, J. Clin. Endocrinol. Metab. 60 (1985) 21–28, https://doi.org/10.1210/JCEM-60-1-21.
[13] Committee for Medicinal Products for Human Use (CHMP), Assessment Report Ketoconazole HRA, Procedure No, EMEA/H/C/003906/0000, 2014. www.ema. europa.eu/contact. (Accessed 21 November 2021).
[14] C.F. Rochlitz, L.E. Damon, M.B. Russi, A. Geddes, E.C. Cadman, Cytotoxicity of ketoconazole in malignant cell lines, Cancer Chemother. Pharmacol. 21 (1988) 319–322, https://doi.org/10.1007/BF00264198.
[15] Y. Chen, H.N. Chen, K. Wang, L. Zhang, Z. Huang, J. Liu, Z. Zhang, M. Luo, Y. Lei, Y. Peng, Z.G. Zhou, Y. Wei, C. Huang, Ketoconazole exacerbates mitophagy to induce apoptosis by downregulating cyclooxygenase-2 in hepatocellular carcinoma, J. Hepatol. 70 (2019) 66–77, https://doi.org/10.1016/J. JHEP.2018.09.022.
[16] N. Weng, Z. Zhang, Y. Tan, X. Zhang, X. Wei, Q. Zhu, Repurposing antifungal drugs for cancer therapy, J. Adv. Res. (2022), https://doi.org/10.1016/J. JARE.2022.08.018.
[17] J.H. Van Tyle, Ketoconazole. Mechanism of action, spectrum of activity, pharmacokinetics, drug interactions, adverse reactions and therapeutic use, Pharmacotherapy 4 (1984) 343–373, https://doi.org/10.1002/J.1875-9114.1984. TB03398.X.
[18] D. Borelli, J.L. Bran, J. Fuentes, R. Legendre, E. Leiderman, H.B. Levine, A. Restrepo, D.A. Stevens, Ketoconazole, an oral antifungal: laboratory and clinical assessment of imidazole drugs, Postgrad. Med. 55 (1979) 657–661, https://doi. org/10.1136/PGMJ.55.647.657.
[19] D.S. Loose, P.B. Kan, M.A. Hirst, R.A. Marcus, D. Feldman, Ketoconazole blocks adrenal steroidogenesis by inhibiting cytochrome P450-dependent enzymes, J. Clin. Invest. 71 (1983) 1495, https://doi.org/10.1172/JCI110903.
[20] O. Shimokawa, M. Niimi, K. Kikuchi, M. Saito, H. Kajiwara, S.I. Yoshida, Relationship between MIC and minimum sterol 14α-demethylation-inhibitory concentration as a factor in evaluating activities of azoles against various fungal species, J. Clin. Microbiol. 43 (2005) 5547, https://doi.org/10.1128/ JCM.43.11.5547-5549.2005.
[21] N. Strushkevich, S.A. Usanov, H.W. Park, Structural basis of human CYP51 inhibition by antifungal azoles, J. Mol. Biol. 397 (2010) 1067–1078, https://doi. org/10.1016/J.JMB.2010.01.075.
[22] Y.Q. Zhang, S. Gamarra, G. Garcia-Effron, S. Park, D.S. Perlin, R. Rao, Requirement for ergosterol in V-ATPase function underlies antifungal activity of azole drugs, PLoS Pathog. 6 (2010) 1000939, https://doi.org/10.1371/JOURNAL. PPAT.1000939.
[23] R.F.M. de Almeida, F.C. Santos, K. Marycz, M. Alicka, A. Krasowska, J. Suchodolski, J.J. Panek, A. Jezierska, R. Starosta, New diphenylphosphane derivatives of ketoconazole are promising antifungal agents, Sci. Rep. 9 (2019), https://doi.org/10.1038/s41598-019-52525-7.
[24] X.L. Guan, C.M. Souza, H. Pichler, G. Dewhurst, O. Schaad, K. Kajiwara, H. Wakabayashi, T. Ivanova, G.A. Castillon, M. Piccolis, F. Abe, R. Loewith, K. Funato, M.R. Wenk, H. Riezman, Functional interactions between sphingolipids and sterols in biological membranes regulating cell physiology, Mol. Biol. Cell 20 (2009) 2083–2095, https://doi.org/10.1091/mbc.E08-11-1126.
[25] R. Starosta, R.F.M. De Almeida, M. Puchalska, A. Białonska, ´ J.J. Panek, A. Jezierska, I. Szmigiel, J. Suchodolski, A. Krasowska, New anticandidal Cu(I) complexes with neocuproine and ketoconazole derived diphenyl(aminomethyl) phosphane: luminescence properties for detection in fungal cells, Dalton Trans. 49 (2020) 8528–8539, https://doi.org/10.1039/D0DT01162B.
[26] R. Starosta, T.C. Santos, A.F. Dinis de Sousa, M.S. Santos, M.L. Corvo, A.I. Tomaz, R.F.M. de Almeida, Assessing the role of membrane lipids in the action of ruthenium(III) anticancer compounds, Front. Mol. Biosci. 9 (2023), https://doi. org/10.3389/fmolb.2022.1059116.

[27] J. Houˇst’, J. Spíˇzek, V. Havlíˇcek, Antifungal Drugs, Metab. 10 (2020) 106, https:// doi.org/10.3390/METABO10030106, 2020, Vol. 10, Page 106.
[28] T. Yamamoto, Y. Umegawa, H. Tsuchikawa, S. Hanashima, N. Matsumori, K. Funahashi, S. Seo, W. Shinoda, M. Murata, The amphotericin B–ergosterol complex spans a lipid bilayer as a single-length assembly, Biochemistry 58 (2019) 5188–5196, https://doi.org/10.1021/ACS.BIOCHEM.9B00835.
[29] B. Jacques, How do the polyene macrolide antibiotics affect the cellular membrane properties? Biochim. Biophys. Acta 864 (1986) 257–304, https://doi.org/10.1016/ 0304-4157(86)90002-X.
[30] B. De Kruijff, R.A. Demel, Polyene antibiotic-sterol interactions in membranes of Acholeplasma laidlawii cells and lecithin liposomes. III. Molecular structure of the polyene antibiotic-cholesterol complexes, Biochim. Biophys. Acta - Biomembr. 339 (1974) 57–70, https://doi.org/10.1016/0005-2736(74)90332-0.
[31] M. Szomek, P. Reinholdt, D. Petersen, A. Caci, J. Kongsted, D. Wüstner, Direct observation of nystatin binding to the plasma membrane of living cells, Biochim. Biophys. Acta - Biomembr. 1863 (2021) 183528, https://doi.org/10.1016/J.BBAMEM.2020.183528.
[32] F. Aresta-Branco, A.M. Cordeiro, H.S. Marinho, L. Cyrne, F. Antunes, R.F.M. de Almeida, Gel domains in the plasma membrane of Saccharomyces cerevisiae: highly ordered, ergosterol-free, and sphingolipid-enriched lipid rafts, J. Biol. Chem. 286 (2011) 5043–5054, https://doi.org/10.1074/jbc.M110.154435.
[33] A. Bento-Oliveira, F.C. Santos, J.T. Marquˆes, P.M.R. Paulo, T. Korte, A. Herrmann, H.S. Marinho, R.F.M. de Almeida, Yeast sphingolipid-enriched domains and membrane compartments in the absence of mannosyldiinositolphosphorylceramide, Biomolecules 10 (2020) 1–24, https:// doi.org/10.3390/biom10060871.
[34] A.G. dos Santos, J.T. Marquˆes, A.C. Carreira, I.R. Castro, A.S. Viana, M.-P. MingeotLeclercq, R.F.M. de Almeida, L.C. Silva, The molecular mechanism of Nystatin action is dependent on the membrane biophysical properties and lipid composition, Phys. Chem. Chem. Phys. 19 (2017) 30078–30088, https://doi.org/ 10.1039/C7CP05353C.
[35] F.C. Santos, J.T. Marquˆes, A. Bento-Oliveira, R.F.M. de Almeida, Sphingolipidenriched domains in fungi, FEBS Lett. 594 (2020) 3698–3718, https://doi.org/ 10.1002/1873-3468.13986.
[36] P. Hassanpour, H. Hamishehkar, B.B. Baroughi, B. Baradaran, S.S. Shotorbani, M. Mohammadi, N. Shomali, L. Aghebati-Maleki, S. Nami, Antifungal effects of voriconazole-loaded nano-liposome on fluconazole-resistant clinical isolates of Candida albicans, biological activity and ERG11, CDR1, and CDR2 gene expression, Assay Drug Dev. Technol. 19 (2021) 453–462, https://doi.org/ 10.1089/ADT.2020.1057.
[37] N. Vera-Gonzalez, ´ C.M. Bailey-Hytholt, L. Langlois, F. de C. Ribeiro, E.L. de S. Santos, J.C. Junqueira, A. Shukla, Anidulafungin liposome nanoparticles exhibit antifungal activity against planktonic and biofilm Candida albicans, J. Biomed. Mater. Res., Part A 108 (2020) 2263–2276, https://doi.org/10.1002/JBM. A.36984.
[38] R. Starosta, R.F.M. de Almeida, Luminescence properties of the antifungal agent ketoconazole and its diphenylphosphane derivatives, J. Lumin. 220 (2020) 116956, https://doi.org/10.1016/j.jlumin.2019.116956.
[39] A. Bento-Oliveira, M.-L.C.J. Moita, R.F.M. de Almeida, R. Starosta, Unraveling environmental effects in the absorption and fluorescence spectra of pmethoxyphenylpiperazine derivatives, Spectrochim. Acta Part A Mol. Biomol. Spectrosc. 306 (2024), https://doi.org/10.1016/j.saa.2023.123583.
[40] G. Rouser, S. Fleischer, A. Yamamoto, Two dimensional thin layer chromatographic separation of polar lipids and determination of phospholipids by phosphorus analysis of spots, Lipids 5 (1970) 494–496, https://doi.org/10.1007/BF02531316.
[41] A.M. De Matos, M.T. Blazquez-S ´ ´ anchez, A. Bento-Oliveira, R.F.M. De Almeida, R. Nunes, P.E.M. Lopes, M. MacHuqueiro, J.S. Cristov´ ao, ˜ C.M. Gomes, C.S. Souza, I. G. El Idrissi, N.A. Colabufo, A. Diniz, F. Marcelo, M.C. Oliveira, O. ´ Lopez, ´ J. G. Fernandez-Bolanos, ˜ P. Datwyler, ¨ B. Ernst, K. Ning, C. Garwood, B. Chen, A. P. Rauter, Glucosylpolyphenols as Inhibitors of Aβ-Induced Fyn Kinase Activation and Tau Phosphorylation: Synthesis, Membrane Permeability, and Exploratory Target Assessment within the Scope of Type 2 Diabetes and Alzheimer’s Disease, J. Med. Chem. 63 (2020) 11663, https://doi.org/10.1021/acs.jmedchem.0c00841.
[42] J. Guill´en, R.F.M. De Almeida, M. Prieto, J. Villalaín, Interaction of a peptide corresponding to the loop domain of the S2 SARS-CoV virus protein with model membranes, Mol. Membr. Biol. 26 (2009) 236, https://doi.org/10.1080/09687680902926203.
[43] Ketoconazole - PubChem, (n.d.). https://pubchem.ncbi.nlm.nih.gov/compo und/ketoconazole (accessed November 21, 2021).
[44] C.S. Ejsing, J.L. Sampaio, V. Surendranath, E. Duchoslav, K. Ekroos, R.W. Klemm, K. Simons, A. Shevchenko, Global analysis of the yeast lipidome by quantitative shotgun mass spectrometry, Proc. Natl. Acad. Sci. U.S.A. 106 (2009) 2136–2141, https://doi.org/10.1073/pnas.0811700106.
[45] D. Marsh. Handbook of Lipid Bilayers, second ed., CRC Press Taylor & Francis Group, Boca Raton FL, 2012 https://doi.org/10.1201/b11712.
[46] A. De Granada-Flor, C. Sousa, H.A.L. Filipe, M.S.C.S. Santos, R.F.M. De Almeida, Quercetin dual interaction at the membrane level, Chem. Commun. 55 (2019) 1750–1753, https://doi.org/10.1039/C8CC09656B.
[47] M.J. Moreno, M. Bastos, A. Velazquez-Campoy, Partition of amphiphilic molecules to lipid bilayers by isothermal titration calorimetry, Anal. Biochem. 399 (2010) 44–47, https://doi.org/10.1016/J.AB.2009.11.015.
[48] A. Khmelinskaia, J.M.T. Marquˆes, A.E.P. Bastos, C.A.C. Antunes, A. Bento-Oliveira, S. Scolari, G.M. da S. Lobo, R. Malho, ´ A. Herrmann, H.S. Marinho, R.F. De Almeida, Liquid-ordered phase formation by mammalian and yeast sterols: a common feature with organizational differences, Front. Cell Dev. Biol. 8 (2020) 337, https://doi.org/10.3389/FCELL.2020.00337.
[49] C. Reyes Mateo, A. Ulises Acuna, ˜ J.C. Brochon, Liquid-crystalline phases of cholesterol/lipid bilayers as revealed by the fluorescence of trans-parinaric acid, Biophys. J. 68 (1995) 978–987, https://doi.org/10.1016/S0006-3495(95)80273- 0.
[50] M.Y. Berezin, S. Achilefu, Fluorescence lifetime measurements and biological imaging, Chem. Rev. 110 (2010) 2641–2684, https://doi.org/10.1021/ CR900343Z.

[51] L.M.S. Loura, R.F.M. de Almeida, A. Coutinho, M. Prieto, Interaction of peptides with binary phospholipid membranes: application of fluorescence methodologies, Chem. Phys. Lipids 122 (2003) 77–96, https://doi.org/10.1016/S0009-3084(02)00180-9.
[52] S.H. White, W.C. Wimley, A.S. Ladokhin, K. Hristova, Protein folding in membranes: determining energetics of peptide-bilayer interactions, Methods Enzymol. 295 (1998) 62–87, https://doi.org/10.1016/S0076-6879(98)95035-2.
[53] N.C. Santos, M. Prieto, M.A.R.B. Castanho, Quantifying molecular partition into model systems of biomembranes: an emphasis on optical spectroscopic methods, Biochim. Biophys. Acta - Biomembr. 1612 (2003) 123–135, https://doi.org/10.1016/S0005-2736(03)00112-3.
[54] A. Coutinho, M. Prieto, Cooperative partition model of nystatin interaction with phospholipid vesicles, Biophys. J. 84 (2003) 3061–3078, https://doi.org/10.1016/ S0006-3495(03)70032-0.
[55] C.R. Mateo, M. Prieto, V. Micol, S. Shapiro, J. Villalaín, A fluorescence study of the interaction and location of (+)-totarol, a diterpenoid bioactive molecule, in model membranes, Biochim. Biophys. Acta 1509 (2000) 167–175, https://doi.org/10.1016/S0005-2736(00)00291-1.
[56] W.C. Wimley, S.H. White, Experimentally determined hydrophobicity scale for proteins at membrane interfaces, Nat. Struct. Biol. 310 (3) (1996) 842–848, https://doi.org/10.1038/nsb1096-842, 1996.
[57] M.A.R.B. Castanho, M.J.E. Prieto, Fluorescence study of the macrolide pentaene antibiotic filipin in aqueous solution and in a model system of membranes, Eur. J. Biochem. 207 (1992) 125–134, https://doi.org/10.1111/J.1432-1033.1992.TB17029.X.
[58] S. Chiu, E. Jakobsson, S. Subramaniam, H. Scott, Combined Monte Carlo and molecular dynamics simulation of fully hydrated dioleyl and palmitoyl-oleyl phosphatidylcholine lipid bilayers, Biophys. J. 77 (1999) 2462, https://doi.org/10.1016/S0006-3495(99)77082-7.
[59] M. Manuel Nuno, C. B, A.R. Miguel, Omiganan interaction with bacterial membranes and cell wall models. Assigning a biological role to saturation, Biochim. Biophys. Acta 1768 (2007) 1277–1290, https://doi.org/10.1016/J.BBAMEM.2007.02.005.
[60] F. Stauffer, M.N. Melo, F.A. Carneiro, F.J.R. Sousa, M.A. Juliano, L. Juliano, R. Mohana-Borges, A.T. Da Poian, M.A.R.B. Castanho, Interaction between dengue virus fusion peptide and lipid bilayers depends on peptide clustering, Mol. Membr. Biol. 25 (2008) 128–138, https://doi.org/10.1080/09687680701633091.
[61] L.C. Naßwetter, M. Fischer, H.A. Scheidt, H. Heerklotz, Membrane-water partitioning – tackling the challenges of poorly soluble drugs using chaotropic cosolvents, Biophys. Chem. 277 (2021) 106654, https://doi.org/10.1016/J. BPC.2021.106654.
[62] J. Seidler, S.L. McGovern, A. Thompson N. Doman, Brian K. Shoichet, Identification and prediction of promiscuous aggregating inhibitors among known drugs, J. Med. Chem. 46 (2003) 4477–4486, https://doi.org/10.1021/ JM030191R.
[63] P.M. Matos, H.G. Franquelim, M.A.R.B. Castanho, N.C. Santos, Quantitative assessment of peptide-lipid interactions. Ubiquitous fluorescence methodologies, Biochim. Biophys. Acta - Biomembr. 1798 (2010) 1999–2012, https://doi.org/10.1016/J.BBAMEM.2010.07.012.
[64] R.C. Weast, CRC Handbook of Chemistry and Physics, CRC Press, Cleveland, Ohio, 1978. https://search.library.wisc.edu/catalog/999469374502121.
[65] N. Martinho, J.M.T. Marquˆes, I. Todoriko, M. Prieto, R.F.M. de Almeida, L.C. Silva, Effect of cisplatin and its cationic analogues in the phase behavior and permeability of model lipid bilayers, Mol. Pharm. 20 (2023) 918–928, https://doi.org/10.1021/acs.molpharmaceut.2c00321.
[66] Y.G. Bachhav, K. Mondon, Y.N. Kalia, R. Gurny, M. Moller, ¨ Novel micelle formulations to increase cutaneous bioavailability of azole antifungals, J. Contr. Release 153 (2011) 126–132, https://doi.org/10.1016/J.JCONREL.2011.03.003.
[67] M. Dzieciuch-Rojek, C. Poojari, J. Bednar, A. Bunker, B. Kozik, M. Nowakowska, I. Vattulainen, P. Wydro, M. Kepczynski, T. Rog, ´ Effects of membrane PEGylation on entry and location of antifungal drug itraconazole and their pharmacological implications, Mol. Pharm. 14 (2017) 1057–1070, https://doi.org/10.1021/acs. molpharmaceut.6b00969.
[68] F. Cicogna, C. Pinzino, S. Castellano, A. Porta, C. Forte, L. Calucci, Interaction of azole compounds with DOPC and DOPC/ergosterol bilayers by spin probe EPR spectroscopy: implications for antifungal activity, J. Phys. Chem. B 117 (2013) 11978–11987, https://doi.org/10.1021/jp406776x.
[69] Itraconazole - PubChem, (n.d.). https://pubchem.ncbi.nlm.nih.gov/compound/Itraconazole (accessed November 21, 2021).
[70] A. Hajare, M.N. Mali, S.M. Sarvagod, S.T. Kurane, S. V Patwardhan, A.S. Dange, Adsorption and partition studies of fluconazole, Asian J. Res. Chem. 2 (2009). https://www.ajrconline.org/AbstractView.aspx?PID=2009-2-2-29.
[71] F.Z. Marok, J.G. Wojtyniak, L.M. Fuhr, D. Selzer, M. Schwab, J. Weiss, W. E. Haefeli, T. Lehr, A physiologically based pharmacokinetic model of ketoconazole and its metabolites as drug–drug interaction perpetrators, Pharmaceutics 15 (2023), https://doi.org/10.3390/PHARMACEUTICS15020679/S1.
[72] A. Daina, O. Michielin, V. Zoete, SwissADME: a free web tool to evaluate pharmacokinetics, drug-likeness and medicinal chemistry friendliness of small molecules, Sci. Rep. 71 (7) (2017) 1–13, https://doi.org/10.1038/srep42717, 2017.
[73] RCSB PDB - 5FSA: Crystal structure of sterol 14-alpha demethylase (CYP51) from a pathogenic yeast Candida albicans in complex with the antifungal drug posaconazole, (n.d.). https://www.rcsb.org/structure/5fsa (accessed October 15, 2021).
[74] M. West, N. Zurek, A. Hoenger, G.K. Voeltz, A 3D analysis of yeast ER structure reveals how ER domains are organized by membrane curvature, J. Cell Biol. 193 (2011) 333, https://doi.org/10.1083/JCB.201011039.
[75] A.G. Manford, C.J. Stefan, H.L. Yuan, J.A. MacGurn, S.D. Emr, ER-to-Plasma membrane tethering proteins regulate cell signaling and ER morphology, Dev. Cell 23 (2012) 1129–1140, https://doi.org/10.1016/J.DEVCEL.2012.11.004.
[76] E. Quon, Y.Y. Sere, N. Chauhan, J. Johansen, D.P. Sullivan, J.S. Dittman, W.J. Rice, R.B. Chan, G. Di Paolo, C.T. Beh, A.K. Menon, Endoplasmic reticulum-plasma membrane contact sites integrate sterol and phospholipid regulation, PLoS Biol. 16 (2018), https://doi.org/10.1371/JOURNAL.PBIO.2003864.

[77] B. Pawar, M. Joshi, S. Srivastava, M. Kanyalkar, In search of a novel antifungal agent: probing molecular interactions of fluconazole and its analogues with model membranes by NMR and DSC techniques, J. Pharm. Pharmacol. 64 (2012) 802–810, https://doi.org/10.1111/J.2042-7158.2012.01489.X.
[78] A. Ambrosini, G. Bossi, S. Dante, B. Dubini, L. Gobbi, L. Leone, M. Grazia Ponzi Bossi, G. Zolese, Lipid-drug interaction: thermodynamic and structural effects of antimicotic fluconazole on DPPC liposomes, Chem. Phys. Lipids 95 (1998) 37–47, https://doi.org/10.1016/S0009-3084(98)00062-0.
[79] A. Kohli, Smriti, K. Mukhopadhyay, A. Rattan, R. Prasad, In vitro low-level resistance to azoles in Candida albicans is associated with changes in membrane lipid fluidity and asymmetry, Antimicrob. Agents Chemother. 46 (2002) 1046, https://doi.org/10.1128/AAC.46.4.1046-1052.2002.
[80] N.K. Khandelwal, N. Chauhan, P. Sarkar, B.D. Esquivel, P. Coccetti, A. Singha, A. T. Coste, M. Guptaa, D. Sanglard, T.C. White, M. Chauvel, C. D'Enfert, A. Chattopadhyay, N.A. Gaur, A.K. Mondal, R. Prasad, Azole resistance in a Candida albicans mutant lacking the ABC transporter CDR6/ROA1 depends on TOR signaling, J. Biol. Chem. 293 (2018) 412–432, https://doi.org/10.1074/jbc. M117.807032.
[81] B.M. Aljaeid, K.M. Hosny, Miconazole-loaded solid lipid nanoparticles: formulation and evaluation of a novel formula with high bioavailability and antifungal activity, Int. J. Nanomed. 11 (2016) 441, https://doi.org/10.2147/IJN.S100625.
[82] C. Serafim, I. Ferreira, P. Rijo, L. Pinheiro, C. Faustino, A. Calado, L. Garcia-Rio, Lipoamino acid-based micelles as promising delivery vehicles for monomeric amphotericin B, Int. J. Pharm. 497 (2016) 23–35, https://doi.org/10.1016/J. IJPHARM.2015.11.034.
[83] D. Butani, C. Yewale, A. Misra, Topical Amphotericin B solid lipid nanoparticles: design and development, Colloids Surf. B Biointerfaces 139 (2016) 17–24, https:// doi.org/10.1016/J.COLSURFB.2015.07.032.
[84] R. Schneiter, B. Brügger, R. Sandhoff, G. Zellnig, A. Leber, M. Lampl, K. Athenstaedt, C. Hrastnik, S. Eder, G. Daum, F. Paltauf, F.T. Wieland, S. D. Kohlwein, Electrospray ionization tandem mass spectrometry (Esi-Ms/Ms) analysis of the lipid molecular species composition of yeast subcellular membranes reveals acyl chain-based sorting/remodeling of distinct molecular species En route to the plasma membrane, J. Cell Biol. 146 (1999) 741, https://doi.org/10.1083/ JCB.146.4.741.

Supplementary procedures

Membrane/water partition thermodynamic quantification

The partition coefficient quantifies the equilibrium distribution of a compound between two phases:

$$K_{\mathrm{p,x}} = \frac{\frac{n_L^c}{n_L + n_L^c}}{\frac{n_W^c}{n_W + n_W^c}} \quad \text{(S1)}$$

where n_L and n_W are the number of moles of lipid and water respectively, while n^c_L and n^c_W are the number of moles of compound, *c*, in the lipid and water phase, respectively; and $K_{\mathrm{p,x}}$ is the mole-fraction partition coefficient of a compound between the lipid and aqueous phases. If we assume that $n_L >> n^c_L$ and that $n_W >> n^c_W$, than:

$$K_{\mathrm{p,x}} = \frac{\frac{n_L^c}{n_L}}{\frac{n_W^c}{n_W}} \quad \text{(S2)}$$

In the literature the partition equilibrium is also quantified considering the volumes of water and lipid phases (V_W and V_L respectively), which in the present work we define as the molar partition coefficient K_p:

$$K_{\mathrm{p}} = \frac{\frac{n_L^c}{V_L}}{\frac{n_W^c}{V_W}} \quad \text{(S3)}$$

K_p and $K_{\mathrm{p,x}}$ are interchangeable using equation 12 of the manuscript.

The mole-fraction of each compound in the lipid phase (χ_L) at a specific concentration of lipid was determined using the following equation:

$$\chi_L = \frac{\mathrm{K}_{p,x}[L]}{[W] + \mathrm{K}_{p,x}[L]} \quad \text{(S4)}$$

where [L] is the total lipid concentration in the suspension, and [W] is the molar concentration of water at the assay temperature (55.5 M).

The standard Gibbs energy ($\Delta G°$) associated with the transfer of a mole of compound from the aqueous phase to the lipid phase was determined using the following equation:

$$\Delta G^{\circ} = -RT \ln K_{\mathrm{p,x}} \quad \text{(S5)}$$

where R is the molar gas constant, 8.314 J·K^{-1}·mol^{-1}, and T is the temperature, 296.15 K.

Supplementary Figures

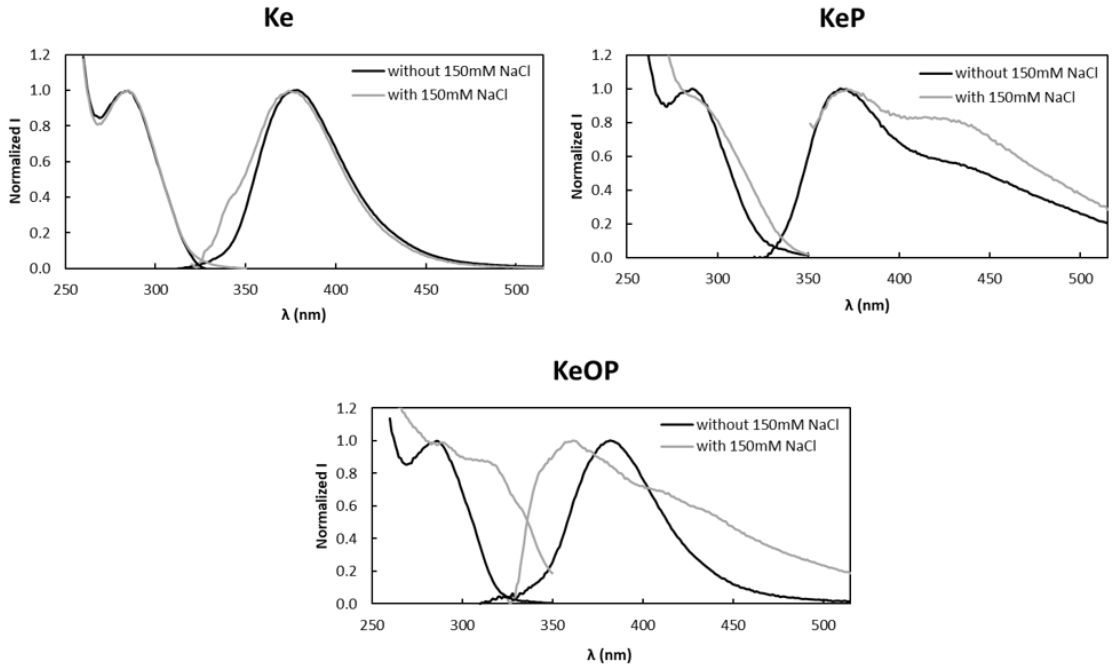

Figure S3. 1: Normalized fluorescence excitation and emission spectra of **Ke**, **KeP** and **KeOP** at 5 µM in HEPES buffer (10 mM, pH 7.4) with 2% DMSO with and without 150 mM NaCl.

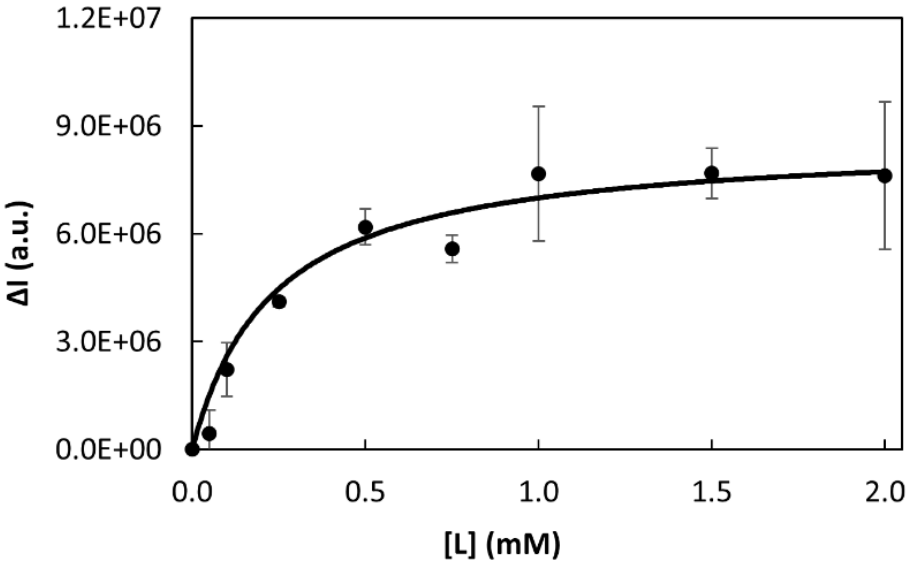

Figure S3. 2: Dependence on lipid concentration, [L], of the fluorescence intensity of **Ke** at 5 µM. The solid line represents the fitting of equation 4 to the experimental data with the fitting parameters $K_{\mathrm{p,x}}$ and ΔI_{max}, with values of (2.40 ± 0.22) x 10^5 and (8.62 ± 0.17) x 10^6 a.u., respectively. ΔI is the difference between the steady state fluorescence intensity of **Ke** in the presence and in the absence of lipid at 370 nm. The values are the mean ± S.D. of at least three independent experiments.

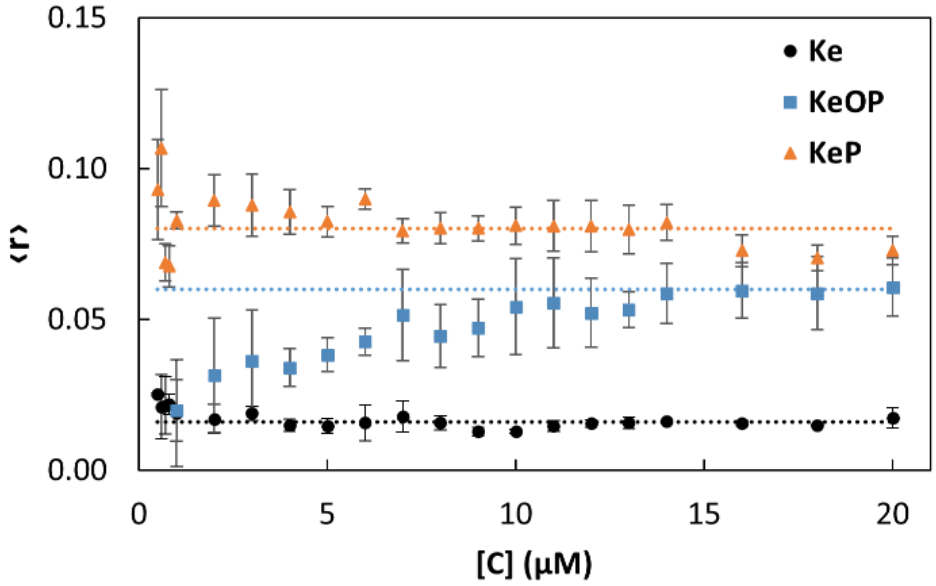

Figure S3. 3: Steady-state fluorescence anisotropy of **Ke** (black circles), **KeP** (orange triangles) and **KeOP** (green squares) in 10mM HEPES (pH 7.4) buffer with 2% DMSO for different compound concentrations, [C]. The dashed lines are guidelines for the mean value along the different compound concentration, except for **KeOP** which is the average value for concentrations larger than 10 µM. The values are the mean ± S.D. of at least three independent experiments.

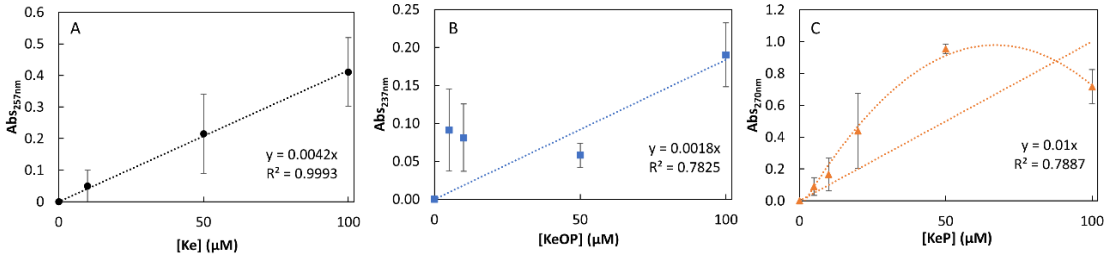

Figure S3. 4: Absorbance at the maximum absorption wavelength of each compound versus concentration of **Ke** (A), **KeOP** (B), **KeP** (C) in 10mM HEPES (pH 7.4) buffer with 2% DMSO. The values are the mean ± S.D. of at least three independent experiments.

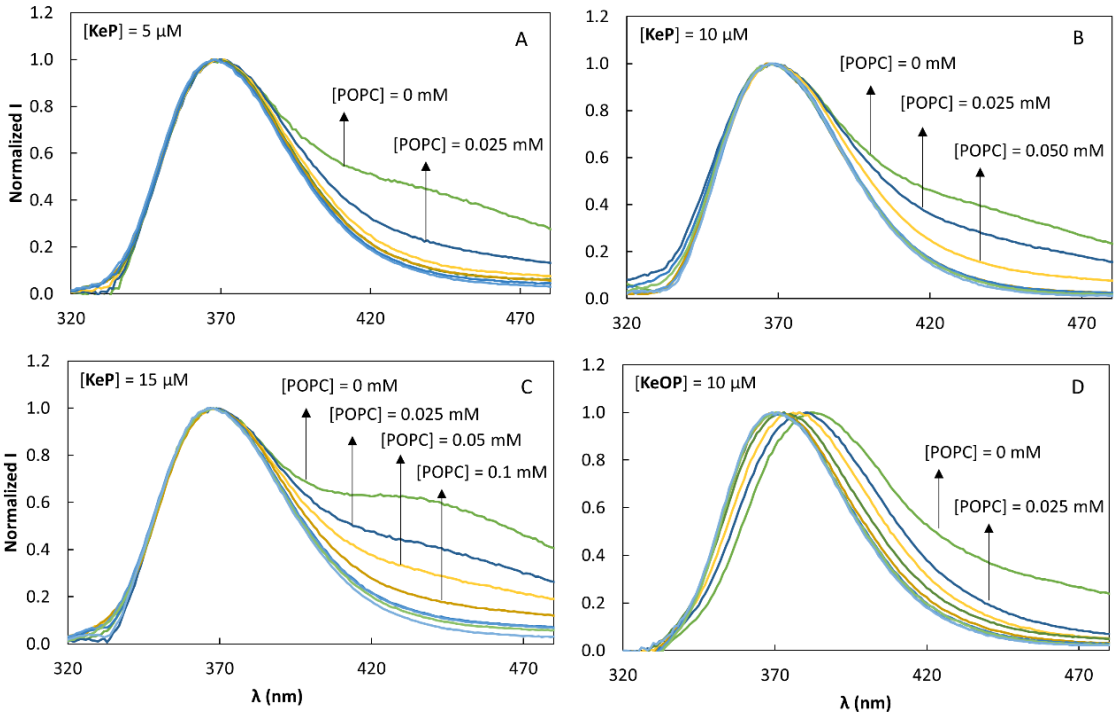

Figure S3. 5: Normalized fluorescence emission spectra of **KeP** and **KeOP** at 10 µM in HEPES buffer (pH 7.4) with 2% DMSO in the presence of different concentrations of POPC. The concentrations of **KeP** was 5 (A), 10 (B) or 15 µM (C), while for **KeOP** it was 10 µM (D).

CHAPTER IV

Diphenylphosphine Oxide: A Motif to Improve Membrane Affinity and Antifungal Activity of Ketoconazole

---

Contribution: Took an active part in the planning of and performed all the experiments. Took an active part in the writing of the paper.

Diphenylphosphine Oxide: A Motif to Improve Membrane Affinity and Antifungal Activity of Ketoconazole

Andreia Bento-Oliveira,[1] Radosław Starosta,[1,2] Rodrigo F. M. de Almeida[1,*]

[1] Centro de Química Estrutural, Institute of Molecular Sciences, Departamento de Química e Bioquímica, Faculdade de Ciências, Universidade de Lisboa, Campo Grande, 1749-016 Lisboa, Portugal.
[2] Faculty of Chemistry, University of Wroclaw, F. Joliot-Curie 14, 50-383 Wroclaw, Poland
* Correspondence: rfalmeida@fc.ul.pt; Tel. : +351-217-500-925

Abstract

The antifungal ketoconazole (**Ke**) and diphenylphosphinomethyl derivatives (**KeP**: Ph_2PCH_2-Ke and **KeOP**: $Ph_2P(O)CH_2$-Ke) have high affinity for a fluid lipid bilayer. Moreover, **KeP**, and particularly **KeOP** interact more efficiently with membranes than **Ke**, inducing extensive membrane leakage, which is probably correlated with its improved antifungal activity. However, it is still unknown how the structural differences between these compounds are affecting their membrane partition and depth. To unravel the relative transverse location of these compounds in a fluid 1-palmitoyl-2-oleoyl-*sn*-glycero-3-phosphocholine (POPC) bilayer, the membrane interaction of two molecules was studied, **4MP** (Ph_2PCH_2-pip-C_6H_4-4-OMe) and its oxide (**4MOP**). These are structurally simplified analogs of **KeP** and **KeOP**, respectively. The mole-fraction partition coefficient ($K_{p,x}$) of **4MP** and **4MOP** between POPC liposomes and aqueous buffer was determined taking advantage of the intrinsic fluorescence of these compounds. The $K_{p,x}$ obtained for **4MP** and **4MOP** were $(4.29 \pm 0.17) \times 10^4$ and $(5.21 \pm 0.82) \times 10^5$, respectively. Surprisingly, the interaction of these more hydrophobic analogs with the membrane is relatively less favorable than **KeP** [$(8.31 \pm 1.60) \times 10^5$] and **KeOP** [$(4.66 \pm 0.72) \times 10^6$]. Moreover, they lie near the surface of the lipid bilayer, in contrast with **Ke**, **KeP** and **KeOP**. Furthermore, a leakage assay was also conducted which showed that **4MP** and **4MOP** do not significantly change the permeability of POPC membranes. Thus, the **Ke** moiety is required for deeper membrane insertion and its presence concomitantly with the phosphine moiety leads to stronger membrane affinity. The higher affinity of both **KeOP** and **4MOP** compared to **KeP** and **4MP**, respectively, and faster and more extensive membrane permeabilization, confirms an important role of $Ph_2P(O)CH_2$-oxygen possibly by affecting the membrane hydration layer. This work evidences the importance of drug-membrane interactions for understanding and improving antifungal activity of this series of compounds.

Keywords
Drug-membrane interaction, antifungal agents, fluorescence spectroscopy, diphenylphosphinomethyl derivatives, phospholipid bilayer

1. Introduction

Fungal infections are a worldwide pressing concern that can have serious consequences both in healthcare and agriculture [1–3]. For instance, invasive fungal infections can cause life-threatening conditions, particularly in immunocompromised individuals to whom even typically non-pathogenic fungi such as *Saccharomyces cerevisiae* can be an issue [4,5]. Moreover, in the agricultural sector, phytopathogenic fungi can lead to significant economic losses due to decreased crop yield and quality [6]. Unfortunately, the fight against these infections is further hindered by the emergence of drug-resistant strains of pathogenic fungi [7,8] belonging to *e.g.* the *Candida* [9,10] and *Aspergillus* [11] genera. Therefore, it is imperative to intensify the search for new and/or improved antifungal therapies to address this urgent problem and mitigate its consequences.

Ketoconazole (**Ke**; Figure 4.1) is an imidazole antifungal drug which inhibits cytochrome P450 sterol-14-α-demethylase (P45014DM) [12–16], an enzyme of the biosynthetic pathway of ergosterol in fungi. Although **Ke** is a relatively potent antifungal agent, it has severe side effects when administered systemically [17,18]. Diphenylphosphinemethyl derivatives (Figure 4.1), **KeP** (Ph_2PCH_2-Ke) and **KeOP** ($Ph_2P(O)CH_2$-Ke) share the same target as **Ke**, with improved antifungal activity, but not increased toxicity towards human cells [19]. These derivatives are active against a yeast strain lacking ergosterol, *erg6*Δ, suggesting alternative modes of action [19,20]. Moreover, recently, we have shown that **Ke**, **KeP** and, particularly **KeOP** have strong affinity and membranotropic abilities towards fluid 1-palmitoyl-2-oleoyl-*sn*-glycero-3-phosphocholine (POPC) membranes [20], disclosing the possibility that the compounds may also act directly on cell membranes in addition to blocking P45014DM active site. Even though **KeP** is more hydrophobic than **KeOP**, the latter has the highest membrane affinity and is the most effective permeabilizing agent, inducing both the fastest and most extensive leakage. This suggests that $Ph_2P(O)CH_2$-oxygen has an important role in the interaction of the compounds with the membrane. The highly polar P=O bond that exists only in **KeOP** renders the oxygen a very high H-acceptor ability, which is in agreement with a stronger stabilization of this compound in the membrane. Moreover, an increased water penetration in the lipid bilayer due to the partition of the compound is expected, which favorably

establishes H-bonds with **KeOP** [21] and correlates with the extensive membrane permeabilization caused by this compound.

To test this hypothesis, it is important to study the membrane interaction of compounds bearing the diphenylphosphine or the diphenylphosphineoxide moieties, but that are structurally simpler, where most of the **Ke** moiety is absent. Nonetheless, these compounds should still have the phenylpiperazine moiety to preserve a fluorophore identical to the other compounds [21,22]. Therefore, to further disclose the details of the interaction of **Ke**, **KeP** and **KeOP** with a fluid lipid bilayer and to better understand the impact of the **Ke** modifications, here we studied the membrane-interaction of two fluorescent model compounds: 1-(4-methoxyphenyl)-4-[(diphenylphosphino)methyl]piperazine (**4MP**) and 1-(4-methoxyphenyl)-4-[(diphenylphosphoryl)methyl]piperazine (**4MOP**), where most of the **Ke** moiety of each of the derivatives is replaced by a methyl group (Figure 4.1)[21,23], leaving a methoxy end on one side of the phenylpiperazine ring system and the diphenylphosphine(oxide) on the other. The membrane/water partition coefficients and the Gibbs energy of transfer from water to the membrane of **4MP** and **4MOP** was determined to clarify the energetic contribution of the **Ke**, diphenyphosphine and oxide moieties for the energetics of membrane interaction.

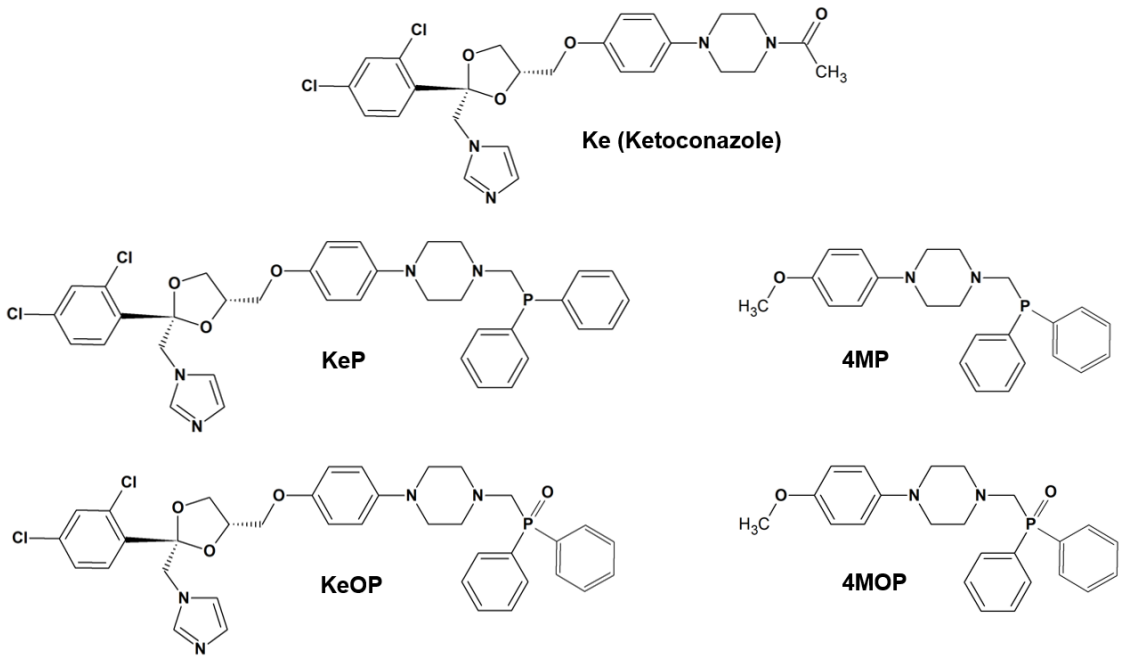

Figure 4. 1: Molecular structures of Ke, KeP, KeOP, 4MP and 4MOP.

Moreover, it is unclear how these structural differences influence compound distribution (relative deepness) along the membrane. Hence, in parallel, a fluorescence quenching assay was carried out for **Ke**, its derivatives **KeP** and **KeOP**, **4MP** and **4MOP**, to assess the relative penetration of the fluorophore phenylpiperazine, in a POPC bilayer. Furthermore, the

membranotropic abilities of **4MP** and **4MOP** were also studied by measuring the changes of the permeability of POPC liposomes in the presence of the compounds.

Comparing the behavior of all the compounds in the presence of POPC bilayers, allowed to conclude that the simultaneous presence of **Ke** and the phosphine moiety allows for a deeper and more effective membrane interaction and confirms the crucial role of the P=O oxygen for improving membrane partition and permeabilizing activity of the compounds.

2. Materials and methods

2.1. Chemicals

POPC was obtained from Lipoid (Ludwigshafen, Germany). DMSO (spectroscopic grade), HEPES and acrylamide were acquired from Fisher Chemical (Waltham, MA, USA). Reagents and solvents used for the syntheses, **Ke** and 5(6)-carboxyfluorescein (CF) were purchased from Merck and used without further purifications. POPC stock solutions in chloroform (spectroscopic grade) were kept at -20 °C under nitrogen and their concentration was determined by phosphate quantification [24]. The compounds were pre-dissolved in DMSO and in all experiments the final DMSO concentration was kept constant at 2%.

The syntheses of **KeP**/**KeOP** [19], and **4MP**/**4MOP** [23] are described in our recent papers.

2.2. Molecular electrostatic potential mapping

To ensure consistency with the previous results [21], the DFT calculations were performed using the Gaussian 2016-C.01 [25] on the ωB97XD/6-311++G(d,p) [26] theory level for the molecular geometries optimized in water (Polarizable Continuum Model - PCM) using the integral equation formalism variant (IEFPCM) [27]. The molecular electrostatic potential (MEP) [28] was calculated using CHelpG scheme [29]. Graphics were prepared using GaussView 6 [30].

2.3. Liposome preparation

LUVs with a mean diameter of 100 nm, containing POPC at 10 mM were prepared by the extrusion method in HEPES buffer (10 mM; pH 7.4), as previously described [20]. These LUVs were then diluted in the same buffer to a final concentration that ranged from 0.025 mM to 2 mM.

2.4. Absorption and Fluorescence Spectroscopy and static light scattering

Absorption spectra were acquired with a Jasco V-560 spectrophotometer (Easton, MD, USA) at room temperature using quartz cuvettes with a 1 cm optical path.

A Fluorolog 3.22 spectrofluorimeter from Horiba Jobin Yvon (Villeneuve D'ascq, France) was used for fluorescence and static light scattering measurements both performed at 23.0 ± 1.0 °C in a sample compartment with magnetic stirring and temperature control, using quartz cuvettes QS from Hellma with optical path of 1 cm in excitation and 0.4 cm in emission.

For the excitation spectra the emission was fixed at 370 nm, and the excitation wavelength was scanned from 260 to 350 nm, while for the emission spectra excitation was fixed at 295 nm, and the emission wavelength was scanned from 310 to 575 nm, with wavelength increments of 1 nm. For spectra acquisition the bandwidths were typically 4 nm in both excitation and emission, and integration time 0.2 s.

For steady-state fluorescence anisotropy measurements, the excitation and emission wavelengths were set to 295 nm and 370 nm, respectively for all compounds. To determine the value of steady-state fluorescence anisotropy, $\langle r \rangle$, the following equation was used:

$$\langle r \rangle = \frac{(I_{VV} - G \times I_{VH})}{(I_{VV} + 2G \times I_{VH})} \quad (1)$$

in which the subscripts indicate the orientation of the excitation and emission polarizers, where V and H correspond to vertical and horizontal orientations and G is a correction factor calculated from the ratio I_{HV} / I_{HH}. An adequate blank was subtracted from each intensity reading. For fluorescence anisotropy measurements the bandwidths were 8 nm.

Time-resolved fluorescence measurements were carried out by the single photon timing technique, using a nanoLED N-280 (λ_{ex} = 279 nm) from Horiba Jobin Yvon (Villeneuve D'ascq, France), using 375 nm as the emission wavelength. The bandwidth was 14.7 nm. The resolution of the detector (TBX from Horiba) was 50 ps. Photon counts were accumulated until reaching 20,000 counts in the peak channel with a time scale of 0.02669 ps/channels, and the number of channels used for analysis was approximately 1000. To obtain the instrument response function diluted Ludox® was used as the scattering agent. The experimental fluorescence intensity decays were analyzed using the software TRFA® version 1.4 (Minsk, Belarus). The fluorescence intensity decays were described by a two exponential model according to equation 2:

$$I(t) = \sum_{i=1}^{n} p_i \exp(-\frac{t}{\tau_i}) \quad (2)$$

A third component was fixed to 10 ps to account for light scattering, and it was not used for the determination of the average fluorescence lifetimes.

After normalizing the pre-exponential factors (p_i), to obtain the normalized pre-exponentials or amplitudes α_i, equation 3 was used to determine the mean fluorescence lifetime (intensity weighted):

$$\langle\tau\rangle = \frac{\sum \alpha_i \tau_i^2}{\sum \alpha_i \tau_i} \tag{3}$$

and equation 4 was used to calculate the amplitude-weighted mean fluorescence lifetime:

$$\bar{\tau} = \sum_{i=1}^{n} \alpha_i \tau_i \tag{4}$$

A reduced χ^2 close to 1 and random distributions of the weighted residuals and of the residuals autocorrelation were the conditions to consider a successful fitting.

2.4.1. Aggregation studies

Absorption, fluorescence, and light scattering measurements were performed for different concentrations of **4MP** and **4MOP** dissolved in 10 mM HEPES (pH 7.4, filtered through paper with 5 μm pores) with 2% DMSO, incubated for 2 h protected from light at room temperature. Static light scattering (Rayleigh) was determined in a spectrofluorimeter as previously described in [20] with both excitation and emission wavelengths set to 550 nm in right angle geometry.

2.4.2. Partition studies

4MP or **4MOP** were added to the LUVs suspensions to a final concentration of 10 μM and incubated for 1 h 30 min at 23.0 ± 1.0 °C.

The membrane/water mole-fraction partition coefficient ($K_{p,x}$) was determined using equation 5 [20,31,32]:

$$\Delta I = \frac{\Delta I_{max}\ K_{p,x}\ [L]}{[W] + K_{p,x}\ [L]} \tag{5}$$

where $\Delta I = I - I_W$ is the difference between the steady state fluorescence intensity at 370 nm of the compound measured in the presence (I) and in the absence (I_W) of LUVs; $\Delta I_{max} = I_L - I_w$ and is the maximum value for this difference, with I_L the limiting value of I corresponding to complete membrane partition of the compound; [L] is the total lipid concentration in the

suspension; $K_{p,x}$ is the mole-fraction partition coefficient of the antifungal between the lipid and aqueous phases; and [W] is the molar concentration of water at the assay temperature (55.5 M).

The standard Gibbs energy ($\Delta G°$) associated with the transfer of a mole of compound from the aqueous phase to the lipid phase was determined using the following equation:

$$\Delta G^{\circ} = -RT \ln K_{p,x} \quad (6)$$

where $K_{p,x}$ has the same meaning as in equation 5; R is the molar gas constant, 8.314 $J \cdot K^{-1} \cdot mol^{-1}$, and T is the absolute temperature, 296.15 K.

The molar fraction of each compound in the lipid phase (χ_L) at a specific concentration of lipid was determined using the following equation:

$$\chi_L = \frac{K_{p,x}[L]}{[W] + K_{p,x}[L]} \quad (7)$$

2.4.3. Fluorescence quenching by acrylamide.

Ke, **KeOP**, **KeP**, **4MP** or **4MOP** were added to the LUVs preparations ([POPC] = 1mM) or to an aqueous solution (10 mM HEPES, pH 7.4) to a final concentration of 10 µM and equilibrated for 1h at 23.0 ± 1.0 °C. Then, acrylamide was added to each individual preparation to a final concentration that ranged from 0 to 0.15 M. The steady-state fluorescence intensity and decays of each sample were measured after 30 min of incubation at 23.0 ± 1.0 °C.

The amplitude-weighted mean fluorescence lifetime of each compound with increasing concentration of acrylamide was plotted in a Stern-Volmer fashion according to the following equation:

$$\frac{\bar{\tau}_0}{\bar{\tau}} = 1 + K_{SV}[Q] \quad (8)$$

where [Q] is the concentration of the quencher acrylamide, $\bar{\tau}$ and $\bar{\tau}_0$ are the amplitude-weighted mean fluorescence lifetimes of the sample in the presence and absence of quencher, respectively, and K_{SV} is the Stern-Volmer constant [33].

The (apparent) bimolecular quenching rate constant, $k_q^{(app)}$, was determined using equation 9:

$$K_{SV} \approx k_q^{(app)} \langle \tau \rangle_0 \quad (9)$$

where $\langle\tau\rangle_0$ is the intensity-weighted average lifetime in the absence of quencher. In the situation of LUV absence, k_q is obtained. However, in the presence of LUVs, the value obtained, k_q^{app} is an apparent k_q, since there are two fluorophore populations with different accessibility to the quencher (corresponding to the compound molecules that remain in aqueous solution and those that are interacting with the lipid phase). As explained in supplementary information its use is justified in the present study.

2.4.4. Permeability assay with 5(6)-carboxyfluorescein

LUVs suspensions with 2 mM of POPC were prepared in 10 mM HEPES buffer containing 40 mM CF. To remove the non-encapsulated CF, the pellet that resulted from LUV centrifugation at 150 000 rcf for 2h (Ultracentrifuge Hitachi CP80NX with P70AT rotor (Tokyo, Japan)), was re-suspended in HEPES buffer (50 mM, pH 7.4), and filtered through a Sephadex G-25 filtration column (Disposable PD Desalting Columns, Merck). The LUVs were then diluted in a 96-well plate to different lipid concentrations ranging from 0.1 to 0.25 mM. CF fluorescence intensity was measured every 2 min, during 14–16 h after the addition of 5 or 10 µM of **4MP** and **4MOP**. Finally, for total LUVs lysis 1 % (v/v) of Triton X-100 was added to each well, and fluorescence intensity was measured to determine the fluorescence intensity corresponding to complete CF release (F_{100}). A temperature-controlled microplate reader SpectraMAX GeminiEM spectrofluorimeter from Molecular Devices (San José, CA, USA) was used to measure the fluorescence intensity of CF, at 25 °C. The excitation and emission wavelengths were set to 492 nm and 530 nm, respectively, and a cut-off filter at 515 nm was used.

The percentage of CF leakage was determined using the following equation:

$$\%\text{CF Leakage} = \frac{F_t - F_0}{F_{100} - F_0} \tag{10}$$

where F_0 is the initial fluorescence intensity measured without the addition of compound, and F_t is the fluorescence intensity value at each time point [20].

Equation 11 [20] was fitted to the experimental data:

$$L = \sum_{i=1}^{n} L_i \left(1 - \exp\left(-\frac{t}{\tau_{Li}}\right)\right) \tag{11}$$

where L_i represents the maximum leakage associated with each kinetic constant, t is the time after the addition of the compounds, and τ_{Li} represents the time constants. The average leakage time constant, $\langle\tau_L\rangle$ can be calculated using the following equations:

$$\langle\tau_L\rangle = \sum \alpha_i^L \tau_{Li} \tag{12}$$

where α_i^L is defined as following:

$$\alpha_i^L = \frac{L_i}{L_{max}} \tag{13}$$

and L_{max} is the sum of all L_i.

2.5. Statistical analysis

All the data, except the fluorescence spectra and decays, are presented as mean ± standard deviation (S.D.) of at least three independent replicates. Representative fluorescence intensity spectra and decays (Figure S4.1 and S4.2) shown are the median result from at least three independent replicates. For the permeability assay, one way ANOVA with Tukey's post-hoc test was used to determine statistical differences. Mean values were considered significantly different for *p*-values below or equal to 0.05.

3. Results and Discussion

3.1. Study of the model compounds 4MP and 4MOP

The main goal of the study of the interaction between **4MP** and **4MOP** and the lipid bilayer was to evaluate the influence of the -$CH_2P(O)Ph_2$ moiety in **KeP** and **KeOP**, *i.e.* the modification of **Ke**, on their interaction with the membrane. Similarly to **Ke** and its derivatives [20], spectroscopic studies of these two compounds, sharing the same fluorophore, were carried out first, in aqueous solution for a range of compound concentrations, and then in the presence of LUVs with increasing POPC concentrations.

3.1.1. Aggregation behavior in aqueous solution

To understand the interaction of these compounds with lipid bilayers, it is relevant to first characterize the compounds in aqueous solution, mainly their aggregation behavior due to their low solubility in water environments [21]. Hence, to achieve this, spectroscopic measurements were conducted with different concentrations of the compounds in buffer solution (HEPES 10 mM, pH 7.4): absorption and static light scattering.

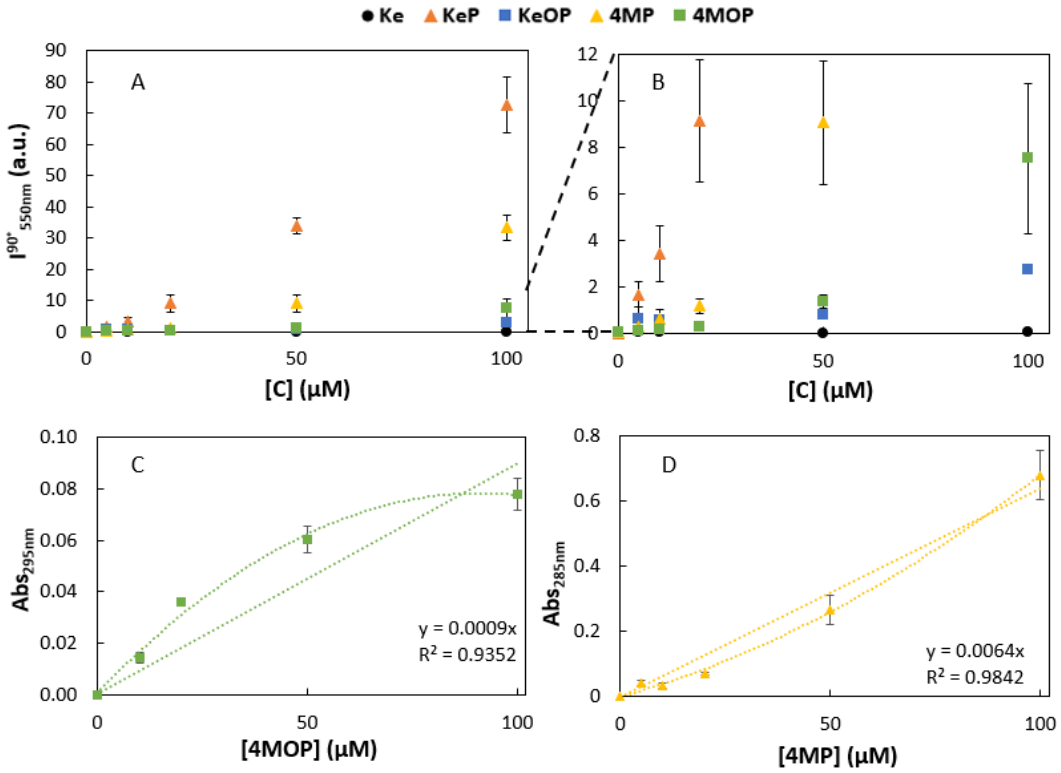

Figure 4. 2: 4MP has a stronger tendency to form aggregates in aqueous solution than 4MOP. A and B) Static light scattering intensity at 550 nm and 90° for **Ke** (black circles), **KeOP** (blue squares), **KeP** (orange triangles) [20], **4MOP** (green squares) and **4MP** (yellow triangles) at concentrations ranging from 5 to 100 μM in 10mM HEPES buffer (pH 7.4) with 2% DMSO. B is a Y-axis zoom-in of panel A as indicated by the dashed lines between the panels. C and D) Absorbance at the maximum absorption wavelength of each compound versus concentration of **4MOP** (C) and **4MP** (D) in 10mM HEPES buffer (pH 7.4) with 2% DMSO. [C] is the compound concentration. The values are the mean ± S.D. of at least three independent experiments.

The results presented in Figure 4.2, show that both **4MP** and **4MOP** can aggregate in aqueous solution, particularly 1) the considerable higher light scattering intensity than that observed for the other compounds, except **KeP** (Figure 4.2 – A and B) and 2) the non-linear dependence of the absorbance of **4MP** and **4MOP** at the maximum wavelength of the respective absorption spectrum on the concentration of the compound (Figure 4.2 – C and D).

It is not possible to precisely determine the concentration at which **4MP** or **4MOP** start to aggregate, however the absorption values at a fixed wavelength of **4MP** deviate from linearity at lower values of concentration than **4MOP** (Figure 4.2 – C and D). Since, **Ke** does not aggregate in aqueous solution, as shown here and in previous studies [20,34], but all other four

compounds aggregate, the diphenylphosphinemethyl moiety is the main cause for the aggregation reported. Nevertheless, **4MOP** has a much weaker tendency to aggregate than **4MP**. It can be clearly observed that the light scattering intensity raises above the value for **Ke** at lower concentrations and by much larger magnitude for **4MP** than **4MOP**. Analogously, it was previously shown that **KeP** starts to aggregate at lower concentrations than **KeOP**, 2 µM and 6 µM respectively ([20] and Figure 4.2 – A and B). Light scattering intensity reaches the highest values for **KeP** and then for **4MP**. Such tendency evidences the important contribution of P=O oxygen atom to reduce compound aggregation. This is probably due to the higher dipole moment [22] and to the stronger ability to participate in H-bonding with water molecules [21]. The differences found in the electron density isosurface of **4MP** *vs* **4MOP**, further corroborate this (Figure 4.3). Particularly, the P=O group has a negative electrostatic potential that is absent in **4MP** that aligns with the different polarity of these two molecules and the ability of the oxygen atom in the oxide derivatives to be an efficient H-bonding acceptor.

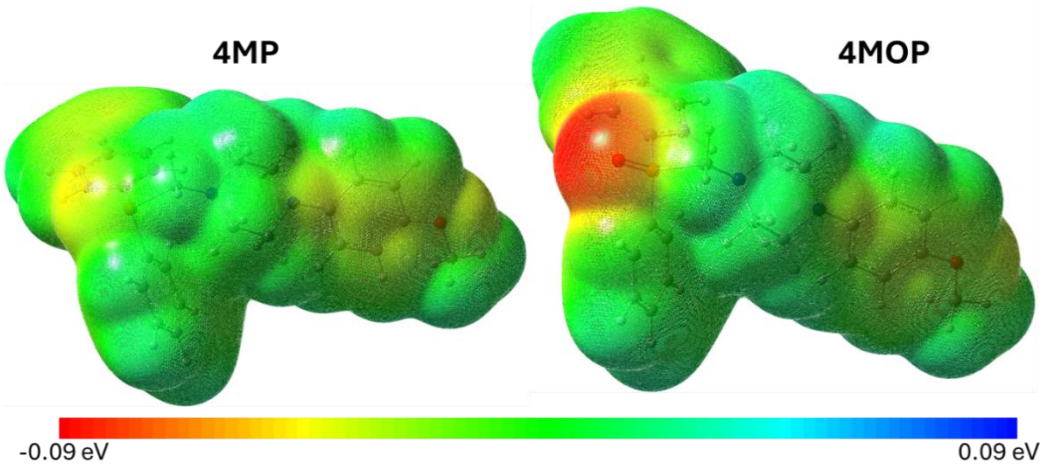

Figure 4. 3: The total electron density isosurface (0.0004 eÅ^{-3}) with mapped molecular electrostatic potential (MEP; from -0.09 (red) to 0.09 eV (blue) for 4MP **and** 4MOP**.**

3.1.2. Quantifying the membrane/water partition of 4MP and 4MOP

The interaction of **4MP** and **4MOP** with POPC bilayers was first studied by analyzing the emission and excitation spectra of these two compounds in buffer only and in LUVs suspensions with different lipid concentrations. The results are summarized in Figure 4.4. As previously performed for **Ke**, **KeP** and **KeOP** [20], the study was made mainly with a compound concentration of 10 µM to obtain a good fluorescence signal-to-noise ratio, minimizing aggregation and being close to the infinite dilution regime.

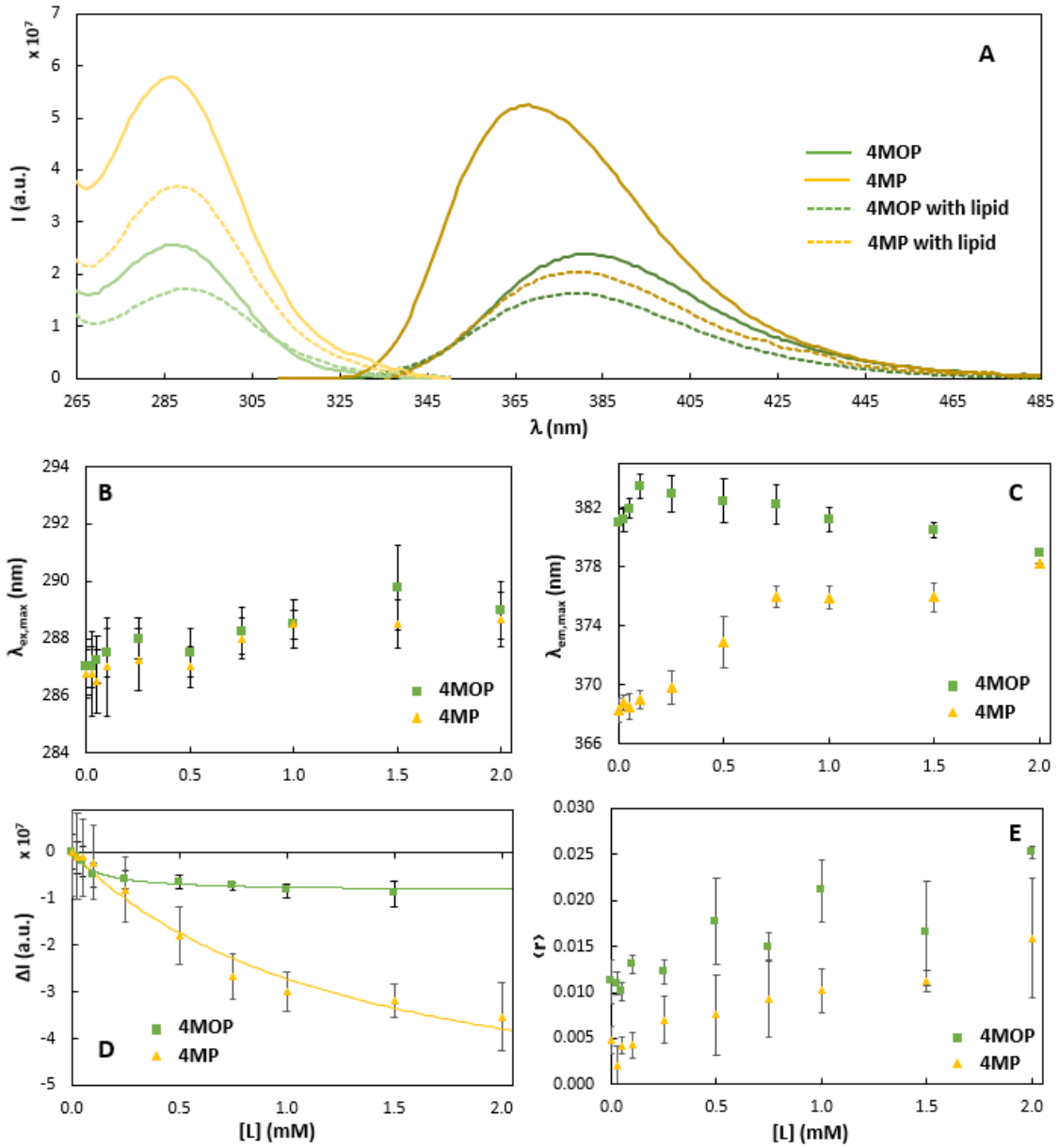

Figure 4. 4: The interaction of 4MOP and 4MP with POPC lipid bilayers can be monitored through their intrinsic fluorescence. (A) Fluorescence excitation (light yellow and green) and emission (dark yellow and green) spectra of **4MOP** (green) and **4MP** (yellow) in buffer (solid line) or in the presence of LUVs prepared with 2 mM of POPC (dashed line). Peak wavelength of excitation ($\lambda_{exc,max}$; B) and emission ($\lambda_{em,max}$; C) spectra, fluorescence intensity (D) and steady-state fluorescence anisotropy, ‹r› (E) of **4MOP** (green squares) and **4MP** (yellow triangles) for increasing lipid concentrations. The solid lines in D represent the fitting of equation 5 to the experimental data. Data in D and E were obtained with excitation at 295 nm and emission collected at 370 nm. The concentration of **4MP** and **4MOP** was 10 µM. The results in B - E are the mean ± S.D. of at least three independent replicates.

The fluorescence intensity of **4MP** and **4MOP** at 370 nm in aqueous solution under the same experimental conditions was 5.16×10^7 (a.u.) and 2.65×10^7 (a.u.) respectively (Figure 4.4 – A), which points at **4MP** having a higher fluorescence quantum yield. Analogous relation was found between **KeP** and **KeOP** quantum yield [20].

In contrast to **Ke**, **KeOP** and **KeP** [20], the presence of lipid led to a decrease in the fluorescence intensity of both **4MP** and **4MOP** (Figure 4.4 – D). Nevertheless, for both

compounds, the presence of lipid led to an increase in anisotropy (Figure 4.4 – E) as observed for the other compounds. Altogether, these alterations of fluorescence properties show that both **4MP** and **4MOP** interact with POPC lipid bilayers.

The presence of lipid induced a rather small red shift of excitation bands of **4MP** and **4MOP** with their maximum wavelengths changing from ca. 286 to 288 nm (Figure 4.4 – B). This shift was particularly small when compared with the one obtained for **KeP** and **KeOP** (12 and 9 nm respectively). The changes in the maxima of the emission bands for **4MP** and **4MOP** differed significantly (Figure 4.4 – C). While the emission spectra of **4MP** underwent a red shift in the presence of lipid with the peak wavelength changing from 368 to 381 nm; the emission spectra of **4MOP** underwent a small red shift of 3 nm with 0.1 mM of POPC, and then for higher concentrations of lipid there was a blueshift and the spectra reached approximately the same wavelengths as without lipid. For both compounds the highest concentration of lipid led to a maximum emission wavelength of ca. 381 nm, suggesting that the fluorophore solvation in the membrane is similar for both compounds. The maximum emission wavelengths obtained for **4MP** and **4MOP** with the highest concentration of lipid is considerably longer than the one found for **Ke**, **KeP** and **KeOP** (between 368 and 371 nm, Table 4.1). This suggests that the microenvironment polarity surrounding the fluorophore in **4MP** and **4MOP** is different than that of the other compounds [21].

The behavior similar in excitation but different in emission of **4MP** and **4MOP** in the presence of POPC can be justified by the differential electronic mechanisms that govern excitation and emission spectra of these compounds [21]. While the excitation is based on a n,$\pi \rightarrow \pi^*$ transition, the emission is $\pi^* \rightarrow \pi$. The observed shifts of the excitation spectra are mainly due to the hydrogen bonds formed by the piperazine nitrogen atom forming a bond to the aromatic ring in the ground state with water molecules at the hydration layer. However, in the excited state this nitrogen adopts a sp^2 hybridization and is no longer able to form hydrogen bonds, leading to a different emission transition. Hence, the different aggregation tendencies of these two compounds justify the different emission shifts observed. **4MP** molecules are predominantly found in aggregates, in which they are to a large extent shielded from the aqueous environment, while in the presence of lipid these aggregates are dissolved, leading to a shift of the emission spectra that is the result of a different polar microenvironment surrounding the compound in aqueous solution and with lipid. Since **4MOP** has a weaker tendency to aggregate, there is a similar environment surrounding the compound while aggregating in aqueous solution and in the membrane at low lipid concentration. Hence, the small hypsochromic shift in the emission of **4MOP** that occurs for lipid concentrations below

0.2 mM, is due to the equilibrium of the aggregate dissolving into monomeric state that is interacting with the membrane. Moreover, for POPC concentrations higher than ca. 0.2 mM a small blue-shift is observed, which corresponds to a situation of only monomers interacting with the membrane. This blue-shift confirms the partition of **4MOP** in aqueous solution towards a less polar environment – the lipid bilayer.

The observed decrease in fluorescence intensity in the presence of the liposomes was somewhat surprising, taking into consideration that for **Ke** and its derivatives an increase was observed with the addition of lipid [20]. This decrease indicates that the quantum yield of **4MP** and **4MOP** is smaller while interacting with the membrane. Particularly, **4MP** seems not to emit when in the membrane since for the limit of infinite lipid concentration its fluorescence intensity is approximately zero (Table 4.1). Interestingly, the decrease observed for **4MP** and **4MOP** follows a typical hyperbolic behavior, despite the negative variation of fluorescence intensity. Therefore, it was possible to fit equation 5 to the variation of fluorescence intensity of **4MP** and **4MOP** with POPC concentration (Figure 4.4 - D) and determine $K_{p,x}$ and ΔI_{max}. The $K_{p,x}$ thereby obtained was (4.29 ± 0.17) x 10^4 and (5.21 ± 0.82) x 10^5 for **4MP** and **4MOP**, respectively. It should be underlined, that the method used to determine the mole-fraction partition coefficient does not consider the aggregation of the compounds, and the values that are obtained correspond to an approximation to the real value.

According to the log $P_{(o/w)}$ values estimated using SwissADME [35], **4MP** (4.22 ± 0.41) is more lipophilic than **4MOP** (3.35 ± 0.23). The partition coefficients for **4MP** and **4MOP** are one order of magnitude smaller than the respective **Ke** derivative counterpart (Table 4.1). Nevertheless, as previously reported for **KeP** and **KeOP** [20], the membrane/water partition coefficient is smaller for **4MP** than for **4MOP**, which is more polar. Not only the membrane/water $K_{p,x}$ of **4MOP** is larger than that of **4MP**, but also the standard Gibbs energy of transfer from water to the membrane differs by a similar amount as it does between **KeOP** and **KeP** (Table 4.1). This result further supports the stabilizing effect of the oxygen atom for the interaction with the membrane, with the probable involvement of H-bonding. The participation and relevance of P=O present in **KeOP** and **4MOP** to participate in hydrogen bond network involving and possibly distorting the membrane hydration layer, is further corroborated by the comparative analysis of the strengths of hydrogen bonds formed by **4MP** or **4MOP** with water and methanol molecules [21].

Time-resolved fluorescence intensity measurements were also performed for **4MP** and **4MOP** in the presence of LUVs with different POPC concentrations with the aim of further understanding the interaction of these two molecules with the lipid bilayer. The mean

fluorescence lifetime (intensity weighted) of **4MOP** in HEPES buffer, 1.49 ns was shorter than for **4MP**, 2.37 ns, in line with the observations for the steady-state fluorescence intensity. While the intensity-weighted mean fluorescence lifetime of **4MP** decreased from 2.37 to 1.68 ns, the intensity-weighted mean fluorescence lifetime of **4MOP** was not significantly affected by the presence of 1 mM of lipid: 1.49 and 1.63 ns in the absence and presence of lipid respectively (Table 4.2), in agreement with a much smaller decrease in steady-state fluorescence intensity for this compound (Figure 4.4 -D).

Table 4. 1: Parameters for the partition of 4MP and 4MOP between POPC bilayer and water at 23 °C. The same parameters are presented for **Ke**, **KeOP** and **KeP** [20]. ([C] = 10 μM; $\lambda_{ex,max,i}$ and $\lambda_{em,max,i}$ are the peak wavelengths of the excitation and emission spectra, respectively, in water (i = aq) or with the highest lipid concentration (i = lip)). $\Delta G°$ was determined using equation 6.

Compound	4MOP	4MP	KeOP	KeP	Ke
$K_{p,x}$	(5.21 ± 0.82) x10^5	(4.29 ± 0.17) x10^4	(4.66 ± 0.72) x10^6	[(8.31 ± 1.60) x10^5][a]	(3.31 ± 0.36) x10^5
ΔI_{max} (a.u.)	-(8.35 ± 1.16) x10^6	-(6.24 ± 1.25) x10^7	(3.20 ± 0.26) x10^6	-	(1.26 ± 0.26) x10^7
$\Delta G°$ (kJ/mol)	-32.41 ± 0.38	-26.26 ± 0.10	-37.81 ± 0.37	-33.56 ± 0.48	-31.30 ± 0.27
I_L/I_W	0.68 ± 0.01	~0	1.51 ± 0.04	1.27	1.37 ± 0.02
r_W	0.011 ± 0.002	0.005 ± 0.002	0.051 ± 0.010	0.079 ± 0.013	0.020 ± 0.001
$\lambda_{ex,max,aq}$ (nm)	286	286	287	284	285
$\lambda_{ex,max,lip}$ (nm)	288	288	296	296	293
$\lambda_{em,max,aq}$ (nm)	381	368	382	368	379
$\lambda_{em,max,lip}$ (nm)	379	381	369	368	371

[a] A different partition model was used for **KeP**, that accounted for the aggregation of the compound in water [20].

The maximum emission wavelength of **4MP** in water is similar to the one obtained for **KeP** under the same conditions. Also, the aggregation study of **4MP** (Figure 4.2) hints at a possible tendency of this compound to aggregate. So, **4MP** could be forming smaller aggregates than **KeP** with a different molecular organization, in which the chromophores are not interacting in the same way as in **KeP**, and therefore do not have the second non-typical band that was observed not only for **KeP** but also for **KeOP** [20], but that could be the cause for **4MP** having the longest lifetime compared to any of the diphenylphosphine moiety-containing compounds (Table 4.2). When **4MP** interacts with the membrane it probably does so at a very shallow location, thus still sensing a rather hydrated environment but is no longer aggregating. Hence, the maximum emission wavelength reaches a value similar to the one obtained in aqueous solution for the compounds that do not aggregate.

3.2. In-depth membrane location of Ke and its derivatives and of the model compounds 4MP and 4MOP

To explore the relative depth of **Ke** and its derivatives in the membrane, and to further characterize the compounds in aqueous solution, a quenching assay with acrylamide was performed both in the presence and in the absence of LUVs with POPC at a concentration of 1 mM.

Aqueous fluorescence quenchers, such as acrylamide and iodide, are often used to explore the accessibility to the aqueous medium of fluorophores interacting with membranes [36,37]. Since acrylamide is hydrophilic, its efficiency as a fluorescence quencher depends on two factors: 1) the fraction of compound effectively in the membrane, and 2) how deeply buried in the membrane the compound is: the more superficial the fluorophore membrane location, the more efficient is the quenching by acrylamide.

According to the $K_{p,x}$ obtained for each compound, at 1 mM of POPC a high fraction of four of the compounds is in the membrane (χ_L > 85%; Table 4.2 - χ_L). The compound **4MP** is the exception, and it would be necessary an amount of lipid higher than 3 mM to achieve a relatively high fraction of the compound in the membrane. Hence, for all compounds, except **4MP**, the quenching in the presence of lipid can be interpreted in terms of the depth of membrane insertion.

Table 4. 2: Summary of the results of the time-resolved fluorescence quenching study of Ke, KeOP, KeP, 4MOP and 4MP at 23 °C by acrylamide, in the presence (Lip.) and absence of POPC (Aq.). [C] = 10 μM. Stern-Volmer constant, K_{SV}, values were obtained from the linear regression performed on the Stern-Volmer plots represented in Figure 4.6. $k_q^{(app)}$ is the (apparent) bimolecular quenching rate constant. See text for further details. χ_L was determined using equation 7.

Compound	χ_L (%)	System	K_{SV} (M^{-1})	$\langle\tau\rangle_0$ (ns)	$k_q^{(app)}$ x 10^9 ($M^{-1}.s^{-1}$)
Ke	86	Aq.	10.4 ± 0.2	2.45 ± 0.02	4.2 ± 0.1
		Lip.	2.0 ± 0.2	2.36 ± 0.01	0.8 ± 0.1
KeOP	99	Aq.	4.6 ± 0.5	1.40 ± 0.17	3.3 ± 0.5
		Lip.	0.6 ± 0.2	1.69 ± 0.48	0.4 ± 0.2
KeP	94	Aq.	3.5 ± 0.1	1.52 ± 0.12	2.3 ± 0.2
		Lip.	≈ 0	1.53 ± 0.03	≈ 0
4MP	44	Aq.	14.3 ± 0.4	2.37 ± 0.05	6.0 ± 0.2
		Lip.	5.6 ± 0.3	1.68 ± 0.24	3.3 ± 0.5
4MOP	90	Aq.	9.4 ± 0.3	1.49 ± 0.03	6.3 ± 0.2
		Lip.	3.7 ± 0.2	1.63 ± 0.17	2.3 ± 0.2

3.2.1. Fluorescence quenching by acrylamide: steady-state study

The Stern-Volmer plots for the quenching of the compounds fluorescence by acrylamide obtained from the measurement of the steady-state fluorescence intensity are shown in Figure 4.5, highlighting the decrease of fluorescence intensity upon increasing quencher concentration. The Stern-Volmer plots of **Ke**, **KeOP** and **4MOP** have much steeper curvatures in aqueous solution than in the presence of lipid (Figure 4.5 – A, B and E). This indicates that the accessibility of these compounds to acrylamide is lower in the presence of lipid bilayers than in their absence, *i.e.*, the membrane is shielding the quenching by acrylamide. For **4MOP** the slope in the presence of lipid is still relatively higher than for **Ke** and **KeOP** (Figure 4.5 - E). These results corroborate the previous interpretation of the spectral shifts, which was that **Ke** and **KeOP** are inserted at a more buried region of the membrane than **4MOP**.

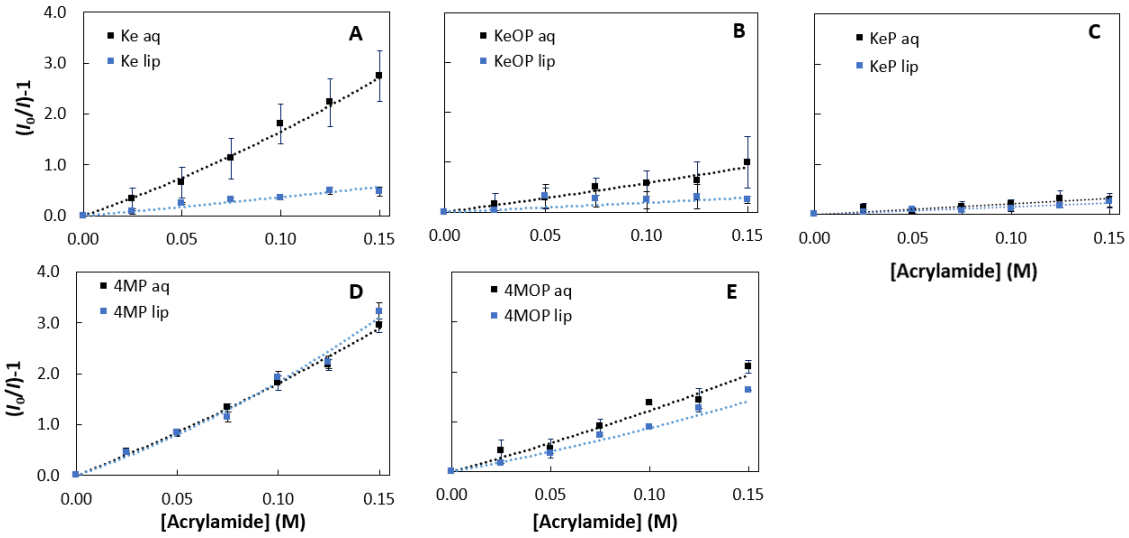

Figure 4. 5: Quenching by acrylamide of the steady-state fluorescence intensity of the compounds. Variation of I_0/I at 375 nm of **Ke** (A), **KeP** (B), **KeOP** (C), **4MP** (D) and **4MOP** (E) in the presence (blue) and absence (black) of LUVs with 1 mM of POPC, for increasing acrylamide concentration. I_0 and I are the fluorescence intensity with and without acrylamide respectively. The dashed lines represent a quadratic fit to the data, except for C, in which a linear regression was used. [C] = 10 µM. The results with error bars are the mean ± S.D. of at least three independent replicates.

For **KeP** and **4MP,** the Stern-Volmer plots in aqueous solutions are essentially overlapped with those obtained in the presence of POPC (Figure 4.5 – C and D). To interpret the quenching data for these compounds, their aggregation in aqueous solution has to be considered. For **KeP**, in both cases the slope is very small. In fact, **KeP** is the compound forming aggregates more readily and larger. As it was shown previously at 10 µM, **KeP** is strongly aggregating in aqueous solution, but not in the presence of 1 mM of POPC [20]. So, in aqueous solution, aggregates of **KeP** might protect the fluorophore from the action of acrylamide in a similar way that the membrane shields **KeP** from the quencher when the compound is membrane-bound.

Therefore, **KeP** is most likely partitioning towards a deeper region of the membrane then **4MP** and **4MOP**. The low quenching efficiency is, in aqueous solution, due to the formation of large aggregates and in the presence of POPC bilayers, to deep membrane insertion.

In the case of **4MP**, the curvatures are approximately as accentuated as for **Ke** in aqueous solution. **4MP** has much lower fluorescence quantum yield when in POPC membranes, and in the presence of lipid, only 44 mol% of the compound is membrane bound. Therefore, in both cases the quenching of the fluorescence emission arising from compound in aqueous solution is being observed.

3.2.2. Fluorescence quenching by acrylamide: time-resolved study

To gain further insight and quantify the fluorescence quenching of the compounds' fluorescence by acrylamide, time-resolved measurements were also performed.

As can be observed in the Stern-Volmer plots obtained from time-resolved data (Figure 4.6), the amplitude-weighted mean fluorescence lifetime of all the compounds decreased in aqueous solution with increasing concentration of acrylamide, indicating a dynamic quenching process. In most cases, the extent of quenching was, however, smaller than the one observed in the steady-state study, showing that in this latter situation both static and dynamic quenching process are in effect. Therefore, a quantitative analysis was performed only for the time-resolved Stern-Volmer plots, to which only dynamic quenching contributes. For all compounds the presence of lipid led to a fluorescence lifetime variation with acrylamide which was less marked than in its absence (Figure 4.6). Hence, there was a decrease of dynamic quenching efficiency for all the compounds. Notably, in the presence of POPC the **KeP** mean fluorescence lifetime remained unchanged.

From the amplitude-weighted mean fluorescence lifetime Stern-Volmer plots with acrylamide in aqueous solution and in the presence of POPC bilayers it is possible to determine the (apparent) bimolecular quenching rate constant, $k_q^{(app)}$, for each compound using equation 9. These values are shown in Table 4.2.

The k_q^{app} obtained for **Ke** in the presence of lipid, 0.8×10^{-9} $M^{-1}.s^{-1}$, was 5.4 times lower than the one obtained in its absence, 4.2×10^{-9} $M^{-1}.s^{-1}$. This difference evidences the insertion of **Ke** in a deep region of the membrane where it is much less accessible to acrylamide, than in aqueous solution. In fact, considering that at the lipid concentration used approximately one sixth of the compound remains in aqueous solution, one could consider that this quenching rate constant has a significant contribution from **Ke** population that is not inserted in the membrane and that membrane-inserted **Ke** would have an even smaller value of k_q. In this case, the value

of k_q retrieved is rather an apparent k_q^{app}, as a simple Stern-Volmer relation is not strictly obeyed (please check supplementary information).

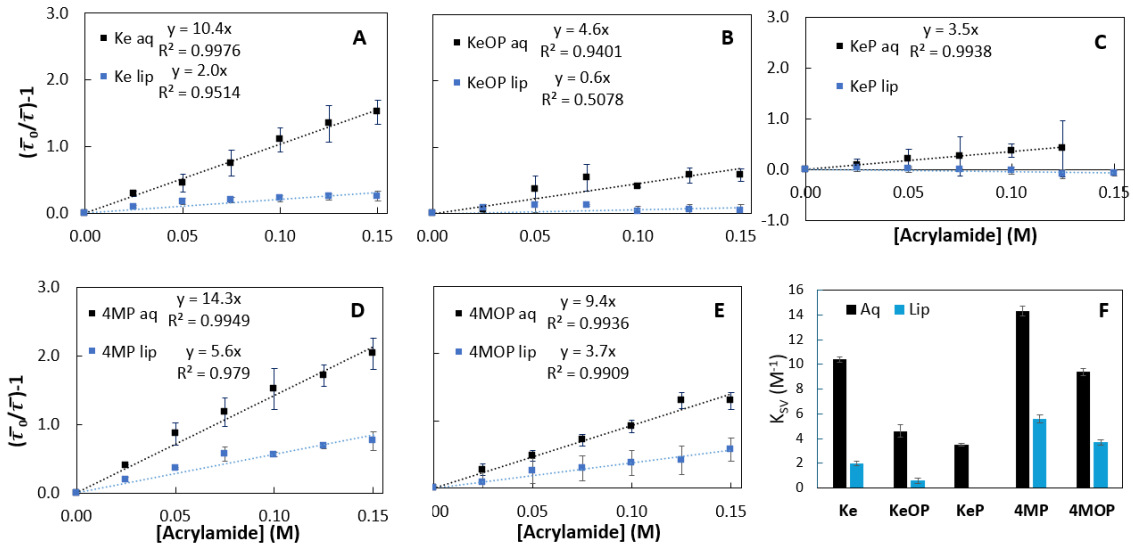

Figure 4. 6: Dynamic quenching by acrylamide. Variation of $\bar{\tau}_0/\bar{\tau}$ at 375 nm of **Ke** (A), **KeP** (B), **KeOP** (C), **4MP** (D) and **4MOP** (E) in the presence (blue) and absence (black) of LUVs with 1 mM of POPC, for increasing acrylamide concentration. $\bar{\tau}_0$ and $\bar{\tau}$ are the amplitude-weighted mean fluorescence lifetime in the absence and presence of acrylamide respectively. The Stern-Volmer constant K_{SV} for each compound in aqueous solution and in the presence of LUVs is also represented in F. The dashed lines represent the linear fit to the data. The equations and R-squared for these fits are represented. [C] = 10 μM. The results with error bars are the mean ± S.D. of at least three independent replicates.

The interaction of another azole antifungal agent, itraconazole, with POPC [38] and POPC/cholesterol bilayers [39] was studied using computational and experimental approaches. For POPC bilayers, it was shown that itraconazole distributes with its long axis along the membrane plane, between the glycerol moiety and the Δ^9 unsaturation of the *sn*-2 acyl chain of POPC [38]. **Ke** and itraconazole are structurally similar, with the exception that itraconazole is a triazole, while **Ke** is an imidazole. Also, itraconazole has one phenyl-triazole group linked to the piperazine ring. Taking in consideration the structural similarities between **Ke** and itraconazole, it is not surprising that both locate in the acyl chain region of the POPC bilayer.

Regarding **KeOP**, the k_q^{app} determined in the presence of lipid was 8.3-fold lower than in its absence (Table 4.2). This ratio for **KeOP** (8.3) is even larger than the one found for **Ke** (5.4). Considering that 99% of the compound is in the membrane and virtually the quenching is from membrane-inserted **KeOP**, the location of **KeOP** is also at a deep region in the membrane, hence with a low accessibility to acrylamide, similar to what was described for **Ke** herein.

The fluorescence lifetime Stern-Volmer plot for **KeP** in buffered solution has a slope similar to the steady-state intensity, while in the presence of lipid the fluorescence lifetime is virtually constant. Thus, in the presence of lipid, there is no dynamic quenching occurring and the bimolecular quenching rate constant is too low to be determined. This corroborates that **KeP** is

also inserting at a deep region in the membrane. The value of k_q in aqueous solution also decreases in the order **Ke**, **KeOP**, **KeP**. The difference between **Ke** and **KeOP** can be, at least in part, justified by the difference in size of the compounds due to the presence of a diphenylphosphoryl moiety that on one hand reduces the diffusion coefficient of **KeOP** when compared to **Ke**, and may reduce the fraction of collisions between compound and quencher that effectively lead to return of the fluorophore to the ground state. However, in the case of **KeP**, the larger decrease is probably due to the formation of aggregates in aqueous solution. In the aggregates, some of the fluorophores may be protected from the solvent and aqueous quencher, and also the diffusion coefficient of the aggregate will be much smaller than that of the monomer, both contributing to smaller quenching efficiency.

The $k_q^{(app)}$ values determined for **4MP** and **4MOP** were only 1.9 and 2.7 times lower in the presence of lipid than in its absence. Moreover, with lipid, the k_q^{app} values of **4MP** and **4MOP**, 3.8 x 10^{-9} and 2.8 x 10^{-9} $M^{-1}.s^{-1}$ respectively, were higher than the ones obtained for **Ke**, **KeP** and **KeOP**, which were closer to zero. This corroborates the previous interpretation regarding the relative location of **4MP** and **4MOP**, *i.e.*, that these compounds are in a more superficial region of the membrane than **Ke**, **KeP** and **KeOP**. The k_q values for these compounds in aqueous solution are larger than for the others, denoting their smaller size, and hence larger diffusion coefficient, and larger exposure of the fluorophore to the quencher. Coincidently, in the presence of POPC liposomes, the bimolecular quenching rate constant changes to values that are similar to the analogue larger compounds in aqueous solution.

3.3. Compounds impact on the permeability of POPC liposomes

Since **4MP** and **4MOP** have a more superficial interaction with a POPC bilayer and lower antifungal activity [23] than **KeP**, **KeOP** and **Ke** itself, and considering that membrane permeabilization may contribute to the mode of action of these compounds [20], it is expected that these smaller compounds have different membranotropic abilities, if at all. To confirm this hypothesis, a leakage assay was conducted.

The change in membrane permeability by the action of a compound can be monitored by measuring the release of CF encapsulated inside LUVs (*e.g.*, [20]). CF is a fluorescent molecule that at relatively high concentrations undergoes self-quenching. Hence, the increase in fluorescence of CF correlates with the release of the probe from the liposomes into the outer buffer solution.

The addition of 10 μM **4MP** or **4MOP** to 0.1mM of POPC membranes did not change the kinetics of leakage significantly when compared to the control (Figure 4.7 – A-C). In fact, for

4MP the increase in CF leakage virtually overlaps with the control, while for **4MOP** is only slightly higher (Figure 4.7 – A). Hence, at this compound and lipid concentration **4MP** and **4MOP** do not change significantly the membrane permeability. Moreover, the leakage observed 1h30 after the addition of compound (L_{1h30}) and the maximum leakage (L_{max}) obtained for **4MP** and **4MOP** are lower than the ones obtained previously for **Ke**, **KeP** and **KeOP** [20] (Figure 4.7 – B), while the average leakage time ($\langle\tau_L\rangle$) is higher for the smaller compounds. Nevertheless, **4MOP** causes a slightly higher (Figure 4.7 - B, L_{max}) and quicker (Figure 4.7 – C) change in permeability than **4MP**.

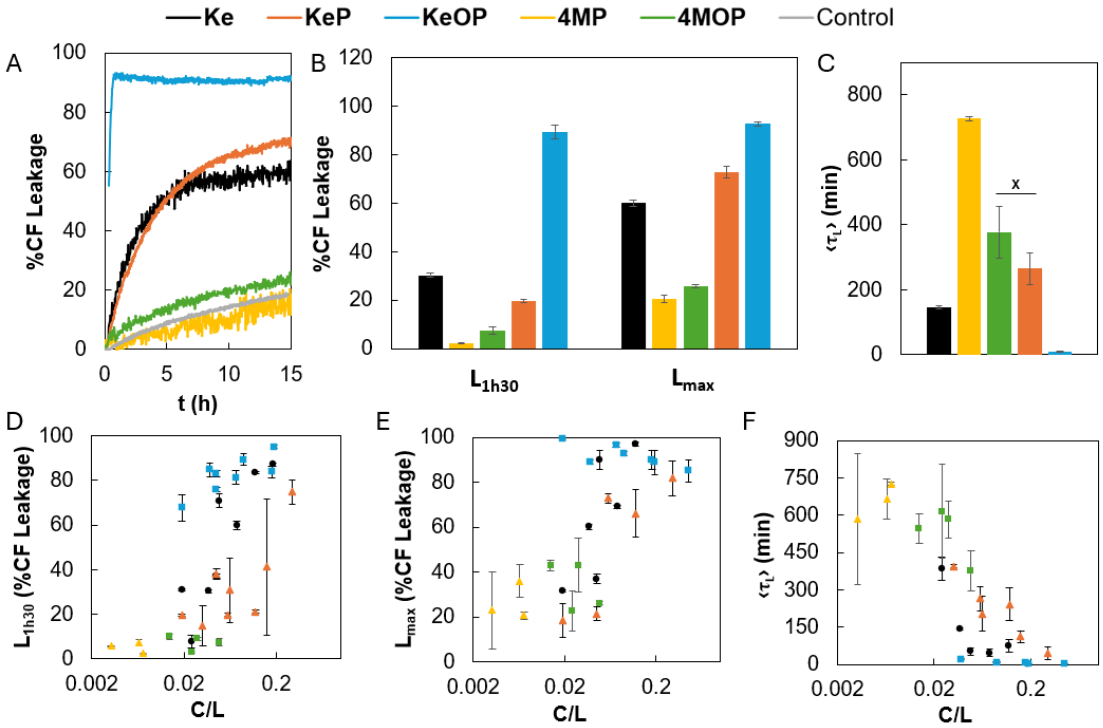

Figure 4. 7: Effect of Ke, 4MP, 4MOP, KeP and KeOP on POPC bilayer permeability. (A–C) The percentage of CF release from LUVs with 0.1 mM of POPC after the addition of 10 μM of each compound, was measured along 14–16 h. (B) Maximum percentage of CF release (L_{max}) and percentage of release 1h30 after the addition of the compound (L_{1h30}). (C) Average leakage time constant ($\langle\tau_L\rangle$) obtained for each compound. (D–F) L_{1h30} (D), L_{max} (E) and $\langle\tau_L\rangle$ (F) after the addition of **Ke**,**4MP, 4MOP**, **KeP** or **KeOP**, at different compound/lipid ratios (C/L). %CF Leakage was calculated using equation 10, while L_{max} and $\langle\tau_L\rangle$ were obtained from equations 11, 12 and 13. The results in B–F are the mean ± S.D. of at least three independent replicates. The results for **Ke**, **KeP** and **KeOP** were originally published in [20]. For B and C, one-way ANOVA reported that multiple comparisons inside each parameter L_{1h30}, L_{max} and $\langle\tau_L\rangle$ are statistically different (p-value ≤ 0.0.5), with the exception of $\langle\tau_L\rangle$ **4MOP** vs **KeP** (represented with a X).

At other ratios of effective membrane concentration of compound/lipid, the same conclusion can be drawn: **4MP** has always lower L_{1h30} and L_{max} and higher $\langle\tau_L\rangle$ than **4MOP**. Moreover, the L_{1h30} and L_{max} for **4MP** and **4MOP** are always lower than the values for **Ke**, **KeOP** and **Ke**, with the exception of **Ke** and **KeP** at ca. 0.02-0.045 effective compound/lipid ratio at which they have values similar to **4MOP**. Furthermore, **4MP** is the slowest compound to induce any change in permeability, followed by **4MOP**.

The little to no ability of **4MP** and **4MOP** to permeabilize POPC liposomes is in line with the superficial interaction and with the moderately low affinity of these compounds for the membrane. This result also correlates with the low antifungal activity of **4MP** and **4MOP** [23] in opposition to their **Ke** derivatives counterparts **KeP** and, particularly, **KeOP** which 1) can strongly interact with the membrane and permeabilize it significantly [20] and 2) have higher antifungal activity than **Ke** itself, particularly against a strain that lacks ergosterol [19].

4. Conclusion

Using fluorescence spectroscopic assays we were able to unravel the relative location of **Ke** and diphenylphosphinemethyl derivatives, **KeP** and **KeOP**. The model compounds **4MP** and **4MOP,** in which the diphenylphosphinomethyl motif is structurally dominant, are interacting with the membrane at a more superficial region, in opposition with the more buried position assumed for **Ke**, **KeOP** and **KeP.** Moreover, a permeability assay allowed to conclude that **4MP** and **4MOP** changed marginally the permeability of POPC membranes when compared to the other compounds, especially **KeOP**. Considering this and that the $K_{p,x}$ values for **KeOP** and **KeP** are higher than for **Ke**, it is possible to conclude that it is the concomitant presence of the **Ke** and the phosphine moieties that allows for a more efficient interaction, and a more buried location in the membrane of the phosphine moiety, with a cumulative effect of the oxygen atom in the phosphine group to facilitate membrane interaction and perturbation and consequent water penetration.

As shown in this work, **4MP** and **4MOP** did not change markedly the membrane permeability, but **4MOP** still induced a higher and quicker leakage than **4MP**. **KeOP** was also much more effective than **KeP** in membrane permeabilization. Moreover, for the later pair of compounds, the participation of the P=O in H-bonding with water of a compound that is penetrating deeper in the bilayer and the presence of such a highly polar bond in the acyl chain region of the lipid bialyer, would induce a stronger and more profound water penetration, and concomitant perturbation of the membrane, explaining the highest permeabilizing activity found for **KeOP** [20]. This permeabilizing ability described in our previous work, is evidence for a possible additional mode of action of this compound, that involves direct action on the plasma membrane of fungi and highlights the importance of the P=O bond. Moreover, despite the presence of this highly polar bond, **KeOP** has higher membrane affinity than **Ke** (and the other derivative).

This study thus supports our hypothesis that **Ke** and particularly its phosphine derivatives may exert their action, at least partially, through their interaction with membrane lipids; and/or

that the interaction with the membrane is relevant for their antifungal activity. Further unraveling of the mechanisms underlying these compound-membrane interactions will provide insights into their pharmaco-kinetics and -dynamics. Paving the way towards antifungal drug improvement.

5. Acknowledgments

This work was funded by *Fundação para a Ciência e Tecnologia* (FCT), I.P./MCTES through national funds under projects EXPL/BIA-BFS/1034/2021, UIDB/00100/2020, UIDP/00100/2020 and LA/P/0056/2020, and doctoral scholarship to A.B.-O. (SFRH/BD/145600/2019).

The DFT calculations have been carried out using resources provided by Wroclaw Centre for Networking and Supercomputing (http://wcss.pl), Grant No. 140.

6. References

[1] K. Kainz, M.A. Bauer, F. Madeo, D. Carmona-Gutierrez, Fungal infections in humans: the silent crisis, Microb. Cell. 7 (2020) 143. https://doi.org/10.15698/MIC2020.06.718.

[2] A. Fausto, M.L. Rodrigues, C. Coelho, The still underestimated problem of fungal diseases worldwide, Front. Microbiol. 10 (2019) 214. https://doi.org/10.3389/fmicb.2019.00214.

[3] D.Z.P. Friedman, I.S. Schwartz, Emerging Fungal Infections: New Patients, New Patterns, and New Pathogens, J. Fungi (Basel, Switzerland). 5 (2019). https://doi.org/10.3390/jof5030067.

[4] P. Muñoz, E. Bouza, M. Cuenca-Estrella, J.M. Eiros, M.J. Pérez, M. Sánchez-Somolinos, C. Rincón, J. Hortal, T. Peláez, Saccharomyces cerevisiae fungemia: An emerging infectious disease, Clin. Infect. Dis. 40 (2005) 1625–1634. https://doi.org/10.1086/429916.

[5] A.J. Riquelme, M.A. Calvo, A.M. Guzmán, M.S. Depix, P. García, C. Pérez, M. Arrese, J.A. Labarca, Saccharomyces cerevisiae fungemia after Saccharomyces boulardii treatment in immunocompromised patients, J. Clin. Gastroenterol. 36 (2003) 41–43. https://doi.org/10.1097/00004836-200301000-00013.

[6] M.C. Fisher, S.J. Gurr, C.A. Cuomo, D.S. Blehert, H. Jin, E.H. Stukenbrock, J.E. Stajich, R. Kahmann, C. Boone, D.W. Denning, N.A.R. Gow, B.S. Klein, J.W. Kronstad, D.C. Sheppard, J.W. Taylor, G.D. Wright, J. Heitman, A. Casadevall, L.E. Cowen, Threats Posed by the Fungal Kingdom to Humans, Wildlife, and Agriculture, MBio. 11 (2020). https://doi.org/10.1128/MBIO.00449-20.

[7] C.M. Hossain, L.K. Ryan, M. Gera, S. Choudhuri, N. Lyle, K.A. Ali, G. Diamond, Antifungals and Drug Resistance, 2 (2022) 1722–1737. https://doi.org/10.3390/ENCYCLOPEDIA2040118.

[8] M.C. Fisher, A. Alastruey-Izquierdo, J. Berman, T. Bicanic, E.M. Bignell, P. Bowyer, M. Bromley, R. Brüggemann, G. Garber, O.A. Cornely, S.J. Gurr, T.S. Harrison, E. Kuijper, J. Rhodes, D.C. Sheppard, A. Warris, P.L. White, J. Xu, B. Zwaan, P.E. Verweij, Tackling the emerging threat of antifungal resistance to human health, Nat. Rev. Microbiol. 2022 209. 20 (2022) 557–571. https://doi.org/10.1038/s41579-022-00720-1.

[9] S.R. Lockhart, K.A. Etienne, S. Vallabhaneni, J. Farooqi, A. Chowdhary, N.P. Govender, A.L. Colombo, B. Calvo, C.A. Cuomo, C.A. Desjardins, E.L. Berkow, M. Castanheira, R.E. Magobo, K. Jabeen, R.J. Asghar, J.F. Meis, B. Jackson, T. Chiller, A.P. Litvintseva, Simultaneous Emergence of Multidrug-Resistant Candida auris on 3 Continents Confirmed by Whole-Genome Sequencing and Epidemiological Analyses, Clin. Infect. Dis. An Off. Publ. Infect. Dis. Soc. Am. 64 (2017) 134. https://doi.org/10.1093/CID/CIW691.

[10] Antimicrobial Resistance in Candida - CDC, (n.d.). https://www.cdc.gov/fungal/diseases/candidiasis/antifungal-resistant.html (accessed May 1, 2023).

[11] S.K. Shishodia, S. Tiwari, J. Shankar, Resistance mechanism and proteins in Aspergillus species against antifungal agents, Mycology. 10 (2019) 151. https://doi.org/10.1080/21501203.2019.1574927.

[12] J.H. Van Tyle, Ketoconazole. Mechanism of action, spectrum of activity, pharmacokinetics, drug interactions, adverse reactions and therapeutic use, Pharmacotherapy. 4 (1984) 343–373. https://doi.org/10.1002/J.1875-9114.1984.TB03398.X.

[13] D. Borelli, J.L. Bran, J. Fuentes, R. Legendre, E. Leiderman, H.B. Levine, A. Restrepo, D.A. Stevens, Ketoconazole, an oral antifungal: laboratory and clinical assessment of imidazole drugs., Postgrad. Med. J. 55 (1979) 657–661. https://doi.org/10.1136/PGMJ.55.647.657.

[14] D.S. Loose, P.B. Kan, M.A. Hirst, R.A. Marcus, D. Feldman, Ketoconazole blocks adrenal steroidogenesis by inhibiting cytochrome P450-dependent enzymes., J. Clin. Invest. 71 (1983) 1495. https://doi.org/10.1172/JCI110903.

[15] O. Shimokawa, M. Niimi, K. Kikuchi, M. Saito, H. Kajiwara, S.I. Yoshida, Relationship between MIC and Minimum Sterol 14α-Demethylation-Inhibitory Concentration as a Factor in Evaluating Activities of Azoles against Various Fungal Species, J. Clin. Microbiol. 43 (2005) 5547. https://doi.org/10.1128/JCM.43.11.5547-5549.2005.

[16] N. Strushkevich, S.A. Usanov, H.W. Park, Structural basis of human CYP51 inhibition by antifungal azoles, J. Mol. Biol. 397 (2010) 1067–1078. https://doi.org/10.1016/J.JMB.2010.01.075.
[17] L.A. García Rodrĭguez, A. Duque, J. Castellsague, S. Pérez-Gutthann, B.H.C. Stricker, A cohort study on the risk of acute liver injury among users of ketoconazole and other antifungal drugs, Br. J. Clin. Pharmacol. 48 (1999) 847–852. https://doi.org/10.1046/J.1365-2125.1999.00095.X.
[18] T.E. Knight, C.Y. Shikuma, J. Knight, Ketoconazole-induced fulminant hepatitis necessitating liver transplantation, J. Am. Acad. Dermatol. 25 (1991) 398–400. https://doi.org/10.1016/0190-9622(91)70214-M.
[19] R.F.M. de Almeida, F.C. Santos, K. Marycz, M. Alicka, A. Krasowska, J. Suchodolski, J.J. Panek, A. Jezierska, R. Starosta, New diphenylphosphane derivatives of ketoconazole are promising antifungal agents, Sci. Rep. 9 (2019). https://doi.org/10.1038/s41598-019-52525-7.
[20] A. Bento-Oliveira, R. Starosta, R.F.M. de Almeida, Interaction of the antifungal ketoconazole and its diphenylphosphine derivatives with lipid bilayers: insights into their antifungal action, Arch. Biochem. Biophys. (2024). https://doi.org/10.1016/j.abb.2024.109919.
[21] A. Bento-Oliveira, M.-L.C.J. Moita, R.F.M. de Almeida, R. Starosta, Unraveling environmental effects in the absorption and fluorescence spectra of p-methoxyphenylpiperazine derivatives, Spectrochim. Acta - Part A Mol. Biomol. Spectrosc. 306 (2024). https://doi.org/10.1016/j.saa.2023.123583.
[22] R. Starosta, R.F.M. de Almeida, Luminescence properties of the antifungal agent ketoconazole and its diphenylphosphane derivatives, J. Lumin. 220 (2020) 116956. https://doi.org/10.1016/j.jlumin.2019.116956.
[23] R. Starosta, R.F.M. de Almeida, M. Puchalska, J. Suchodolski, D. Derkacz, A. Krasowska, Anticandidal Cu(I) Complexes with Neocuproine and 1-(4-Methoxyphenyl)Piperazine Based Diphenylaminomethylphosphine: Is Cu-Diimine Moiety a Pharmacophore?, J. Inorg. Biochem. 248 (2023) 112355. https://doi.org/10.1016/j.jinorgbio.2023.112355.
[24] G. Rouser, S. Fleischer, A. Yamamoto, Two dimensional thin layer chromatographic separation of polar lipids and determination of phospholipids by phosphorus analysis of spots, Lipids. 5 (1970) 494–496. https://doi.org/10.1007/BF02531316.
[25] M.J. Frisch, G.W. Trucks, H.B. Schlegel, G.E. Scuseria, M.A. Robb, J.R. Cheeseman, G. Scalmani, V. Barone, G.A. Petersson, H. Nakatsuji, X. Li, M. Caricato, A.V. Marenich, J. Bloino, B.G. Janesko, R. Gomperts, B. Mennucci, H.P. Hratchian, J. V. Ortiz, A.F. Izmaylov, J.L. Sonnenberg, D. Williams-Young, F. Ding, F. Lipparini, F. Egidi, J. Goings, B. Peng, A. Petrone, T. Henderson, D. Ranasinghe, V.G. Zakrzewski, J. Gao, G. N. Rega, D.J. Fox, Gaussian 16, Revision C.01, (2019) Gaussian, Inc., Wallingford CT.
[26] J. Da Chai, M. Head-Gordon, Long-range corrected hybrid density functionals with damped atom–atom dispersion corrections, Phys. Chem. Chem. Phys. 10 (2008) 6615–6620. https://doi.org/10.1039/B810189B.
[27] J. Tomasi, B. Mennucci, R. Cammi, Quantum mechanical continuum solvation models, Chem. Rev. 105 (2005) 2999–3093. https://doi.org/10.1021/CR9904009/.
[28] J.S. Murray, K. Sen, Molecular electrostatic potentials, concepts and applications., Elsevier, Amsterdam eBook, 1996.
[29] C.M. Breneman, K.B. Wiberg, Determining atom-centered monopoles from molecular electrostatic potentials. The need for high sampling density in formamide conformational analysis, J. Comput. Chem. 11 (1990) 361–373. https://doi.org/10.1002/JCC.540110311.
[30] GaussView, Version 6, Dennington, Roy; Keith, Todd A.; Millam, John M. Semichem Inc., Shawnee Mission, KS, 2016., (n.d.).
[31] S.H. White, W.C. Wimley, A.S. Ladokhin, K. Hristova, Protein folding in membranes: Determining energetics of peptide-bilayer interactions, Methods Enzymol. 295 (1998) 62–87. https://doi.org/10.1016/S0076-6879(98)95035-2.
[32] A. Coutinho, M. Prieto, Cooperative partition model of nystatin interaction with phospholipid vesicles, Biophys. J. 84 (2003) 3061–3078. https://doi.org/10.1016/S0006-3495(03)70032-0.
[33] C.R. Mateo, R.F.M. de Almeida, L.M.S. Loura, M. Prieto, From Lipid Phases to Membrane Protein Organization: Fluorescence Methodologies in the Study of Lipid-Protein Interactions, (2006) 1–33. https://doi.org/10.1007/3-540-28435-4_1.
[34] J. Seidler, S.L. McGovern, A. Thompson N. Doman, Brian K. Shoichet, Identification and Prediction of Promiscuous Aggregating Inhibitors among Known Drugs, J. Med. Chem. 46 (2003) 4477–4486. https://doi.org/10.1021/JM030191R.
[35] A. Daina, O. Michielin, V. Zoete, SwissADME: a free web tool to evaluate pharmacokinetics, drug-likeness and medicinal chemistry friendliness of small molecules, Sci. Reports 2017 71. 7 (2017) 1–13. https://doi.org/10.1038/srep42717.
[36] M. Manuel Nuno, C. B., Miguel A. R., Omiganan interaction with bacterial membranes and cell wall models. Assigning a biological role to saturation, Biochim. Biophys. Acta. 1768 (2007) 1277–1290. https://doi.org/10.1016/J.BBAMEM.2007.02.005.
[37] H. Sónia Troeira, C. Miguel A. R. B., Environmental factors that enhance the action of the cell penetrating peptide pep-1 A spectroscopic study using lipidic vesicles, Biochim. Biophys. Acta. 1669 (2005) 75–86. https://doi.org/10.1016/J.BBAMEM.2004.11.017.
[38] M. Dzieciuch-Rojek, C. Poojari, J. Bednar, A. Bunker, B. Kozik, M. Nowakowska, I. Vattulainen, P. Wydro, M. Kepczynski, T. Roǵ, Effects of membrane PEGylation on entry and location of antifungal drug itraconazole and their pharmacological implications, Mol. Pharm. 14 (2017) 1057–1070. https://doi.org/10.1021/acs.molpharmaceut.6b00969.
[39] C. Poojari, A. Zak, M. Dzieciuch-Rojek, A. Bunker, M. Kepczynski, T. Róg, Cholesterol Reduces Partitioning of Antifungal Drug Itraconazole into Lipid Bilayers, ACS Appl. Mater. Interfaces. 124 (2020) 2139. https://doi.org/10.1021/acs.jpcb.9b11005.

Supplementary Information

Apparent bimolecular quenching rate constant considering two fluorophore populations with different accessibility to the quencher

For purposes of simplification, when any fluorescence (F) is mentioned, it is valid for both steady-state intensity and mean lifetime (amplitude-weighted).

If there are two fluorophore populations in the medium, then the total fluorescence that is being measured in the absence of quencher (F_0) corresponds to the sum of the fluorescence emitted by each of those populations:

$$F_0 = F_{0_a} + F_{0_b} \tag{S1}$$

In the present study, F_{0_a} and F_{0_b} are the fluorescence of the compound in aqueous solution and in the lipid bilayer respectively, in the absence of quencher.

Also, the fraction of fluorescence emitted by each population (f_a or f_b) is equal to:

$$f_a = \frac{F_{0_a}}{F_0} \tag{S2}$$

$$f_b = \frac{F_{0_b}}{F_0} \tag{S3}$$

The variation of fluorescence (F) with quenching concentration [Q], considering two populations, one accessible (a) to the quencher, undergoing dynamic quenching with a Stern-Volmer constant K_{SV}, and a population inaccessible such as when the compound is buried in the membrane b which does not undergo quenching, can be given by:

$$\frac{F}{F_0} = \frac{f_a}{1 + K_{SV}[Q]} + f_b = \frac{f_a + f_b\,(1 + K_{SV}[Q])}{1 + K_{SV}[Q]} \tag{S4}$$

This is equivalent to:

$$\frac{F_0}{F} = \frac{1 + K_{SV}[Q]}{f_a + f_b\,(1 + K_{SV}[Q])} \tag{S5}$$

Therefore, it is possible to determine the slope of the Stern-Volmer plot by determining its first derivative:

$$\frac{d\left(\frac{\mathrm{F_0}}{F}\right)}{d[\mathrm{Q}]} = \frac{K_{\mathrm{SV}}}{\mathrm{f_a} + \mathrm{f_b}\ (1 + K_{\mathrm{Sv}}[\mathrm{Q}])} + \frac{(1 + K_{\mathrm{Sv}}[\mathrm{Q}])\mathrm{f_b}K_{\mathrm{SV}}}{[\mathrm{f_a} + \mathrm{f_b}\ (1 + K_{\mathrm{Sv}}[\mathrm{Q}])]^2} = \\ = \frac{K_{\mathrm{SV}}[\mathrm{f_a} + \mathrm{f_b}\ (1 + K_{\mathrm{SV}}[\mathrm{Q}]) - \mathrm{f_b}K_{\mathrm{SV}} - \mathrm{f_b}{K_{\mathrm{SV}}}^2[\mathrm{Q}]]}{[\mathrm{f_a} + \mathrm{f_b}\ (1 + K_{\mathrm{SV}}[\mathrm{Q}])]^2} \quad \text{(S6)}$$

The slope for low concentrations of quencher can be approximated to the limit of the derivative when [Q] approaches zero:

$$\left[\frac{d\left(\frac{\mathrm{F_0}}{F}\right)}{d[\mathrm{Q}]}\right]_{[Q]=0} = \frac{K_{\mathrm{SV}}(\mathrm{f_a} + \mathrm{f_b}) - \mathrm{f_b}K_{\mathrm{SV}}}{(\mathrm{f_a} + \mathrm{f_b})^{\,2}} = \frac{\mathrm{f}_a K_{\mathrm{SV}}}{1^2} = \mathrm{f}_a K_{\mathrm{SV}} \quad \text{(S7)}$$

This slope is an apparent Stern-Volmer constant obtained from a linear regression applied to the Stern-Volmer plot. This apparent constant is in fact the product of the Stern-Volmer constant for the accessible population multiplied by its fraction of emitted fluorescence. If the quantum yield of the fluorophore is not markedly different for both populations in the absence of quencher, this fraction is similar to the mole fraction of fluorophore in each population. This is valid for several of the compounds studied in this work, where the amplitude-weighted mean fluorescence lifetime is not markedly affected by the presence of lipid. In these situations, if the compound in the membrane is virtually inaccessible to the quencher, the apparent Stern-Volmer constant should be close to the product of χ_W (molar fraction of the compound in aqueous solution) times K_{SV} in water. This is the case for **Ke**, where $\chi_W = 0.14$ and K_{SV} in water is is 10.4 hence it is expected to obtain a K_{SV} app $\approx 1.5\ M^{-1}$ in the presence of lipid. The experimental value was $2.0 \pm 0.2\ M^{-1}$. Moreover, when f_b is closer to 1 (once again, according to χ_L in Table 4.2), then the "slope" of the Stern-Volmer plots (Figure 4.5) is a good approximation to K_{SV} and the biomolecular quenching constant k_q determined from this value is in fact close to the real k_q for membrane-bound compound. Such is the case of **KeOP** for which k_q^{app} was $(0.4 \pm 0.2)\ x10^9\ M^{-1}.s^{-1}$. This is particularly valid for lower quenching concentrations at which the deviation from linearity is not significant. In the cases of **4MP** and **4MOP**, this calculation would yield a very different value from the one experimentally determined. This is because for these model compounds, the true K_{SV} and k_q^{app} for the membrane-bound population is much larger than zero. Threfore, this corroborates the conclusions in the main text, that **Ke** and its derivatives are buried deep in the lipid bilayer whereas the model compounds have a much more superifical location.

Supplementary Figures

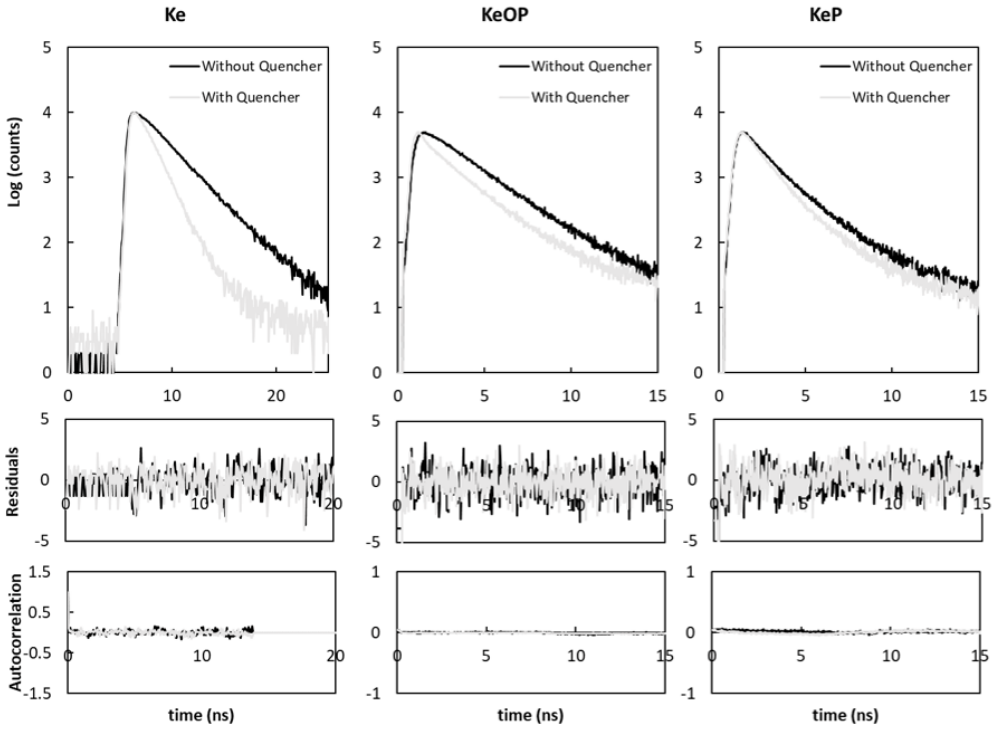

Figure S4. 1: Fluorescence intensity decays of **Ke**, **KeOP** and **KeP** in the presence of LUVs ([POPC] = 1mM) with (grey) and without (black) hydrophilic quencher ([Acrylamide] = 1.5 mM). The residuals and autocorrelation obtained from the fit of equation 2 to the data are also represented. The decays correspond to one replicate but are representative of the average results. [C] = 10 μM.

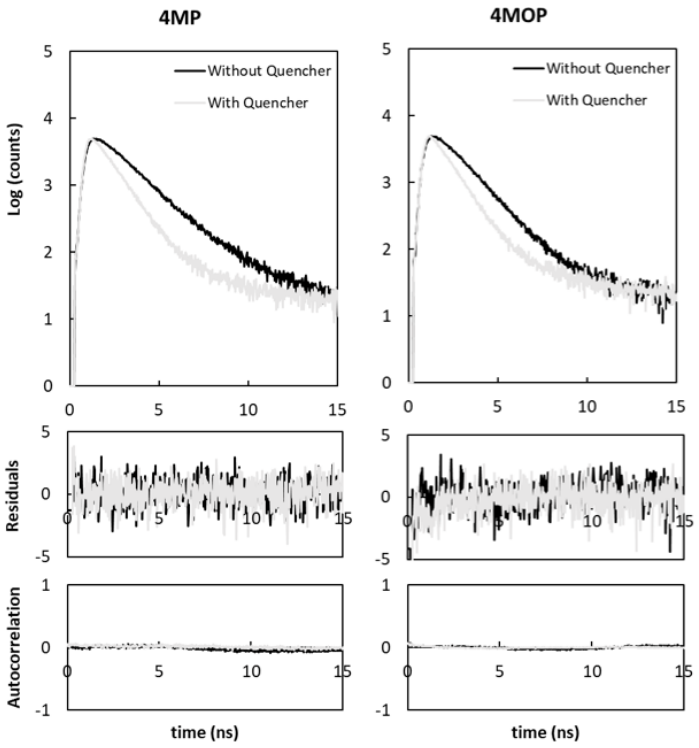

Figure S4. 2: Fluorescence intensity decays of **Ke**, **KeOP** and **KeP** in the presence of LUVs ([POPC] = 1mM) with (grey) and without (black) hydrophilic quencher ([Acrylamide] = 1.5 mM). The residuals and autocorrelation obtained from the fit of equation 2 to the data are also represented. The decays correspond to one replicate but are representative of the average results. [C] = 10 μM.

CHAPTER V

THE ROLE OF MEMBRANE LIPID COMPOSITION IN MEDIATING THE ANTIFUNGAL ACTIVITY OF KETOCONAZOLE: EMPHASIS ON STEROLS AND SPHINGOLIPIDS

Contribution: Took an active part in the planning of and performed all the experiments. Took an active part in the writing of the paper.

The Role of Membrane Lipid Composition in Mediating the Antifungal Activity of Ketoconazole: Emphasis on Sterols and Sphingolipids

Andreia Bento-Oliveira,[1] Radosław Starosta,[1,2] Rodrigo F. M. de Almeida[1,*]

[1] Centro de Química Estrutural, Institute of Molecular Sciences, Departamento de Química e Bioquímica, Faculdade de Ciências, Universidade de Lisboa, Campo Grande, 1749-016 Lisboa, Portugal.
[2] Faculty of Chemistry, University of Wroclaw, F. Joliot-Curie 14, 50-383 Wroclaw, Poland
* Correspondence: rfalmeida@fc.ul.pt; Tel. : +351-217-500-925

Abstract

Ketoconazole (**Ke**) is an important antifungal drug which has high affinity and can permeabilize a fluid 1-palmitoyl-2-oleoyl-*sn*-glycero-3-phosphocholine (POPC) bilayer. However, it was never uncovered if this azole has a different interaction with membranes containing different lipid composition and biophysical properties.

To test possible specific drug-lipid or -lipid phases interactions the membrane/water partition coefficient of **Ke** for POPC liposomes containing fungal (ergosterol and phytoceramide) or mammalian (cholesterol and ceramide) sterol or sphingolipids was quantified. Moreover, a leakage assay was also performed for each of these systems.

Ke has more affinity towards POPC only membranes ($(3.03 \pm 0.36) \times 10^5$) followed by ergosterol-, phytoceramide- and ceramide-containing membranes, which had similar values: $(1.51 \pm 0.19) \times 10^5$, $(1.46 \pm 0.08) \times 10^5$ and $(1.34 \pm 0.17) \times 10^5$, respectively. Furthermore, this azole causes similar membrane disturbance to POPC only and ergosterol- or phytoceramide-containing membranes, while it was the highest for POPC/ceramide and the lowest for POPC/cholesterol liposomes. Moreover, the presence of sterols hindered the change in permeability (it was the slowest) caused by **Ke**, while sphingolipids facilitated it.

The results suggest that **Ke** interacts preferentially with membranes containing ergosterol instead of cholesterol, while the interaction with membranes with sphingolipids was similar between each other.

Overall, this work shows that the membrane-interaction of **Ke** is different according to the lipid composition, suggesting that these interactions are important for the biological activity of azoles and should be considered in the design of new therapeutic agents.

Keywords:
Ketoconazole, Fluorescence spectroscopy, drug-membrane interaction, membrane permeability, ergosterol, phytoceramide

1. Introduction

Ketoconazole (**Ke**) (Figure 5.1) is an effective antifungal agent against a wide range of fungal pathogens. The main mode of action of this azole is through the inhibition of cytochrome P450 sterol-14-α-demethylase, an enzyme of the ergosterol (Erg) biosynthetic pathway [1–3]. This inhibition causes the decrease of Erg levels, compromising the integrity of the fungal plasma membrane, leading to cell death. Together with membrane disruption, the inhibition of Erg synthesis caused by **Ke** also leads to the accumulation of toxic sterol intermediates such as 14α-methyl-3,6-diol [4] adding to membrane stress. Moreover, **Ke** disrupts the cation homeostasis within the cell since it impairs the function of vacuolar proton pump V-ATPase [5,6]. Unfortunately, **Ke** has severe side effects to humans, particularly hepatotoxicity [7,8]. That is why **Ke** is mainly used in shampoos to treat dandruff [9,10] and in emulsions and ointments for eradicating superficial mycosis [9]. **Ke** can also inhibit steroid synthesis, being used in cases where there is an excess of androgen levels, such as those found in Cushing's syndrome [11]. Furthermore, **Ke** has also potential as an anticancerogenic agent has revealed by a number of studies [12–15].

We showed recently that **Ke** has a moderately high affinity towards fluid membranes containing 1-palmitoyl-2-oleoyl-*sn*-glycero-3-phosphocholine (POPC). In fact, this interaction changes the permeability of the membrane [16]. Moreover, this compound most probably integrates with the membrane in a relatively deep region, along the hydrocarbon lipid tails [17]. Hence, there might be a relevance for the interaction of **Ke** with membranes, which is directly or indirectly correlated with the activity of the drug as an antifungal agent. Nevertheless, it was never explored if **Ke** interaction with membranes depends on lipid composition, and/or on membrane biophysical properties, which are also modulated by lipid composition. There is also the possibility for **Ke** to have preferences towards specific lipid phases. For example, the membrane partition and pore-forming activity of the antifungal polyene nystatin is increased in the presence of highly ordered gel domains [18].

The main aim of this work was to explore the different interaction of **Ke** with membranes containing POPC mixed in relevant molar percentage of the major sterol or sphingolipid backbone found in fungi (Erg and phytoceramide (Phycer)) vs the mammalian ones (cholesterol (Chol) and ceramide (Cer)). While POPC alone forms highly fluid membranes in a liquid-disordered phase (l_d), increasing the molar fraction of those sterols induces the formation of a liquid-ordered phase (l_o) [19–21], more ordered than a l_d, but less than a gel phase. Particularly, at 30 mol% of Erg (the major fungal sterol) or Chol (the major mammalian sterol) with POPC,

a coexistence of l_d and l_o phases can be detected [22,23]. At the same molar percentage in a mixture with POPC, Erg induces the formation of a higher molar fraction of l_o than Chol [19–21]. On the other hand, Chol has a stronger ability to increase membrane dipole potential, which has been correlated with the presence of the relatively long saturated aliphatic chain found in the molecular structure of Chol, but not Erg (Figure 5.1) [21].

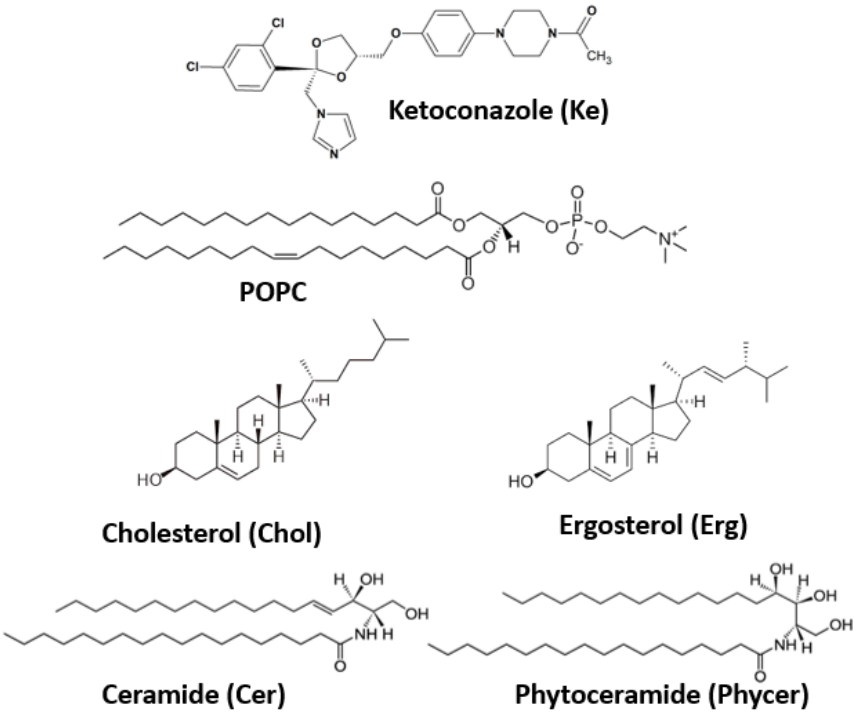

Figure 5. 1: Molecular structure of ketoconazole (Ke; 1-[4-[4-[[2-(2,4-dichlorophenyl)-2-(imidazole-1-ylmethyl)-1,3-dioxolan-4-yl]methoxy]phenyl]piperazin-1-yl]ethanone), 1-palmitoyl-2-oleoyl-*sn*-glycero-3-phosphocholine (POPC), Cholesterol (Chol), Ergosterol (Erg), Ceramide (Cer; *N*-stearoyl-D-erythro-sphingosine) and Phytoceramide (Phycer; *N*-stearoyl 4-hydroxysphinganine) used in this work.

Sphingolipids such as Cer or Phycer – the major hydrophobic backbone of complex sphingolipids in mammals and fungi, respectively – induce the formation of highly ordered gel domains with different biophysical properties [24,25]. Mammalian cells also have sphingolipids with a Phycer backbone [26] but not in significant levels, with some exceptions such as in the uppermost epidermal layer [27,28]. The presence of the additional hydroxyl group present in Phycer at C4 of the sphingoid base but absent in Cer which has a *trans* unsaturation instead (Figure 5.1) results in higher melting temperature of the domains rich in this fungal sphingolipid when mixed with POPC. [25,29]. Moreover, it was shown that at 20 mol% of either of these sphingolipids in binary mixtures with POPC, there is a coexistence of a l_d with a gel phase [25,29]. At this molar percentage of sphingolipid, the gel phase membrane fraction is more than the double for Phycer-containing bilayers than the gel phase found for Cer-containing ones. Furthermore, Cer-rich gel has a more pure and rigid arrangement than Phycer,

which organizes with POPC in highly stable and rigid stoichiometric complexes [25]. For instance, at 20 mol% of Phycer, the l_d phase coexists with a phase formed by 3:1 POPC/Phycer complexes. Indeed, the stability of these complexes together with the similarity of the biophysical properties reported for POPC liposomes containing 20 mol% of Phycer and yeast cells [25,30], aligns with the existence of sphingolipid-enriched domains (SLEDs) in the fungal plasma membrane, which are usually not found in mammalian cells [30].

To quantify the affinity of **Ke** towards POPC/Erg, POPC/Chol, POPC/Cer and POPC/Phycer the mole-fraction partition coefficient ($K_{p,x}$) was determined by following the intrinsic fluorescence properties of the *p*-methoxyphenyl piperazine moiety in **Ke** with increasing lipid concentration. Moreover, a permeability assay was also conducted to verify if the interaction of **Ke** was changing the integrity of the membrane according to the lipid present in the bilayer. This work highlights specific **Ke**-lipid interactions and/or -lipid phases and how it could correlate with antifungal drug activity.

2. Materials and methods

2.1. Chemicals

POPC was obtained from Lipoid (Ludwigshafen, Germany), and Cer and Phycer from Merck (Darmstadt, Germany). DMSO (spectroscopic grade), HEPES and Erg were acquired from Thermo Fisher Scientific (Waltham, MA, USA). Chemicals and solvents, including **Ke**, 5(6)-carboxyfluorescein (CF) and Chol were purchased from Merck and used without further purification. POPC stock solutions in chloroform (spectroscopic grade) were kept at -20 °C under nitrogen and their concentration was determined by phosphate quantification [31]. Erg, Chol, Cer and Phycer were quantified using a simple gravimetry assay in a balance with 10^{-5} g precision. Erg stock solutions were freshly prepared for each assay, and dissolved in chloroform only when used, and Erg exposure to light and air was minimized.

2.2. Liposome preparation

LUVs with a mean diameter of 100 nm or ca. 200 nm, containing the lipids in the desired molar proportions were prepared by the extrusion method in HEPES buffer (10 mM; pH 7.4), as previously described [16]. Each time the sample containers were opened, the sample was bubbled with a nitrogen stream. LUVs extruded through filters with different pore diameter were used for sterol (100 nm) vs sphingolipids (400 nm) containing systems. Moreover, for liposomes containing POPC only the experiments were conducted for both liposome size and

the results were virtually the same (comparison not shown), hence the results obtained for sterols and sphingolipids are regarded as directly comparable. The results presented for POPC systems (including partition and permeability assays) are for the liposomes with 100 nm of diameter. For systems with sphingolipids, the pore diameter and hence the size of the LUVs was larger than the typical 100 nm since, during the extrusion process, Phycer can be retained in the pore of the membrane filter if the pores are smaller. This is probably due to the tendency of this sphingolipid to form highly rigid structures, such as lamellar crystalline phases and tight complexes with POPC [25].

2.3. Absorption and fluorescence spectroscopy

A Fluorolog 3.22 spectrofluorimeter from Horiba Jobin Yvon (Villeneuve D'ascq, France) was used for fluorescence measurements performed at 23.0 ± 1.0 °C in a sample compartment with magnetic stirring and temperature control, using quartz cuvettes QS from Hellma with optical path of 1 cm in excitation and 0.4 cm in emission.

For steady-state fluorescence anisotropy measurements, the excitation and emission wavelengths were set to 295 nm and 370 nm, respectively. For the excitation spectra the emission was fixed at 370 nm, and the excitation wavelength was scanned from 260 to 350 nm, while for the emission spectra excitation was fixed at 295 nm, and the emission wavelength was scanned from 310 to 575 nm, with wavelength increments of 1 nm. For spectra acquisition the bandwidths were typically 4 nm in both excitation and emission, and integration time 0.2 s.

To determine the value of steady-state fluorescence anisotropy, $\langle r \rangle$, the following equation 1 was used:

$$\langle r \rangle = \frac{(I_{VV} - G \times I_{VH})}{(I_{VV} + 2G \times I_{VH})} \quad (1)$$

in which the subscripts indicate the orientation of the excitation and emission polarizers, where V and H correspond to vertical and horizontal orientations and G is a correction factor calculated from the ratio I_{HV}/I_{HH}. An adequate blank was subtracted from each intensity reading. For fluorescence anisotropy measurements the bandwidths were 8 nm in both excitation and emission.

2.3.1. Partition experiments

LUVs with 3 to 5 mM of total lipid, were diluted in HEPES buffer to a final concentration in the 0.025 mM to 1.5 mM range. **Ke** was added to the LUV suspensions to a final concentration of 10 μM and 2% DMSO and incubated for 1 h 30 min at 23.0 ± 1.0 °C.

The variation of fluorescence anisotropy of **Ke** with lipid concentration was used to determine the partition coefficient (K_p), by fitting the following equation to the experimental data:

$$\langle r \rangle_{ke} = \frac{r_W \left(\frac{1}{\gamma_L [L]} - 1\right) + r_L K_p \frac{\Phi_L}{\Phi_W}}{\frac{1}{\gamma_L [L]} - 1 + K_p \frac{\Phi_L}{\Phi_W}} \quad (2)$$

where the ratio $\frac{\Phi_L}{\Phi_W}$ (fluorescence quantum yield of **Ke** in lipid / fluorescence quantum yield of **Ke** in aqueous solution) was taken as equal to I_L / I_W determined from the components of polarized light, *i.e.* $I = I_{VV} + 2G$ x I_{VH} (the denominator in equation 1). γ_L is the average molar volume of the lipids, which was considered equal to γ_{POPC} [32] x POPC mol% + γ_S x S mol%, with S being Erg [33], Chol [34], Phycer [35] or Cer [36]. The determined γ_L was 0.644 M^{-1}, 0.647 M^{-1}, 0.676 M^{-1} and 0.680 M^{-1} for Erg, Chol, Phycer and Cer, respectively. Note that liposomes with POPC mixed with these sterols or sphingolipids have a coexistence of two lipid-phases, and for this calculation, it was assumed that POPC and S have the same molar volume in both these phases. r_W and r_L are the fluorescence anisotropy values for the compound in aqueous solution (with no lipid) and in the lipid phase respectively.

Equation 2 allows to determine the molar Nernst partition coefficient K_p, which relates with the mole-fraction partition coefficient $K_{p,x}$ according to equation 3 [37]:

$$K_p = K_{p,x} \frac{\gamma_W}{\gamma_L} \quad (3)$$

where γ_W is the molar volume of water, 0.018 M^{-1}.

The standard Gibbs free energy ($\Delta G°$) associated with the transfer of a mole of compound from the aqueous phase to the lipid phase was determined using equation 4:

$$\Delta G^{\circ} = -RT \ln K_{p,x} \quad (4)$$

where R is the molar gas constant, 8.314 $J \cdot K^{-1} \cdot mol^{-1}$, and T is the absolute temperature of the assay, 296 K.

The molar fraction of each compound in the lipid phase (χ_L) at a specific concentration of lipid was determined using equation 5:

$$\chi_L = \frac{K_{p,x}[L]}{[W] + K_{p,x}[L]} \quad (5)$$

where [L] is the total lipid concentration in the suspension; and [W] is the molar concentration of water at the assay temperature (55.5 M).

2.3.2. Leakage Assays

LUVs with 2 mM of total lipid were prepared in HEPES buffer containing 40 mM of CF. In order to remove the non-encapsulated CF, the pellet that resulted from LUV centrifugation at 150 000 *g* for 2h (Ultracentrifuge Hitachi CP80NX with P70AT rotor (Tokyo, Japan)), was re-suspendend in HEPES buffer (50 mM, pH 7.4), and filtered through a Sephadex G-25 filtration column (Disposable PD Desalting Columns, Merck). The LUVs were then diluted in a 96-well plate to different lipid concentration ranging from 0.1 to 0.25 mM. CF fluorescence intensity was measured every 1 min, during 14-16 hours after the addition of 5-20 μM of **Ke**. Finally, for total LUVs lysis 1% (V/V) of Triton was added to each well, and fluorescence intensity was measured to determine the maximum percentage of release of CF (F_{100}). The measurements were also performed to the corresponding blanks (each lipid system with DMSO only), and a CF leakage lower than 10% was obtained, which was subtracted to each sample.

The percentage of CF leakage was determined using equation 6:

$$\%\text{CF Leakage} = \frac{F_t - F_0}{F_{100} - F_0} \tag{6}$$

where F_0 is the initial fluorescence intensity measured without the addition of compound, and F_t is the fluorescence intensity value at each time point [16].

Equation 7 [16] was fitted to the experimental data:

$$L = \sum_{i=1}^{n} L_i \left(1 - \exp\left(-\frac{t}{\tau_{Li}}\right)\right) \tag{7}$$

where L_i represents the maximum leakage associated with each kinetic constant, *t* is the time after the addition of the compounds, and τ_{Li} represents the time constants. The average leakage time constant, $\langle\tau_L\rangle$ can be calculated using equations 8 and 9:

$$\langle\tau_L\rangle = \sum \alpha_i \tau_{Li} \tag{8}$$

where α_i is defined as following:

$$\alpha_i = \frac{L_i}{L_{max}} \quad (9)$$

and L_{max} is the sum of all L_i.

A microplate reader SpectraMAX GeminiEM spectrofluorimeter from Molecular Devices (San José, CA, USA) was used in leakage assays to measure the fluorescence intensity of CF, at 25 °C. The excitation and emission wavelengths were set to 492 nm and 530 nm, respectively, and a cut-off filter at 515 nm was used.

2.4. Statistical Analysis

All the results, except the fluorescence spectra and the CF leakage curves, are presented as mean ± standard deviation (S.D.) of at least three independent replicates, unless stated otherwise. Representative fluorescence intensity spectra and CF leakage curves shown are a median result from at least three independent replicates. The statistical significance was determined using one way ANOVA with Tukey's post-hoc test. Mean values were considered significantly different for *p*-values below or equal to 0.05.

3. Results

3.1. Ketoconazole partition with membranes containing mammalian vs fungal lipids

To explore the partition of **Ke** with membranes containing different lipids the fluorescence properties of **Ke** were measured in the presence of POPC/Erg, POPC/Chol, POPC/Cer and POPC/Phycer LUVs with increasing total lipid concentration. Using a similar approach we have previously determined the $K_{p,x}$ of **Ke** towards a simpler lipid system containing only POPC and the value obtained was $K_{p,x} = (3.31 \pm 0.36)\ x10^5$) [16].

The percentage of Cer and Phycer used was 20 mol% since it is an approximation to the amount of sphingolipids in the plasma membrane of fungi [38–40] and bilayers with this percentage of ceramides have already been biophysically characterized [24,25].

3.1.1. Overcoming the problem of sterol auto-fluorescence in the study of Ke in the presence of Erg-containig liposomes

Regarding the sterols, ideally the liposomes would contain the approximate percentage of sterol in the plasma membrane of yeast, 40 mol% [41,42]. Nevertheless, during optimization in the bilayers with Erg (but not with Chol), the signal from the blank represented 50% or more of the signal from the respective sample containing **Ke**. Moreover, the fluorescence intensity of **Ke** decreased with lipid concentration (Figure S5.1 – A), which could indicate that 1) there is

an interaction of the compound with the liposomes, and 2) that this interaction led to a smaller fluorescence quantum yield of the compound. However, since the blank itself presents fluorescence and is subtracted from the sample, this could also be due to a problem of overcorrection. Moreover, the spectra of **Ke** is distorted for higher lipid concentrations and a closer look at the spectra of the blanks (Figure S5.1 – B and Figure S5.2) show a clear fluorescence spectral envelope, that is similar to the one from dehydroergosterol (DHE) in chloroform (Figure S5.1 - C). Moreover, the excitation and emission peaks of our samples and that of DHE are approximately the same, 325 and 375-380 nm, respectively. Mass spectrometry confirmed the presence of less than 5 mol% of DHE in Erg stocks (data not shown). This corresponds to less than 2 mol% of total lipid in the LUV suspensions, which does not affect the general biophysical properties of the membranes under analysis [43]. However, DHE is used as a fluorescent membrane probe, as an analogue for Erg or Chol [44,45] having an additional double bond in the ring system conjugated with the two double bonds that are present in Erg. This conjugated triene is responsible for the absorption and fluorescence properties of DHE.

Even though the presence of DHE below 2 mol% does not influence the biophysical properties of the membrane it is necessary to minimize its contribution regarding fluorescence properties and **Ke** partition quantification. Hence, to quantify the partition of **Ke** towards liposomes containing Erg it was necessary to adjust several experimental variables. First to decrease even more the maximum concentration of DHE, liposomes were prepared with 30 mol% of Erg instead of 40 mol%, which is still within the range of reported values for the expected amount of sterol in the plasma membrane of fungi and mammals.

Even with this alteration, due to the presence of DHE it is not possible to use the fluorescence intensity of the samples to quantify the partition of **Ke** towards membranes containing Erg. Hence a new approach was considered. Instead of considering the signal from the preparation without **Ke** as a background to be subtracted to the signal of the preparation with **Ke**, it was assumed that there is a second fluorescent species (DHE) in the latter, and this is the only fluorescent species present in the former. This way, the anisotropy of **Ke** alone could be determined considering the additive properties of anisotropy, and that the value measured is the sum of the anisotropy of each fluorescent species, **Ke** and the DHE ($\langle r \rangle_{ke}$ and $\langle r \rangle_{DHE}$ respectively) weighted by the corresponding fractional fluorescence intensity, *f,* of each:

$$\langle r \rangle_{total} = \langle r \rangle_{ke} f_{ke} + \langle r \rangle_{DHE} f_{DHE} \quad (10)$$

Note that $f_{ke} + f_{DHE} = 1$, and $f_{DHE} = I_{DHE}/I_{tot}$. I_{tot} is the fluorescence intensity from the preparation with **Ke** and Erg; I_{DHE} is the fluorescence intensity from the sample without **Ke**. Thus, it is possible to solve the equation to find $\langle r \rangle_{ke}$. Likewise, $\langle r \rangle_{DHE}$ corresponds to the anisotropy of the samples that does not contain **Ke** (which would be the typical blank in a classical methodology fluorescence assay; the only fluorescence species in this sample is the contaminant DHE). Moreover, to obtain a background to subtract to each fluorescent intensity value, the blank used to determine $\langle r \rangle_{DHE}$ and $\langle r \rangle_{total}$ corresponded to the samples containing POPC and Chol in the same mol% of Erg (30 mol%) and the total lipid concentration of the respective sample. With Chol instead of Erg there is no contamination with a fluorescent species, hence the values measured come mainly from the light scattering by the liposomes which is similar in POPC/Erg and POPC/Chol samples and other light artifacts, so the fluorescence intensity values are background corrected. This background was always less than 5% of the fluorescence signal considering the measurements without polarizer and the different polarization components used to obtain the anisotropy (equation 1).

With these methodological alterations it was possible to obtain the membrane/water partition coefficient of **Ke**.

The minimization of the contamination of DHE was not enough to not influence the excitation spectra of **Ke** with mixtures containing Erg due to the spectral overlap of the contaminant with the azole (blank representing ~30-40% of the total intensity of the sample). Therefore, the fluorescence intensity obtained in the emission spectra is not reliable to accurately determine K_p. Nevertheless, the maximum emission peak does not depend on the excitation energy. The variation of the maximum wavelength peak for the emission of **Ke** with total lipid concentration is represented in Figure 5.2 – D.

3.2.2. Summary of the partition of Ke towards the different binary mixtures

The change in 1) the fluorescence intensity (Figure S5.1 - A and S5.3), 2) fluorescence anisotropy (Figure 5.2 - A) and 3) the peak wavelength of both the excitation and emission spectra of **Ke** with increasing lipid concentration for all lipid systems reveals that this antifungal drug interacts with membranes containing the sterols or sphingolipids in study. The fit of equation 2 to the experimental data (Figure 5.2 – A) allowed to estimate the partition coefficient of **Ke** towards lipid bilayers containing POPC, POPC/Erg, POPC/Chol, POPC/Cer and POPC/Phycer (Figure 5.2 – B).

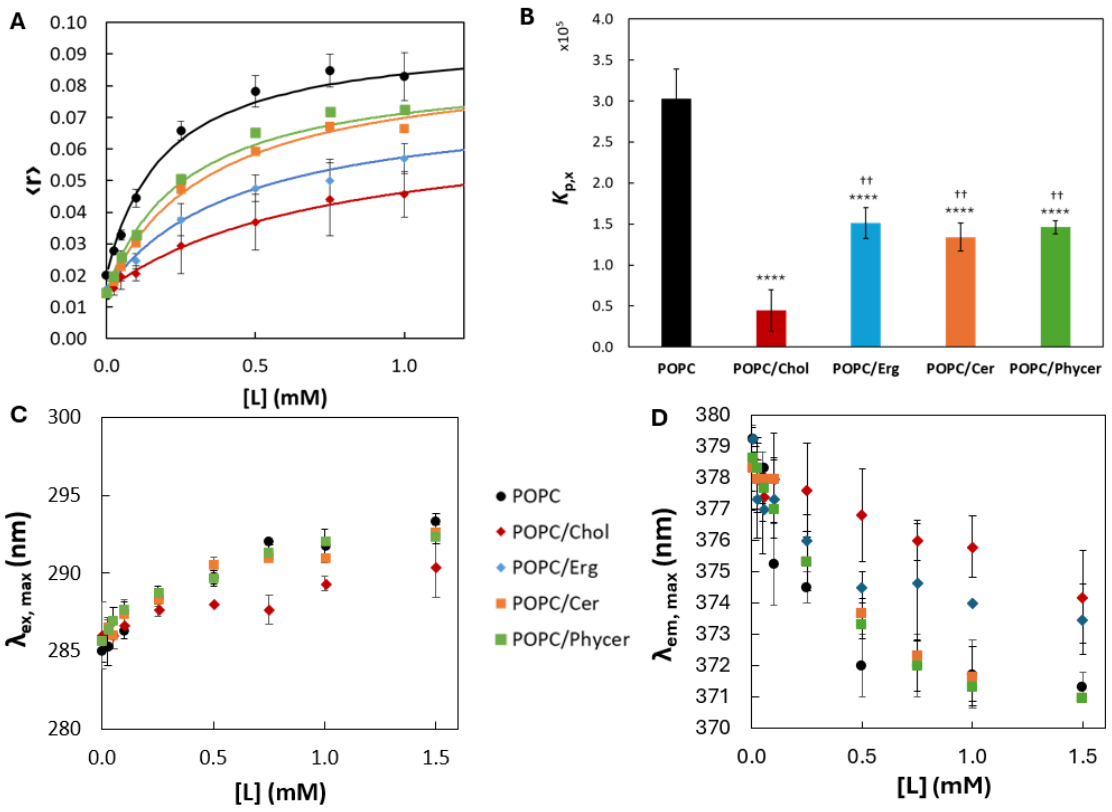

Figure 5. 2: Determination of the mole-fraction partition coefficient of Ke **to membranes containing POPC with Chol, Erg, Cer and Phycer.** Variation of the fluorescence anisotropy (A), excitation (C) and emission (D) wavelength peak of **Ke** with total lipid concentration of liposomes containing POPC with and without Chol, Erg, Cer and Phycer. The mole-fraction partition coefficient ($K_{p,x}$) of **Ke** in the different lipid systems is also represented (B). For systems with Erg and Chol 30 mol% of sterol was used, while with Cer and Phycer 20 mol% was used. In C, the values for POPC/Erg are not represented since, as mentioned in the text, the presence of the contaminant DHE distorted the excitation spectra envelope of **Ke** in this membrane system. The solid lines in A represent the fitting of equation 2 to the experimental data. Data was obtained with excitation at 295 nm and emission collected at 370 nm. The concentration of **Ke** was 10 µM. The results are the mean ± S.D. of at least three independent replicates. The results obtained for POPC were already published by us [16]. †† p-value ≤ 0.01 in comparison between each lipid system with POPC/Chol; **** p-value ≤ 0.001 in comparison between each lipid system with POPC only. The data for the POPC system was retrieved from [16].

Considering the partition coefficients determined, **Ke** has higher affinity towards liposomes containing POPC only than with any of the lipids used in this work (Figure 5.2 – B). Interestingly, the affinity of **Ke** is similar for the Cer- and Phycer-containing systems being approximately half of the value obtained for POPC only LUVs. The affinity of **Ke** towards membranes containing Erg was similar to those containing Cer and Phycer ones, but higher as compared to the Chol-containing ones.

The peak wavelength of excitation and emission of **Ke** spectra shifted 8 nm (red and blue-shifted, respectively) in the presence of POPC, POPC/Cer and POPC/Phycer liposomes, while for Erg and Chol containing-membranes the shift still occurred but to smaller extents - ~4-5 nm (Figure 5.2 – C and D).

Table 5. 1: Parameters for Ke partition between water and POPC, POPC/Erg, POPC/Chol, POPC/Phycer, POPC/Cer bilayers at 23 °C. [C] = 10 μM; $\lambda_{ex,max,i}$ and $\lambda_{em,max,i}$ are the peak wavelengths of the excitation and emission spectra, respectively, in water (i = aq) or with the highest lipid concentration (i = lip). $\Delta G°$ was determined using equation 4. The $K_{p,x}$ was estimated using equation 2 and 3. For systems with Erg and Chol, 30 mol% of sterol was used, while with Cer and Phycer 20 mol% was used. The data obtained for POPC was already published [16]. The $\lambda_{ex,max,lip}$ for the POPC/Erg membrane was not possible to determine, due to the presence of DHE spectral overlapping with that of **Ke**.

Lipid mixture	POPC	POPC/Erg	POPC/Chol	POPC/Phycer	POPC/Cer
$K_{p,x}$	(3.03 ± 0.36) x10^5	(1.51 ± 0.19) x10^5	(4.44 ± 2.51) x10^4	(1.46 ± 0.08) x10^5	(1.34 ± 0.17) x10^5
$\Delta G°$ (kJ/mol)	-31.30 ± 0.27	-29.36 ± 0.31	-26.35 ± 1.39	-29.28 ± 0.14	-29.07 ± 0.31
I_L/I_W	1.37 ± 0.02	0.71 ± 0.02	1.47 ± 0.10	1.41 ± 0.20	1.19 ± 0.08
r_W			0.016 ± 0.002		
r_L	0.094 ± 0.005	0.076 ± 0.004	0.055 ± 0.020	0.086 ± 0.001	0.086 ± 0.003
$\lambda_{em,max,aq}$ (nm)			379		
$\lambda_{em,max,lip}$ (nm)	371	374	374	371	371
$\lambda_{ex,max,aq}$ (nm)			285		
$\lambda_{ex,max,lip}$ (nm)	293	-	290	292	293

3.2. Impact of ketoconazole on membrane permeability

Now that the partition of **Ke** with membranes containing Erg, Chol, Cer or Phycer has been quantified, a question that arises is if such interaction is disturbing the membrane properties. To answer it, a CF leakage assay was conducted with LUVs with binary mixtures of POPC and Erg or Chol 30 mol%, or Cer or Phycer 20 mol%. In this assay, CF is encapsulated in the liposomes at high concentrations at which its fluorescence quantum yield is lower due to self-quenching. After the addition of a compound, if it increases the permeability of the membrane, CF will be released to the outer medium, and its dilution will cause a fluorescence increase. Therefore, it is possible to track the leakage of CF, *i.e.* a compound ability to change membrane permeability, by monitoring its fluorescence intensity.

Ke changes the permeability of all the LUVs under study which is revealed by the increase of the percentage of CF release (Figure 5.3 - A). After the addition of 10 μM of **Ke** to LUVs with 0.1 mM of total lipid the maximum leakage of CF (L_{max}) obtained for liposomes with Erg, Cer or Phycer was similar to the values obtained for POPC (Figure 5.3 – B). Nevertheless, systems with Chol had lower values of L_{max} than POPC and the other sterol Erg, meaning that LUVs that contain Chol are less susceptible to permeability changes by **Ke**. Moreover, higher values of the maximum probe leakage are reached for Chol systems at lower effective compound concentration than for Erg (Figure 5.3 – E). Regarding the systems with sphingolipids, the L_{max} was higher for Cer- than Phycer-containing liposomes for 10 μM of compound and 0.1 mM of total lipid. However, for similar effective compound/lipid ratio in the

membrane the maximum leakage that results from **Ke** is approximately the same for both liposomal compositions (Figure 5.3 – E).

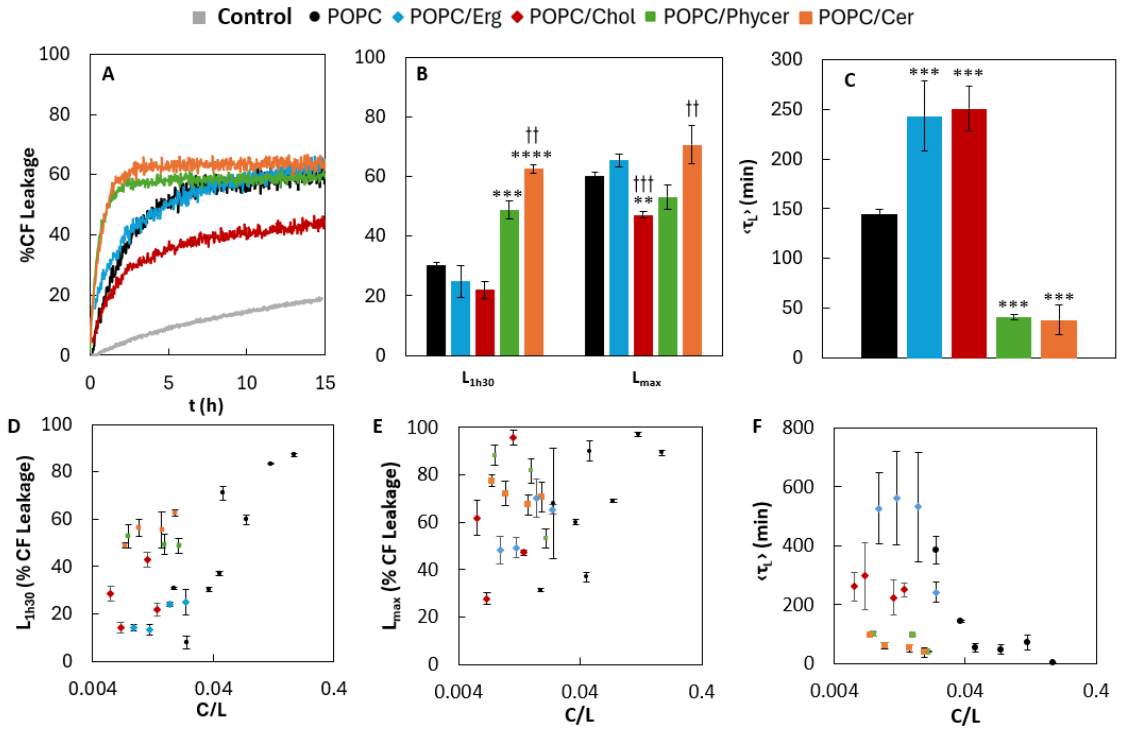

Figure 5. 3: Effect of Ke on the permeability of membranes composed by POPC, POPC/Erg, POPC/Chol, POPC/Cer and POPC/Phycer. For binary systems the sterol amount was 30 mol%, and the sphingolipid amount was 20 mol%. (A-C) The percentage of CF release from LUVs with 0.1 mM of total lipid after the addition of 10 μM of **Ke**, was measured along 14-16 hours. (B) Maximum percentage of CF release (L_{max}) and 1h30 (L_{1h30}) after the addition of the compound. (C) Average leakage time constant ($\langle\tau_L\rangle$) obtained for each compound. (D-F) L_{1h30} (D), L_{max} (E) and $\langle\tau_L\rangle$ (F) after the addition of **Ke**, at different compound/lipid ratios (C/L). %CF Release was calculated using equation 6, while L_{max} and $\langle\tau_L\rangle$ were obtained from equations 7 to 9. The results in B-F are the mean ± S.D. of at least three independent replicates. The data obtained for POPC was already published [16]. * represents the comparison between each lipid system with POPC only, while † represents the comparison between the mammalian lipid vs the fungal one, *i.e.* Chol vs Erg or Cer vs Phycer. **,†† p-value ≤ 0.01; ***,††† p-value ≤ 0.001; ****p-value ≤ 0.0001.

The average leakage time of CF through LUVs containing either of the sterols in study was approximately the same and significantly longer than the values obtained for POPC samples. The opposite was observed for the systems with sphingolipids, in which significantly slower average leakage times were reported (Figure 5.3 – C and F). This suggests that the presence of sterols is hindering the permeabilizing ability of **Ke** with the membrane, while sphingolipids are facilitating it.

4. Discussion

Although there are several studies aimed at increasing **Ke** effectiveness through its encapsulation in liposome formulations [46–48], it was only very recently that the interaction of this azole with a lipid bilayer was characterized [16,17]. In these previous studies the membrane was composed of POPC only and in a single highly fluid l_d state. The affinity of **Ke**

to POPC bilayers is moderately high [16], distributing in a relatively deep region of the membrane [17].

Herein the interaction of **Ke** with liposomes containing different lipids was carried out, with the goal of uncovering differential dependency of the membrane-drug interaction on lipid composition which could possibly evidence specific drug-lipid interactions or the preference for certain lipid phases. In this work we showed that **Ke** partitions towards liposomes containing POPC mixed with sterols and sphingolipid backbones that are a staple of either the fungal or mammalian lipidome: Erg and Phycer vs Chol and Cer.

Investigating the interaction with the sphingolipid backbones Phycer and Cer instead of the more complex sphingolipids of yeast and mammalians which would also differ in the polar headgroup (inositolphosphorylceramides and sphingomyelin, respectively) is relevant since **Ke** distributes in a relatively deep region of the membrane [17], of low polarity at the level of hydrophobic tails of lipids, shielded from interactions with the aqueous phase.

The membrane/water partition coefficients for POPC/Erg, POPC/Phycer and POPC/Cer lipid systems were all similar, but lower than the one obtained with POPC only and statistically higher than the one obtained for POPC/Chol liposomes (Figure 5.2 - B). Hence **Ke** has the strongest affinity for POPC membranes when compared with the others. This could be due to the fact that POPC membranes are totally in a l_d, while in the other systems a coexistence of this fluid phase and a more rigid one is expected [19–21,24,25] as previously mentioned in the introduction.

As shown in our previous paper the fluorescence excitation and emission peak wavelengths of the *p*-methoxyphenyl piperazine motif depend on different conditions [49]. Excitation depends to some extent on aggregation of the compound with this motif, but mostly on formation of hydrogen bonds (HBs) with solvent molecules, depending almost linearly on the solvent's HB acidity. On the other hand, the emission solely depends on the polarity of the environment. Undoubtedly, all indicates that the surrounding environment of **Ke** is different while partitioning towards each membrane system. Since the emission and the excitation of **Ke** changed equally while partitioning towards Cer, Phycer and POPC membranes, it indicates that the polarity and HB acidity of the direct environment of the compound is very similar in these cases. For membranes with sterols the shift of the excitation wavelength (in this case we only have the values for Chol) and the emission was lower than for the previous three. This means that, the microvicinity of **Ke** is more polar and more able to form HBs in membranes with sterols than with sphingolipids. A gel phase is typically less hydrated than an l_o which is less hydrated than an l_d. Since with 20 mol% of the sphingolipids used in this work mixed with

POPC there is a coexistence of an l_d and a gel phase, it would be expected that the emission peak wavelength would be lower than for both types of membranes: with an l_d/l_o coexistence (sterol-containing membranes) and l_d only (POPC). While this is observed for the sterol case, the values for the POPC membranes are virtually overlapping with those of the sphingolipids systems. This could be explained by the compound being partitioning mainly towards the l_d phase and being excluded from the gel phase – and the compound distribution is similar with POPC only and POPC/Cer and POPC/Phycer.

This partition of **Ke** towards l_d phase is further corroborated with the fact that the total extent of leakage can in some way be related to the partition constant. When equilibrium is attained, and no more **Ke** is being transferred to the membrane the maximum leakage capacity is reached. This is similar for all binary systems except POPC/Chol for which **Ke** has a lower K_p. However, the maximum leakage is similar for POPC and the other binary mixtures (again except Chol) even though the K_p is larger for POPC. This can be justified by the hypothesis proposed herein that the azole molecules probably predominate in l_d regions /interfacial regions and the local concentration of **Ke** in l_d + interfaces ends up being similar to its local concentration in pure POPC membranes.

Therefore, the presence of highly fluid membranes may facilitate the interaction of the compound with the membrane. Nevertheless, **Ke** is faster permeabilizing liposomes containing either of the sphingolipids used in this work – Phycer and Cer – rather than bilayers with sterols or POPC only. In the lipid systems with sphingolipids a coexistence of a gel phase with a fluid phase is expected [24,25]. Gel-l_d interfacial regions have packing defects and are preferential sites for many small molecules to locate in heterogeneous membranes. A small perturbation in these regions that already have higher water penetration and water/small ion permeability could facilitate the interaction of the compound with the membrane [50] and its permeabilizing activity.

Since, the amount of gel phase in bilayers with Phycer is higher than in Cer-containing liposomes at the same molar proportions [24,25] and **Ke** is preferentially partitioning towards l_d and to the gel-l_d interfaces a different average leakage time and $K_{p,x}$ should be expected between these two systems. Nevertheless, apart from some situations where the leakage is slightly faster and more extensive for Cer-containing membranes, those parameters are similar for membranes with Phycer and Cer. This could be justified by the fact that the gel organization and topographic distribution is different for a membrane that contains Phycer or Cer, particularly regarding the interface layout/pattern and extent, which could cancel-out the effect of different molar fractions of the gel phase [24,25].

Comparing the two sterols, the partition of **Ke** is more efficient towards Erg-containing liposomes than Chol. This is an interesting result as it shows that there seems to be a preference towards Erg - the major fungal sterol. Furthermore, for the same compound and lipid concentration, **Ke** leads to higher disturbance of Erg-containing membranes than Chol-ones. This could be due to a preference towards Erg itself that **Ke** has, and/or the l_o phase formed by Erg membranes which have different biophysical properties (such as molar fraction of the l_o phase or dipole potential) [19–21] that facilitate **Ke** interaction. The presence of Chol in membranes is known to increase the dipole potential of membranes more than Erg or even their precursor zymosterol [21]. Drug-membrane interaction is affected by the dipole potential of the membrane [51–53]. For instance, if the dipolar moment of a compound aligns with the dipole potential of the membrane, then the interaction is more efficient/favorable. In this situation the opposite might be occurring, and **Ke** dipole moment is not aligning with the membrane dipole potential. In fact, the presence of **Ke** in the membranes used in this work might be changing other properties of the membrane, besides permeability, such as the dipole potential itself, a recurrent membranotropic feat by a number of compounds [54], such as anesthetics [55,56].

Despite the moderately high affinity of **Ke** towards POPC/Erg liposomes, membrane insertion is diminishing the quantum yield of the azole as shown by the value of I_L/I_W below 1 (Table 5.1). The same does not occur for POPC/Chol membranes, with the I_L/I_W value being 1.47 ± 0.10. Since this phenomenon only occurs in the presence of Erg it is possible that specific lipid-drug interactions are occurring between **Ke** and Erg, such as π-π stacking involving the diene in Erg ring and the aromatic ring of the **Ke** fluorophore. Alternatively, the partition towards the Erg-containing membrane could cause the molecules to be more closely together causing inter molecular self-quenching if, for instance, **Ke** has a preference for Erg-rich l_o phase. This decrease in quantum yield could be also related to a more superficial location of **Ke** in POPC/Erg liposome. In fact, two model compounds, **4MP** (1 (4 methoxyphenyl)-4-[(diphenylphosphino)methyl]piperazine) and **4MOP** (1-[(diphenylphosphoryl)methyl]-4-(4-methoxyphenyl)piperazine), containing virtually the same fluorophore which have a superficial location in POPC membranes also undergo a decrease of their fluorescence intensity upon partitioning to the lipid bilayer [17].

The lower affinity of **Ke** towards sterol-containing membranes is also in line with a possible more superficial location of the compound in these membranes when compared with POPC only liposomes. This is evidenced by the shift of the emission spectra peak wavelength in the presence of the highest lipid concentration for the systems containing Erg or Chol towards

higher values (374 nm) than for POPC (371 nm) (Table 5.1). Taking into consideration this shift in emission peak wavelength, a similar relative location is expected for **Ke** in Erg-membranes as in Chol-ones. In fact, if one considers that the polarity and hydration of the membrane with and without sterol is different (higher hydration for POPC) then the wavelength scale for each membrane system is different according to these biophysical properties. Indeed, considering the different membrane polarity, the emission peak wavelength obtained for sterol, of 374 nm, confirms the more superficial interaction of **Ke** with sterol membranes than POPC ones. Interestingly, the mole-fraction partition coefficient of **4MP**, a fluorescent model compound that contains the same fluorophore as **Ke**, towards POPC membranes [17] is similar to the one obtained for **Ke** towards Chol-ones. Therefore, it is possible that the interaction of **Ke** with a Chol containing membrane is similar to the one found for **4MP** with POPC ones.

Despite the clear differences between **Ke** interaction with fungal or mammalian sterols, the same can not be said for sphingolipids used in this work. For instance, the affinity of this azole is the same towards membranes containing Cer or Phycer with the same molar percentage. Moreover, the average leakage time of liposomes with either of these lipids due to the presence of **Ke** is virtually the same. The only exception is the maximum leakage percentage which for Cer is higher than for Phycer systems. Nevertheless, this only occurs specifically at 10 μM of **Ke** and 0.1 mM of lipid. If the effective compound/lipid ratio in the membrane (Figure 5.3 – E) is considered than it seems that Cer and Phycer share similar maximum leakage values after the addition of **Ke**. Therefore, all results point to no preferential interaction of **Ke** with either of these sphingolipids. Nonetheless, the POPC/Phycer and POPC/Erg in the molar proportions used in this work, are biophysically reliable model membrane systems for outer and inner leaflet, respectively, of the yeast plasma membrane [21,25]. In the mammalian case, POPC/Chol is the model membrane mixture which approaches some properties of the mammalian plasma membrane [19,21], as Chol is the single most abundant lipid and is represented in high amounts in both bilayer leaflets, while the biophysical properties of POPC/Cer do not truly reminisce that of any domains present in the mammalian plasma membrane, except perhaps upon stress or pro-apoptotic situations where Cer levels rise and Cer-rich platforms might form [29]. In this way, when comparing the lipid mixtures that mimic leaflets or domains of the yest plasma membrane with POPC/Chol, we find that **Ke** has a higher partition to the former. Moreover, the $K_{p,x}$ and permeabilizing ability of **Ke** towards POPC/Phycer or POPC/Erg is significantly higher than for POPC/Chol. This suggests that **Ke** has a preferential interaction with fungal membranes *vs* mammalian ones.

Even though the antifungal mode of action of **Ke** is through the inhibition of a transmembrane enzyme in the endoplasmic reticulum (ER) [1,57–59], its interaction with membranes must be considered to better understand its activity. Thus, the compound must reach the target either by crossing the plasma membrane or distributing along it and traffic via the endomembrane cell system. Imbalances in sphingolipid and sterol content in fungal plasma membrane have been correlated with increased susceptibility to azoles, since changes in these lipids affect the drug efflux pumps activity [60–62]. For instance, *Candida glabrata Cgipt1*Δ mutants that accumulate mannosylinositolphosphorylceramide (MIPC) instead of mannosyldiinositolphosphorylceramide ($M(IP)_2C$; the major complex sphingolipid found in the plasma membrane of most yeast) in the plasma membrane, have higher susceptibility to azole action than the wild-type one [63]. Also, in *Cgipt1*Δ mutants the overall membrane fluidity is increased [63]. This is in line with the results of the current work that show **Ke** with a stronger affinity for fluid-membranes than more rigid ones. Essentially, with a more fluid membrane **Ke** is able to distribute more efficiently in the plasma membrane. If azoles reach the target transmembrane enzyme in the ER *via* the endomembrane system, then a more fluid membrane increases the amount of compound that inhibits the enzyme. However, it is important to consider that the differences in **Ke**-membrane affinity could be due to the rigidity of the membranes, but also due to drug-lipid specific interactions.

5. Conclusions

In order to explore the interaction of **Ke** with different lipids and lipid phases, the affinity of this drug towards membranes containing POPC and Erg, Chol, Phycer or Cer in biologically justified molar proportions was quantified. For the same systems the permeabilizing abilities of **Ke** were determined using a permeability assay.

The results evidence that this antifungal drug interacts with both fluid and more ordered membranes, including those with a coexistence of l_d with l_o or gel phases. Also, **Ke** has particularly higher affinity and leads to higher permeability towards Erg-containing membranes than Chol. Nevertheless, there is still significant partition and disturbance of Chol-containing membranes, which actually might be also responsible for a relatively high cytotoxicity towards mammalian cells and adverse side effects when administrated orally. Additionally, the presence of sphingolipids appears to facilitate **Ke** permeabilizing ability. The comparison of the results obtained for the systems with Phycer and Erg *vs* Chol allows to anticipate that **Ke** has more affinity and permeabilizing ability towards fungal membranes than mammalian ones.

These findings are pertinent to improve the understanding of the mode of action and model pharmacokinetics of **Ke** itself. It is now highlighted that membrane lipid diversity must be considered in the development of new antifungal agents. Also, the differential interaction of **Ke** with different lipids offers a pathway to design more effective and targeted therapies, potentially reducing side effects that are associated with broad-spectrum antifungal drugs. These aspects are all relevant since they all help fighting the increasing numbers of fungal infections and fungal resistance to the drugs available in the market.

6. References

[1] N. Strushkevich, S.A. Usanov, H.W. Park, Structural basis of human CYP51 inhibition by antifungal azoles, J. Mol. Biol. 397 (2010) 1067–1078. https://doi.org/10.1016/J.JMB.2010.01.075.

[2] D.S. Loose, P.B. Kan, M.A. Hirst, R.A. Marcus, D. Feldman, Ketoconazole blocks adrenal steroidogenesis by inhibiting cytochrome P450-dependent enzymes., J. Clin. Invest. 71 (1983) 1495. https://doi.org/10.1172/JCI110903.

[3] M. Borgers, H. Van den Bossche, M. De Brabander, The mechanism of action of the new antimycotic ketoconazole, Am. J. Med. 74 (1983) 2–8. https://doi.org/10.1016/0002-9343(83)90507-7.

[4] A. Lupetti, R. Danesi, M. Campa, M. Del Tacca, S. Kelly, Molecular basis of resistance to azole antifungals, Trends Mol. Med. 8 (2002) 76–81. https://doi.org/10.1016/S1471-4914(02)02280-3.

[5] Y.Q. Zhang, S. Gamarra, G. Garcia-Effron, S. Park, D.S. Perlin, R. Rao, Requirement for Ergosterol in V-ATPase Function Underlies Antifungal Activity of Azole Drugs, PLoS Pathog. 6 (2010) 1000939. https://doi.org/10.1371/JOURNAL.PPAT.1000939.

[6] A. Luna-Tapia, M.E. Kerns, K.E. Eberle, B.S. Jursic, G.E. Palmer, Trafficking through the Late Endosome Significantly Impacts Candida albicans Tolerance of the Azole Antifungals, Antimicrob. Agents Chemother. 59 (2015) 2410. https://doi.org/10.1128/AAC.04239-14.

[7] L.A. García Rodrĩguez, A. Duque, J. Castellsague, S. Pérez-Gutthann, B.H.C. Stricker, A cohort study on the risk of acute liver injury among users of ketoconazole and other antifungal drugs, Br. J. Clin. Pharmacol. 48 (1999) 847–852. https://doi.org/10.1046/J.1365-2125.1999.00095.X.

[8] T.E. Knight, C.Y. Shikuma, J. Knight, Ketoconazole-induced fulminant hepatitis necessitating liver transplantation, J. Am. Acad. Dermatol. 25 (1991) 398–400. https://doi.org/10.1016/0190-9622(91)70214-M.

[9] F.D. Choi, M.L.W. Juhasz, N. Atanaskova Mesinkovska, Topical ketoconazole: a systematic review of current dermatological applications and future developments, Https://Doi.Org/10.1080/09546634.2019.1573309. 30 (2019) 760–771. https://doi.org/10.1080/09546634.2019.1573309.

[10] P. V. Poojary, S. Sarkar, A.A. Poojary, P. Mallya, R. Selvaraj, A. Koteshwara, J.M. Aranjani, S. Lewis, Novel anti-dandruff shampoo incorporated with ketoconazole-coated zinc oxide nanoparticles using green tea extract, J. Cosmet. Dermatol. 23 (2024) 563–575. https://doi.org/10.1111/JOCD.16027.

[11] C. Viecceli, A.C.V. Mattos, V.N. Hirakata, S.P. Garcia, T. da C. Rodrigues, M.A. Czepielewski, Ketoconazole as second-line treatment for Cushing's disease after transsphenoidal surgery: systematic review and meta-analysis, Front. Endocrinol. (Lausanne). 14 (2023) 1145775. https://doi.org/10.3389/FENDO.2023.1145775/BIBTEX.

[12] D. Doheny, S. Manore, S.R. Sirkisoon, D. Zhu, N.R. Aguayo, A. Harrison, M. Najjar, M. Anguelov, A.O. Cox, C.M. Furdui, K. Watabe, T. Hollis, A. Thomas, R. Strowd, H.W. Lo, An FDA-Approved Antifungal, Ketoconazole, and Its Novel Derivative Suppress tGLI1-Mediated Breast Cancer Brain Metastasis by Inhibiting the DNA-Binding Activity of Brain Metastasis-Promoting Transcription Factor tGLI1, Cancers (Basel). 14 (2022). https://doi.org/10.3390/CANCERS14174256.

[13] S. Naftalovich, E. Yefenof, Y. Eilam, Antitumor effects of ketoconazole and trifluoperazine in murine T-cell lymphomas, Cancer Chemother. Pharmacol. 28 (1991) 384–390. https://doi.org/10.1007/BF00685694.

[14] V. Patel, B. Liaw, W. Oh, The role of ketoconazole in current prostate cancer care, Nat. Rev. Urol. 15 (2018) 643–651. https://doi.org/10.1038/S41585-018-0077-Y.

[15] N. Weng, Z. Zhang, Y. Tan, X. Zhang, X. Wei, Q. Zhu, Repurposing antifungal drugs for cancer therapy, J. Adv. Res. (2022). https://doi.org/10.1016/J.JARE.2022.08.018.

[16] A. Bento-Oliveira, R. Starosta, R.F.M. de Almeida, Interaction of the antifungal ketoconazole and its diphenylphosphine derivatives with lipid bilayers: insights into their antifungal action, Arch. Biochem. Biophys. (2024). https://doi.org/10.1016/j.abb.2024.109919.

[17] A. Bento-Oliveira, R. Starosta, R.F.M. de Almeida, Diphenylphosphine oxide: a motif to improve membrane affinity and antifungal activity of ketoconazole, Under Revis. (2024).

[18] A.G. dos Santos, J.T. Marquês, A.C. Carreira, I.R. Castro, A.S. Viana, M.-P. Mingeot-Leclercq, R.F.M. de Almeida, L.C. Silva, The molecular mechanism of Nystatin action is dependent on the membrane biophysical properties and lipid composition, Phys. Chem. Chem. Phys. 19 (2017) 30078–30088. https://doi.org/10.1039/C7CP05353C.

[19] R.F.M. de Almeida, E. Joly, Crystallization around solid-like nanosized docks can explain the specificity, diversity, and stability of membrane microdomains., Front. Plant Sci. 5 (2014) 72. https://doi.org/10.3389/fpls.2014.00072.

[20] J.M. Vanegas, M.F. Contreras, R. Faller, M.L. Longo, Role of unsaturated lipid and ergosterol in ethanol tolerance of

model yeast biomembranes, Biophys. J. 102 (2012) 507–516. https://doi.org/10.1016/j.bpj.2011.12.038.
[21] A. Khmelinskaia, J.M.T. Marquês, A.E.P. Bastos, C.A.C. Antunes, A. Bento-Oliveira, S. Scolari, G.M. da S. Lobo, R. Malhó, A. Herrmann, H.S. Marinho, R.F. De Almeida, Liquid-ordered phase formation by mammalian and yeast sterols: a common feature with organizational differences, Front. Cell Dev. Biol. 8 (2020) 337. https://doi.org/10.3389/FCELL.2020.00337.
[22] L. Silva, A. Coutinho, A. Fedorov, M. Prieto, Competitive binding of cholesterol and ergosterol to the polyene antibiotic nystatin. A fluorescence study, Biophys. J. 90 (2006) 3625–3631. https://doi.org/10.1529/biophysj.105.075408.
[23] R.F.M. de Almeida, A. Fedorov, M. Prieto, Sphingomyelin/phosphatidylcholine/cholesterol phase diagram: boundaries and composition of lipid rafts., Biophys. J. 85 (2003) 2406–16. https://doi.org/10.1016/S0006-3495(03)74664-5.
[24] S.N. Pinto, L.C. Silva, A.H. Futerman, M. Prieto, Effect of ceramide structure on membrane biophysical properties: The role of acyl chain length and unsaturation, Biochim. Biophys. Acta - Biomembr. 1808 (2011) 2753–2760. https://doi.org/10.1016/J.BBAMEM.2011.07.023.
[25] J.T. Marquês, A.M. Cordeiro, A.S. Viana, A. Herrmann, H.S. Marinho, R.F.M. de Almeida, Formation and Properties of Membrane-Ordered Domains by Phytoceramide: Role of Sphingoid Base Hydroxylation., Langmuir. 31 (2015) 9410–21. https://doi.org/10.1021/acs.langmuir.5b02550.
[26] Y. Mizutani, A. Kihara, Y. Igarashi, Identification of the human sphingolipid C4-hydroxylase, hDES2, and its up-regulation during keratinocyte differentiation, FEBS Lett. 563 (2004) 93–97. https://doi.org/10.1016/S0014-5793(04)00274-1.
[27] Y. Masukawa, H. Narita, H. Sato, A. Naoe, N. Kondo, Y. Sugai, T. Oba, R. Homma, J. Ishikawa, Y. Takagi, T. Kitahara, Comprehensive quantification of ceramide species in human stratum corneum, J. Lipid Res. 50 (2009) 1708–1719. https://doi.org/10.1194/JLR.D800055-JLR200.
[28] R. T'Kindt, L. Jorge, E. Dumont, P. Couturon, F. David, P. Sandra, K. Sandra, Profiling and characterizing skin ceramides using reversed-phase liquid chromatography-quadrupole time-of-flight mass spectrometry, Anal. Chem. 84 (2012) 403–411. https://doi.org/10.1021/AC202646V.
[29] L. Silva, R.F.M. De Almeida, A. Fedorov, A.P.A. Matos, M. Prieto, Ceramide-platform formation and -induced biophysical changes in a fluid phospholipid membrane, Mol. Membr. Biol. 23 (2006) 137–148. https://doi.org/10.1080/09687860500439474.
[30] F. Aresta-Branco, A.M. Cordeiro, H.S. Marinho, L. Cyrne, F. Antunes, R.F.M. de Almeida, Gel domains in the plasma membrane of Saccharomyces cerevisiae: highly ordered, ergosterol-free, and sphingolipid-enriched lipid rafts., J. Biol. Chem. 286 (2011) 5043–54. https://doi.org/10.1074/jbc.M110.154435.
[31] G. Rouser, S. Fleischer, A. Yamamoto, Two dimensional thin layer chromatographic separation of polar lipids and determination of phospholipids by phosphorus analysis of spots, Lipids. 5 (1970) 494–496. https://doi.org/10.1007/BF02531316.
[32] S. Chiu, E. Jakobsson, S. Subramaniam, H. Scott, Combined monte carlo and molecular dynamics simulation of fully hydrated dioleyl and palmitoyl-oleyl phosphatidylcholine lipid bilayers, Biophys. J. 77 (1999) 2462. https://doi.org/10.1016/S0006-3495(99)77082-7.
[33] F. Foglia, A.F. Drake, A.E. Terry, S.E. Rogers, M.J. Lawrence, D.J. Barlow, Small-angle neutron scattering studies of the effects of amphotericin B on phospholipid and phospholipid-sterol membrane structure, Biochim. Biophys. Acta. 1808 (2011) 1574–1580. https://doi.org/10.1016/J.BBAMEM.2011.02.012.
[34] A.I. Greenwood, S. Tristram-Nagle, J.F. Nagle, Partial molecular volumes of lipids and cholesterol, Chem. Phys. Lipids. 143 (2006) 1. https://doi.org/10.1016/J.CHEMPHYSLIP.2006.04.002.
[35] N-(2-hydroxyhexadecanoyl)-4-hydroxysphinganine | ChemSpider, (n.d.). https://www.chemspider.com/Chemical-Structure.28533113.html?rid=e797b369-13ba-4799-a29e-e397f2de57f4 (accessed April 11, 2024).
[36] Ceramide (d18:1/16:0) | ChemSpider, (n.d.). https://www.chemspider.com/Chemical-Structure.4446677.html (accessed April 11, 2024).
[37] P.M. Matos, H.G. Franquelim, M.A.R.B. Castanho, N.C. Santos, Quantitative assessment of peptide-lipid interactions. Ubiquitous fluorescence methodologies, Biochim. Biophys. Acta - Biomembr. 1798 (2010) 1999–2012. https://doi.org/10.1016/J.BBAMEM.2010.07.012.
[38] D.K. Breslow, Sphingolipid Homeostasis in the Endoplasmic Reticulum and Beyond, Cold Spring Harb. Perspect. Biol. 5 (2013) 1–16. https://doi.org/10.1101/CSHPERSPECT.A013326.
[39] G. Daum, N.D. Lees, M. Bard, R. Dickson, Biochemistry, Cell Biology and Molecular Biology of Lipids of Saccharomyces cerevisiae, Yeast. 14 (1998) 1471–1510. https://doi.org/10.1002/(SICI)1097-0061(199812)14:16.
[40] R.C. Dickson, R.L. Lester, Yeast sphingolipids, Biochim. Biophys. Acta - Gen. Subj. 1426 (1999) 347–357. https://doi.org/10.1016/S0304-4165(98)00135-4.
[41] N. Pedroso, A.C. Matias, L. Cyrne, F. Antunes, C. Borges, R. Malhó, R.F.M. de Almeida, E. Herrero, H.S. Marinho, Modulation of plasma membrane lipid profile and microdomains by H2O2 in Saccharomyces cerevisiae, Free Radic. Biol. Med. 46 (2009) 289–298. https://doi.org/10.1016/j.freeradbiomed.2008.10.039.
[42] G. Daum, G. Tuller, T. Nemec, C. Hrastnik, G. Balliano, L. Cattel, P. Milla, F. Rocco, A. Conzelmann, C. Vionnet, D.E. Kelly, S. Kelly, E. Schweizer, H.J. Schüller, U. Hojad, E. Greiner, K. Finger, Systematic analysis of yeast strains with possible defects in lipid metabolism., Yeast. 15 (1999) 601–14. https://doi.org/10.1002/(SICI)1097-0061(199905)15:7<601::AID-YEA390>3.0.CO;2-N.
[43] D. Wüstner, Fluorescent sterols as tools in membrane biophysics and cell biology, Chem. Phys. Lipids. 146 (2007) 1–25. https://doi.org/10.1016/J.CHEMPHYSLIP.2006.12.004.
[44] L.M. Solanko, D.P. Sullivan, Y.Y. Sere, M. Szomek, A. Lunding, K.A. Solanko, A. Pizovic, L.D. Stanchev, T.G. Pomorski, A.K. Menon, D. Wüstner, Ergosterol is mainly located in the cytoplasmic leaflet of the yeast plasma

membrane, Traffic. 19 (2018) 198–214. https://doi.org/10.1111/TRA.12545.
[45] R.F.M. De Almeida, L.M.S. Loura, M. Prieto, A. Watts, A. Fedorov, F.J. Barrantes, Cholesterol Modulates the Organization of the γM4 Transmembrane Domain of the Muscle Nicotinic Acetylcholine Receptor, Biophys. J. 86 (2004) 2261. https://doi.org/10.1016/S0006-3495(04)74284-8.
[46] A.A. Aljohani, M.A. Alanazi, L.A. Munahhi, J.D. Hamroon, Y. Mortagi, M. Qushawy, G.M. Soliman, Binary ethosomes for the enhanced topical delivery and antifungal efficacy of ketoconazole, OpenNano. 11 (2023) 100145. https://doi.org/10.1016/J.ONANO.2023.100145.
[47] N. Dudhipala, A.A. AY, Amelioration of ketoconazole in lipid nanoparticles for enhanced antifungal activity and bioavailability through oral administration for management of fungal infections, Chem. Phys. Lipids. 232 (2020) 104953. https://doi.org/10.1016/J.CHEMPHYSLIP.2020.104953.
[48] S. Raut, N. Gargate, S. Ugale, K.N. Gujar, H. Kapare, Formulation and Development of Hyaluronic Acid based Gel with Ketoconazole-Loaded Nanostructured Lipid Carriers in Fungal Infection, Pharm. Nanotechnol. 11 (2023) 344–354. https://doi.org/10.2174/2211738511666230310103017.
[49] A. Bento-Oliveira, M.-L.C.J. Moita, R.F.M. de Almeida, R. Starosta, Unraveling environmental effects in the absorption and fluorescence spectra of p-methoxyphenylpiperazine derivatives, Spectrochim. Acta - Part A Mol. Biomol. Spectrosc. 306 (2024). https://doi.org/10.1016/j.saa.2023.123583.
[50] R.M. Cordeiro, Molecular Structure and Permeability at the Interface between Phase-Separated Membrane Domains, J. Phys. Chem. B. 122 (2018) 6954–6965. https://doi.org/10.1021/ACS.JPCB.8B03406/SUPPL_FILE/JP8B03406_SI_002.ZIP.
[51] T. Asawakarn, J. Cladera, P. O'Shea, Effects of the membrane dipole potential on the interaction of saquinavir with phospholipid membranes and plasma membrane receptors of Caco-2 cells, J. Biol. Chem. 276 (2001) 38457–38463. https://doi.org/10.1074/JBC.M103269200.
[52] J. Cladera, I. Martin, J.M. Ruysschaert, P. O'Shea, Characterization of the sequence of interactions of the fusion domain of the simian immunodeficiency virus with membranes. Role of the membrane dipole potential, J. Biol. Chem. 274 (1999) 29951–29959. https://doi.org/10.1074/JBC.274.42.29951.
[53] J. Guillén, P.K.J. Kinnunen, J. Villalaín, Membrane insertion of the three main membranotropic sequences from SARS-CoV S2 glycoprotein, Biochim. Biophys. Acta. 1778 (2008) 2765–2774. https://doi.org/10.1016/J.BBAMEM.2008.07.021.
[54] S.S. Efimova, O.S. Ostroumova, Modulation of the Dipole Potential of Model Lipid Membranes with Phytochemicals: Molecular Mechanisms, Structure–Activity Relationships, and Implications in Reconstituted Ion Channels, Membranes (Basel). 13 (2023). https://doi.org/10.3390/MEMBRANES13040453.
[55] D.S. Cafiso, Dipole potentials and spontaneous curvature: membrane properties that could mediate anesthesia, Toxicol. Lett. 100–101 (1998) 431–439. https://doi.org/10.1016/S0378-4274(98)00217-3.
[56] B.M. Davis, J. Brenton, S. Davis, E. Shamsher, C. Sisa, L. Grgic, M.F. Cordeiro, Assessing anesthetic activity through modulation of the membrane dipole potential, J. Lipid Res. 58 (2017) 1962–1976. https://doi.org/10.1194/JLR.M073932.
[57] J.H. Van Tyle, Ketoconazole. Mechanism of action, spectrum of activity, pharmacokinetics, drug interactions, adverse reactions and therapeutic use, Pharmacotherapy. 4 (1984) 343–373. https://doi.org/10.1002/J.1875-9114.1984.TB03398.X.
[58] D. Borelli, J.L. Bran, J. Fuentes, R. Legendre, E. Leiderman, H.B. Levine, A. Restrepo, D.A. Stevens, Ketoconazole, an oral antifungal: laboratory and clinical assessment of imidazole drugs., Postgrad. Med. J. 55 (1979) 657–661. https://doi.org/10.1136/PGMJ.55.647.657.
[59] RCSB PDB - 5FSA: Crystal structure of sterol 14-alpha demethylase (CYP51) from a pathogenic yeast Candida albicans in complex with the antifungal drug posaconazole, (n.d.). https://www.rcsb.org/structure/5fsa (accessed October 15, 2021).
[60] K. Mukhopadhyay, T. Prasad, P. Saini, T.J. Pucadyil, A. Chattopadhyay, R. Prasad, Membrane sphingolipid-ergosterol interactions are important determinants of multidrug resistance in Candida albicans., Antimicrob. Agents Chemother. 48 (2004) 1778–87.
[61] J. Gao, H. Wang, Z. Li, A.H.H. Wong, Y.Z. Wang, Y. Guo, X. Lin, G. Zeng, Y. Wang, J. Wang, Candida albicans gains azole resistance by altering sphingolipid composition, Nat. Commun. 9 (2018). https://doi.org/10.1038/S41467-018-06944-1.
[62] J. Song, X. Liu, R. Li, Sphingolipids: Regulators of azole drug resistance and fungal pathogenicity, Mol. Microbiol. 114 (2020) 891–905. https://doi.org/10.1111/MMI.14586.
[63] G. Shahi, M. Kumar, N.K. Khandelwal, A. Banerjee, P. Sarkar, S. Kumari, B.D. Esquivel, N. Chauhan, A. Chattopadhyay, T.C. White, N.A. Gaur, A. Singh, R. Prasad, Inositol Phosphoryl Transferase, Ipt1, Is a Critical Determinant of Azole Resistance and Virulence Phenotypes in Candida glabrata, J. Fungi (Basel, Switzerland). 8 (2022). https://doi.org/10.3390/JOF8070651.
[64] L.M.S. Loura, M. Prieto, Dehydroergosterol structural organization in aqueous medium and in a model system of membranes, Biophys. J. 72 (1997) 2226–2236. https://doi.org/10.1016/S0006-3495(97)78866-0.

Supplementary Material

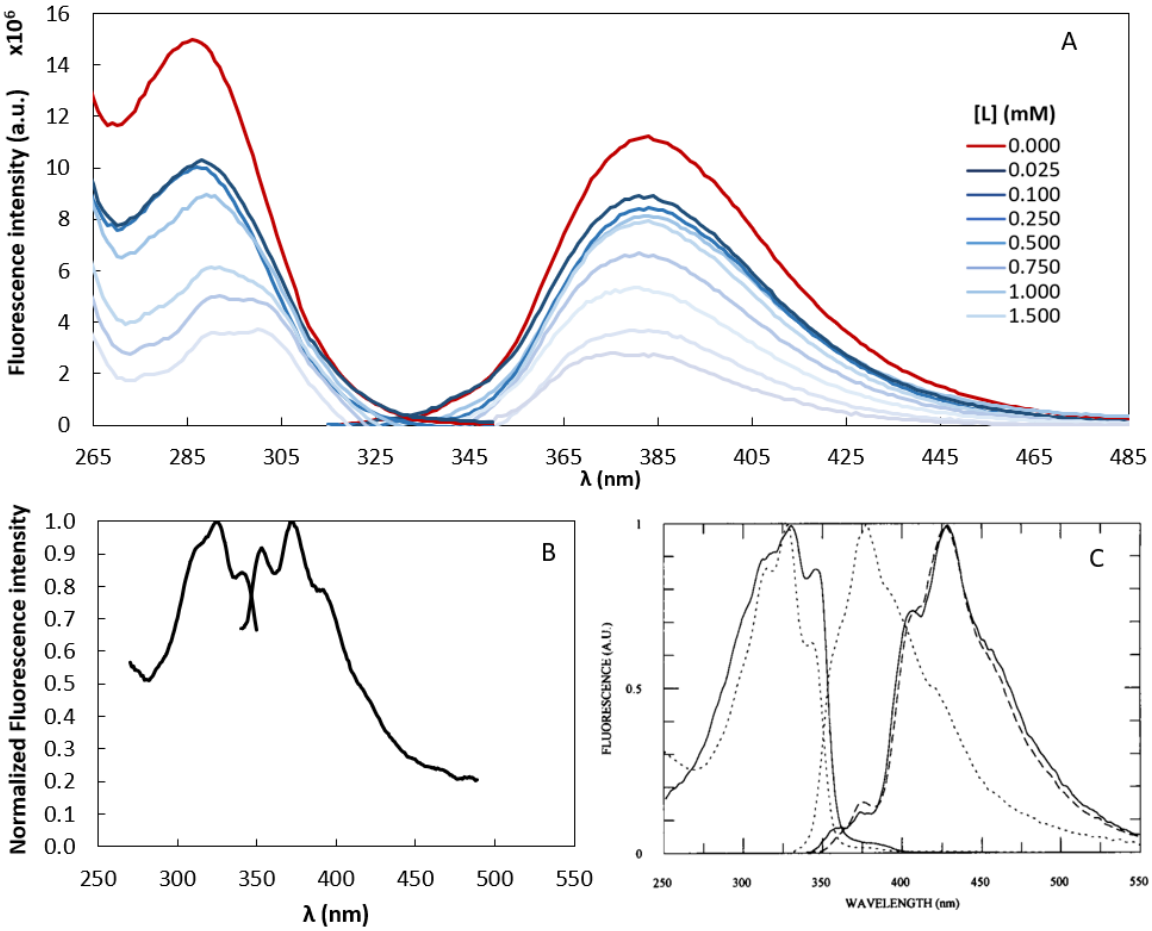

Figure S5. 1: **Ke fluorescence spectra in the presence of POPC/Erg 40 mol% liposomes.** (A) Fluorescence excitation and emission spectra of **Ke** for increasing lipid concentrations. (B) Normalized fluorescence excitation and emission spectra of the blank samples, *i.e.* containing only POPC/Erg 40 mol% ([L] = 1 mM) liposomes without **Ke**, comparable to (C) the spectra of DHE (figure reproduced from [64]). In C the solid lines represent DHE in buffer (50 mM Tris-HCl, pH 7.4, 50 mM NaCl, 0.2 mM EDTA), the dots DHE in chloroform solution and the dashed lines the polycrystalline powder. Please note that the spectra in B were obtained with the acquisition parameters (such as excitation and emission wavelengths) used for the spectra of **Ke**, hence the truncated edges.

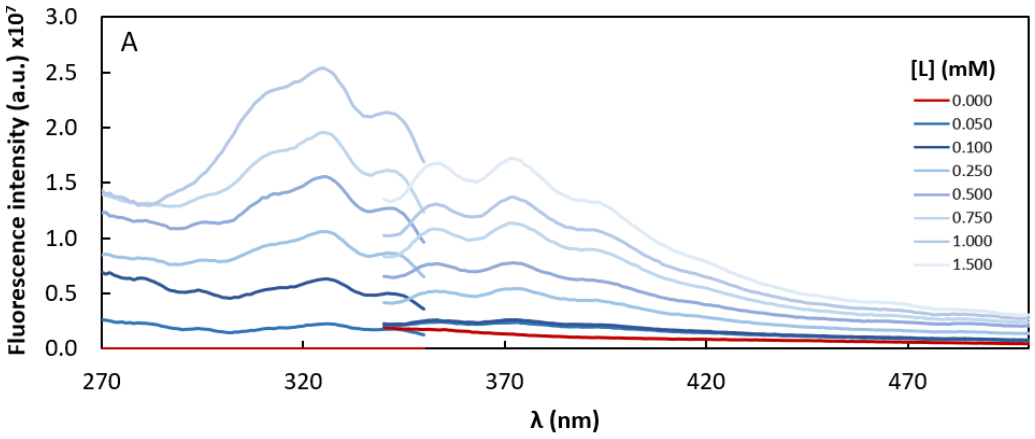

Figure S5. 2: Excitation and emission spectra obtained with parameters of Ke (please check the methods section) but without this compound and only POPC with 40 mol% of Erg in different total lipid concentration.

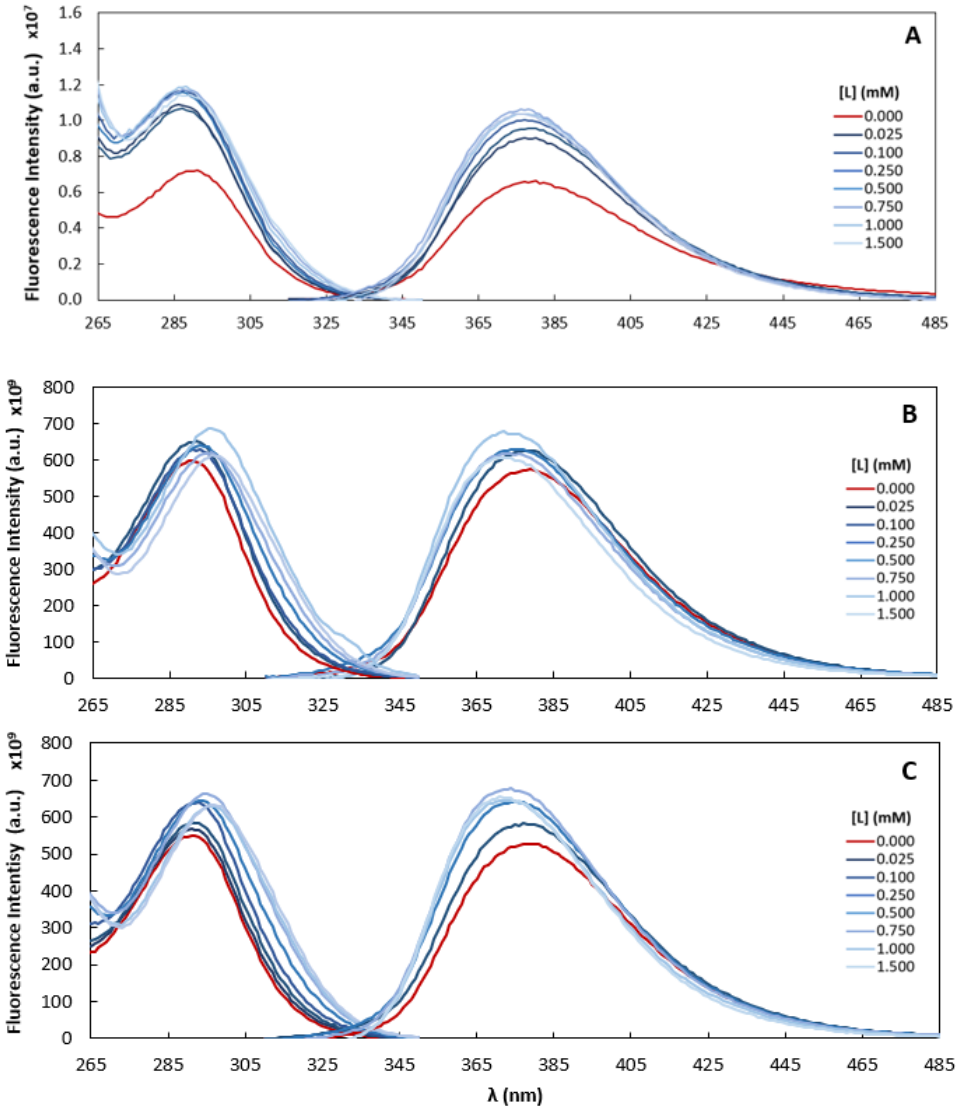

Figure S5. 3: Interaction of Ke with POPC/Chol, POPC/Cer and POPC/Phycer lipid bilayers monitored through its intrinsic fluorescence. The fluorescence excitation and emission spectra of **Ke** for increasing total lipid concentration are represented for systems with 30 mol% of Chol (A), 20 mol% of Cer (B) or 20 mol% of Phycer (C) mixed with POPC. The concentration of **Ke** was 10 µM.

CHAPTER VI

PREFERENTIAL INTERACTION OF THE ANTIFUNGAL NYSTATIN WITH PHYTOCERAMIDE-CONTAINING MEMBRANES

Contribution: Took an active part in the formal analysis, investigation, writing and preparation of the original draft and visualization. I conducted the nystatin activity assay and analysed the data from the lipid monolayers.

Preferential Interaction of the Antifungal Nystatin with Phytoceramide-Containing Membranes

Andreia Bento-Oliveira[1], Mafalda Guimarães[1], Franscesca Fedeli[1], Joaquim T. Marquês[1], Liana C. Silva[2,*], Rodrigo F. M. de Almeida[1,*]

[1] Centro de Química Estrutural, Institute of Molecular Sciences, Departamento de Química e Bioquímica, Faculdade de Ciências, Universidade de Lisboa, Campo Grande, 1749-016 Lisboa, Portugal.

[2] Research Institute for Medicines (iMed.ULisboa), Faculdade de Farmácia, Universidade de Lisboa, 1649-003 Lisboa, Portugal

* Correspondence: Rodrigo F.M. de Almeida rfalmeida@fc.ul.pt, Tel. : +351-217-500-925;
Liana C. Silva lianacsilva@ff.ulisboa.pt; Tel:. +351 217 946 429 (ext. 14244)

Abstract

Sphingolipid-enriched domains (SLEDs) are a unique feature of the fungal plasma membrane, as they are highly rigid ergosterol depleted gel domains found in growing fungi. Sphingolipids predominate in the outer leaflet of the fungal plasma membrane, while ergosterol is mainly localized in the inner one, supporting the hypothesis that polyene antifungal drugs may actually target sphingolipids, particularly SLEDs, instead of ergosterol in the fungal plasma membrane.

Nystatin (Nys) is a polyene which fungicidal activity results from the formation of pores in the membrane of fungal cells. Although Nys has a preference for forming pores in ordered lipid bilayers it is still unknown if the activity of this antifungal drug is enhanced by the presence of fungal sphingolipids (or SLEDs) vs mammalian ones. To clarify this, the interaction of Nys with the membrane was studied in model systems containing ceramide (Cer) or phytoceramide (Phycer): the major backbone of mammalian or fungal sphingolipids, respectively.

In 1-palmitoyl-2-oleoyl-*sn*-glycerol-3-phosphocholine (POPC) based liposomes, the steady-state and time-resolved fluorescence properties of Nys were clearly altered by the presence of Phycer but not Cer, suggesting a preferential interaction of Nys with Phycer- but not Cer-rich domains. Moreover, Nys had a stronger influence in the compressibility properties of Phycer monolayers than Cer ones. Finally, the pore-forming activity of the polyene towards POPC/Phycer and POPC/Cer liposomes was quantified by using a H^+/K^+ exchange assay. In general, Nys activity tends to be higher in liposomes containing Phycer rather than Cer, which is especially noticeable at longer incubation times and/or higher Nys concentrations.

The preference of Nys for Phycer-rich domains, which mimic fungal membrane SLEDs, versus Cer-rich domains, points to a potential role of SLEDs in the antifungal activity of Nys, and its higher activity towards fungal cells than mammalian ones.

Keywords

Nystatin, Membrane model systems, Phytoceramide, Ceramide, Fluorescence spectroscopy, Membrane compressibility properties

1. Introduction

Currently, a frightening number of fungal infections that no longer respond to the existent antifungal therapies is found, especially among immunocompromised patients [1–3]. It is relevant that new or improved antifungal drugs are developed in order to fight these infections. However, the development of antifungal drugs is complex due to the resemblance of fungi and mammals, sharing similar targets which lead to potential toxicity risk.

Polyenes represent the oldest class of antifungal drugs available in the market, and are characterized by powerful fungicidal activity, wide spectrum of action and low resistance rate. However, this category of compounds has toxicity problems which severely limit their use. Nystatin (Nys) is a Food and Drug Administration (FDA) approved antifungal agent [4] that, as a polyene, has a macrolactonic ring containing conjugated double bonds (2+4), *O*-linked to a D-mycosamine group (Figure 6.1). This macrolide polyene was first discovered in bacterium *Streptomyces noursei* in the early 1950s. There are three different components of Nys, A_1, A_2 and A_3, all with biological activity [5,6], but the component that is typically used in marketed drugs is A_1, which was the one used in the present work (Figure 6.1).

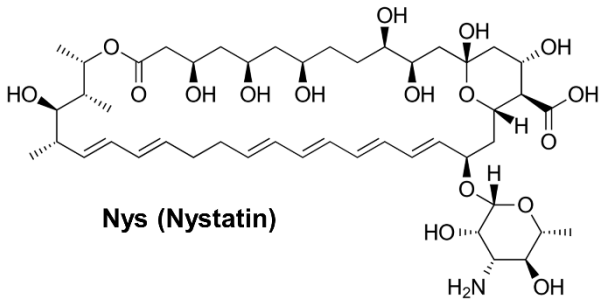

Figure 6. 1: Molecular structure of the antifungal drug Nystatin (Nys) A_1.

Nys has fungistatic activity against various types of yeasts and fungi, mainly from the genus *Candida*. However, the free drug has low absorption from the gastrointestinal tract and

is also toxic and ineffective when administered systemically due to its hydrophobic nature. Therefore, it is currently used in topical vaginal, cutaneous and oral treatment [7,8].

Regarding its mechanism of action, the most accredited model is that Nys forms small-diameter pores in the plasma membrane of fungi, by formation of stoichiometric Nys-Ergosterol (Erg) complexes that promote leakage of cytoplasmic components and membrane disruption leading to cell death. Nys has a preference towards Erg, the major sterol found in fungal membranes, when compared to cholesterol, that grants selective toxicity of this compound against fungal cells [9,10]. However, there are controversies regarding the role of Erg and its indispensability in the mechanism of action of polyene antifungals. For instance, yeast strains with similar sterol content but different sphingolipid profile have different sensitivity to the drug [11,12]. Moreover, polyene macrolides are active in sterol-free highly ordered lipid bilayers [13]. Particularly Nys has a strong pore-forming activity in membranes with 1,2-dipalmitoyl-*sn*-glycero-3-phosphocholine (DPPC)/1-palmitoyl-2-oleoyl-*sn*-glycerol-3-phosphocholine (POPC) or sphingomyelin/POPC that have gel phases but no sterol [13]. Also, the partition of Nys is stronger towards membranes containing gel phases [13] in opposition to more fluid membranes [13,14]. Another aspect to consider is the similar tetraene motif of Nys with *trans*-parinaric acid (*t*-PnA), a fluorescent membrane probe that partitions preferentially towards gel domains [15–18]. Due to this, it seems that Nys has a preference towards membranes containing gel-phases.

Under physiological conditions while it is not possible to find gel domains in membranes of mammals, the fungal plasma membrane contains distinct gel domains, the sphingolipid-enriched domains (SLEDs) [16,18]. SLEDs are a feature of the fungal plasma membrane being different from the prototypical mammalian sphingolipid/cholesterol rich domains, lipid rafts, since in terms of composition SLEDs contain close to no sterol, and biophysically these lipid domains are highly ordered gel domains [19]. Some of the functions attributed to these lipid domains include adaptation to stress [18,20–25], cell division [26], trafficking and signaling [18,27–29].

There are differences at the headgroup, chain length and hydroxylation of sphingolipids of fungi when comparing with those of mammals [19], that account for different sphingolipid domains in each phylogenetic kingdom. Ceramide (Cer) and phytoceramide (Phycer) are the major backbone for complex sphingolipids in mammals and fungi respectively. At the molecular level both molecules result from a sphingoid or long chain base bound to a fatty acid. However, the sphingoid base of Phycer, phytosphingosine, has an additional hydroxyl group instead of a *trans* double bond at C-4, when compared to the sphingosine of Cer (Figure 6.2).

At room temperature, both molecules can induce the formation of highly ordered gel domains with different biophysical properties [24,30].

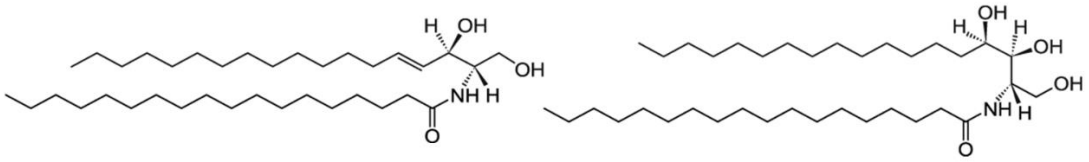

Figure 6. 2: Molecular structure of Ceramide (*N*-stearoyl-D-*erythro*-sphingosine; left) and Phytoceramide (*N*-stearoyl 4-hydroxysphinganine; right) used in this work.

In this work, Nys preference towards sterol-free membranes containing Phycer *vs* Cer, was explored. The fluorescence properties of Nys were studied in the presence of liposomes containing POPC with either Cer or Phycer, to better understand the interaction of this tetraene antifungal with sterol-free membranes. Also, the pore-forming activity of Nys in liposomes with the same composition was evaluated. Finally, different quantities of Nys were added to monolayers of Phycer or Cer, to determine how the presence of Nys affects the compressibility and mean molecular area of each monolayer. All results point to a preferential interaction of Nys with Phycer in detriment of Cer-enriched domains.

2. Materials and Methods

2.1. Chemicals

POPC was obtained from Lipoid (Ludwigshafen, Germany). Cer and Phycer were purchased from Merck (Darmstadt, Alemanha). DMSO and HEPES were acquired from Fisher Chemical (Waltham, MA, USA). Pyranine, Nys, and the other reagents were purchased from Merck and used without further purifications.

POPC stock solutions concentration was determined by phosphate quantification [37] and kept at -20 °C in chloroform. Cer and Phycer were quantified using a gravimetry assay with a highly precision balance (10^{-5} g precision), and then kept at -20 °C in chloroform/methanol (2:1). The Nys stock solution was stored at -20 °C always protected from light and its concentration was determined spectroscopically with a Jasco V-560 spectrophotometer (Easton, MD, USA) using a molar absorption coefficient of 6.3 x 10^4 $M^{-1}cm^{-1}$ at 303 nm in ethanol [13]. For the studies with lipid monolayers, Nys was dissolved in chloroform to allow for a quicker solvent evaporation, and its quantity was determined by gravimetry.

2.2. Nystatin fluorescence properties in the presence of liposomes

2.2.1. Liposome preparation

Large unilamellar vesicles (LUVs) containing POPC, POPC/DPPC, POPC/Cer or POPC/Phycer with the desired ratio of lipids were prepared as previously described [38], but instead of 100 nm membrane filters, 400 nm were used in the current work. Briefly, an adequate volume of the stock solution of lipid was evaporated under a nitrogen stream to form a lipid film and left in a vacuum desiccator overnight to remove all organic solvent. The film was hydrated by adding HEPES buffer (10 mM pH 7.4, 150 mM NaCl) and the final lipid concentration was 1 mM. The samples were mixed in a vortex for a few minutes and were left for 1 h at room temperature before starting freeze/thaw cycles. The cycles were repeated 5 times using liquid nitrogen and a water bath set to 50 °C. The multilamellar vesicles suspension was subjected to extrusion through polycarbonate Nucleopore Track Etch Membrane filters with 400 nm pore size from Whatman® (GE Healthcare, Little Chalfont, UK) by using a Mini-extruder from Merck under constant heating conditions at a temperature above the melting temperature of the gel domains [24,31]. The sample, during the extrusion, was passed through the filter 21 times to guarantee a homogeneous dimensional distribution of the liposomes, which was confirmed by dynamic light scattering (Table S6.1). The LUVs suspension thus obtained, after reaching room temperature, was left at 4 °C to stabilize overnight.

2.2.2. Fluorescence Spectroscopy Measurements

Before any measurement, the antifungal agent, Nys, was added to have a final concentration of 5, 10, 15 and 20 μM in 1 mM of LUVs and left incubating for 2 h at room temperature, protected from light.

Fluorescence measurements were carried out on a Fluorolog 3-22 spectrofluorimeter from Horiba Jobin-Yvon (Villeneuve D'ascq, France) in right angle geometry, at 23.0 ± 1.0 °C in a sample compartment with temperature-control and magnetic stirring, using quartz cuvettes from Hellma Analytic (Mülheim, Germany). The spectrofluorimeter was equipped with a 450 W Xenon arc lamp, double monochromators in both excitation and emission, and with Glan-Thompson polarizers. Fixed wavelength of excitation (λ_{ex}) and emission (λ_{em}), 304 nm and 404 nm, respectively, were used to carry out steady-state measurements [13]. Both in excitation and emission the values of bandwidth were 4 nm, while for anisotropy measurements the bandwidths were 8 nm. Data was corrected for inner filter effects according to the optical path lengths used in excitation and emission.

To determine the value of steady-state fluorescence anisotropy, ⟨r⟩, the following Equation (1) was used:

$$\langle r \rangle = \frac{(I_{VV} - G \times I_{VH})}{(I_{VV} + 2G \times I_{VH})} \quad (1)$$

in which the subscripts indicate the orientation of the excitation and emission polarizers, where V and H correspond to vertical and horizontal orientations and *G* is a correction factor for the different sensitivity of the detector to each light polarization plane and corresponds to the ratio I_{HV} / I_{HH}. An adequate blank was subtracted from each intensity reading.

A nanoLED source N-320, from Horiba Jobin-Yvon was used for the excitation of Nys at 315 nm for time-resolved fluorescence measurement by single-photon counting technique. The TBX detector (Horiba) used has a time resolution of 50 ps. In the peak channel, the number of counts was 20 000 and the number of channels was approximately 1000. The instrument response function for reconvolution was obtained using a diluted Ludox (from Sigma) suspension as a scatterer. For the analysis of fluorescence decays the program TRFA Data Processor (Minsk, Belarus) version 1.4 was used. The fluorescence intensity decays of Nys were described by a multiexponential model according to the following equation.

$$I(t) = \sum_{i=1}^{n} p_i \exp\left(-\frac{t}{\tau_i}\right) \quad (2)$$

The pre-exponential factors (p_i), were normalized to obtain the normalized pre-exponential or amplitude α_i, that were then used to determine the intensity- ($\langle\tau\rangle$) or amplitude- ($\bar{\tau}$) weighted mean fluorescence lifetime according to the following equations, respectively:

$$\langle\tau\rangle = \frac{\sum \alpha_i \tau_i^2}{\sum \alpha_i \tau_i} \quad (3)$$

$$\bar{\tau} = \sum_{i=1}^{n} \alpha_i \tau_i \quad (4)$$

Values of χ^2 were considered acceptable below 1.5 for the more complex decays, and in general, they were below 1.2. To judge the quality of the fit, visual inspection of the residuals and autocorrelation plots was also made.

The background obtained from liposomes with ethanol only instead of Nys, were appropriately subtracted in all fluorescence measurements.

2.3. Nystatin activity assays with pyranine

LUVs containing POPC, POPC/DPPC (50 mol%), POPC/Cer and POPC/Phycer (20 mol% of the sphingolipids) at 3 mM were prepared in K-buffer (20 mM HEPES, 100 mM K_2SO_4, pH 7.4) containing 0.5 mM pyranine as described in section 2.2.1.

The pyranine outside the LUVs was separated using a Sephadex G-25 filtration column (Disposable PD Desalting Columns, Merck) equilibrated with K-buffer. Each LUV suspension was incubated for 10 minutes with carbonyl cyanide-*p*-trifluoromethoxyphenylhydrazone (FCCP) to a FCCP:lipid ratio of 1:470. The transmembrane potassium gradient (3.3:1 $[K^+]_{in}$:$[K^+]_{out}$) was obtained by adding K-free buffer (20 mM HEPES-KOH, pH 7.4; 230 mM sucrose; 3 mM NaN_3).

The sample was loaded to a 96 well Greiner black/clear bottom microplate, and the fluorescence intensity was measured at 510 nm after excitation at 405 nm and 450 nm, for 10 minutes in a microplate reader Spectramax Gemini EM from Molecular Devices (San José, CA, USA), at 24 °C. Nys was added to a final concentration of either 5 or 15 μM, and fluorescence was measured for 42 minutes. Valinomycin dissolved in DMSO was added to a final concentration of 13.4 μM, and the fluorescence was measured for 10-20 minutes. Finally, Triton X-100 was added at 1% (v/v), and a final 10–20-minute measurement was performed.

2.4. Compressibility curves of lipid monolayers

Lipid monolayers were formed in a Kibron (Helsinki, Finland) Microthrough G2 Langmuir-Blodgett, in an aqueous surface of phosphate buffered saline (10 mM phosphate, 2.7 mM KCl, 137 mM NaCl, pH 7.4; PBS) at room temperature. All measurements were performed with stirring. The probe was calibrated with Milli-Q water (18 MΩ) using as a reference the surface tension of water at 24 °C (71.8 mN/m [39]). Before adding any lipid solution, compressibility isotherms curves were measured with just the buffer, to confirm the purity of the water interface and that the surface pressure was constant.

Lipids were spread along the buffer surface using a glass syringe, and for 10 min the Langmuir-Blodgett trough was left untouched to guarantee the evaporation of the organic solvent. The quantities of POPC, Phycer and Cer added were respectively 7.5×10^{-9}, 9.0×10^{-9} and 1.5×10^{-8} mol. Compressibility curves were measured with a compression speed of 10 mm/min, until it reached 40 mN/m, avoiding the collapse of the monolayer. For all monolayers, 2 to 3 isothermal compression semi-cycles were performed. After measuring the

curves for the lipid monolayers, Nys was added to the same system, according to the desired Nys/lipid ratio, and more compressibility measurements were performed.

Monolayers containing only Nys (in the absence of lipid) were also prepared with different quantities of the polyene (Figure S6.3 – B).

For the lipid monolayers to which Nys was added, the excess area per molecule (A_{ex}) at π = 20 mN/m was determined using the following equation [40]:

$$A_{ex} = A_{Lip+Nys} - \left(A_{Lip}\chi_{Lip} + A_{Nys}\chi_{Nys}\right) \quad (5)$$

where A_{Lip} and A_{Nys} are the average area per molecule of lipid and Nys at π = 20mN/m, respectively, obtained from the monolayers prepared with each component solely (Figure S3 - A and B), and $A_{Lip+Nys}$ being the average area per molecule in the mixture with the two components, obtained from the mixed monolayers in Figure 6.7 – A-C. χ_{Lip} and χ_{Nys} are the molar fraction of lipid and Nys, respectively.

2.5. Dynamic light scattering

The average size of the liposomes and polydispersity index (PDI) was determined by dynamic light scattering (DLS) on a Zetasizer Nano S instrument (Malvern instrument, UK). The liposome suspension was adequately diluted with HEPES buffer, usually 10 times, to reduce the high turbidity of the sample that could alter the results. Average particle diameter and PDI were obtained from the average of three measurements (10 runs, 2s/run).

2.6. Statistical analysis

The results are presented as mean ± standard deviation (S.D.), and the sample dimension and number of biologically independent replicates are given with the results. The statistical significance was determined using one or two-way Anova with Tukey's *post-hoc*. Mean values were considered significantly different for *p* values below or equal to 0.05.

3. Results

3.1. Different interaction of Nys with POPC, Phycer or Cer lipid bilayers

To understand if the interaction of Nys with membranes containing Phycer or Cer is different, the intrinsic fluorescence properties of Nys were studied in the presence of liposomes containing POPC and each one of these sphingolipids at 10 or 20 mol%.

The LUVs used in these studies and in the activity assays (Section 3.3) had a larger diameter (~200 nm) compared to the typical 100 nm liposomes used in previous studies on Nys-

membrane interactions (*e.g.* [9,13]). This larger vesicle size was chosen because Phycer tends to form highly rigid structures when distributed along the membranes. In smaller vesicles, these lipids are constrained closer together, increasing this rigidity and potentially causing the sphingolipids to be retained by the filter used to prepare the LUVs

3.1.1. Steady-state fluorescence of Nys

Assuming that the formation of Nys oligomers in the membrane are the main factors that affects the fluorescence spectra of this drug [41] detailed study of these spectral changes is essential to understand the interaction between Nys and POPC liposomes enriched with Cer or Phycer. The emission spectra of Nys both in the presence of Cer- and Phycer-containing membranes shows the centered emission band at 404 nm (Figure S6.1). Also, the excitation spectra showed three peaks resulting from the characteristic vibrational progression of the absorption band of a tetraene-containing compound [42].

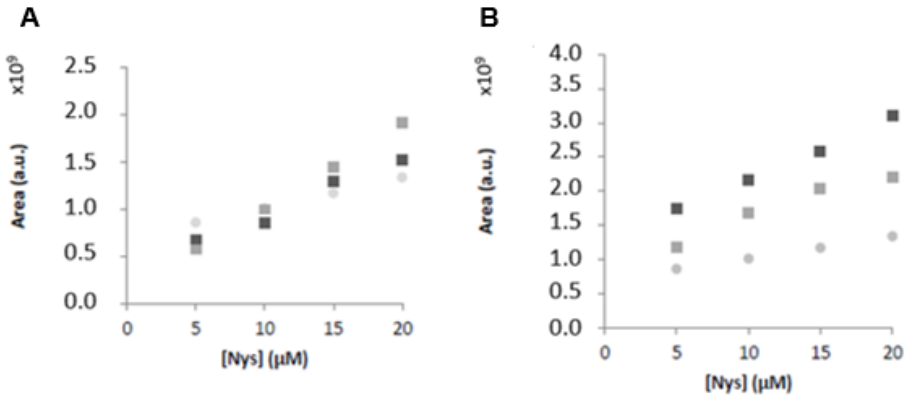

Figure 6. 3: Effect of the presence of Cer and Phycer in Nys fluorescence spectra. Area under the curve of the excitation spectra in the presence of POPC LUVs 100 mol% (grey circles), 10 (grey squares) and 20 mol% (black squares) of Cer (A) and Phycer (B).

In all systems, there is a consistent linear increase in the areas under the curve of excitation spectra with Nys concentration, as anticipated (Figure 6.3). Interestingly, at 5 and 10 μM of the drug, the area under the curve of the excitation spectra inversely decreases with the increase in Cer gel fraction (Figure 6.3 – A). This trend appears to vary at 15 μM, and notably at 20 μM, where the area under the spectra seems to be higher in the sample with the higher gel fraction. A different result was obtained with Phycer liposomes. The intensity of the excitation spectra increases according to the increase in Phycer mol%.

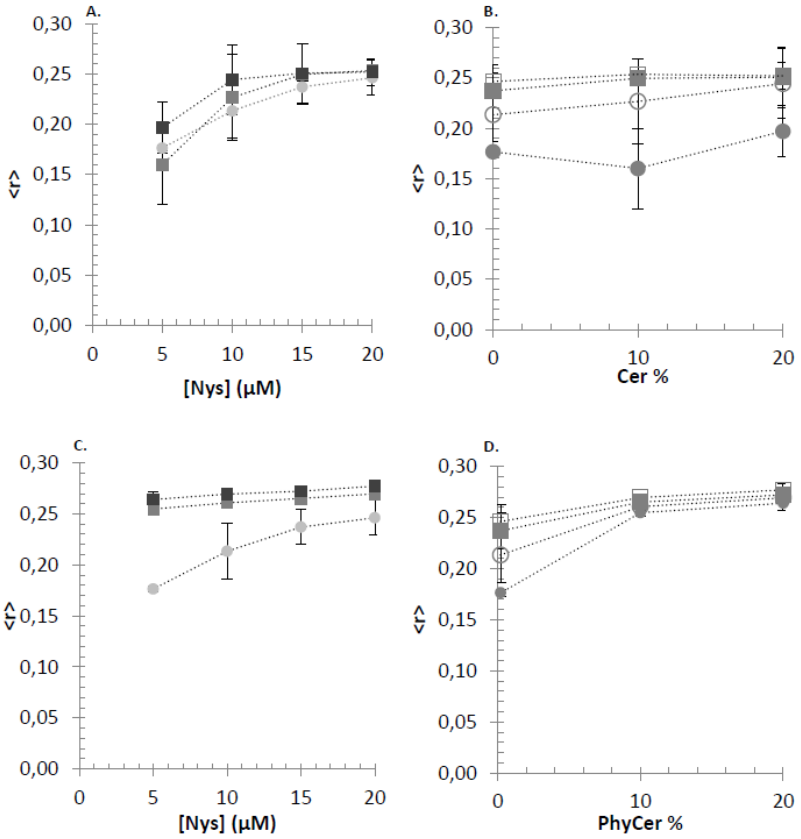

Figure 6. 4: Effect of the presence of Cer (A and B) and Phycer (C and D) in Nys fluorescence anisotropy. For the fluorescence anisotropy plotted as a function of Nys concentration (A and C), grey circles represent POPC LUVs 100 mol%, while grey squares and black squares represent the 10 and 20 mol%, respectively, of sphingolipid in LUVs with POPC. For the fluorescence anisotropy plotted as a function of sphingolipid mol%, the Nys concentration was 5 (●),10 (○), 15 (▪) and 20 µM (□). The excitation wavelength was set to 303 nm and emission was collected at 404 nm. The values are the mean ± S.D. of at least three independent replicates.

Figure 6.4 shows the steady-state fluorescence anisotropy of Nys plotted as a function of the molar fractions of Cer (χ_{Cer}) and Phycer (χ_{Phycer}), as well as Nys concentration. An increase in Nys anisotropy is observed with χ_{Phycer} (Figure 6.4 - D), particularly noticeable from 0 to 10 mol%, with a slight increase from 10 to 20 mol%. Interestingly in liposomes containing 10 mol% and 20 mol% of Phycer, the anisotropy values are independent of Nys concentrations (Figure 6.4 - C). In contrast, in Cer containing membranes, the anisotropy shows an hyperbolic trend with increasing Nys concentration (Figure 6.4 - A), but no substantial differences when comparing the effects of the same Nys concentration across different Cer containing membranes (Figure 6.4 - B). In general, the increase in anisotropy values represent a reduction in Nys mobility [42] and therefore data suggest that Phycer has a more pronounced influence on Nys rotational diffusion, reaching values of 0.277 ± 0.004, compared to the maximum of Cer, 0.25 ± 0.01. This suggests a greater preference and binding capacity of Nys for Phycer.

3.1.2. Time-resolved measurements of Nys fluorescence

To further explore the interaction of Nys with membranes containing POPC and Cer or Phycer, the fluorescence intensity decays of the antifungal were acquired. The fluorescence intensity decay contains important information on the molecular environment surrounding the fluorophore. Although it may be sensitive to the polarity of the system, the degree of hydration, viscosity and the presence of fluorescence quencher is less sensitive to artefacts such as light scattering and / or inner filter. Mainly, an increase in mean fluorescence lifetime may occur either as a result of increased membrane packing [41] or the formation of Nys oligomers [14].

The fluorescence emission decay kinetics of Nys was measured for the different lipid mixtures as a function of increasing quantities of Nys. Generally, the total number of exponentials required to describe the intensity decay curve of Nys was three, though sometimes a fourth exponential was also required, judged according to the fitting criteria: $\chi 2$ values, random-weighted residuals and autocorrelation plots.

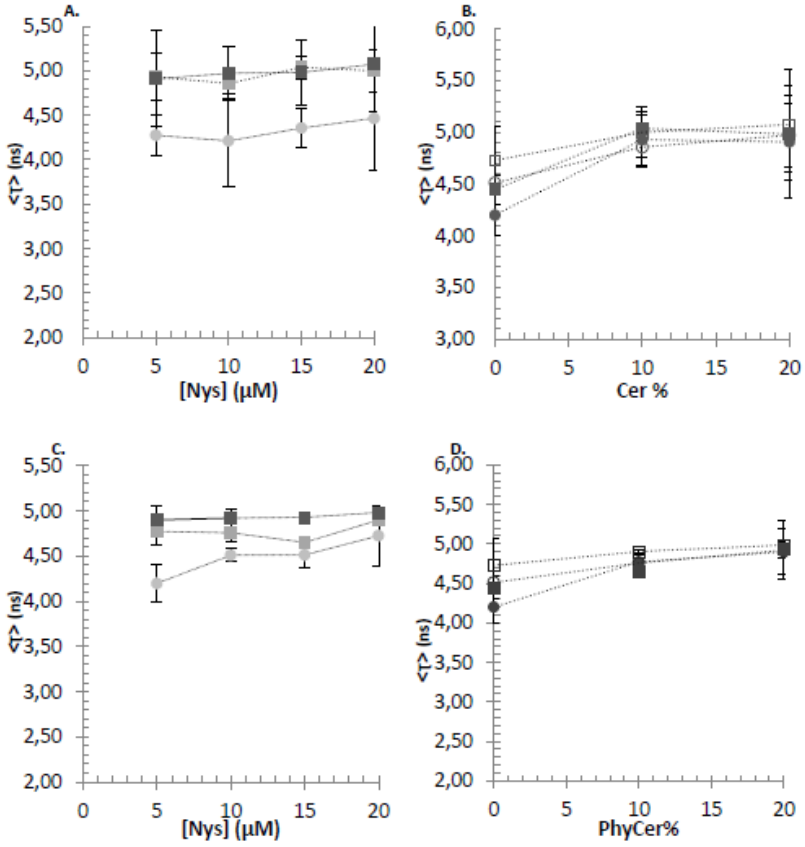

Figure 6. 5: Effect of the presence of Cer (A and B) and Phycer (C and D) in Nys intensity-weighted mean fluorescence lifetime. For the intensity-weighted mean fluorescence lifetime ($\langle\tau\rangle$) plotted as a function of Nys concentration (A and C), grey circles represent POPC LUVs 100 mol%, while grey squares and black squares represent the 10 and 20 mol%, respectively, of sphingolipid in LUVs with POPC. For the mean fluorescence lifetime plotted as a function of sphingolipid mol%, the Nys concentration was 5 (●),10 (○), 15 (▪) and 20 µM (□). The values are the mean ± S.D. of at least three independent replicates.

For each membrane composition non-significant changes in Nys fluorescence lifetime were observed upon increasing Nys concentration (Figure 6.5 – A and C). For example, the fluorescence lifetime of the binary mixture POPC/Phycer 10 mol% change from 4.77 ± 0.15 ns to 4.90 ± 0.03 ns from the lowest to the highest concentration of Nys. On the other hand, an increase in the fluorescence lifetime was observed in membranes containing increasing amounts of Cer or Phycer (Figure 6.5 – B and D). The same behavior occurs for the other systems and concentration of the antifungal drug. On the other hand, upon changing the composition in lipid vesicles from 0 mol% to 10 mol% and 20 mol% of the different ceramides, an increase in lifetime is observed according to the increase of the gel phase. However, the increase in Nys mean fluorescence lifetime is different between the two binary mixtures, showing a dependence on the type of lipid or more specifically, on the type of sphingolipid, in this case. Within Phycer-containing membranes, Nys mean fluorescence lifetime steadily increases according to the increase of the fraction of gel. In opposition, in Cer-containing membranes the difference between 10 mol% and 20 mol% does not appear to be so marked, but the variation in gel phase fraction, in this case, is also much smaller, going from 8 to 23% in the case of Cer, while for Phycer it changes from 23 to 77%. The mean fluorescence lifetime of Nys obtained for 20 mol% of Cer and 10 mol% of Phycer, which have the same gel fraction (~23%) have approximately the same value for all Nys concentration, except 15 μM. For this Nys concentration the values for Phycer are slightly shorter than for Cer.

3.1.3. Ratiometric fluorescence of Nys with sphingolipid to POPC only systems – a new approach to compare the interaction of Nys with different membranes

To mitigate distortions introduced by inner filter effects, better assess changes in fluorescence intensity with increasing sphingolipid amounts, and understand the underlying reasons for these intensity changes, we calculated the ratio of steady-state fluorescence intensity obtained in the presence and absence of Cer or Phycer, as well as those displayed by the amplitude-weighted mean fluorescence lifetime ($\bar{\tau}$). Nys is virtually non-fluorescent in aqueous solution, thus the amplitude-weighted mean fluorescence lifetime reflects the fluorescence quantum yield of the drug inserted in the membrane. However, the total fluorescence intensity also depends on the fraction of Nys incorporated in the lipid bilayer, reflecting the partition of Nys between water and each lipid system analyzed. Therefore, this comparison enables to determine whether the intensity trend aligns with that of the $\bar{\tau}$. Notably, significant differences emerge between Cer and Phycer containing mixtures in terms of the ratiometric values for $\bar{\tau}$ and the average area of the excitation spectra of Nys (IF) (see Figure 6.6). Specifically, the ratio

for $\bar{\tau}$ is similar or higher than the ratio of the average fluorescence intensity maximum in the case of Cer, whereas the opposite trend is observed for Phycer. Moreover, both the ratios of $\bar{\tau}$ and the intensity maximum are generally higher in the case of Phycer. For instance, the ratio of $\bar{\tau}$ in the case of Phycer reaches values around 1.4, whereas in the case of Cer, it ranges from 1 to 1.2. However, for the two binary sphingolipid systems, the $\bar{\tau}$ ratio remains approximately independent of Nys concentration, suggesting that the organization of Nys is similar across all concentrations and sphingolipid amounts.

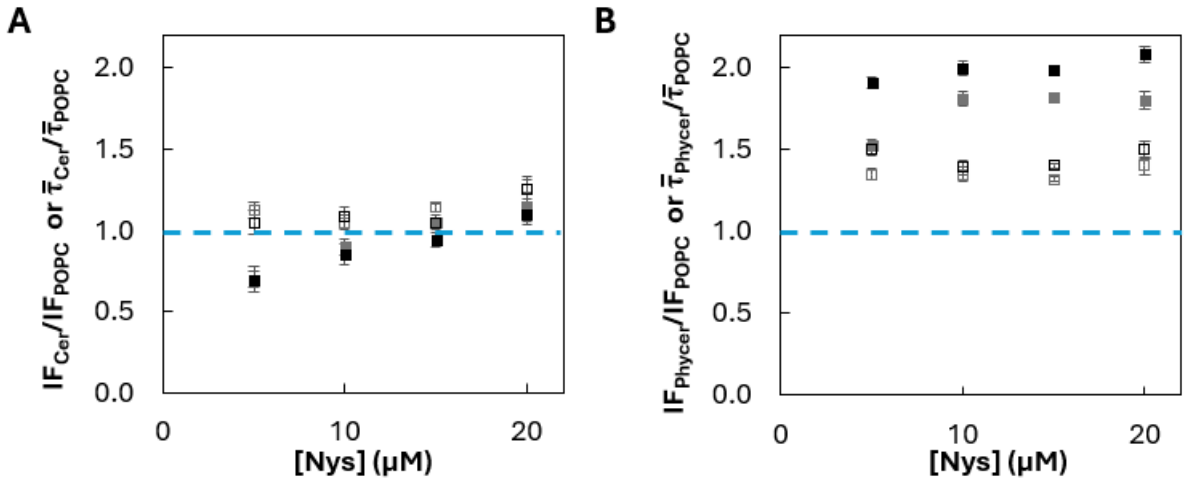

Figure 6. 6: Effect of Cer and Phycer on Nys fluorescence intensity and lifetime. Ratios of (full squares) total fluorescence intensity (IF, area under the excitation spectra) of Nys and (open squares) Nys amplitude-weighted mean fluorescence lifetime ($\bar{\tau}$) between mixtures containing 10 mol% (grey) and 20 mol% (black) of (A) Cer or (B) Phycer and POPC alone, are shown as a function of Nys concentration. The blue dashed line highlights where the systems with sphingolipids have the same value as POPC alone (ratio = 1). Values are the mean ± S.D. from at least three independent replicates.

These observations indicate that Nys has a greater affinity/partition for membranes containing Phycer compared to those with Cer. The intensity ratios for Phycer are higher than the lifetimes ratios for all Nys concentration. Moreover, the intensity ratios increase with the fraction of Phycer more than the lifetime ratios. In contrast, for Cer, the results suggest that the mammalian sphingolipid backbone does not enhance and may even decrease Nys partitioning into the membrane. This is demonstrated by the intensity ratios (IF_{Cer}/IF_{POPC}) in Cer- containing membranes, which are lower than 1 for Nys concentrations below 20 μM. This data shows that Nys has higher partition towards membranes that contain Phycer *vs* Cer.

3.2. Nystatin interaction with Phycer and Cer monolayers

The binary POPC/sphingolipid mixtures studied above display a coexistence between a fluid and a gel phase. The size and the properties of both the gel domains and the interface between the gel and fluid phases are distinct for Cer and Phytocer containing membranes [24,31]. To further investigate the differences in interactions between Nys and either Phycer or

Cer, pure monolayers containing Cer or Phycer were prepared in a Langmuir-Blodgett trough. These studies allow for a direct evaluation of the effects of Nys on the biophysical properties of the membranes.

Figure 6.7 and Figure S6.3 show the isotherms, *i.e.*, the surface pressure (π) as a function of average molecular area (*A*) for monolayers of POPC, Phycer, and Cer. Figure S6.3 specifically shows the isotherms of the lipids in the absence of Nys to clearly illustrate their compressibility. Among the lipids, Cer exhibits the steepest isotherm slope, followed by Phycer, and then POPC. The POPC monolayer forms at a higher area value compared to both sphingolipids, with Phycer forming at the lowest area values. This indicates that POPC is the most compressible lipid, which is expected given its larger molecular area, particularly regarding its headgroup. The different compressibility behaviors of Cer and Phycer are attributed to their structural differences, specifically the presence of hydroxylation in Phycer, which is absent in Cer.

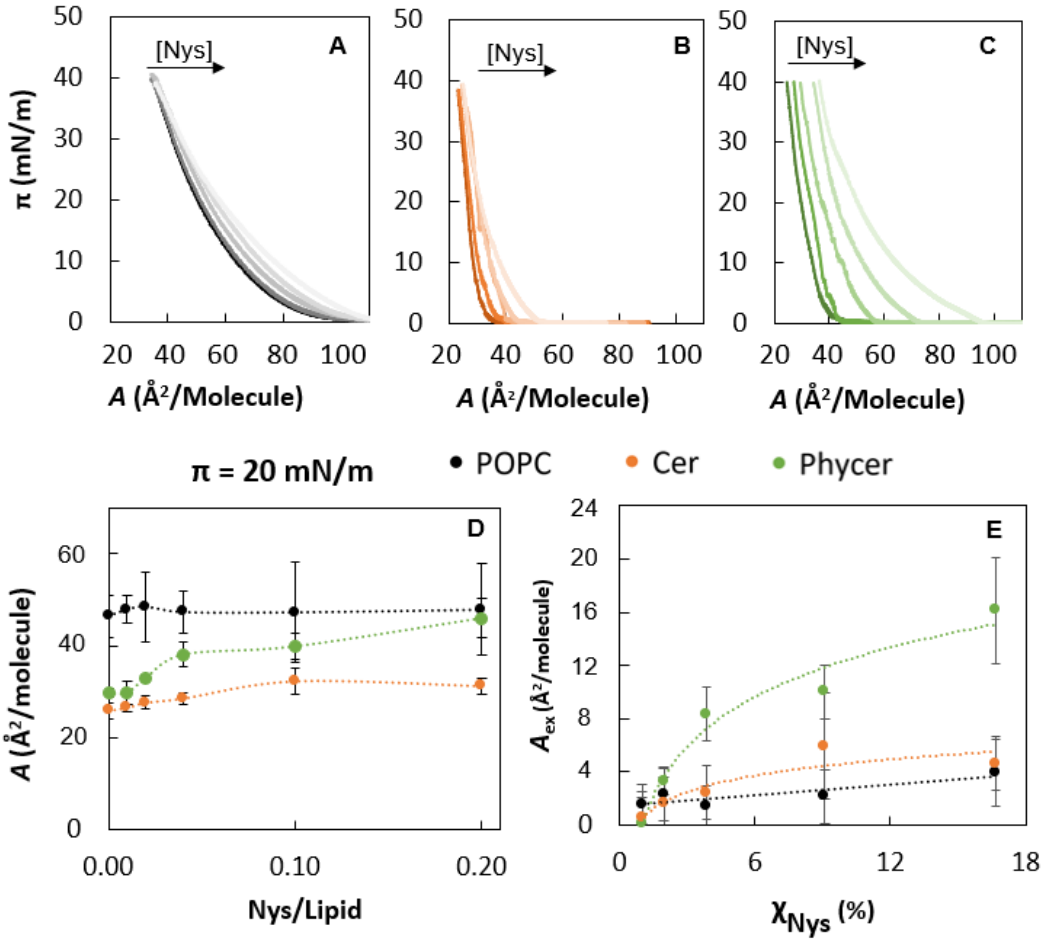

Figure 6. 7: Nys influence on the compressibility of POPC, Cer and Phycer monolayers. Representative isothermic curves of POPC (A), Cer (B) and Phycer (C) on an aqueous subphase at 24 °C with increasing concentration of Nys (black arrow). (D) Area plotted as a function of lipid/Nys ratio, π = 20 mN/m. (E) Excess area (A_{ex}) determined for each lipid monolayer after the addition of different Nys quantities. In D and E the dashed lines are to merely guide the eye, and the results are the mean ± S.D. for at least three independent replicates. The gradient of color in A-C indicates the increase of Nys amounts from

darker to lighter colors. The Nys/lipid ratios were: 0:1; 1:5, 1:10, 1:25, 1:50, 1:100. The aqueous subphase was PBS: 1 mM phosphate, 2.7 mM KCl, 137 mM NaCl, pH 7.4.

Nys was incrementally added to each lipid monolayer, and representative isotherms are presented in Figure 6.7 – A-C. The addition of Nys led to an increase in the area at which all lipid monolayers formed. However, this increase was more pronounced for Phycer compared to Cer and notably greater when compared with POPC. This differential expanding effect of Nys can be further analyzed by plotting the mean molecular area as a function of the Nys/lipid ratio, with surface pressure (π) fixed at 20 mN/m (Figure 6.7 – D). The plot clearly illustrates the pronounced increase in area for Phycer monolayers upon the addition of the antifungal agent compared to the other two lipids. Without Nys, the area at 20 mN/m is approximately 29.6 ± 0.8 Å^2, while with the highest Nys/lipid ratio used (1/5), it increases to 46 ± 4.2 Å^2.

The determination of the excess area (Figure 6.7 – E) allows to quantitively compare the expanding effect of Nys in the monolayers. For POPC this area does not vary with increasing Nys molar fraction. Statistical analysis shows that the excess area for POPC and Cer is not significantly different for any of the Nys:lipid ratios used, yet these two are significantly different from the excess area observed for Phycer, *i.e,* the addition of Nys increased significantly the excess area of Phycer monolayers and did so in a significantly different manner than for POPC and Cer.

The impact of Nys on the compressibility curves suggests a preferential interaction with Phycer monolayers over Cer or POPC.

3.3. Nystatin increases the K^+ permeability more efficiently in membranes containing Phycer than Cer

In the preceding sections, it was established that Nys exhibits distinct and stronger interactions with Phycer-containing membranes compared to Cer-containing ones. However, it remains unverified whether the pore-forming ability of Nys also differs between these systems.

Nys channel formation on lipid bilayers can be quantified using H^+/K^+ exchange assays, leveraging on pyranine fluorescence sensitivity to pH [43]. This involves vesicle formation in a high-potassium buffer with pyranine, removal of external pyranine via molecular exclusion chromatography, and equilibration of H^+ ions using FCCP. The subsequent addition of Nys to these vesicles induces potassium efflux, triggering H^+ influx and acidification of the vesicle interior, resulting in a shift in pyranine fluorescence excitation maximum wavelength from 450 to 405 nm and decreased emission ratio at these wavelengths. To quantify Nys pore formation effectiveness, the percentage of potassium gradient dissipation is determined by comparing

gradient dissipation induced by Nys with total gradient dissipation achieved by valinomycin addition.

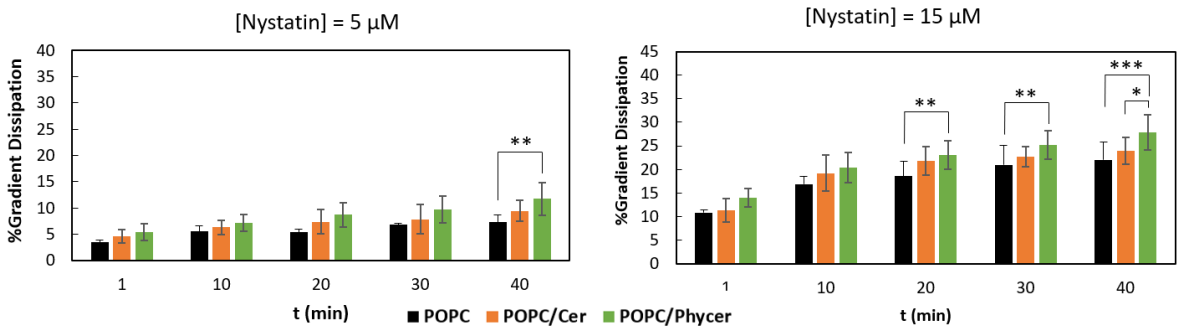

Figure 6. 8: Nys increase in K^+ permeability of different lipid bilayers. Nys was added to the LUV preparation at a final concentration of 5 µM or 15 µM. LUVs were prepared with POPC (black), POPC/Cer (20 mol%; orange) and POPC/Phycer (20 mol%; green). The percentage of gradient dissipation was calculated at different time points after the addition of Nys. The results with error bars are the mean ± S.D. for at least eleven independent replicates. * $p \leq 0.05$; ** $p \leq 0.01$; *** $p \leq 0.001$.

The amount of Cer and Phycer incorporated into the vesicles was set at 20 mol%, to mimic the sphingolipid content typically found in the plasma membrane of mammals and fungi [44–47]. Furthermore, considering the phase diagrams of each lipid mixture [24,30], this proportion of sphingolipids and POPC is anticipated to result in a coexistence of fluid and gel phases.

The variation of the fluorescence intensity ratio $I_{\lambda ex = 450nm} / I_{\lambda ex = 405nm}$ after the addition of Nys, valinomycin and Triton X-100 (Figure S6.4 – A and B), aligned with previous observations [13]. However, the initial ratio values for the POPC/DPPC system were slightly lower (~0.9) compared to the previously reported value of ~1, possibly due to the larger diameter of the LUVs in this study (Table S6.1). Interestingly, while the initial ratio was similar for LUVs containing only POPC, those with Cer and Phycer had slightly lower starting values (~0.8), indicating greater permeability to H^+ in line with the expected for a membrane with gel/fluid phase coexistence [48].

Overall, higher Nys concentrations (15 µM) led to increased gradient dissipation compared to lower concentrations (5 µM), likely due to a higher effective Nys/lipid ratio promoting pore formation. DPPC-containing membranes consistently exhibited the highest gradient dissipation percentages at all time points (Figure S6.4 – C and D).

After adding 5 µM of Nys, gradient dissipation in Phycer and Cer systems did not significantly differ from that in POPC, except for the Phycer membrane after 40 minutes, showing a slightly higher dissipation gradient. However, with triple the Nys concentration (15 µM), Phycer membranes began to exhibit significantly higher gradient dissipation compared to POPC after 20 minutes, with the difference becoming more pronounced over time.

At the final time point, Phycer gradient dissipation surpassed that of Cer, highlighting the distinct behavior of Phycer-containing membranes under Nys exposure.

4. Discussion

Nys is one of the oldest polyene macrolides that is used as an antifungal agent. Although there are several studies regarding its mode of action and interaction with membranes, there is still plenty to uncover regarding its specificity and activity towards the fungal plasma membrane. In the classical and for a long time most accepted mechanism, Nys pore formation on membranes is Erg-dependent. This theory is being questioned by results that show that this polyene has high partition preference towards ordered gel phases that are Erg-free [13], compared to a POPC-rich fluid phase [41]. The evidence of the interaction of polyene macrolides with gel domains together with the discovery of the presence of SLEDs that lack Erg in the plasma membrane of yeast [18] has recently raised the hypothesis of a sterol-independent mechanism of action for this class of compounds.

The main aim of this work was to investigate the interaction of Nys with membranes containing either a mammalian or a fungal sphingolipid: Cer, the major hydrophobic backbone of sphingolipids found in the mammalian cells and the more hydroxylated Phycer, the counterpart found in plants and fungal cells (Figure 6.2). These two sphingolipid backbones represent two simple systems that could be useful for understanding the differences between mammals and fungi concerning their sensitivity to Nys. At room temperature, bilayers with 20 mol% of Cer or Phycer mixed with POPC display a coexistence of a gel and a fluid phase [24,31]. Nevertheless, for Cer containing systems there is approximately 23 mol% of gel phase, while with Phycer this value goes up to 77 mol%. Moreover, the presence of the additional hydroxyl group in the sphingoid base of Phycer that is absent in Cer, leads to an increase of the T_m. Indeed, Cer shows a T_m of around 90 °C [32,33] while for Phycer it reaches 100 °C [34,35]. Furthermore, the two sphingolipids give rise to different organization of the membrane, as a result from the different phases observed for Cer and Phycer at the same temperature and/or composition. For instance, POPC:Phycer organize in highly stable 3:1 and 1:2 complexes which exhibit properties distinct from both the fluid and gel states. These complexes coexist between 25 mol% and 66.7 mol% of Phycer up to approximately 40 °C. Below 25 mol%, a fluid phase enriched in POPC coexists with complex 3:1 (POPC:Phycer), while above 66.7 mol%, complex 1:2 (POPC/Phycer) coexists with the lamellar crystalline phase [24]. Mixed with POPC, Cer does not form these complexes, and, in turn, leads to a different molecular arrangement. Below

50 °C, a coexistence of fluid and gel phases occurs for mixtures of Cer and POPC. Also, with χ_{Cer} higher than 80 mol% only gel phases are found [31]. At 20 mol% of sphingolipid, the Cer-enriched gel phase is more rigid than Phycer-rich domains as evidenced by the fluorescence anisotropy and mean fluorescence lifetime of *t*-PnA while labelling POPC/Cer liposomes being significantly higher than with POPC/Phycer [24,31]. As mentioned previously, this fluorescent probe partitions preferentially towards gel domains, reporting on its properties [15–18]. Moreover, DPH (1,6-diphenyl-1,3,6-hexatriene) is a fluorescent membrane probe which partitions equally towards different lipid phase with the exception of Cer-rich domains, from which it is excluded [31,36] while it is not from Phycer-rich phases [24].

The hydrophobic chain packing and order of gel domains, as well as the global membrane order in liposomes containing 20 mol% of Phycer and POPC [24] are similar to those reported for SLEDs in yeast cells [16], evidencing that Phycer liposomes mixed with POPC mimic the yeast plasma membrane. Furthermore, the highly stable and rigid stoichiometric complexes formed between this sphingolipid and POPC accounts for the stability of gel domains in the yeast plasma membrane [24].

To confirm if there is a stronger affinity and activity of the drug towards Cer or Phycer, different membrane model systems containing each of these lipids were prepared, and their interaction with Nys was studied using different techniques.

The $\chi_{sphingolipid}$ used for the studies with liposomes (10-20 mol%) was chosen due to a number of reasons: 1) 10-20 mol% is within the range of sphingolipid fraction in the plasma membrane of yeasts [44–46], 2) the properties of Phycer-rich phases at this molar fraction replicate several biophysical properties of gel domains found in the plasma membrane of yeast [16,18,24] ; 3) at higher percentages of Cer or Phycer than the values used and at the lipid concentration (1 mM), the formation of crystals becomes more probable. The lipid concentration was not lower than 1 mM to guarantee a relatively high Nys partition towards the membrane.

First, we took advantage of the intrinsic fluorescence of Nys and measured its properties in the presence of liposomes with different lipid mixtures. All mixtures were composed of POPC, a very common phospholipid in eukaryotic membranes, that has a low T_m and is widely characterized, which facilitates the comparison with previous studies [49,50]. In general, the results of Nys fluorescence in the presence of LUVs with just POPC are widely confirmed and consistent with the previous studies found in the literature. For instance, the mean fluorescence lifetime of Nys in POPC membranes show values of approximately 5 ns, as previously found in the study with sphingomyelin or DPPC-enriched POPC LUVs [13]. Also the anisotropy

values found in this work are similar to the ones found in a previous study in which it was explored how different sterols affect Nys aggregation [10].

The spectra obtained for Cer and Phycer systems closely resemble those observed for liposomes prepared with cholesterol or Erg. The presence of 30 mol% cholesterol did not alter the emission and excitation spectra of Nys compared to liposomes containing only POPC. However, in the presence of liposomes with 10 and 30 mol% Erg, the spectra of Nys exhibited significant rearrangements, indicative of Nys aggregate formation within the membrane [10]. While the spectral variations observed for Cer and Phycer were not as pronounced as those seen with Erg vesicles, they could suggest an initial formation of aggregates. Notably, the excitation spectra of Nys in the presence of Cer and Phycer showed a greater increase in the intensity of the 0-0 vibrational peak, particularly at higher Nys concentrations.

The increase in the fluorescence intensity and amplitude-weighted mean fluorescence lifetime of Nys in the presence of LUVs containing Phycer when compared with POPC-only LUVs, confirms that Nys prefers Phycer-containing highly ordered domains. The anisotropy values of Phycer (Figure 6.5) behave similarly to those of the mean fluorescence lifetime (Figure 6.5), indicating a more rigid environment surrounding Nys when compared to the absence of sphingolipids, *i.e.* vesicles with only POPC. The fluorescent tetraene function of the Nys molecule could be further stabilized within these ordered domains as confirmed by the increase in the average fluorescence lifetime. A similar behavior has been observed in studies conducted with *t*-PnA in the same binary lipid mixture of POPC with Phycer [24]. *T*-PnA is a membrane probe with the same fluorophore as Nys. However, it is important to consider that there are some structural differences between the two compounds, such as the presence of a rigid ring in Nys that renders it less sensitive to the fluidity of the membrane environment in opposition to *t*-PnA. The anisotropy values of *t*-PnA increased significantly from 5 to 20-25 mol% of Phycer. A similar trend was observed for Nys in this work, although the differences between 10 and 20 mol% are not as marked as for *t*-PnA. Comparable behavior is observed for the mean fluorescence lifetime both in the case of *t*-PnA and Nys. Therefore, this similar trend could suggest a preference of Nys for incorporation into Phycer-enriched domains. However, the mean fluorescence lifetime of Nys determined in this work has only a modest increase, especially when compared to what was observed previously with liposomes containing POPC/Erg [10], POPC/sphingomyelin or POPC/DPPC [13]. Furthermore, in the latter case, in the gel phase the long lifetime component of Nys reached values around approximately 45 ns already with very small gel fractions, as in the case of DPPC system. However, in the present work this did not occur, and the maximum values reached were less or near 15 ns. Another

important difference that needs to be highlighted between this study and the previous ones, is that in the one conducted with LUVs containing POPC and 30 mol% of Erg the mean fluorescence lifetime shows only a slightly increase from 5 to 10 μM of Nys, but from 10 μM up to 15 μM a drastic increase was observed, a behavior that does not occur in the systems studied in this work. This difference could be explained by not having enough Cer or Phycer to allow the same trend. Another plausible explanation is that Nys high partition towards the gel phases of the membranes with sphingolipids is inducing the formation of an aggregate in the membranes with lipid in between Nys molecules. A situation different from the formation of Nys pore observed for membranes with Erg. Also, the gel-liquid disordered interface could be stabilizing the interaction of the polyene with the membrane. Also possible is that the orientation of Nys in the pores formed in the systems studied herein could be different than those formed in other membranes, where the chromophore is closely stacked giving rise to excitonic interaction clearly observed in the fluorescence spectra. Such excitonic bands were not observed with the lipid compositions used in this work.

The positive impact of Phycer on the membrane partition of Nys, is strongly supported by the comparison of the values of the ratio of steady-state fluorescence intensity obtained from integration of the excitation spectra with the ratio of $\bar{\tau}$. The representation of these values in the same graphic allow to detect that the ratio of fluorescence intensity maximum is higher than that of $\bar{\tau}$, as detailed above, and these strongly suggested incorporation of more Nys into the membrane in the presence of Phycer. Moreover, permeability assays were also performed using Phycer and POPC LUVs which showed that the presence of Nys induced ion leakage, confirming the partition of the drug towards the membrane. Since the analysis of the ratio of the fluorescence intensity and $\bar{\tau}$ for lipid systems with and without sphingolipids was used, the determination of the partition coefficient of Nys to the lipid bilayers was not necessary. Moreover, to determine the partition coefficient, it would have been required to use increasing lipid concentrations, in order to have a rigorously determined partition behavior. For lipid concentrations higher than those used in this work, the formation of sphingolipid crystals is prone to occur [31]. In addition, since LUVs with higher diameter (~200 nm) had to be used for the current work, light scattering would be stronger especially for the highest lipid concentration, which could interfere with the accuracy of the fluorescence measurements.

The case of Cer is more complex unlike Phycer-systems. Generally, with Cer it was more difficult to obtain reproducible results, both in the Nys fluorescence assays and the isotherms of monolayers measurements. This might be due to the chemical structure of Cer or because it is more hydrophobic than its 4'-hydroxylated counterpart. The unexpected behavior observed

in the fluorescence spectra, particularly in the emission spectrum of Nys, may be attributed to the formation of nearly pure ordered domains by Cer, known for their remarkable rigidity [31]. Therefore, especially for lower concentrations of Nys the presence of Cer could decrease the partition to the membrane so, there is less Nys found in the membrane. This would explain the inversion in the fluorescence intensity emitted by Nys in the different lipid mixtures and for different concentrations. The fluorescence anisotropy follows trends that are very different from those obtained in a study of biophysical properties of the binary system POPC/Cer with *t*-PnA. *T*-PnA anisotropy presented a sharp increase with Cer mol% that reached a plateau around Cer mole fraction of 20 mol% [31]. Considering the differences described in the results for fluorescence anisotropy, mean fluorescence lifetime and the ratios of $\bar{\tau}$ and area of excitation spectra obtained for the membranes with Cer *vs* Phycer it is possible to conclude that the behavior of Nys in the presence of Cer is almost the opposite of that in the presence of Phycer, which concur to the interpretation that, unlike with Phycer, Nys seems to be mostly excluded from Cer-rich domains.

The increase of the mean fluorescence lifetime of Nys in both Cer and Phycer enriched phase is evidence for an incipient formation of Nys oligomers, since a greater packing inside the ordered phase stabilizes the chromophores prolonging the mean fluorescence lifetime by reducing its non-radiative decay rate. Nys is not forming the same oligomers as seen in the case of Erg [10] or sphingomyelin [13], as the values of the long lifetime component obtained in this work (Figure S6.2) and for those systems are different. The trend of the mean fluorescence lifetime as function of Nys concentration (Figure 6.5), highlights that the decay parameters are independent of drug concentration on both Cer and Phycer cases. Because the decay values depend on the average number of fluorescent oligomers occupying the membrane, these results suggest that the important factor for the formation of long-lived species is the presence of a sphingolipid-enriched gel phase and not the concentration of Nys. Instead, in fluid phase membrane, *i.e.* LUVs with 100 mol% of POPC, the parameters values increase with Nys concentration. This could be due to some increase in rigidity of the membrane induced by Nys itself or that in the fluid phase there is a smaller tendency of Nys to aggregate being the increase in concentration crucial for the formation of oligomers.

The results of the activity of Nys with pyranine suggest that the drug permeabilized more effectively the membranes containing Phycer than the ones with Cer. POPC at room temperature organizes in fluid lipid bilayers [51], while the other systems (POPC/DPPC, POPC/Cer and POPC/Phycer have a coexistence of fluid and gel phases [24,31]. Moreover, the equimolar mixture of POPC/DPPC is the one that contains higher amount of gel phase and less

of liquid disordered [24,31,51] followed by POPC/Phycer [24], and finally POPC/Cer. The same trend is found for Nys ability to permeabilize the membrane: the activity was the highest for the POPC/DPPC system, followed by POPC/Phycer, POPC/Cer and finally POPC alone Therefore, Nys evidently partitions preferentially and is more active towards gel phases, which is in agreement with previous results that showed that Nys action is higher the less amount of fluid phases are in the system [13].

This different behavior of Nys in the presence of domains formed by Cer and Phycer could be due to the different organization between these two sphingolipid species in a POPC matrix, and/or because the additional hydroxyl group present on Phycer can facilitate the interaction with Nys. At this point it should be reminded that, according to the available phase diagrams from POPC/Cer [31] and POPC/Phycer [24], the gel formed by Cer is almost a pure Cer phase, which is extremely rigid, and this might be related to the exclusion of Nys. Moreover, for the Cer mole fractions used, the gel is a minor phase. On the contrary, for the mole fraction of Phycer used, the ordered phase is composed by a stoichiometric complex where Phycer only represent 25 mol%, the remainder lipid being POPC. Moreover, the fraction of gel phase at the Phycer concentrations tested is much higher than the gel fraction in POPC/Cer mixtures for the same sphingolipid concentrations. Another feature to consider is that since Phycer bilayers contain more gel phase than Cer ones, there is a bigger interface area between fluid and gel phases. Hence, this interfaces with lipid packing defects may facilitate the interaction of Nys with the membrane that end up leading to pore formation.

Interestingly, according to the monolayer compressibility assay performed in this work, at a specific surface pressure (π = 20mN/m), the average molecular area (A) of Phycer increases significantly with the addition of Nys. The same is not observed for monolayers of Cer or POPC. In other words, Nys is affecting markedly the compressibility properties of Phycer monolayers, but not of Cer or POPC. Moreover, the excess area determined for each lipid monolayer mixed with different Nys quantities, increased significantly for Phycer monolayers but not for Cer nor POPC. This expanding effect is reminiscent of the observation by atomic force microscopy in supported lipid bilayers of POPC mixed with palmitoylsphingomyelin (PSM) or DPPC at different molar proportions. With increasing PSM or DPPC fraction, the gel fraction also increases and so did 1) the membrane/water partition coefficient of the drug and 2) the area of the gel but not the fluid phase [13]. The relative increase observed was similar to the one observed for Phycer monolayers. Furthermore, the increase of excess area observed for the Phycer monolayer after the addition of Nys is similar to that observed with monolayers for the same range of Nys:lipid ratios [40]. It coud be that the additional hydroxyl group in Phycer

that is lacking in Cer could establish hydrogen bonds which would justify these changes in Phycer packaging with Nys. The monolayers are formed exclusively by the sphingolipid, therefore in this case, thre are no stoichiometric complexes being formed with POPC. Phycer alone is able to interact differently with Nys than Cer or POPC. Additionally, correlating with the results of the permeability assay conducted in this work, the excess area observed for Phycer is probably due to the formation of pores which is more significant in membranes that contain Phycer rather than Cer. The area of the aqueous lumen of the pore will contribute to the expansion of the monolayer.

A positive excess area is usually considered as the result of a repulsive interaction between the two components, and this would mean that the interation of Nys would be less favourable with Phycer monolayers than with Cer or POPC ones. However, the partition of Nys to the membrane is enhaned in the presence of DPPC or PSM gel domains, and these domains also undergoe an expansion. As stated above, a similar expansion was observed upon Nys addition to DPPC monolayers. Thus, in this particular case, a larger excess area does not mean a less favourable interaction, but on the contrary, a more favourable interaction. This is probably due to the fact that excess area is calculated comparing the experimental value for the mixture with an ideal mixture where the interactions between molecules of each component are the same as they are with one another in the mixutre. However, this would mean that we would have to compare a lipid bilayer (or monolayer) of lipid with a bilayer of Nys (or a monolayer organized as that of a lipid) but Nys alone does not form a lipid bilayer. Together with the additional area created by the pores that may be forming, the positive excess area calculated, in the case of Nys interacting with lipids, is a result of a preferential interaction.

The results present in this work clearly show a preferential interaction of Nys with Phycer containing bilayers with no sterol present, challenging the classical mode of action of this drug in which the pore forming mechanism of Nys occurs through stereospecific interactions with Erg. Hence the model for the action of Nys needs an update in which the interaction with sphingolipids is relevant. Another relevant fact is that the transversal distribution of both sphingolipids and Erg is not equitative among the exoplasmic and the cytoplasmic leaflet of the yeast plasma membrane. In fact, there is evidence that the inner layer is ca. 4-fold enriched in Erg when compared to the outer one [52], while sphingolipids predominate in the outer layer [53,54]. Therefore, one possibility is that when Nys first interacts with the outer layer of the fungal plasma membrane it encounters SLEDs, rich in sphingolipids with Phycer backbone that can act as gateways for the drug which then can more easily reach Erg in the inner leaflet, efficiently forming pores.

If this hypothesis is verified, it also justifies why there is a toxicity associated with Nys. Although Nys has a preferential interaction with Erg rather than cholesterol, Nys can form pores in model membranes containing cholesterol [55]. Nonetheless, Nys is more active towards yeast cells with Erg in the plasma membrane than when this sterol is substituted with cholesterol [56]. Moreover, there are evidence for cholesterol to be evenly distributed along the plasma membrane in many mammalian cell types [57] and since in these cells there is no need of SLEDs as gateways for the drug to reach the sterol, it still forms pores. Nevertheless, the cholesterol distribution in mammalian plasma membrane remains a subject of discussion [57,58].

5. Conclusion

We investigated the interaction of the antifungal polyene Nys with membrane model systems containing the major sphingolipid backbone of fungi and mammals: Phycer and Cer, respectively. Using the intrinsic fluorescence properties of Nys it was possible to show that Nys interacts preferably with Phycer-containing membranes over Cer-containing. Moreover, the compressibility of Phycer monolayers is clearly more affected by the presence of Nys than Cer, which can be related to a higher ability of Nys to insert in Phycer monolayers and more strongly affect the lipid packing in those monolayers. These effects in turn explain the highest activity towards Phycer-containing liposomes than Cer, also found in this work. Overall, all the results point to Nys having a higher affinity and pore-forming activity towards membranes containing the fungal sphingolipid backbone than the mammalian.

Interestingly, all the studies were performed without Erg which challenges the old classic mode of action of Nys in which Erg was indispensable for the formation of Nys pores in membranes. The results in this work support the hypothesis that the mechanism of action of Nys is not entirely specific towards a target such as Erg, but possibly also towards different types of ordered lipid domains, namely gel domains, that are present in the fungal membrane. Furthermore, these gel domains are found in fungal plasma membranes - SLEDs - but not in mammalian ones.

A new model is proposed for the action of Nys which considers SLEDs present in the outer leaflet of the fungal plasma membrane as gateways for the drug to interact with the membrane and reach the Erg that is predominantly in the inner leaflet and forms pores with the sterol. This new model takes into account the different results obtained in studies with model systems and *in vivo* with yeast cells.

This type of approach is relevant for the design of new or improved antifungal drugs that have membranes and particularly lipid domains as targets, in hope to find a more efficient and less toxic agent.

Acknowledgements

This work was funded by Fundação para a Ciência e Tecnologia (FCT), I.P./MCTES through national funds under projects EXPL/BIA-BFS/1034/2021, UIDB/00100/2020, UIDP/00100/2020, UIDB/04138/2020 and LA/P/0056/2020, and doctoral scholarship to A.B.-O. (SFRH/BD/145600/2019).

6. References

1. Fisher, M.C.; Hawkins, N.J.; Sanglard, D.; Gurr, S.J. Worldwide emergence of resistance to antifungal drugs challenges human health and food security. *Science* **2018**, *360*, 739–742.
2. Rhodes, J. Rapid Worldwide Emergence of Pathogenic Fungi. *Cell Host Microbe* **2019**, *26*, 12–14.
3. Hossain, C.M.; Ryan, L.K.; Gera, M.; Choudhuri, S.; Lyle, N.; Ali, K.A.; Diamond, G. Antifungals and Drug Resistance. **2022**, *2*, 1722–1737.
4. Nystatin Monograph for Professionals - Drugs.com Available online: https://www.drugs.com/monograph/nystatin.html (accessed on May 3, 2023).
5. Zielinski, J.; Golik, J.; Pawlak, J.; Borowski, E.; Falkowski, L. The structure of nystatin A3, a component of nystatin complex. *J. Antibiot. (Tokyo).* **1988**, *41*, 1289–1291.
6. Mitrofanova, V.G.; Shenin, I.D.; Mirgorodskaia, O.; Derzhavets, A.A.; Matveeva, E.; Grinberg, G.E.; Apter, I.M.; Golubkova, L. [Determination of nystatin component composition using HPLC and TLC with densitometry]. *Antibiot. i khimioterapiia = Antibiot. chemoterapy [sic]* **1991**.
7. Nystatin Cream: Package Insert - Drugs.com Available online: https://www.drugs.com/pro/nystatin-cream.html (accessed on Jul 17, 2023).
8. Nystatin Uses, Side Effects & Warnings - Drugs.com Available online: https://www.drugs.com/mtm/nystatin.html (accessed on Jul 17, 2023).
9. Silva, L.; Coutinho, A.; Fedorov, A.; Prieto, M. Competitive binding of cholesterol and ergosterol to the polyene antibiotic nystatin. A fluorescence study. *Biophys. J.* **2006**, *90*, 3625–3631.
10. Coutinho, A.; Silva, L.; Fedorov, A.; Prieto, M. Cholesterol and ergosterol influence nystatin surface aggregation: relation to pore formation. *Biophys. J.* **2004**, *87*, 3264–3276.
11. Komor, E.; Weber, H.; Tanner, W. Greatly decreased susceptibility of nonmetabolizing cells towards detergents. *Proc. Natl. Acad. Sci. U. S. A.* **1979**, *76*, 1814–1818.
12. Leber, A.; Fischer, P.; Schneiter, R.; Kohlwein, S.D.; Daum, G. The yeast mic2 mutant is defective in the formation of mannosyl-diinositolphosphorylceramide. *FEBS Lett.* **1997**, *411*, 211–214.
13. dos Santos, A.G.; Marquês, J.T.; Carreira, A.C.; Castro, I.R.; Viana, A.S.; Mingeot-Leclercq, M.-P.; de Almeida, R.F.M.; Silva, L.C. The molecular mechanism of Nystatin action is dependent on the membrane biophysical properties and lipid composition. *Phys. Chem. Chem. Phys.* **2017**, *19*, 30078–30088.
14. Coutinho, A.; Prieto, M. Cooperative partition model of nystatin interaction with phospholipid vesicles. *Biophys. J.* **2003**, *84*, 3061–3078.
15. Sklar, L.A.; Hudson, B.S.; Simoni, R.D. Conjugated polyene fatty acids as fluorescent probes: Synthetic phospholipid membrane studies. *Biochemistry* **1977**, *16*, 819–828.
16. Bento-Oliveira, A.; Santos, F.C.; Marquês, J.T.; Paulo, P.M.R.; Korte, T.; Herrmann, A.; Marinho, H.S.; de Almeida, R.F.M. Yeast sphingolipid-enriched domains and membrane compartments in the absence of mannosyldiinositolphosphorylceramide. *Biomolecules* **2020**, *10*, 1–24.
17. de Almeida, R.F.M.; Loura, L.M.S.; Prieto, M. Membrane lipid domains and rafts: current applications of fluorescence lifetime spectroscopy and imaging. *Chem. Phys. Lipids* 2009, *157*, 61–77.
18. Aresta-Branco, F.; Cordeiro, A.M.; Marinho, H.S.; Cyrne, L.; Antunes, F.; de Almeida, R.F.M. Gel domains in the plasma membrane of Saccharomyces cerevisiae: highly ordered, ergosterol-free, and sphingolipid-enriched lipid rafts. *J. Biol. Chem.* **2011**, *286*, 5043–54.
19. Santos, F.C.; Marquês, J.T.; Bento-Oliveira, A.; de Almeida, R.F.M. Sphingolipid-enriched domains in fungi. *FEBS Lett.* **2020**, *594*, 3698–3718.
20. Marquês, J.T.; Marinho, H.S.; de Almeida, R.F.M. Sphingolipid hydroxylation in mammals, yeast and plants – An integrated view. *Prog. Lipid Res.* **2018**, *71*, 18–42.
21. Grossmann, G.; Opekarová, M.; Malinsky, J.; Weig-Meckl, I.; Tanner, W. Membrane potential governs lateral segregation of plasma membrane proteins and lipids in yeast. *EMBO J.* **2007**, *26*, 1–8.
22. Herman, P.; Vecer, J.; Opekarova, M.; Vesela, P.; Jancikova, I.; Zahumensky, J.; Malinsky, J. Depolarization affects the lateral microdomain structure of yeast plasma membrane. *FEBS J.* **2015**, *282*, 419–434.
23. Santos, F.C.; Lobo, G.M.; Fernandes, A.S.; Videira, A.; De Almeida, R.F.M. Changes in the biophysical properties of the cell membrane are involved in the response of neurospora crassa to staurosporine. *Front. Physiol.* **2018**, *9*.
24. Marquês, J.T.; Cordeiro, A.M.; Viana, A.S.; Herrmann, A.; Marinho, H.S.; de Almeida, R.F.M. Formation and Properties of Membrane-Ordered Domains by Phytoceramide: Role of Sphingoid Base Hydroxylation. *Langmuir* **2015**, *31*, 9410–21.
25. Malinsky, J.; Tanner, W.; Opekarova, M. Transmembrane voltage: Potential to induce lateral microdomains. *Biochim. Biophys. Acta* **2016**, *1861*, 806–811.
26. Clay, L.; Caudron, F.; Denoth-Lippuner, A.; Boettcher, B.; Frei, S.B.; Snapp, E.L.; Barral, Y. A sphingolipid-dependent diffusion barrier confines ER stress to the yeast mother cell. *Elife* **2014**, *2014*.
27. Gaigg, B.; Timischl, B.; Corbino, L.; Schneiter, R. Synthesis of sphingolipids with very long chain fatty acids but not ergosterol is required for routing of newly synthesized plasma membrane ATPase to the cell surface of yeast. *J. Biol. Chem.* **2005**, *280*, 22515–22522.
28. Watanabe, R.; Funato, K.; Venkataraman, K.; Futerman, A.H.; Riezman, H. Sphingolipids Are Required for the Stable Membrane Association of Glycosylphosphatidylinositol-anchored Proteins in Yeast. *J. Biol. Chem.* **2002**, *277*, 49538–49544.
29. Heese-Peck, A.; Pichler, H.; Zanolari, B.; Watanabe, R.; Daum, G.; Riezman, H. Multiple functions of sterols in yeast endocytosis. *Mol. Biol. Cell* **2002**, *13*, 2664–2680.

30. Pinto, S.N.; Silva, L.C.; Futerman, A.H.; Prieto, M. Effect of ceramide structure on membrane biophysical properties: The role of acyl chain length and unsaturation. *Biochim. Biophys. Acta - Biomembr.* **2011**, *1808*, 2753–2760.
31. Silva, L.; De Almeida, R.F.M.; Fedorov, A.; Matos, A.P.A.; Prieto, M. Ceramide-platform formation and -induced biophysical changes in a fluid phospholipid membrane. *Mol. Membr. Biol.* **2006**, *23*, 137–148.
32. Shah, J.; Duclos, R.I.; Shipley, G.G. Structure and thermotropic properties of 1-stearoyl-2-acetyl-phosphatidylcholine bilayer membranes. *Biophys. J.* **1994**, *66*, 1469–1478.
33. Sot, J.; Aranda, F.J.; Collado, M.I.; Goñi, F.M.; Alonso, A. Different Effects of Long- and Short-Chain Ceramides on the Gel-Fluid and Lamellar-Hexagonal Transitions of Phospholipids: A Calorimetric, NMR, and X-Ray Diffraction Study. *Biophys. J.* **2005**, *88*, 3368–3380.
34. Raudenkolb, S.; Wartewig, S.; Neubert, R.H.H. Polymorphism of ceramide 3. Part 2: A vibrational spectroscopic and X-ray powder diffraction investigation of N-octadecanoyl phytosphingosine and the analogous specifically deuterated d35 derivative. *Chem. Phys. Lipids* **2003**, *124*, 89–101.
35. Garidel, P. Structural organisation and phase behaviour of a stratum corneum lipid analogue: ceramide 3A. *Phys. Chem. Chem. Phys.* **2006**, *8*, 2265–2275.
36. Megha; London, E. Ceramide selectively displaces cholesterol from ordered lipid domains (rafts): implications for lipid raft structure and function. *J. Biol. Chem.* **2004**, *279*, 9997–10004.
37. Rouser, G.; Fleischer, S.; Yamamoto, A. Two dimensional thin layer chromatographic separation of polar lipids and determination of phospholipids by phosphorus analysis of spots. *Lipids* **1970**, *5*, 494–496.
38. Bastos, A.E.P.; Marinho, H.S.; Cordeiro, A.M.; de Soure, A.M.; de Almeida, R.F.M. Biophysical properties of ergosterol-enriched lipid rafts in yeast and tools for their study: characterization of ergosterol/phosphatidylcholine membranes with three fluorescent membrane probes. *Chem. Phys. Lipids* **2012**, *165*, 577–588.
39. *CRC handbook of chemistry and physics*; Haynes, W.M., Ed.; 95th Editi.; CRC Press: Boca Raton, USA, 2014;
40. Hąc-Wydro, K.; Dynarowicz-Łatka, P. Interaction between nystatin and natural membrane lipids in Langmuir monolayers--the role of a phospholipid in the mechanism of polyenes mode of action. *Biophys. Chem.* **2006**, *123*, 154–161.
41. Coutinho, A.; Prieto, M. Self-association of the polyene antibiotic nystatin in dipalmitoylphosphatidylcholine vesicles: a time-resolved fluorescence study. *Biophys. J.* **1995**, *69*, 2541–2557.
42. Castanho, M.A.R.B.; Coutinho, A.; Prieto, M.J.E. Absorption and fluorescence spectra of polyene antibiotics in the presence of cholesterol. *J. Biol. Chem.* **1992**, *267*, 204–209.
43. Launay, M.; Tripier, M.; Guizerix, J.; Viriot, M.L.; Andre, J.C. Pyranine used as a fluorescent tracer in hydrology: pH effects in determination of its concentration. *J. Hydrol.* **1980**, *46*, 377–383.
44. Breslow, D.K. Sphingolipid Homeostasis in the Endoplasmic Reticulum and Beyond. *Cold Spring Harb. Perspect. Biol.* **2013**, *5*, 1–16.
45. Daum, G.; Lees, N.D.; Bard, M.; Dickson, R. Biochemistry, Cell Biology and Molecular Biology of Lipids of Saccharomyces cerevisiae. *Yeast* **1998**, *14*, 1471–1510.
46. Dickson, R.C.; Lester, R.L. Yeast sphingolipids. *Biochim. Biophys. Acta - Gen. Subj.* **1999**, *1426*, 347–357.
47. Rautenbach, M.; Troskie, A.M.; Vosloo, J.A. Antifungal peptides: To be or not to be membrane active. *Biochimie* **2016**, *130*, 132–145.
48. Khmelinskaia, A.; Marquês, J.M.T.; Bastos, A.E.P.; Antunes, C.A.C.; Bento-Oliveira, A.; Scolari, S.; Lobo, G.M. da S.; Malhó, R.; Herrmann, A.; Marinho, H.S.; et al. Liquid-ordered phase formation by mammalian and yeast sterols: a common feature with organizational differences. *Front. Cell Dev. Biol.* **2020**, *8*, 337.
49. Ejsing, C.S.; Sampaio, J.L.; Surendranath, V.; Duchoslav, E.; Ekroos, K.; Klemm, R.W.; Simons, K.; Shevchenko, A. Global analysis of the yeast lipidome by quantitative shotgun mass spectrometry. *Proc. Natl. Acad. Sci. U. S. A.* **2009**, *106*, 2136–2141.
50. Marsh, D. *Handbook of lipid bilayers*; 2nd ed.; CRC Press Taylor & Francis Group: Boca Raton FL., 2012; ISBN 9781420088328.
51. Shoemaker, S.D.; Vanderlick, T.K. Material studies of lipid vesicles in the Lα and Lα-gel coexistence regimes. *Biophys. J.* **2003**, *84*, 998–1009.
52. Solanko, L.M.; Sullivan, D.P.; Sere, Y.Y.; Szomek, M.; Lunding, A.; Solanko, K.A.; Pizovic, A.; Stanchev, L.D.; Pomorski, T.G.; Menon, A.K.; et al. Ergosterol is mainly located in the cytoplasmic leaflet of the yeast plasma membrane. *Traffic* **2018**, *19*, 198–214.
53. Koval, M.; Pagano, R.E. Intracellular transport and metabolism of sphingomyelin. *Biochim. Biophys. Acta - Lipids Lipid Metab.* **1991**, *1082*, 113–125.
54. Van Meer, G. Lipid Traffic in Animal Cells. *Annu. Rev. Cell Biol.* **1989**, *5*, 247–275.
55. Silva, L.; Coutinho, A.; Fedorov, A.; Prieto, M. Nystatin-induced lipid vesicles permeabilization is strongly dependent on sterol structure. *Biochim. Biophys. Acta - Biomembr.* **2006**, *1758*, 452–459.
56. Szomek, M.; Reinholdt, P.; Petersen, D.; Caci, A.; Kongsted, J.; Wüstner, D. Direct observation of nystatin binding to the plasma membrane of living cells. *Biochim. Biophys. Acta - Biomembr.* **2021**, *1863*, 183528.
57. Steck, T.L.; Lange, Y. Transverse distribution of plasma membrane bilayer cholesterol: Picking sides. *Traffic* **2018**, *19*, 750–760.
58. Buwaneka, P.; Ralko, A.; Liu, S.L.; Cho, W. Evaluation of the available cholesterol concentration in the inner leaflet of the plasma membrane of mammalian cells. *J. Lipid Res.* **2021**, *62*.

Supplementary Material

Supporting Information

In this work, the inner filter effect is more pronounced for the emission spectra than the excitation one because the excitation is carried out at the maximum absorption wavelength. The excitation spectra spans all the wavelengths, including those where absorption is much smaller and the inner filter is negligible. Therefore, the results from the excitation spectra are more reliable and are the ones considered in the manuscript for Figure 6.3 and Figure 6.6.

Stability of the vesicles containing Cer and Phycer

Since the liposomes used in this work were prepared with a bigger membrane filter pore (400 nm, instead of the typical 100 nm), the dimensions and polydispersity index (PDI) of the particles of the LUVs used were monitored in the absence of Nys. Dynamic light scattering (DLS) was performed and the average vesicle size estimated was around 200-300 nm according to the 400 nm pore size of the filter. It was noted that the dimensions increased slightly with the increase of Cer, whereas a small decrease with the increase of Phycer was noticed, this can be related with the fact that the first POPC/Phycer complex is thinner than the fluid, an unusual behavior that this system displays revealed by atomic force microscopy and X-ray scattering [24]. The PDI was relatively high (ranging from 0.3-0.4 for all samples). This can prevent an accurate size determination and can also translate in high particles size distribution. The diameter represents an important characteristic of model membrane systems since the curvature radius modulates the phospholipid packing in the lipid vesicles and could also condition its stability and interfacial properties. The light scattering was measured by adequate diluting the sample with the same buffer used for their preparation, namely, HEPES buffer. Only the control of each system, *i.e.*, without Nys, was measured. For more detail see Table S6.1.

Table S6. 1: DLS characterization of the liposomes prepared with different lipid mixtures studied in this work.

Composition	Size (nm)	PDI
POPC 100 mol%	239.0 ± 7.5	0.32
Cer 10 mol%	252.0 ± 3.3	0.39
Cer 20 mol%	316.0 ± 7.3	0.41
Phycer 10 mol%	197.0 ± 17.1	0.31
Phycer 20 mol%	181.0 ± 6.0	0.31

Supporting Figures

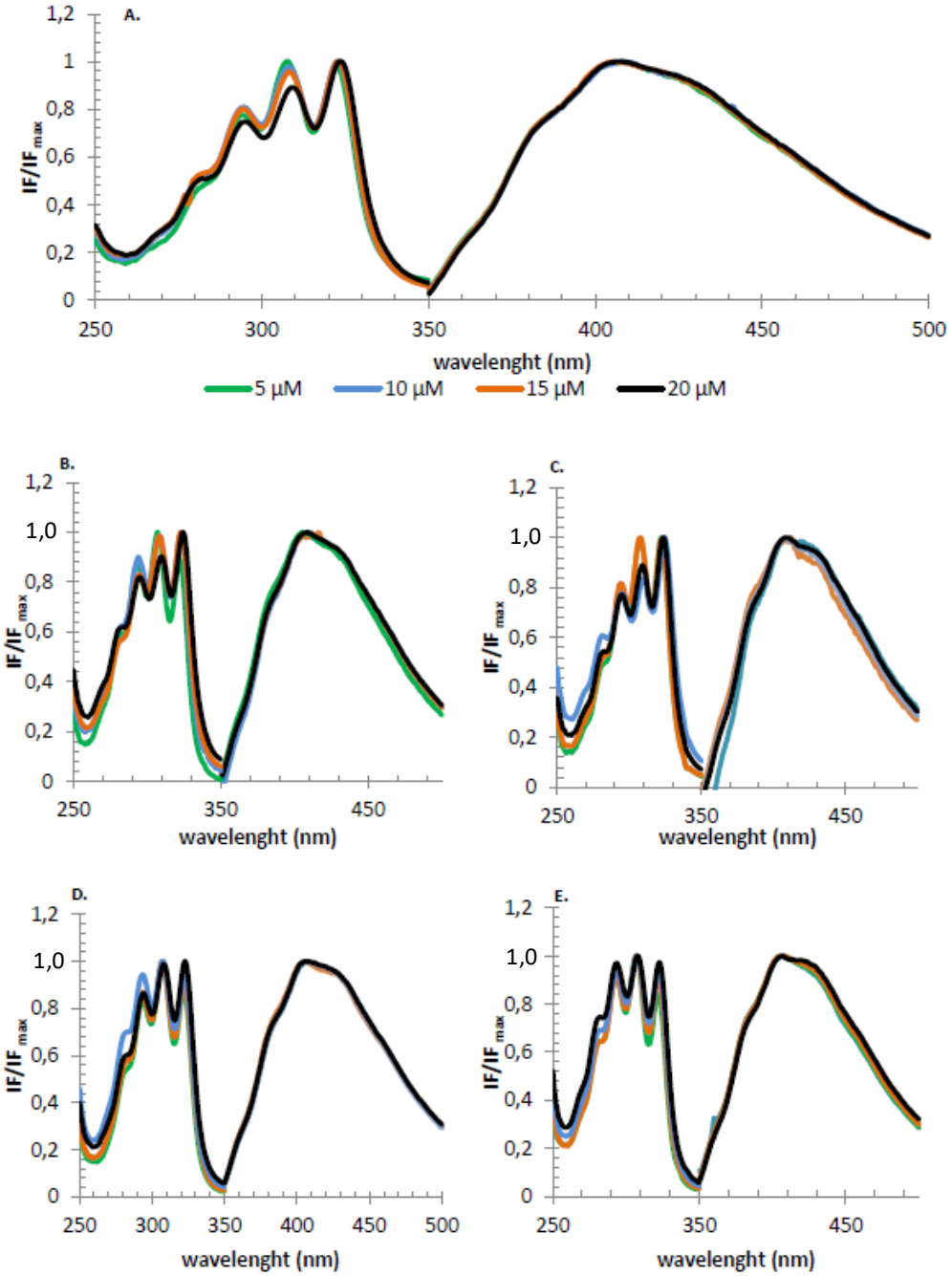

Figure S6. 1: Normalized excitation and emission spectra of Nys with liposomes containing POPC (A) and 10 and 20 mol% of Cer (B and C) and Phycer (D and E), respectively. Nys concentration was 5, 10, 15 or 20 µM. IF is the fluorescence intensity of Nys. For the excitation spectra emission was collected at 404 nm, while for the emission spectra the excitation wavelength was 303 nm.

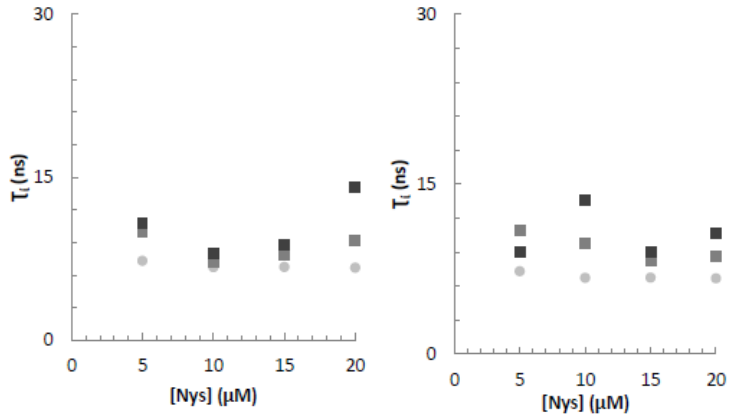

Figure S6. 2: Effect of the fraction of gel-phase on the long lifetime component of Nys. The values of long lifetime component of Nys were measured in presence of POPC 100 mol% ( ), 10 mol% ( ) and 20 mol% ( ) of Cer (right) and Phycer (left). The values are the mean ± S.D. of at least three independent replicates. Nys longest lifetime component provideS important information about the organization of Nys in different membrane environments. The formation of oligomers can be identified by the presence of a very long lifetime component. There were no significant differences among all lipid mixtures, but an increase was observed with the amount of the two different sphingolipids. This could mean a stronger tendency to aggregate with the increase of fraction of gel. Moreover, the value between these two mixtures is not so different, although in both cases a slight increase on the value of the long lifetime component was observed going from fluid to gel phase. For instance, in the absence of gel phase, *i.e.* 100 mol% of POPC, values of about 6 to 7 ns are observed, while in the presence of gel, values greater than 10 ns are reached.

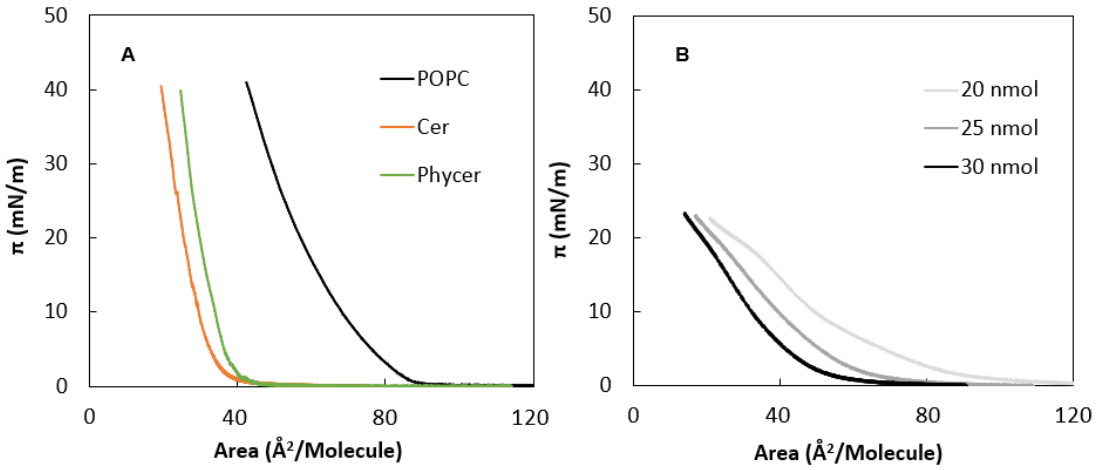

Figure S6. 3: Representative isothermic curves of solely POPC, Cer and Phycer (A), and Nys (B) on an aqueous subphase at 24 °C. The amount of Nys used in the curves is represented. The aqueous subphase was PBS: 1 mM phosphate, 2.7 mM KCl, 137 mM NaCl, pH 7.4.

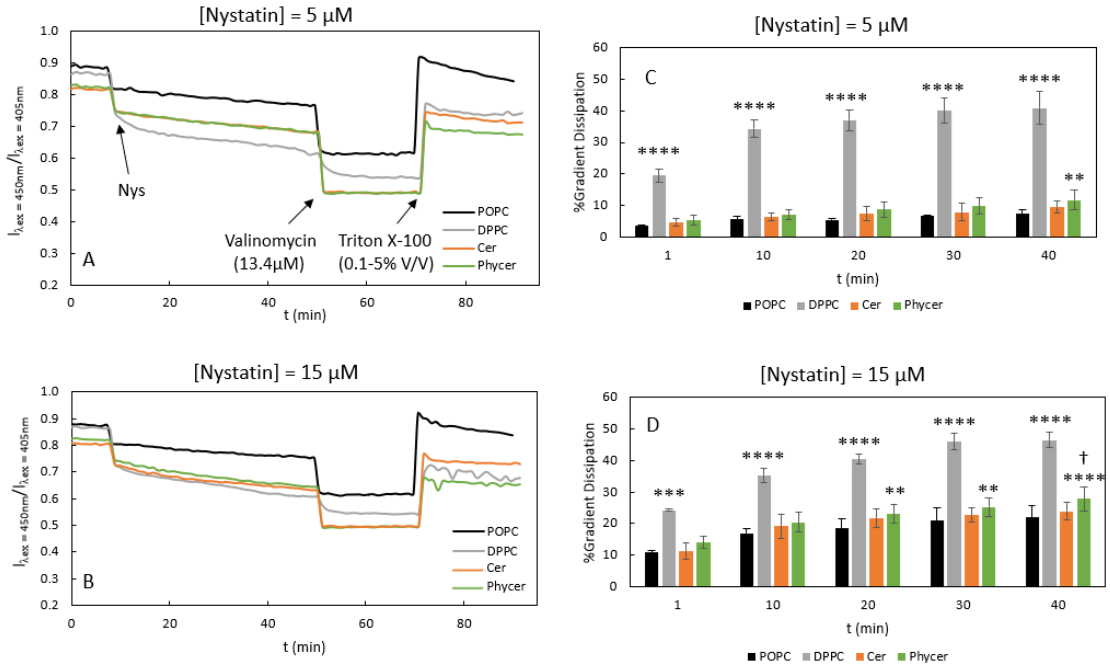

Figure S6. 4: Nys permeabilization effect on different lipid bilayers. Nys was added to the LUV preparation at a final concentration of 5 µM (A and C) or 15 µM (B and D). LUVs were prepared with POPC (black), POPC/DPPC (50 mol%; grey), POPC/Cer (20 mol%; orange) and POPC/Phycer (20 mol%; green). In A and B, $I_{\lambda ex\,=\,450nm}/\ I_{\lambda ex\,=\,405nm}$ represents the ratio between the emission fluorescence of pyranine after excitation with 450 and 405 nm, respectively. The time points at which Nys, the protonophore valinomycin and the detergent Triton X-100 were added to the samples are also represented. The percentage of gradient dissipation was calculated at different time points after the addition of Nys. Each result in A and B are from one replicate only, that is representative of the results. The results with error bars are the mean ± S.D. for at least eleven independent replicates. ** represent the statistical comparison of the results of POPC with the other systems, while † represent the statistical comparison of Phycer system with the Cer one. † $p \leq 0.05$; ** $p \leq 0.01$; *** $p \leq 0.001$; **** $p \leq 0.0001$.

CHAPTER VII

Final Conclusions and Future Perspectives

As highlighted throughout this thesis the rising of mortality rates caused by fungal infections is a pressing concern that deserves our attention. The antifungal drugs already available in the market are not many nor diverse in their mode of action. Moreover, these drugs have several side effects which in many cases are harmful towards humans. Because of this, some drugs are only used topically or orally in extreme cases. Also, the concentration of drug used can not be high due to the side effects mentioned, and in some cases the dose is not enough to completely eradicate the infection and instead contributes to the development of fungal resistance – a problem that adds to the increasing incidence of severe fungal infections. Another point worth mentioning is that even in diagnostics a fungal infection is not the first option to be considered, and in many cases antibacterial and antiviral drugs are firstly used, leaving the fungus to grow freely and in some cases develop resistance.

Due to those issues, it is relevant to find either new targets and/or new antifungal drugs. The present thesis addressed both these matters by exploring the plasma membrane of the budding yeast *Saccharomyces cerevisiae* as an antifungal drug target, taking advantage of its biophysical properties that are clearly distinct from the mammalian counterpart. In parallel, the study of the interaction of compounds representative of two distinct classes of antifungal drugs (azoles and polyenes) with membranes was carried out. The mode of action described for these two classes of antifungal drugs involves directly or indirectly alteration on the plasma membrane compromising its integrity and/or function.

This chapter starts with a compilation of the main conclusions reached throughout the thesis, followed by an attempt to tie them together, *i.e.*, disclose interconnections, analogies and mutual impact of the studies that were presented separately, but at the end of the day are all pieces of the same puzzle. In summary, from the presented data the following conclusions can be drawn:

- The presence of the major complex sphingolipid mannosyldiinositolphosphorylceramide ($M(IP)_2C$) in the plasma membrane of *S. cerevisiae* is important for proper hydrophobic chain packing of sphingolipids in the gel domains of wild-type cells, *i.e.* the size and charge of the headgroup of sphingolipids that enrich sphingolipid-enriched domains (SLEDs) is relevant for their rigidity;
- However, the biophysical properties more related to sterols /sterol-rich domains (SRDs) are not significantly affected;
- $M(IP)_2C$ should be a major component of the SLEDs. In the original publication where SLEDs were firstly introduced (Aresta-Branco et al. 2011) it was proposed that SLEDs

were rich in inositolphosphorylceramide (IPC) due to the smaller headgroup that were more prone to pack in rigid gel domains an also because the average melting temperature of SLEDs in yeast was similar to that of IPC isolated from yeast reconstituted in liposomes (Klose et al. 2010);

- SLEDs are relevant for the formation and stability of the MCP (membrane compartment that contains the H^+-ATPase Pma1p) possibly being enriched in this compartment but not MCC (membrane compartment that contains the arginine permease Can1p);
- The concomitant presence of ketoconazole (**Ke**) and the diphenylphosphine moieties allows for a more efficient interaction and in a relatively deep region of a fluid membrane, with a cumulative effect of the oxygen atom in the phosphine group;
- This interaction of **Ke** and derivatives with a fluid membrane causes an increase of the permeability of a fluid membrane, and again the oxygen atom in the phosphine group significantly increases the efficiency and speed of the permeabilizing ability of the compounds;
- The ability of the diphenylphosphine derivatives of **Ke** to strongly permeabilize a fluid membrane correlates with the possible additional mode of action proposed for these compounds. In fact, this permeabilizing ability could be their primary mode of action instead of the inhibition of the ergosterol (Erg) biosynthetic pathway – the classical mechanism of action of azoles;
- **Ke** has higher affinity towards membranes containing the major fungal sterol, Erg than the major mammalian one, cholesterol (Chol);
- The presence of sphingolipids facilitates the increase of membrane permeability caused by **Ke**;
- The presence of the major fungal sphingolipid backbone, phytoceramide (Phycer), in lipid bilayers, influences more the interaction of the polyene antifungal nystatin (Nys) with the membranes, than the mammalian counterpart, ceramide (Cer).

The biophysical study of the yeast plasma membrane in the current thesis brings us one step closer to uncovering the mysteries of the fungal plasma membrane. Interestingly, the relevance of SLEDs for the MCP and Pma1p function aligns perfectly with recent literature, that show that Pma1p is surrounded by sphingolipids and low amount of sterol (van 't Klooster et al. 2020) and that the hexameric conformation of Pma1p depends on a pool of lipids surrounded by the protein that are in a highly ordered organization (Zhao et al. 2021). Tacking

this into consideration we hypothesize that the ordered lipids surrounded by Pma1p hexamer correspond to SLEDs.

Diphenylphosphine **Ke** derivatives used in this work have an additional mode of action, that according to the data presented in this thesis (chapter III), points to membrane permeability disturbance. Antifungal drugs that act directly on the plasma membrane are not susceptible to certain resistance mechanisms that occur inside the cell. Hence, these derivatives are able to avoid certain resistance mechanisms, mainly overexpression of drug exporters.

As mentioned previously, current antifungal drugs have relatively severe side effects – a result of the similarities between human and fungal cells. Nevertheless, it is interesting that the results of this thesis show that both Nys and **Ke**, which have different modes of action against fungi and high toxicity towards human cells, have differential interaction with fungal lipids than mammalian ones. The development of new antifungal agents needs to consider this toxicity that is associated with most antifungal drugs. The different membrane interactions reported here for structurally different compounds further help to identify the molecular features relevant in drug development. Worth highlighting are the effects of the addition of the oxygen atom in the **Ke** diphenylphosphine derivatives (**KeOP** – oxide derivative) which was able to increase significantly the efficiency of the partition of the drugs towards fluid membranes and, most importantly, its ability to increase membrane permeability. This ability correlates with their additional mode of action mentioned before.

To confirm this hypothesis of **KeOP** targeting SLEDs it would be interesting to conduct similar experiments as the ones in chapter III, in which using the intrinsic fluorescence properties of this compound, its partition and permeabilizing ability towards membranes containing sphingolipids would be quantified. It would be interesting to study first the interaction of this compound towards gel membranes without sphingolipids, such as DPPC (1,2-diparlmitoyl-*sn*-glycero-3-phosphocholine) or sphingomyelin, which could point to **KeOP** having or not any preference towards gel domains; and then with different sphingolipids, such as Phycer and Cer, which would demonstrate the relevance of the hydroxyl group present in Phycer but not Cer, or ideally with $M(IP)_2C$ (as shown in chapter II the main sphingolipid enriching SLEDs).

Evidently for both **Ke** diphenylphosphine derivatives and Nys, the presence of SLEDs in the fungal plasma membrane is a factor to consider in membrane-drug interactions studies. In the development of new antifungal drugs, one must now consider the existence of a possible new target, these highly ordered gel SLEDs. Moreover, even if not a target, the presence of SLEDs in the fungal plasma membrane should now be considered since SLEDs are thought to

be in the outer leaflet of the plasma membrane, hence, after the cell wall, are amongst the first entities that a drug encounters.

Studies conducted with the objective of better understand the biophysical properties of the fungal plasma membrane are therefore relevant and timely, as previously stated. Recent literature shows the relevance of these studies to find new ways to fight pathogenic fungi (Hajdu et al. 2021), unravel SLEDs as targets of antifungal agents (Steigenberger et al. 2022) and explore the resistance mechanisms against the already available antifungal drugs (Kalli et al. 2023; Shahi et al. 2022; Urbanek et al. 2022).

SLEDs in the plasma membrane of fungal cells are evidently a feature of fungi and already considered in well-regarded reviews from literature (Athanasopoulos et al. 2019; Renne & Ernst 2023). Nonetheless, recent review articles which focus on sphingolipids in fungi and their correlation with antifungal resistance (Kalra et al. 2024), and sphingolipid membrane trafficking in yeast *vs* plants (Fougère et al. 2024), do not mention these domains. It seems that SLEDs remain overlooked or unknown for some Authors. Another option is that SLEDs are considered as synonyms of yeast lipid rafts. In fact, certain studies report the presence of lipid rafts in the fungal plasma membrane (Bagnat et al. 2000; Du & London 2024; Mollinedo 2012). The liquid-ordered (l_o)-sphingolipid/sterol enriched lipid rafts might exist in the plasma membrane of yeast, probably not as much as in mammals due to Erg being mostly on the inner leaflet, while sphingolipids are in the outer leaflet. However, in several studies the domains described as rafts are either SLEDs or SRDs. In these studies, the methodologies used to detect these domains are based on *e.g.* 1) the use of fluorescent probes, that report on membrane fluidity and not composition (*e.g.* Klose et al. 2010); or 2) using detergent-resistant membrane extraction which also includes sphingolipid gel domains (SLEDs) (Schroeder et al. 1998); or 3) the use of proteins such as Pma1p as lipid rafts markers, which interact with SLEDs (*e.g.* Bagnat et al. 2000). Therefore, even though l_o domains are detected in the yeast plasma membrane, it is possible that they are not the typical sphingolipid/sterol lipid rafts. Moreover, a mixture of glycerophospholipids with sterols in certain molar percentages has a coexistence of l_o with liquid-disordered or gel phases (*e.g.* reviewed in (de Almeida & Joly 2014)). Hence, the l_o detected for the fungal plasma membrane, could be a result from the glycerophospholipids and Erg on its inner leaflet.

Although a very thorough approach was performed in the development of this work, some new questions arose that definitely require further studies to be solved. Using the data presented

in this thesis and relevant literature, we present some hypothesis or future experiments that try to answer the most intriguing problems:

What is the actual relevance of SLEDs and Erg (or SRDs?) for the formation of the Nys pore in membranes?

It is possible to conclude from the data on chapter VI and from previous articles (dos Santos et al. 2017; Komor et al. 1979; Leber et al. 1997), that Nys is able to form pores in membranes free of sterol. Hence, the Nys sterol-dependent mode of action needs to be revised to include recent results (not only from this thesis) that 1) show that Nys can still form pores in highly ordered gel membranes (dos Santos et al. 2017; Komor et al. 1979; Leber et al. 1997), 2) Nys has a preference towards Erg rather than Chol (Szomek et al. 2021) and 3) Erg is mainly located in the inner leaflet of the fungal plasma membrane (Solanko et al. 2018). Giving an answer to the question entailed, we hypothesize that Nys first interacts with SLEDs on the outer leaflet of the membrane which serve as gateways for the drug to reach the inner leaflet enriched in Erg (SRDs), forming pores more efficiently.

What is the distribution, structure and composition of MCP and MCC/ SLEDs and SRDs among the two leaflets of fungal membranes?

The results from chapter II already provide some info regarding the SLEDs being enriched in $M(IP)_2C$, and since the MCP is interrelated with SLEDs, this compartment is most likely enriched in this complex sphingolipid. It would be interesting to conduct a similar study as in chapter II, in which the biophysical properties of the plasma membrane of the yeast *Schizosaccharomyces pombe* would be studied, particularly in search of gel domains in its plasma membrane. This study would be relevant since *S. pombe* lacks $M(IP)_2C$, having MIPC as the most complex sphingolipid, containing high levels of free Phycers and IPC (Shui et al. 2010). Hence it would show not only the possible presence of SLEDs in yet another fungal species, but also, further reveal how IPCs modulate gel properties using a wild-type strain. In contrast, the biophysical properties of the plasma membrane of *isc1*Δ *S. cerevisiae* mutant cells lacking inositol sphingolipid phospholipase C should also be investigated, because this strain should contain more $M(IP)_2C$ in the plasma membrane than the wild-type (Sawai et al. 2000).

Considering that sphingolipids are mostly in the outer leaflet and Erg in the inner leaflet of the fungal plasma membrane, then most likely SLEDs and SRDs are enriching the outer and inner leaflet of the plasma membrane respectively. Also, the MCP and the MCC are interrelated with SLEDs and SRDs respectively, hence the same respective distribution in the membrane is expected. Nevertheless, this is only a simple description of the organization of the membrane

as other factors should be considered such as: 1) certain proteins that are specific of some compartments, such as Pma1p (MCP), are transmembrane proteins, and, since it is evidenced that Pma1p surrounds SLEDs (Zhao et al. 2021), which signifies that in this case locally, SLEDs might be in both membrane leaflets; 2) other membrane compartments exist; 3) different conditions change membrane organization; 4) interdigitation is probably occurring with the sphingolipids that enrich SLEDs due to its very long chain of 24 or 26 carbons in length. Regarding this fourth point, it should be interesting to study the properties of SLEDs in yeast that have sphingolipids with shorter chains instead of the typical 24-26. Moreover, mutant yeasts with sphingolipids that have shortened very long chains and lower levels of these lipids are resistant to a polyene antifungal drug, syringomycin E (Stock et al. 2000).

*Is the membrane permeabilizing ability of **Ke** derivatives their primary mode of action?*

Membrane permeabilization is important for the antifungal activity of the diphenylphosphine derivatives of **Ke**, particularly of the oxide derivative, **KeOP**. The minimal inhibitory concentration (MIC) values and compound concentration range for membrane permeabilization indicate that this could be an important additional mechanism of action for these compounds, especially **KeOP**. Nonetheless, membrane perturbation is most probably not the sole mechanism of action of these compounds, since the MIC value for a *S. cerevisiae* mutant that lacks the main drug exporters AD1-8, is ~60 (for **KeP** and **KeOP**) and ~300 (for **Ke**) times lower than for the wild-type (de Almeida et al. 2019). If membrane disruption were the only mechanism, lack of main drug exporter would likely not affect MIC values so markedly.

However, to confirm that it is the primary mode of action of these **Ke** derivatives other experiments would be necessary. For instance, an uptake assay with rhodamine-6G (Mukhopadhyay et al. 2002) with yeast cells would allow to confirm *in vivo* the permeabilizing ability of these compounds observed only in model membranes in chapter III. In this assay rhodamine-6G is added to cells in suspension and after an incubation period, the rhodamine that remains outside the cells is removed with centrifugations. The fluorescence of rhodamine-6G measured after this process is only from the fluorophore inside the cell. Hence, it is possible to conduct this assay comparing the passive diffusion of rhodamine-6G with and without the addition of **Ke** derivatives, *i.e.* the permeabilizing ability of these compounds in cells. Using incubation periods with the drug that are lower than the time it takes azoles to reach the target (sterol synthesis) inside the cell, would confirm if the drug is faster at permeabilizing the membrane or inhibiting sterol synthesis.

*Does the oxide diphenylphosphine derivative of **Ke**, **KeOP**, targets SLEDs?*

The oxygen atom in **KeOP** grants the molecule strong affinity towards fluid membranes, the ability to increase membrane permeability, and to form hydrogen bonds. This hydrogen bonding ability means that the compound may interact differently or even specifically with different membrane regions of the fungal plasma membrane such as SLEDs. Moreover, the sphingolipids that enrich SLEDs are organized in a highly ordered network in which hydrogen bonding is relevant. Furthermore, and as highlighted in the chapter V and VI of this thesis, the major backbone of fungal sphingolipids has extra hydroxylations when compared to the mammalian one. Therefore, these hydroxyl groups could also be relevant for the interaction of **KeOP** with SLEDs. Hence, this compound could even be a stronger membrane perturbing agent towards these gel domains. Since SLEDs and the MCP are interrelated, as reported in chapter II of this thesis, the perturbation of SLEDs would cause a disturbance in the MCP and to the cellular functions associated with it – mainly ion and proton homeostasis.

Why evolution "decided" that fungi would have gel in their membranes but not mammals? Is it an adaptive characteristic of non-motile organisms such as plants?

In the current thesis the main comparison of the plasma membrane properties and composition being made is between yeast and mammals. It has yet to be discovered if there are gel domains in the plasma membrane of plants. This becomes more interesting when comparing the sphingolipidome of the three kingdoms. Similarly to fungi, Phycer also exists in plants, but the end result instead of IPCs is glucosylceramides and glycosyl inositol phosphoryl ceramides (GIPCs) (Mamode Cassim et al. 2020). It is possible that this GIPCs, which are not that different from IPCs, having only more sugars in the headgroup but similar backbone (Phycer), have analogous biophysical behavior as IPCs in fungi, and are organized in gel domains. The functions associated with SLEDs listed in chapter I, are mainly related with mechanisms of adaptation to stress. If truly gel domains exist in the plasma membrane of plants, then similar functions might be associated.

This type of studies further discloses how structural differences in lipids change membrane properties, but most importantly are particularly relevant to have a better overview of the evolution of sphingolipids across different kingdoms.

Overall, the conclusions drawn in this chapter answer the questions proposed in the Aims section, and the main goals of the project were achieved. Each chapter works as a puzzle piece of a bigger picture, paving the way to fight fungal infections and their human mortality rate and the problems faced in crop and timber industries.

References

Aresta-Branco F, Cordeiro AM, Marinho HS, Cyrne L, Antunes F, de Almeida RFM. (2011). Gel domains in the plasma membrane of Saccharomyces cerevisiae: highly ordered, ergosterol-free, and sphingolipid-enriched lipid rafts. *J. Biol. Chem.* 286(7):5043–54

Athanasopoulos A, André B, Sophianopoulou V, Gournas C. (2019). Fungal plasma membrane domains. *FEMS Microbiol. Rev.*

Bagnat M, Keränen S, Shevchenko A, Shevchenko A, Simons K. (2000). Lipid rafts function in biosynthetic delivery of proteins to the cell surface in yeast. *Proc. Natl. Acad. Sci. U. S. A.* 97(7):3254–59.

de Almeida RFM, Joly E. (2014). Crystallization around solid-like nanosized docks can explain the specificity, diversity, and stability of membrane microdomains. *Front. Plant Sci.* 5:72

de Almeida RFM, Santos FC, Marycz K, Alicka M, Krasowska A, et al. (2019). New diphenylphosphane derivatives of ketoconazole are promising antifungal agents. *Sci. Rep.* 9(1):

Du BB, London E. (2024). Lipid rafts form in S. cerevisiae plasma membrane and are modulated by growth conditions. *Biophys. J.* 123(3):96a.

Fougère L, Mongrand S, Boutté Y. (2024). The function of sphingolipids in membrane trafficking and cell signaling in plants, in comparison with yeast and animal cells. *Biochim. Biophys. acta. Mol. cell Biol. lipids*. 1869(3):.

Hajdu T, Szabó K, Jakab Á, Pócsi I, Dombrádi V, Nagy P. (2021). Biophysical experiments reveal a protective role of protein phosphatase Z1 against oxidative damage of the cell membrane in Candida albicans. *Free Radic. Biol. Med.* 176:222–27

Kalli S, Vallieres C, Violet J, Sanders J-W, Chapman J, et al. (2023). Cellular Responses and Targets in Food Spoilage Yeasts Exposed to Antifungal Prenylated Isoflavonoids. *Microbiol. Spectr.* 11(4):

Kalra S, Tanwar S, Bari VK. (2024). Insights into the role of sphingolipids in antifungal drug resistance. *Fungal Biol. Rev.* 47:100342

Klose C, Ejsing CS, García-Sáez AJ, Kaiser HJ, Sampaio JL, et al. (2010). Yeast Lipids Can Phase-separate into Micrometer-scale Membrane Domains. *J. Biol. Chem.* 285(39):30224.

Mamode Cassim A, Grison M, Ito Y, Simon-Plas F, Mongrand S, Boutté Y. (2020). Sphingolipids in plants: a guidebook on their function in membrane architecture, cellular processes, and environmental or developmental responses. *FEBS Lett.* 594(22):3719–38.

Mollinedo F. (2012). Lipid raft involvement in yeast cell growth and death. *Front. Oncol.* 2:

Mukhopadhyay K, Kohli A, Prasad R. (2002). Drug Susceptibilities of Yeast Cells Are Affected by Membrane Lipid Composition. *Antimicrob. Agents Chemother.* 46(12):3695.

Renne MF, Ernst R. (2023). Membrane homeostasis beyond fluidity: control of membrane compressibility. *Trends Biochem. Sci.* 48(11):963–77.

Sawai H, Okamoto Y, Luberto C, Mao C, Bielawska A, Domae N, Hannun A. (2000). Identification of ISC1 (YER019w) as inositol phosphosphingolipid phospholipase C in Saccharomyces cerevisiae. *J. Biol. Chem.* 275(50): 39793.

Schroeder RJ, Ahmed SN, Zhu Y, London E, Brown DA. (1998). Cholesterol and Sphingolipid Enhance the Triton X-100 Insolubility of Glycosylphosphatidylinositol-anchored Proteins by Promoting the Formation of Detergent-insoluble Ordered Membrane Domains. *J. Biol. Chem.* 273(2): 1150-7

Shahi G, Kumar M, Khandelwal NK, Banerjee A, Sarkar P, et al. (2022). Inositol Phosphoryl Transferase, Ipt1, Is a Critical Determinant of Azole Resistance and Virulence Phenotypes in Candida glabrata. *J. fungi (Basel, Switzerland)*. 8(7)

Shui G, Guan XL, Low CP, Chua GH, Goh JSY, et al. (2010). Toward one step analysis of cellular lipidomes using liquid chromatography coupled with mass spectrometry: application to Saccharomyces cerevisiae and Schizosaccharomyces pombe lipidomics. *Mol. Biosyst.* 6(6):1008–17.

Solanko LM, Sullivan DP, Sere YY, Szomek M, Lunding A, et al. (2018). Ergosterol is mainly located in the cytoplasmic leaflet of the yeast plasma membrane. *Traffic.* 19(3):198–214.

Steigenberger J, Mergen C, De Roo V, Geudens N, Martins JC, Heerklotz H. (2022). The effect of membrane thickness on the membrane permeabilizing activity of the cyclic lipopeptide tolaasin II. *Front. Mol. Biosci.* 9:1064742

Stock, SD, Hama, H, Radding, JA, Young, DA, Takemoto, JY. (2000). Syringomycin E inhibition of Saccharomyces cerevisiae: Requirement for biosynthesis of sphingolipids with very-long-chain fatty acids and mannoseand phosphoinositol-containing head groups. *Antimicrob. Agents Chemother*. 44: 1174–1180.

Szomek M, Reinholdt P, Petersen D, Caci A, Kongsted J, Wüstner D. 2021. Direct observation of nystatin binding to the plasma membrane of living cells. *Biochim. Biophys. Acta - Biomembr.* 1863(2):183528

Urbanek AK, Muraszko J, Derkacz D, Łukaszewicz M, Bernat P, Krasowska A. (2022). The Role of Ergosterol and Sphingolipids in the Localization and Activity of Candida albicans' Multidrug Transporter Cdr1p and Plasma Membrane ATPase Pma1p. *Int. J. Mol. Sci.* 23(17):9975.

van 't Klooster JS, Cheng T-Y, Sikkema HR, Jeucken A, Moody B, Poolman B. (2020). Periprotein lipidomes of Saccharomyces cerevisiae provide a flexible environment for conformational changes of membrane proteins. *Elife*. 9:

Zhao P, Zhao C, Chen D, Yun C, Li H, Bai L. (2021). Structure and activation mechanism of the hexameric plasma membrane H+-ATPase. *Nat. Commun. 2021 121*. 12(1):1–11.